MAR2PROTECT

D4.3 Report on the REACH Tool for GC and CC impacts on GW chemical status

CETAQUA ANDALUCÍA

AQUATEC

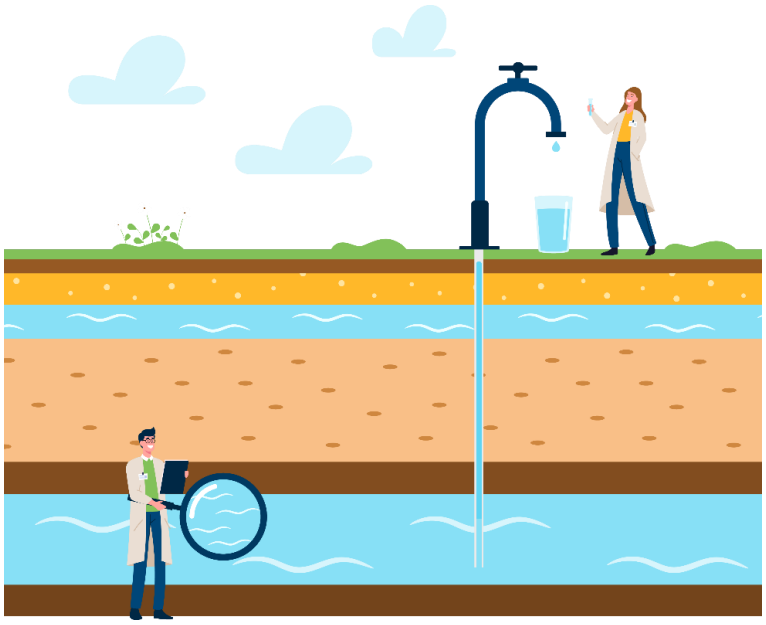

This project has received funding from the European Union's Horizon Europe research and innovation programme under grant agreement No GA 101082048

Funded by the European Union

GRANT AGREEMENT NUMBER: 101082048

PROJECT ACRONYM: MAR2PROTECT

PROJECT TITLE: "Preventing Groundwater Contamination Related to Global and Climate Change through a Holistic Approach Based on Managed Aquifer Recharge"

PROJECT Duration: 1st December 2022 - 30th November 2026 (48 months)

WEBSITE: https://mar2protect.eu/

PARTNERS AND ASSOCIATED PARTNERS ACRONYMS

ACRONYM	PARTNER
ADTA	ÁGUAS DO TEJO ATLÂNTICO
AQUATEC	AFFILIATED ENTITY OF CETAND. WATER PRIVATE COMPANY (VEOLIA GROUP), SPAIN
CETAND	CENTRO ANDALUZ DE INVESTIGACIONES DEL AGUA
CIIMAR	CENTRO INTERDISCIPLINAR DE INVESTIGAÇÃO MARINHA E AMBIENTAL, PORTUGAL
CT	CITY OF CAPE TOWN
DU	DUNEA DUIN & WATER
FEUGA	FUNDACIÓN EMPRESA UNIVERSIDAD GALLEGA, SPAIN
FHNW	UNIVERSITY OF APPLIED SCIENCES AND ARTS NORTHWESTERN SWITZERLAND
HERA	HOLDING ENERGIA RISORSE AMBIENTE
IHE	IHE DELFT INSTITUTE FOR WATER EDUCATION, THE NETHERLANDS
IT	INSTITUTO DE TELECOMUNICAÇOES, PORTUGAL
ISSBAT	INST. SUPÉR. DES SCIENCES BIOLOGIQUES APPLIQUÉES DE TUNIS
KTU	KAUNAS UNIVERSITY OF TECHNOLOGY, LITHUANIA
NOVA	NOVA ID FCT – ASSOCIAÇÃO PARA A INOVAÇÃO E DESENVOLVIMENTO DA FACULDADE DE CIÊNCIAS E TECNOLOGIA DA UNIVERSIDADE NOVA DE LISBOA, PORTUGAL
SU	STELLENBOSCH UNIVERSITY, SOUTH AFRICA
UNIBO	UNIVERSITY OF BOLOGNA, ITALY

This project has received funding from the European Union's Horizon Europe research and innovation programme under grant agreement No GA 101082048

Funded by the European Union

Abbreviation / Acronym:

AEMET: State Meteorological Agency (Spain) 34
CC: Climate Change 4
CMIP: Coupled Model Intercomparison Project Phase 106
DERA: Reference Spatial Data of Andalucía 34
DMA: Water Framework Directive 34
DS: Demo sites 15
EC: Electrical Conductivity 84
EO: Earth Observation 14
GC: Global Change 4
GCMs: Global Climate Models 50
GW: Groundwater 4
IFAPA: Andalusian Institute of Agricultural and Fisheries Research and Training 34
IGME: Spanish Geological Survey 60
IGN: National Geographic Institute 34
LULC: Land Use Land Cover 14
m.a.s.l: Meters above sea level 28
MAE: Mean Absolute Error 38
MAR: Managed Aquifer Recharge 115
MDA: Mean Directional Accuracy 38
NE: North East 18
PET: Potential Evapotranspiration 35
RAIF: Andalusian Network of Alert and Phytosanitary Information 34
RCMs: Regional Climate Models 50
RCPs: Representative Concentration Pathways 14
REACH: *REACH (gRoundwatEr quAlity CHange)* 14
RMSE: Root Mean Squared Error 38
SAIH: Automatic Hydrological Information Systems 34
SHAP: SHapley Additive exPlanations 40
sMAPE: Symmetric Mean Absolute Percentage Error 39
Sñ1: Señorío 1 58
Sñ2: Señorío 2 58
Sñ3: Señorío 3 58
SO: Specific Objective 16
SPEI: Standardised Precipitation Evapotranspiration Index 15
SPI: Standardised Precipitation Index 15
SSP: Shared Socioeconomic Pathways 106
UMA: University of Málaga 60
WKT: Well Known Text 50

This project has received funding from the European Union's Horizon Europe research and innovation programme under grant agreement No GA 101082048

Funded by the European Union

Executive Summary

The following document is Deliverable 4.3 "Report on the REACH Tool for Global Change (GC) and Climate Change (CC) impacts on groundwater (GW) chemical status" of the MAR2PROTECT project, funded by the European Union's Horizon Europe research and innovation programme under grant agreement Number 101082048.

This report will be the main output of T4.2. It will show the results obtained by the REACH Tool, considering three functional approaches: physical (MOD-REACH; e.g., groundwater flow modelling for simulating the impacts of climate trends on GW chemical status), data-driven (DATA-REACH; past correlations between climate indices and GW quality variables to extrapolate into the future) and overlay-based models (GIS- REACH; vulnerability and risk mapping for different pollution types including spatial explanatory variables).

Deliverable Number	WP / T
D4.3	WP4 / T4.2

Lead Beneficiary	Deliverable Author (S)
Cetaqua Andalucía	Francisco Nuñez (CETAND) Jose Manuel Nieto (CETAND) Lupicinio García (CETAND) (Organisation)

Beneficiaries	Deliverable Co-Author (S)
Aquatec	Irene Marín (AQUATEC) Nicolás Tapia Morales (AQUATEC) Ana Ortuño Morales (AQUATEC)

Planned Delivery Date	Actual Delivery Date
31/05/2024	29/05/2024

Type of deliverable	PU	Public, fully open, e.g. web (Deliverables flagged as the public will be automatically published in the CORDIS project's page))	**X**
	SEN	Sensitive, limited under the conditions of the Grant Agreement	

This project has received funding from the European Union's Horizon Europe research and innovation programme under grant agreement No GA 101082048

Funded by the European Union

Revision History

Version	Date	Author	Document history/approvals
01	15/05/2024	CETAQUA	V0
02	16/05/2024	NOVA/UNIBO	V1
03	21/05/2024	CETAQUA	V2
04	24/05/2024	NOVA	V3
05	18/10/2024	CETAQUA	V4

Acknowledgement: The work described in this report has been funded by the European Union from the Horizon Europe research and innovation Programme (HORIZON-CL6-2022-ZEROPOLLUTION-01), Research and Innovation Action under the Grant Agreement No 101082048.

Index

This project has received funding from the European Union's Horizon Europe research and innovation programme under grant agreement No GA 101082048

Funded by the European Union

This project has received funding from the European Union's Horizon Europe research and innovation programme under grant agreement No GA 101082048

Funded by the European Union

This project has received funding from the European Union's Horizon Europe research and innovation programme under grant agreement No GA 101082048

Funded by the European Union

INDEX OF FIGURES

This project has received funding from the European Union's Horizon Europe research and innovation programme under grant agreement No GA 101082048
Funded by the European Union

This project has received funding from the European Union's Horizon Europe research and innovation programme under grant agreement No GA 101082048
Funded by the European Union

This project has received funding from the European Union's Horizon Europe research and innovation programme under grant agreement No GA 101082048
Funded by the European Union

This project has received funding from the European Union's Horizon Europe research and innovation programme under grant agreement No GA 101082048

Funded by the European Union

INDEX OF TABLES

This project has received funding from the European Union's Horizon Europe research and innovation programme under grant agreement No GA 101082048
Funded by the European Union

This project has received funding from the European Union's Horizon Europe research and innovation programme under grant agreement No GA 101082048
Funded by the European Union

1 INTRODUCTION

This report is part of WP4, specifically, it is the output of Task 4.2. *Global and climate change scenarios and GW quality: REACH (gRoundwatEr quAlity CHange) tool,* where the REACH Tool for a reliable assessment of the impacts of GC and CC on GW is developed. The report will show the results obtained by the tool, considering three functional approaches: physical (MOD-REACH; groundwater flow modelling for simulating the impacts of climate trends on GW chemical status), data-driven (DATA-REACH; past correlations between climate indices and GW quality variables to extrapolate into the future) and overlay-based models (GIS-REACH; vulnerability and risk mapping for different pollution types including spatial explanatory variables). REACH will include downscaling procedures to regionalize global climate projections, Land Use Land Cover (LULC) predictions, projected sea level rise scenarios to locate potential areas in which MAR could be proposed as a solution and different RCPs (Representative Concentration Pathways). A deeper analysis of MAR potential areas using EO techniques will be assessed in Deliverable 4.4 (MAR suitability and feasibility mapping and cost-benefit analysis of MAR projects).

The report will also serve as input for Task 4.6 - M-AI-R DSS integrated platform for MAR management and risk assessment & mitigation strategies. The REACH Tool is one of the integral parts of the M-AI-R-DSS as well as the DRONE and RAINREC models which will be further developed in Deliverable 4.5 (DRONE & RAINREC: Data-driven & hybrid forecasting models for simulating MAR yield variable).

The REACH tool is one of several components that make up M-AI-R DSS (Decision Support System) a tool designed for the efficient management of groundwater artificial recharge using both conventional and non-conventional water resources. Specifically, REACH has been developed as a solution to enhance the understanding of the main processes that condition the groundwater (GW) bodies' chemical and quantitative status.

Through the application of diverse approaches (physical models, GIS and data analytics), the aim has been to generate a set of results that provide insights into what is happening, why it is happening, and what is likely to happen in the future.

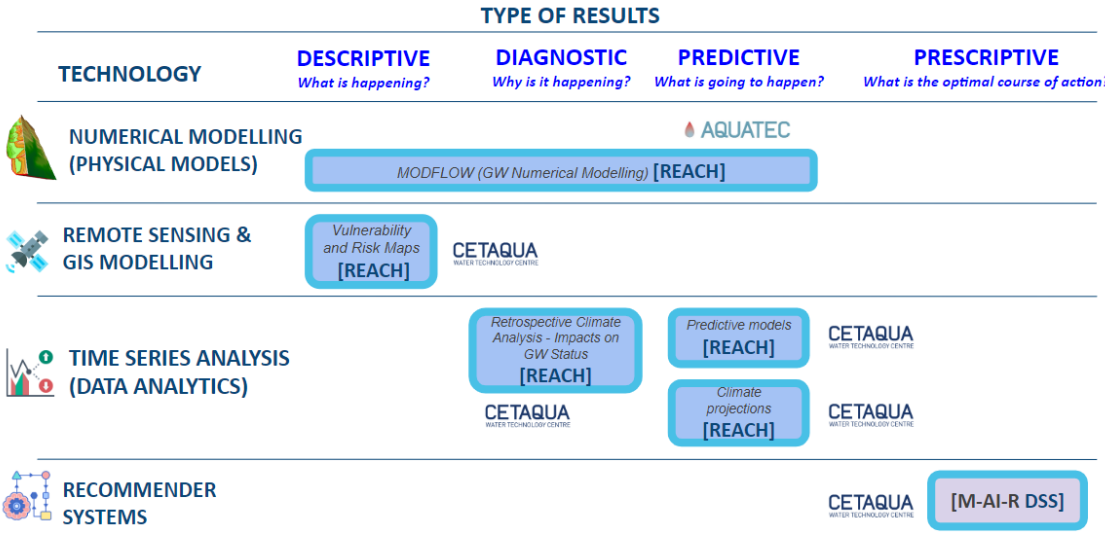

Figure 2.1-1 Classification of expected results.

The initial approach of this study involves the use of physical models to create a three-dimensional numerical model of the coastal aquifer of the Señorío de Marbella. The

This project has received funding from the European Union's Horizon Europe research and innovation programme under grant agreement No GA 101082048
Funded by the European Union

objective is to understand the hydrogeological relationships between the aquifer and the sea, which is vital as this aquifer is a key water supply source for the local population. The water demands in Marbella are satisfied with a mix of surface water, desalinated water, and groundwater (this last one represents 40-50%). While the connection between different alluvial aquifers is evident, the relationship between the deeper Pliocene aquifers is less clear. The existing geological mapping is often insufficient to clarify the geometry of these Pliocene aquifers, particularly in the coastal line where the salt intrusion occurs.

A thorough understanding of the boundaries and geometry of Marbella's deep aquifers would enable optimised management and potentially increase the volume of available water resources.

The next approach to be addressed involves vulnerability and risk mapping. Groundwater pollution risk is a significant social issue, given that groundwater sources supply drinking water to millions globally, so it is important to consider both the physical parameters of the environment and the population perspective (Raucher, 1983; Shechter, 1985; Ducci, 1999; Darmendrail, 2001; Perles *et al*., 2004). Within the scope of this project, a groundwater risk assessment methodology will be developed, designed for wide applicability across European groundwater bodies.

Another approach to be addressed in this study is retrospective climate analysis. The intensification of droughts due to climate change highlights the importance of effective water resource management, especially in Mediterranean coastal areas with high tourist activity where water demand significantly increases. A comparative analysis has been conducted between the Standardised Precipitation Index (SPI) and the Standardised Precipitation Evapotranspiration Index (SPEI) in the Western Costa del Sol. This analysis aims to detect potential temporal deterioration, both quantitative and chemical, of the Marbella-Estepona groundwater body (060.040) associated with drought events.

One of the predictive approaches of this research involves training and validating various machine learning models. These models will provide monthly probabilistic predictions of different variables to support decision-making focused on groundwater quality and quantity in the context of global and climatic change. The focus will be on different wells distributed in the Marbella-Estepona groundwater body (060.040) and on the main reservoirs of the area for this purpose.

The study also includes climate projections from 7 demo sites (DS), providing a comprehensive understanding of the potential impacts of climate change on groundwater resources.

In the following pages, the specific objectives of each of the approaches that constitute the REACH tool will be detailed, along with the methodology followed in each case to achieve these objectives and the final results and conclusions that have been obtained.

The REACH tool is divided into three analytics modules: MOD-REACH (physical modelling-based approach), DATA-REACH (data-driven-based approach), and GIS-REACH (geospatial approach). This categorization has been used to structure the technical results in the sections below.

The replication of these results has been performed in:

- MOD-REACH: DS6 (Marbella, Spain).

This project has received funding from the European Union's Horizon Europe research and innovation programme under grant agreement No GA 101082048

Funded by the European Union

- DATA-REACH: DS6 (Marbella, Spain). A replication in DS4 (Emilia Romagna, Italy) of the predictive models will be performed in T4.5 to compare results between both modelling approaches DRONE and DATA-REACH.
- GIS-REACH: DS3 (Frielas, Portugal), DS4 (Emilia Romagna, Italy), DS5 (Cape Flats, South Africa) and DS6 (Marbella, Spain).

2 SCOPE AND OBJECTIVES

This report is the output of task 4.2 and will serve as an input to task 4.6. It is related to the first objective of the WP4: Better understanding of GC/CC impacts on GW contamination. It responds to SO4 (To predict the impacts of global and climate change on GW quality in a specific context with the innovative REACH - gRoundwatErquAlityCHange - tool) and it is related to SO5 as REACH Tool is part of the M-AI-R-DSS.

The scope and objectives of each of the analytic modules will be explained in the following sections.

2.1 MOD-REACH

This section is based on the development of a three-dimensional numerical model of underground flow in the coastal aquifer of the Señorío de Marbella that will allow:

- To know the geometry and boundaries of the deep aquifers used for the supply to Marbella, from the integration of geological data from drilling and geophysics.
- To specify the hydrogeological relationships between the El Señorío aquifer and the sea.
- To establish future simulation scenarios (new points to implement MAR schemes).

2.2 DATA-REACH

2.2.1 RETROSPECTIVE CLIMATE ANALYSIS

The objectives pursued in the execution of this part of the tool are as follows:

- Conducting a comparative analysis of two climate indices (SPI and SPEI) at different meteorological stations on the Western Costa del Sol.
- Identifying drought periods based on the generated climate indices.
- Assessing potential deterioration in the chemical and quantitative status of the Marbella-Estepona groundwater body associated with drought periods detected by the climate indices.

2.2.2 PREDICTIVE MODELS

This component of the tool aims to train and validate various machine learning models that provide monthly probabilistic predictions of different variables to support decision-making focused on groundwater quality in the context of global and climatic change.

It will focus on various wells belonging to the Marbella-Estepona groundwater body (060.040) and on the main reservoirs for this purpose.

2.3 GIS-REACH

The vulnerability and risk mapping of a specific area through the REACH tool will allow to:

This project has received funding from the European Union's Horizon Europe research and innovation programme under grant agreement No GA 101082048

Funded by the European Union

- Identify areas more sensitive to pollution within the groundwater body.
- Identify the main pressures in the area that can contribute to groundwater pollution.
- Allocate optimal areas to address groundwater protection actions.

2.4 CLIMATE PROJECTIONS

In this stage, the goal is to apply downscaling procedures to regionalize global climate projections at the 7 Mar2protect demo sites, allowing for a more accurate representation of their climate behaviour minimising the bias associated with large-scale dimensional projections. This will be achieved through the simulation of various RCP scenarios. The objective of downloading climate projections has been to characterise the future trends of two climate drivers (precipitation and temperature). These climate projections will be tested as inputs of DRONE and RAINREC models (D4.5), as well as for assessing the impacts of climate change in the activation or not of the Spanish MAR scheme (D4.6), respectively.

3 METHODOLOGY

As mentioned before, the REACH Tool is made of three analytical modules: MOD-REACH, DATA-REACH and GIS-REACH. The following Figure shows a schematic approach of each part of the REACH Tool and the methodologies applied.

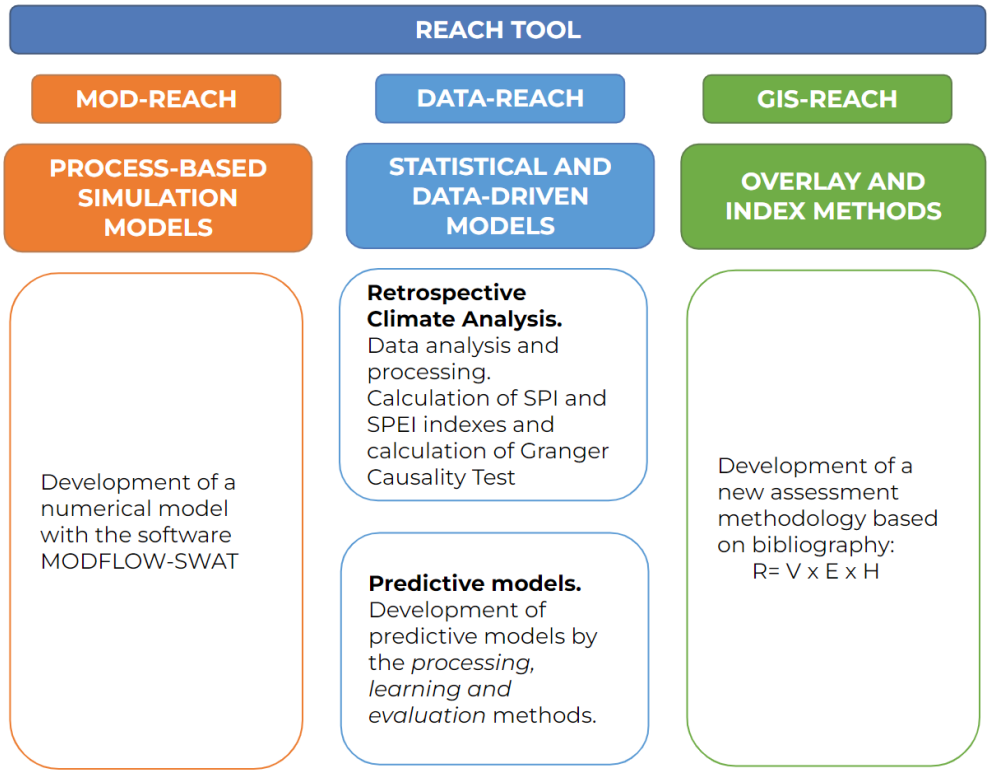

Figure 3-1 REACH Tool components and the methodologies applied in each of them.

This section contains an explanation of the construction and development of each of the modules of the REACH tool.

3.1 MOD-REACH

The detrital Señorío Aquifer is made up of conglomerates, sands and sandy silts of the Pliocene, of high permeability, which dip from 5 to 10° towards the sea, with which it

This project has received funding from the European Union's Horizon Europe research and innovation programme under grant agreement No GA 101082048
Funded by the European Union

contacts on a front of 3.2 km. It is a multilayer set about 100 m thick, which is confined in its southern half. The pumping tests carried out, around Señorío 4 borehole, show a transmissivity of 1,995 m^2/day and a storage coefficient of $5.7x10^{-3}$. The aquifer is naturally recharged through the infiltration of rainfall on permeable outcrops (7.1 km^2) and, to a lesser extent, by percolation of the runoff from the Nagüeles stream, which is fed by springs from Sierra Blanca. However, this stream is captured near its source to supply a nearby development, at a rate of 10 L/s. Currently, MAR is produced through the Señorío 4 and 2 boreholes, with water coming from the Camoján spring located NE of the aquifer, around the edge of Sierra Blanca.

The aquifer has been exploited for more than three decades both for the supply of the Marbella core, as well as for urbanizations from other surveys. The aquifer discharges naturally towards the sea and also from extractions in the Señorío 1, 2 and 3 wells, as well as from other private use operations. For the 2000-2022 time series, the average inputs by direct infiltration have been evaluated at 1.6 hm^3/year with an infiltration rate of 35%. The average volume of artificial recharge is quantified at 0.13 hm^3/year. As for the extractions, the Señorío wells present an average exploitation of 0.56 hm^3/year and the private use wells of 0.65 hm^3/year (or at least that was the flow they extracted before the year 2000), which together represent an average pumping of 1.2 hm^3/year.

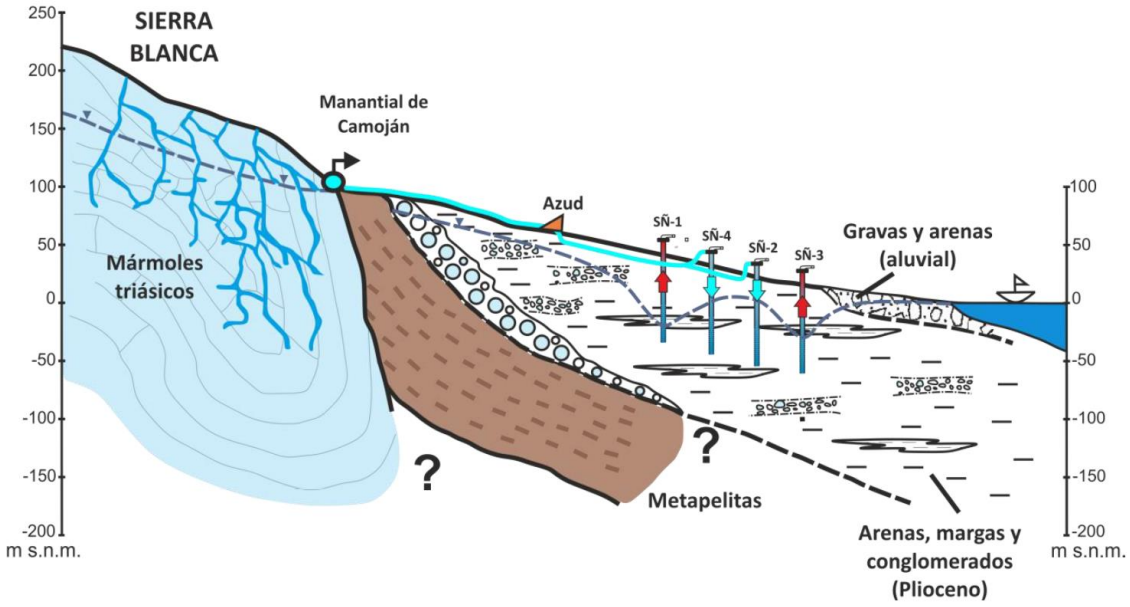

Figure 3.1-1 Hydrogeological scheme of the Señorío de Marbella aquifer and artificial recharge (source: Argamasilla, 2017).

The piezometric levels of the Señorío aquifer show a marked periodic succession associated with the seasonality of precipitation, with rapid rises in response to autumn and winter rainfall and abrupt drops in summer, with minimum values of 7 m below sea level. Specifically, the piezometric series of the Señorío 2 and Torreverde drillings (Figure 3.1-2), in the summer months between 2000 and 2003 reached negative levels, with minimums close to 4 m below sea level.

This project has received funding from the European Union's Horizon Europe research and innovation programme under grant agreement No GA 101082048
Funded by the European Union

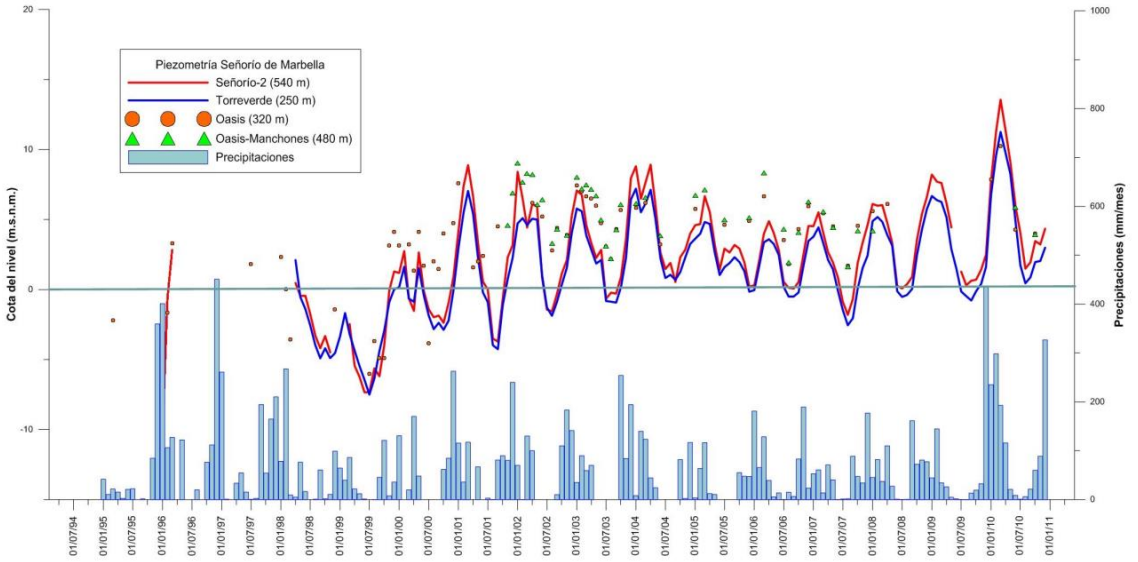

Figure 3.1-2 Evolution of the piezometric level in the aquifer of the Señorío of Marbella (source: Study of recharge in the detrital coastal aquifer of the Señorío of Marbella, 2012).

The piezometric level rise occurs after rainy periods, which indicates that the aquifer has a rapid response to the natural recharge due to rainfall.

From 1998 to 2004, negative levels were recorded in the aquifer and the negative trend of the levels continued until August 2007 (the month in which the levels approached 3 m below sea level). Since 2008, the aquifer has maintained a progressive piezometric rise and reached a historical maximum in March 2010, in the Señorío 2 well (13.5 m above sea level), due to the heavy rainfalls at the end of 2009 and the beginning of 2010. Generally, in most of the Pliocene aquifer, the average piezometric level is between 10 and 40 m deep.

The numerical model is carried out, trying to reproduce the hydrogeological conceptualization previously exposed in the best possible way.

3.1.1 GEOMETRY

The structure or geometry of the numerical model consists of a total of three layers or hydrogeological units, which group the main lithological units of the study area based on their hydrogeological properties. In this way, and as developed in this section, the numerical model consists of three layers: two surface layers of a detrital nature and a third corresponding to the impermeable basement.

The construction of the geometry of the numerical model began with an extensive task of collecting and analysing geological information obtained from multiple sources. Table 3.1-1 compiles the databases consulted, as well as Table 3.1-2 synthesises the reviewed technical studies.

Table 3.1-1 Databases consulted.

Type of information	Database	Source
Stratigraphic columns	Private litholibrary	Hidralia S.A
Stratigraphic columns	Public litholibrary	Geological and Mining Institute of Spain (IGME)
Location of water points	Water Point Database	Geological and Mining Institute of Spain (IGME)
Geological descriptions	Documentary Information System	Geological and Mining Institute of Spain (IGME)

This project has received funding from the European Union's Horizon Europe research and innovation programme under grant agreement No GA 101082048
Funded by the European Union

Type of information	Database	Source
Geophysical profiles	Geophysical Information System (SIGEOF)	Geological and Mining Institute of Spain (IGME)
Geological descriptions	GeoPortal	Ministry of Agriculture and Fisheries, Food and Environment

Table 3.1-2 Articles reviewed.

Title	Author/s	Year
Contribution to the knowledge of the geometry and boundaries of the Pliocene aquifers of Marbella and Estepona (province of Malaga) through the application of geophysical techniques	Damián Sánchez García, Jesús Galindo Zaldívar, Francisco José Martínez Moreno, Alberto Barrera García, Ana Ortuño Morales, Juan Antonaya Avi, Gustavo Calero Díaz, Lourdes González Castillo, Gemma Ercilla Zárraga, Ana Ruiz Constan and Marina Arnaldos	2017
New data on the age of transgressive Miocene formations in the Baetic Internal Zones: the San Pedro de Alcántara Formation (Province of Málaga).	Aguado, R., Feinberg, H., Durán Delgado, M., Martín Algarra, A., Esteras, M. and Didón, J.	1990
Hydrogeological cartography of the Municipality of Marbella. Unpublished report.	AQUAGEST ON S.A. INGEMISA	1995
Factors controlling groundwater salinization and hydrogeochemical processes in coastal aquifers from southern Spain. Science of the Total Environment, 580: 50–68.	Argamasilla, M., Barberá, J.A. and Andreo, B.	2017
Hydrogeological Atlas of the province of Malaga. Geological and Mining Institute of Spain and Diputación de Málaga. Madrid, 155-160.	Lupiani Moreno, E.	2007

As an example of the information reviewed, the following figures show the location of some of the lithological soundings, stations and geophysical profiles used to develop the geometry of the numerical model. These figures have been extracted from the study “Increase of the available resource through the improvement of the knowledge of the limits and geometry of the aquifers of Marbella (Geomar project), 2017".

This project has received funding from the European Union’s Horizon Europe research and innovation programme under grant agreement No GA 101082048
Funded by the European Union

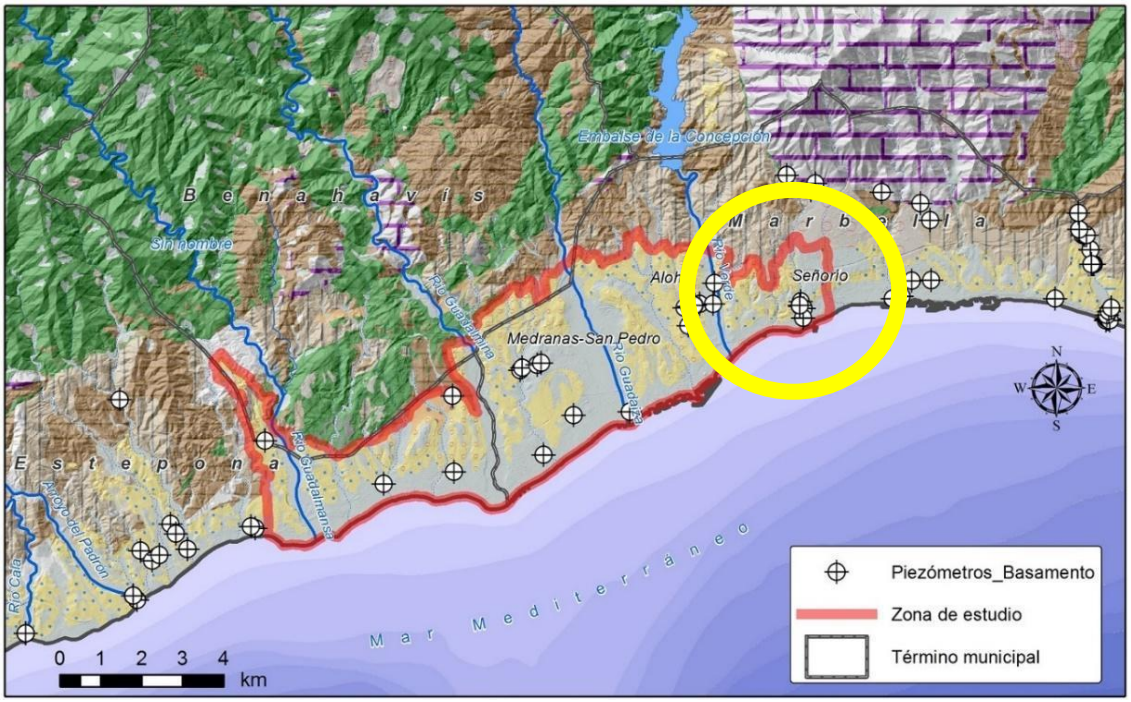

Figure 3.1-3 Location of the lithological column boreholes collected within the framework of the GEOMAR project.

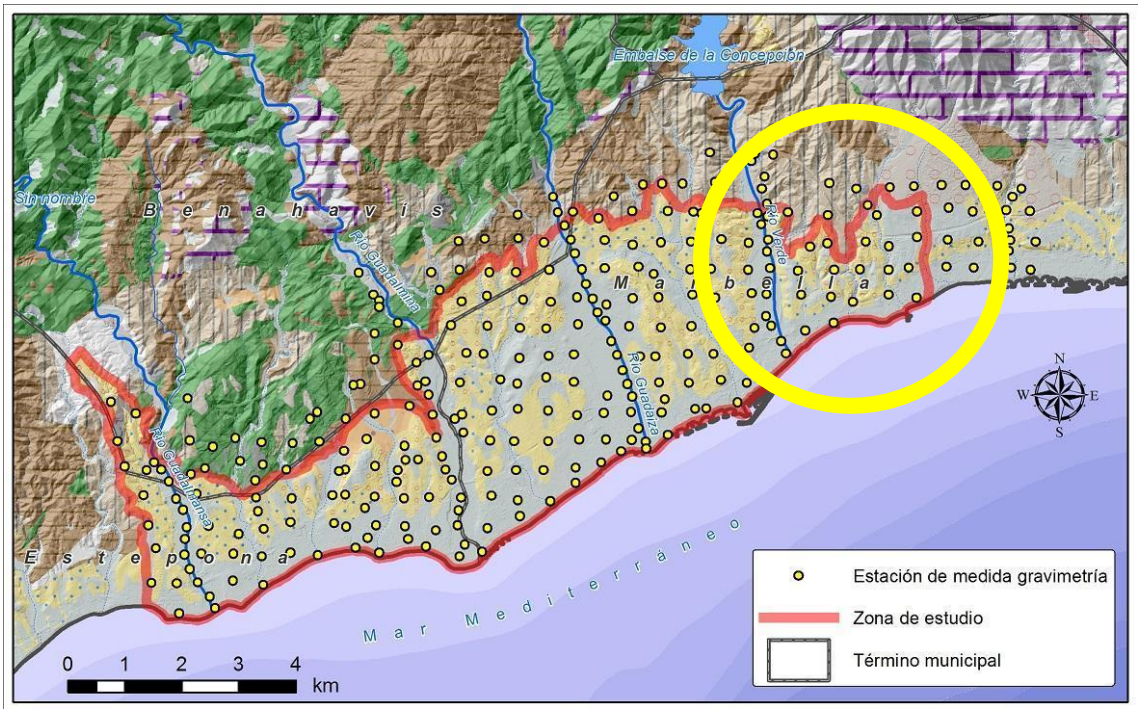

Figure 3.1-4 Geographical location of the gravimetry stations in the GEOMAR project.

This project has received funding from the European Union's Horizon Europe research and innovation programme under grant agreement No GA 101082048

Funded by the European Union

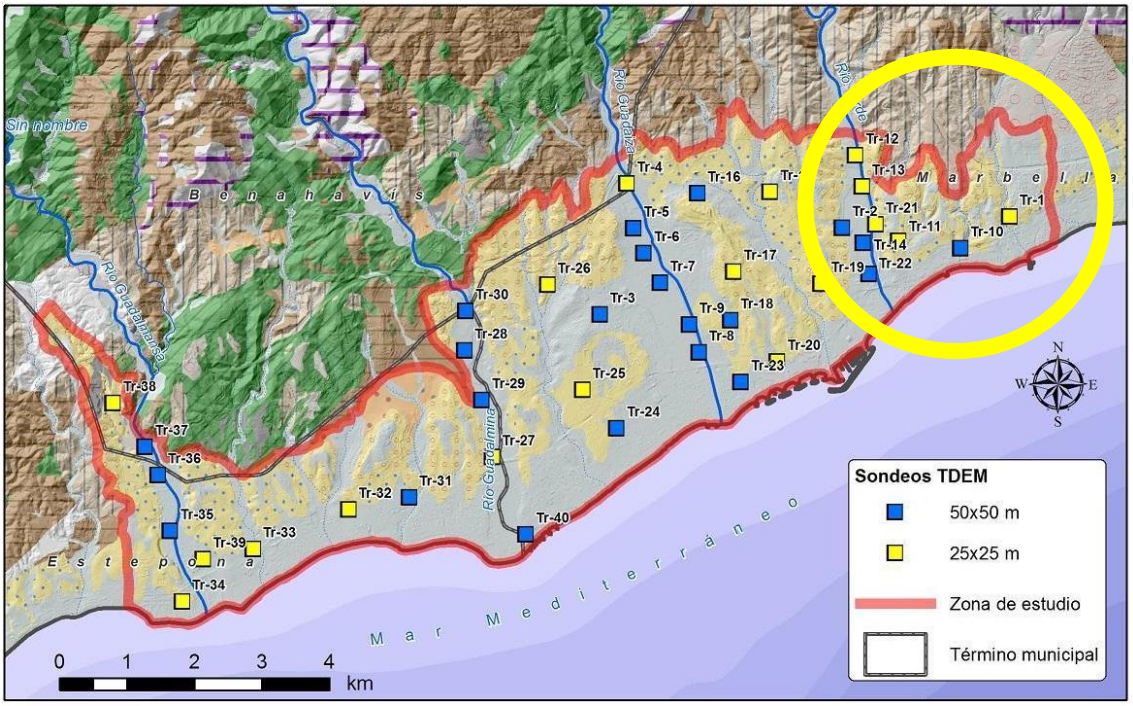

Figure 3.1-5 Location of the 40 TDEM wells carried out in the GEOMAR project.

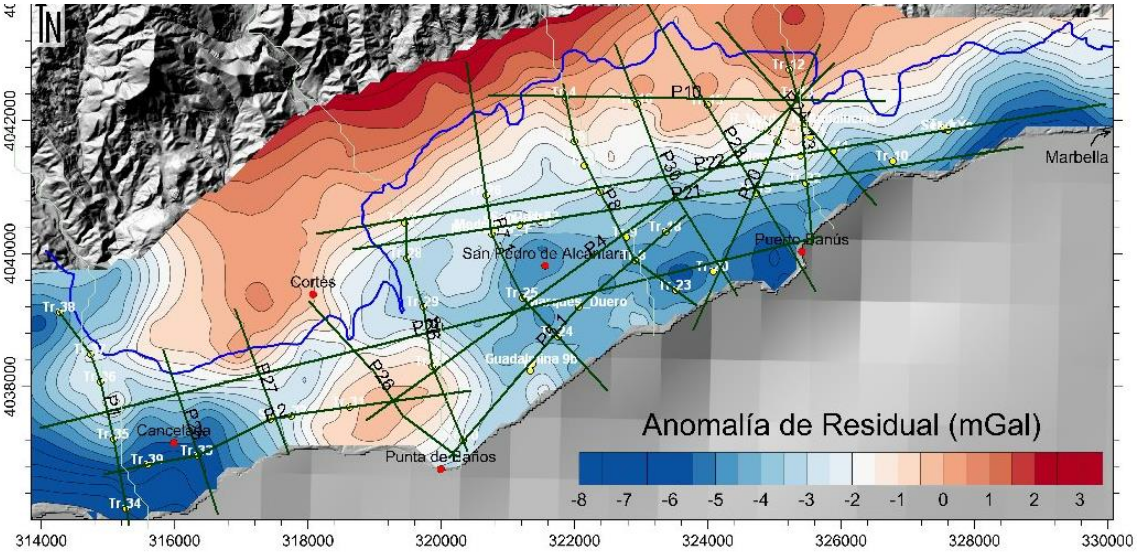

Figure 3.1-6 Drawing of the gravimetric profiles of the GEOMAR project.

As shown in the preceding figures, the gravimetric profiles used to define the geometry of the numerical model in the Señorío have been those that cross points TR10 and TR1, whose interpreted geology is presented below.

This project has received funding from the European Union's Horizon Europe research and innovation programme under grant agreement No GA 101082048

Funded by the European Union

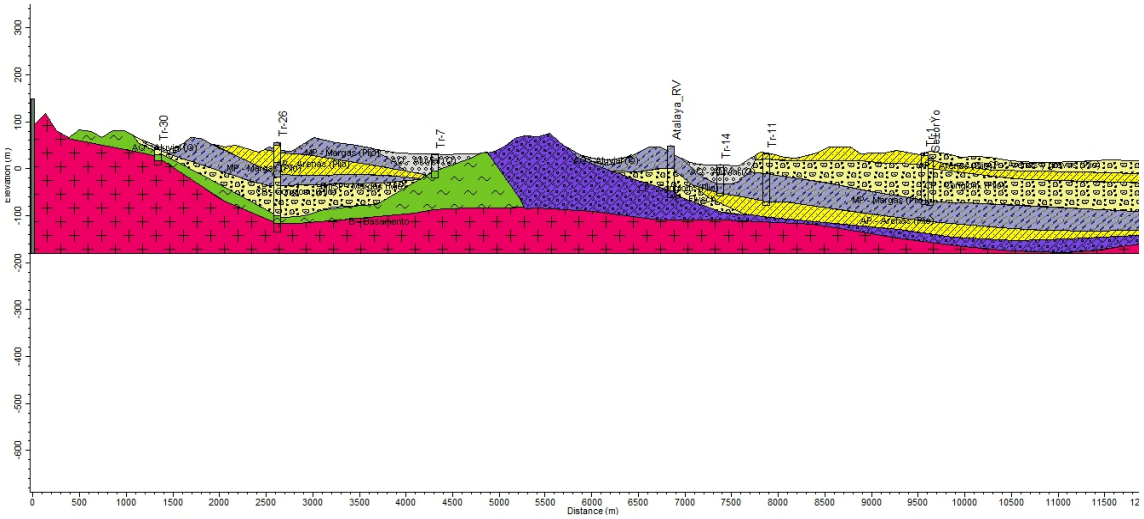

Figure 3.1-7 Geological profile that crosses TR1.

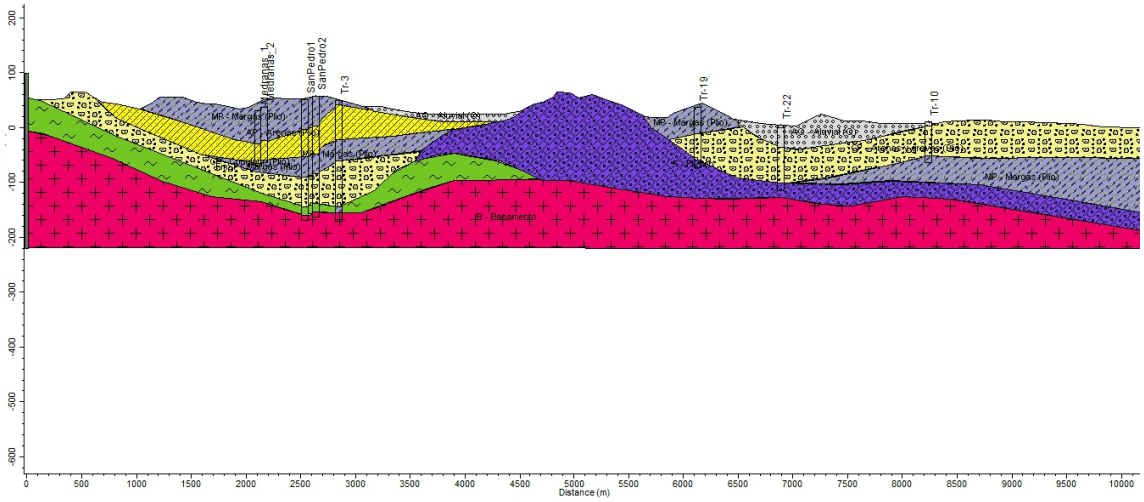

Figure 3.1-8 Geological profile that crosses TR10.

After analysing the set of information regarding the spatial distribution of geological materials, as well as their respective ages, characteristics and hydraulic properties, it was decided to group them into a total of 3 hydrogeological units, which are the geometric basis of the hydrogeological numerical model. In descending order, these hydrogeological units are:

1. Hydrogeological unit 1: Quaternary detrital aquifer/aquitard.
2. Hydrogeological unit 2: Pliocene detrital aquifer.
3. Hydrogeological unit 3: Paleozoic aquitard/aquiclude, corresponding to the basement.

For the construction of the geometry of each hydrogeological unit, the HydroGeo Analyst software has been used. This software allows the generation of three-dimensional surfaces from the geological information analysed. The following figures show the contact surfaces of each hydrogeological unit.

This project has received funding from the European Union's Horizon Europe research and innovation programme under grant agreement No GA 101082048
Funded by the European Union

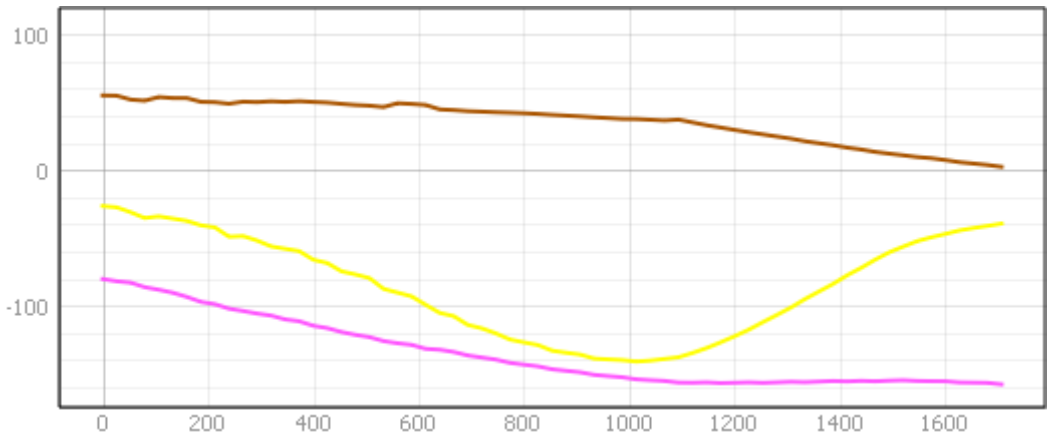

Figure 3.1-9 2D profile of aquifer layers from rasters.

The volumes of each Hydrogeological Unit are visualized in the following figures.

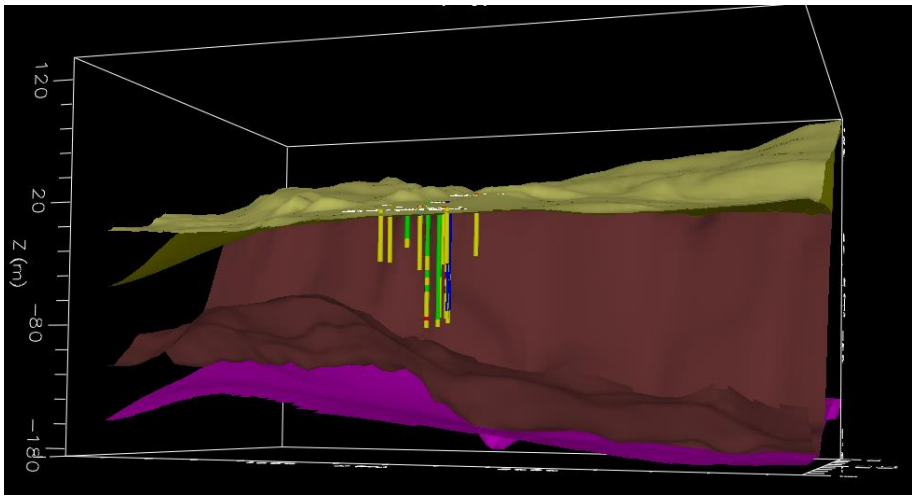

Figure 3.1-10 3D view of aquifer layers from the South in the numerical model.

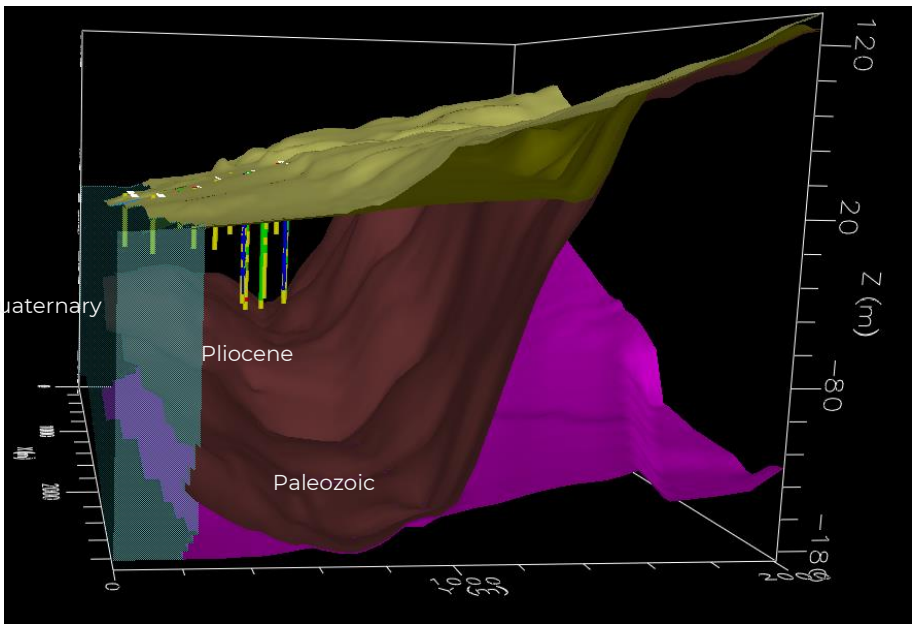

Figure 3.1-11 3D view of aquifer layers from the East in the numerical model.

This project has received funding from the European Union's Horizon Europe research and innovation programme under grant agreement No GA 101082048

Funded by the European Union

After analysing the lithology and geometry of the area, the extension of the numerical model is established, which has an approximate area of 6 km^2.

Figure 3.1-12 In red, an extension of the numerical model with the base orthophoto.

For ease of operation and understanding of the numerical model, it is rotated so that the main orientation is North-South.

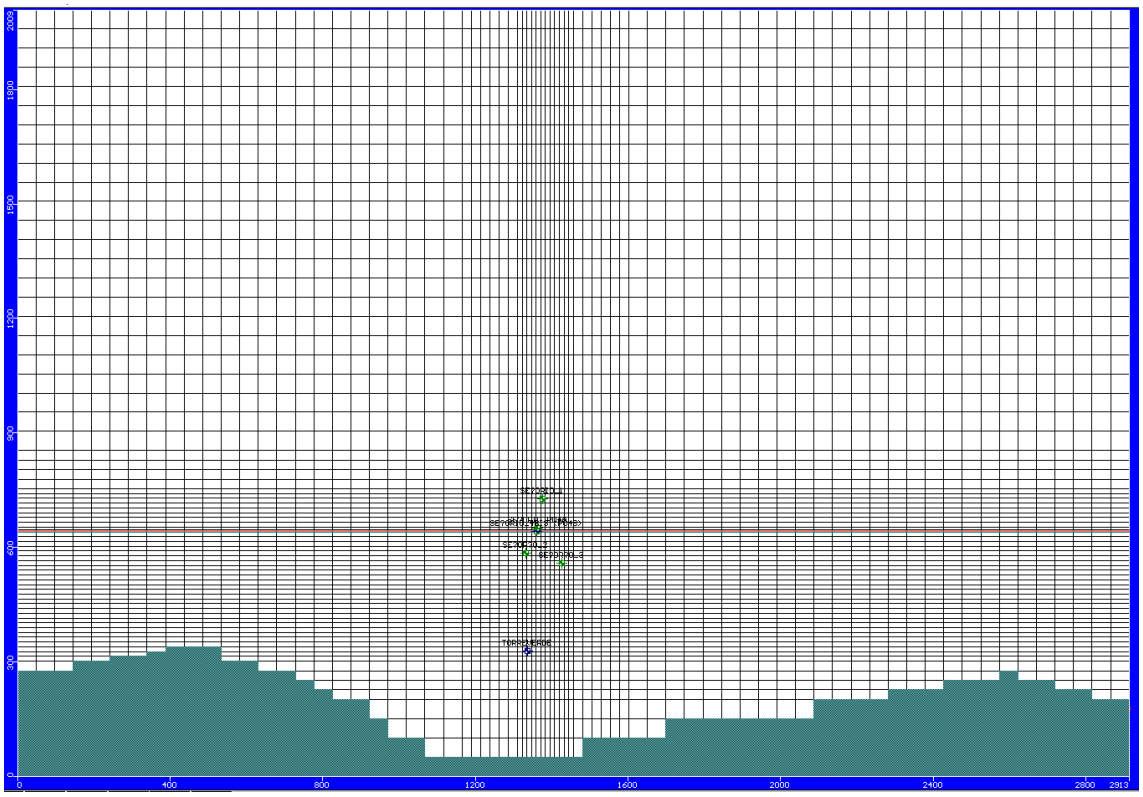

Figure 3.1-13 Mastery of the model in the plant.

This project has received funding from the European Union's Horizon Europe research and innovation programme under grant agreement No GA 101082048

Funded by the European Union

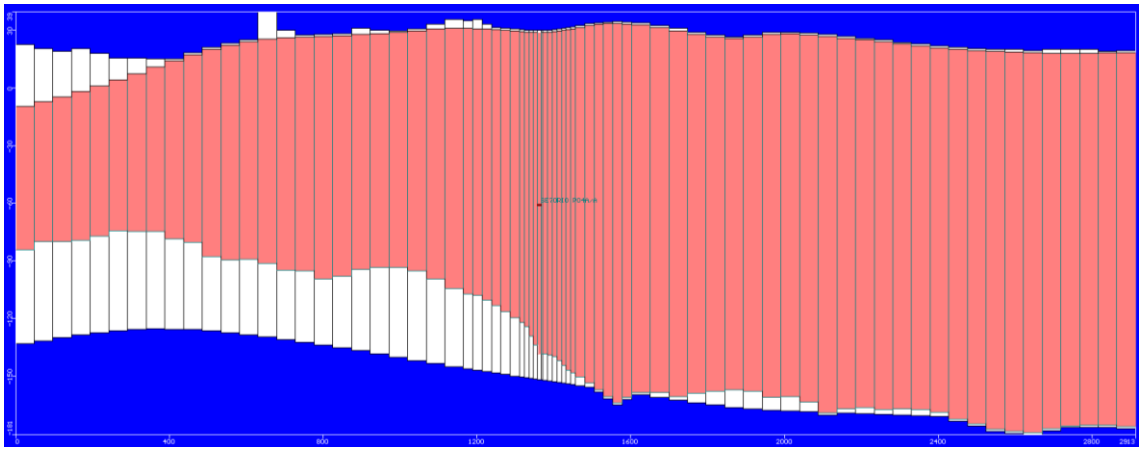

Figure 3.1-14 EW profile in manor 4.

3.1.2 SPATIAL DISCRETIZATION

The horizontal discretization of the numerical model domain has been carried out with 50x50 m cells, increasing the refining in the areas where the Señorío and Torreverde wells are located until reaching a cell size of 10x10 m.

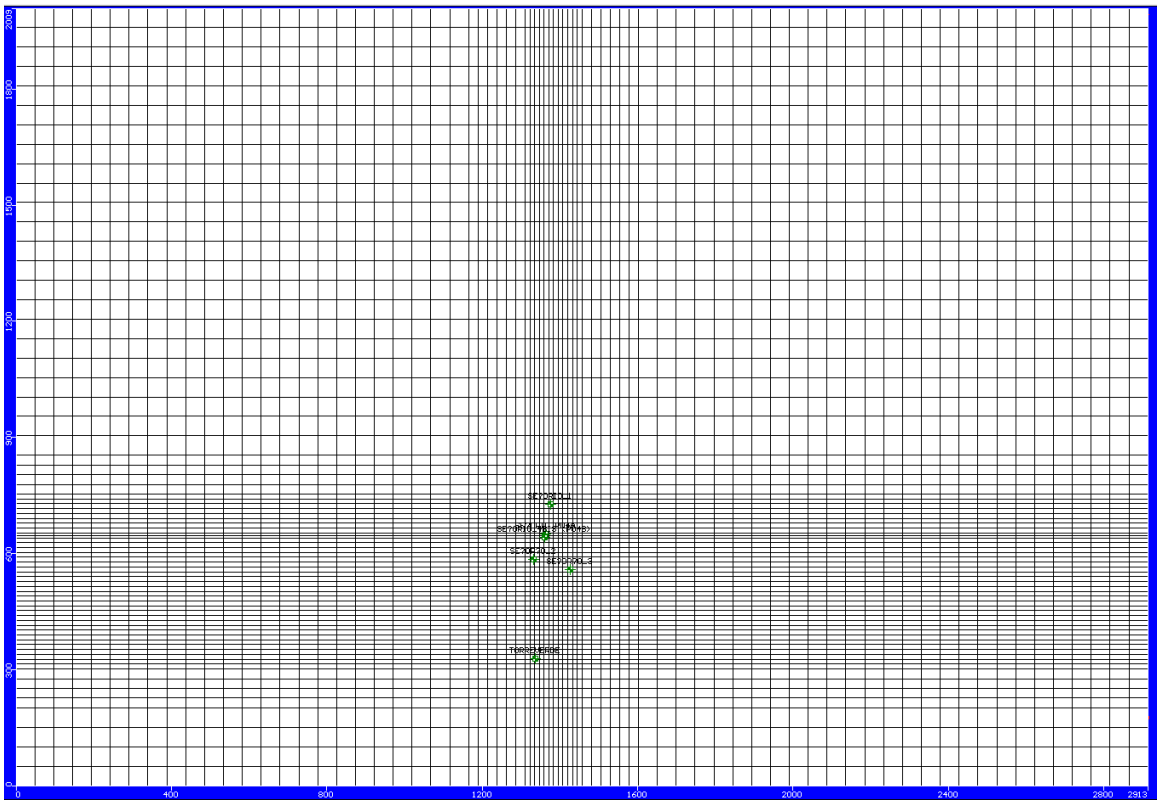

Figure 3.1-15 Horizontal discretization of the domain.

The vertical spatial discretization has been carried out from the HydroGeo Analyst software in which a total of 3 hydrogeological units were defined from which the 3 layers in which the numerical model is defined were defined.

This project has received funding from the European Union's Horizon Europe research and innovation programme under grant agreement No GA 101082048

Funded by the European Union

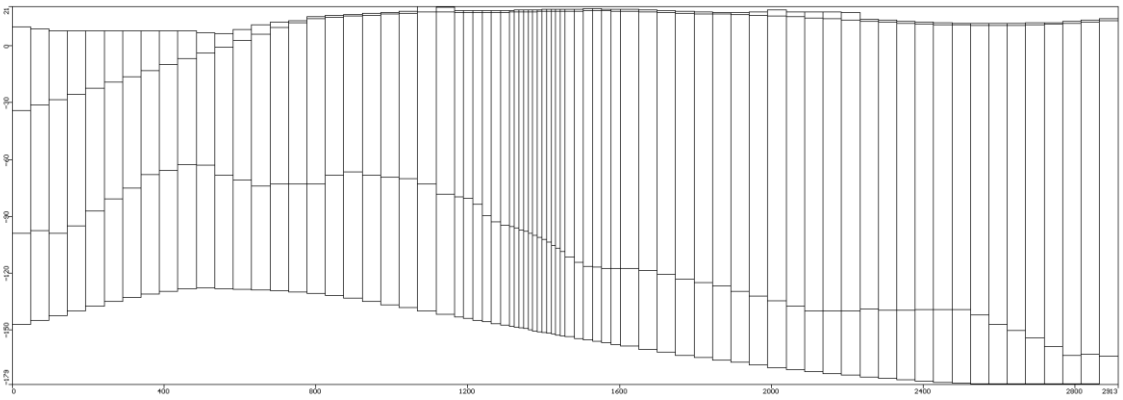

Figure 3.1-16 Vertical discretization of the domain.

The southern edge of the aquifer from the shoreline has been considered inactive cells. The following figure shows the active cells in white and the inactive cells in green.

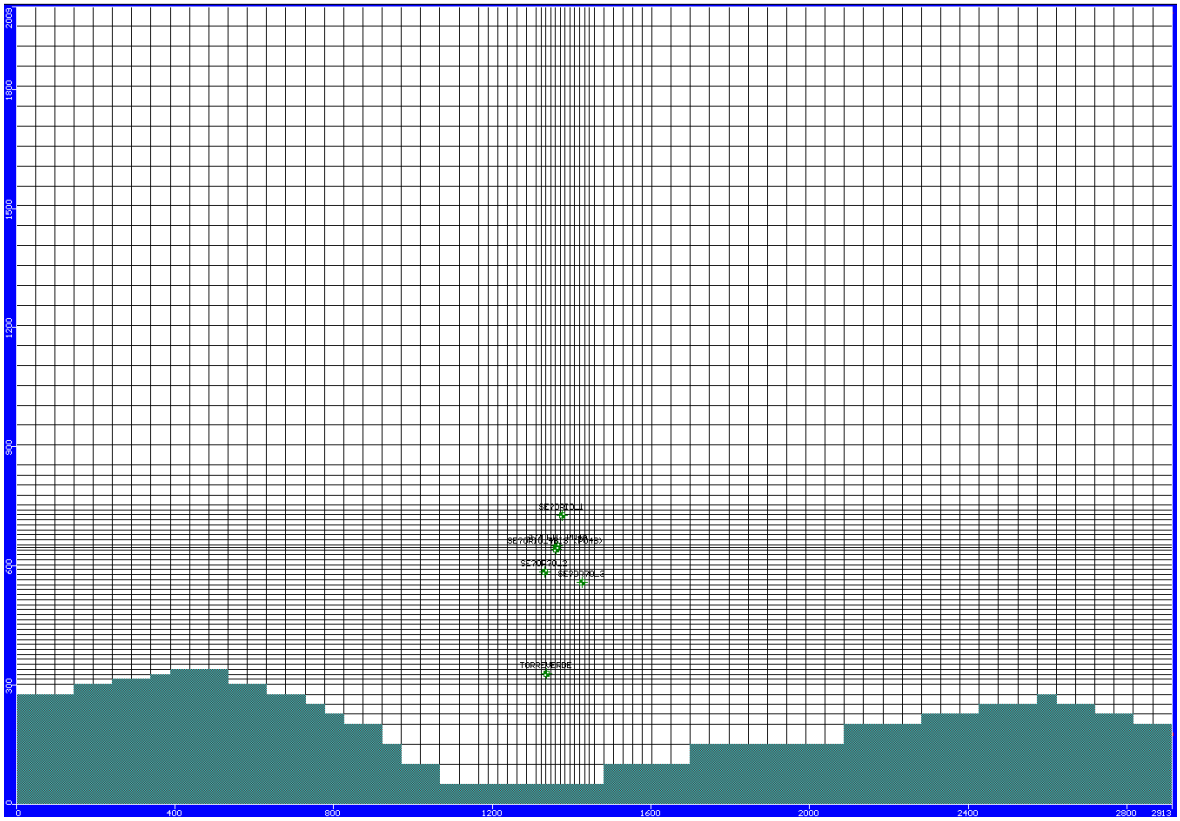

Figure 3.1-17 Active (blank) and inactive (green) cells.

3.1.3 BOUNDARY CONDITIONS

3.1.3.1 RECHARGE

Precipitation infiltration has been incorporated with the Recharge module, corresponding to one recharge per unit area for each time step. This recharge has been assigned to the most superficial layer (Hydrogeological Unit 1), throughout its area.

This project has received funding from the European Union's Horizon Europe research and innovation programme under grant agreement No GA 101082048

Funded by the European Union

The precipitation inputs have been assigned, in the model, to monthly steps for the period between 2000 and 2022, based on the data from the Red Hidrosur network recorded in the rain gauge located in the La Concepción reservoir.

Table 3.1-3 Rainfall station used.

Station	Type of station	X UTM	Y UTM	Z (m a.s.l.)	Temperature Record (years)	Rainfall Record (years)
La Concepción Reservoir (Málaga province)	Reservoir	324643	4045234	110	2000-2022	2000-2022

The following table shows the data at the annual level. The average annual rainfall is 638.8 mm/y. The assigned infiltration rate (35 %) corresponds to a theoretical value according to the materials in the area, which means an average recharge per rainwater infiltration of 224.9 mm/y, or 1.6 hm^3/y.

Table 3.1-4 Annual recharge.

YEAR	PRECIPITATION (mm)	INFILTRATION (hm^3/y)	YEAR	PRECIPITATION (mm)	INFILTRATION (hm^3/y)
2000	533	1.32	2012	518.00	1.29
2001	829.05	2.06	2013	856.00	2.13
2002	520.95	1.29	2014	352.40	0.88
2003	642.70	1.60	2015	554.00	1.38
2004	881.60	2.19	2016	418.30	1.04
2005	406.55	1.01	2017	721.23	1.79
2006	604.00	1.50	2018	684.80	1.70
2007	623.50	1.55	2019	455.80	1.13
2008	723.00	1.80	2020	570.40	1.42
2009	620.00	1.54	2021	405.10	1.01
2010	1396.00	3.47	2022	401.60	1.00
2011	976.00	2.43	**Average**	**638.87**	**1.59**

3.1.3.2 CONSTANT LEVEL AND RIVERS

To reproduce the transfer of flow from the aquifer to the sea, a constant level has been assigned along the coastline at 0 m.a.s.l.

This project has received funding from the European Union's Horizon Europe research and innovation programme under grant agreement No GA 101082048

Funded by the European Union

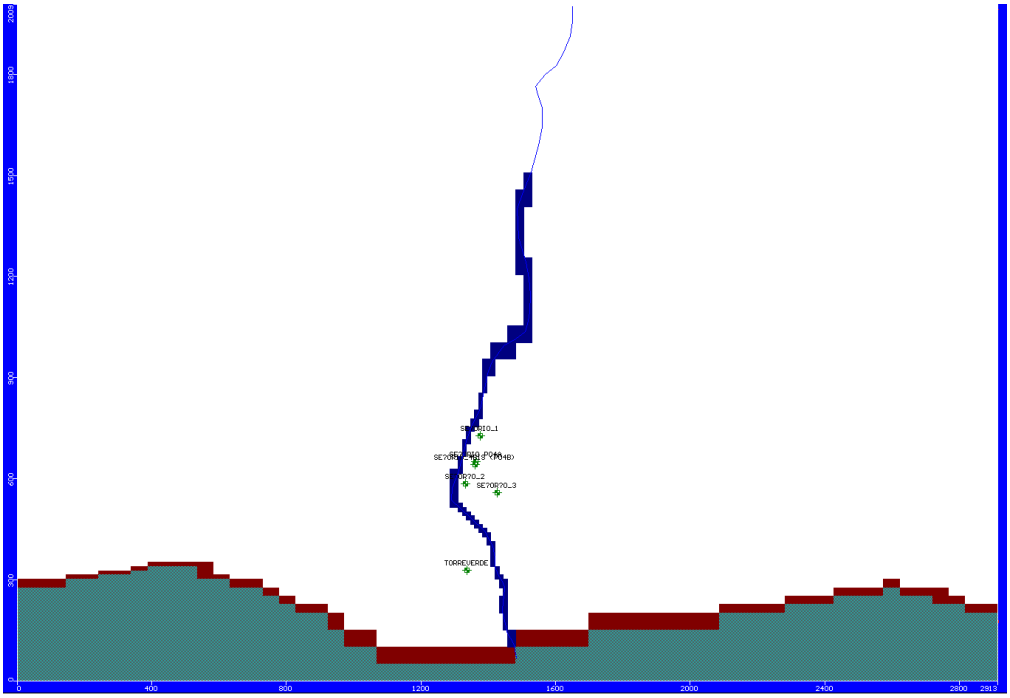

Figure 3.1-18 In brown, constant level cells, in blue river cells.

Through the River function, the Nagüeles stream has been assigned, which crosses the aquifer from north to south, very close to the Señorío wells.

3.1.3.3 PUMPING/INJECTION

10 wells have been incorporated with the Pumping Well function, of which 3 function as extraction and injection (Sñ1, Sñ2 and Sñ-3), one, Sñ4, only for injection, and 6 of them (other users) as exclusively pumping wells. The following table shows their main characteristics as well as the ownership and source of the information pertaining to them.

Table 3.1-5 Pumping/Injection Wells.

Well	Use	X UTM	Y UTM	Z (m a.s.l.)	Prof. (m)	Owner	Concessionaire company
Sñ1	Extraction /injection	327465	4041812	27	103	Marbella City Council	Hidralia, S.A.
Sñ 2	Extraction /injection	327469	4041663	26	114		
Sñ 3	Extraction /injection	327567	4041669	21	110		
Sñ 4	Injection	327478	4041735	26	92		
Well-1	-	-	-	-	-	Private	-
Well-2	-	-	-	-	-		
Well-3	-	-	-	-	-		
Well-4	-	-	-	-	-		
Well-5	-	-	-	-	-		
Well-6	-	-	-	-	-		

This project has received funding from the European Union's Horizon Europe research and innovation programme under grant agreement No GA 101082048

Funded by the European Union

The Señorío wells (Sñ1 to Sñ-4), correspond to municipal management boreholes, perfectly located and controlled in terms of flow and level. The other 6 are private wells, whose control since 2000 has been difficult to maintain, so their activity is not known with certainty.

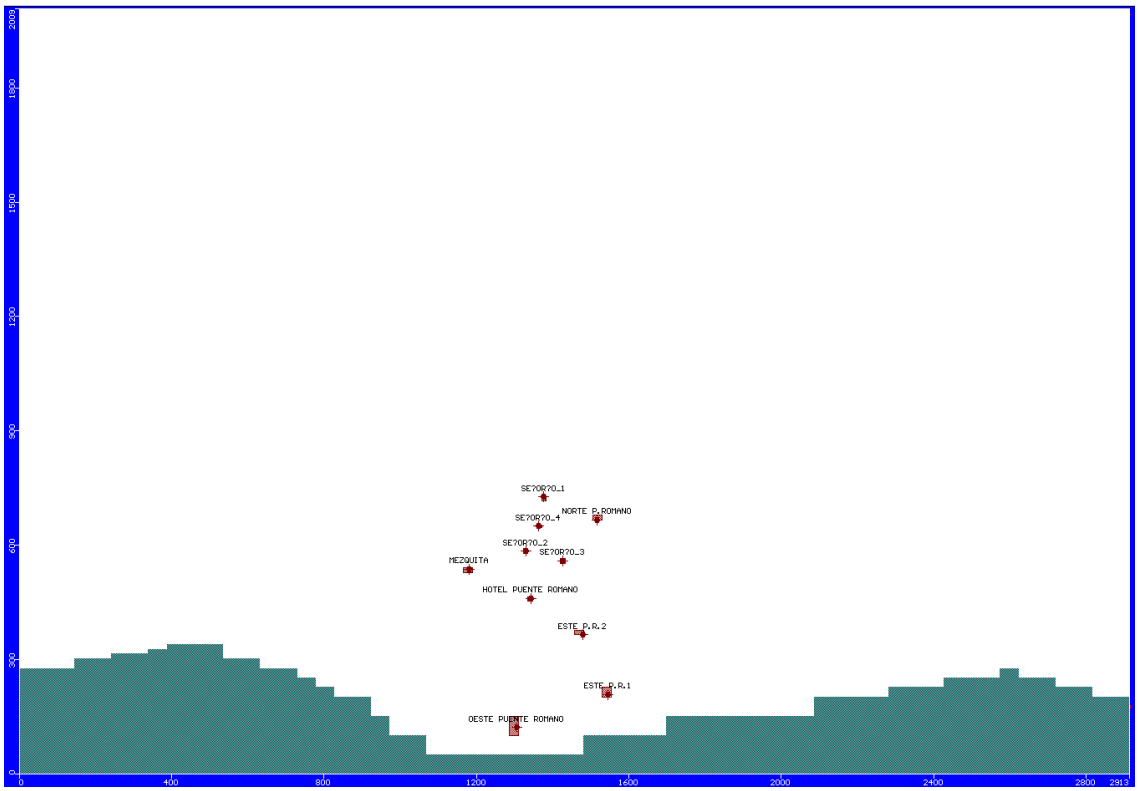

Figure 3.1-19 Location of the extraction and injection boreholes in the model.

The following table shows the annual values of the set of wells of Señorío and other users.

Table 3.1-6 Extraction values and injection of the wells of the model (hm^3/y).

YEAR	EXTRACTION SEÑORÍO	INJECTION SEÑORÍO	EXTRACTION OTHER USERS	TOTAL (HM^3/Y)
2000	-0.67	+0.17	-0.65	-1.15
2001	-0.49	+0.16	-0.65	-0.98
2002	-0.41	+0.12	-0.65	-0.93
2003	-0.59	+0.24	-0.65	-1.00
2004	-0.59	+0.25	-0.65	-0.99
2005	-0.65	+0.19	-0.65	-1.11
2006	-0.67	+0.20	-0.65	-1.12
2007	-0.58	+0.14	-0.65	-1.09
2008	-0.63	+0.24	-0.65	-1.04
2009	-0.80	+0.28	-0.65	-1.17
2010	-0.97	+0.20	-0.65	-1.42
2011	-1.10	+0.00	-0.65	-1.75
2012	-0.53	+0.00	-0.65	-1.18
2013	-0.43	+0.13	-0.65	-0.95

This project has received funding from the European Union's Horizon Europe research and innovation programme under grant agreement No GA 101082048
Funded by the European Union

YEAR	EXTRACTION SEÑORÍO	INJECTION SEÑORÍO	EXTRACTION OTHER USERS	TOTAL (HM^3/Y)
2014	-0.55	+0.01	-0.65	-1.19
2015	-0.31	+0.03	-0.65	-0.93
2016	-0.32	+0.07	-0.65	-0.90
2017	-0.58	+0.11	-0.65	-1.12
2018	-0.38	+0.03	-0.65	-1.00
2019	-0.60	+0.00	-0.65	-1.25
2020	-0.24	+0.01	-0.65	-0.88
2021	-0.40	+0.00	-0.65	-1.05
2022	-0.43	+0.05	-0.65	-1.03
AVERAGE	**-0.56**	**+0.12**	**-0.65**	**-1.10**

3.1.3.4 PIEZOMETERS

In order to allow the calibration and adjustment of the numerical model, a total of 6 piezometric points with water level measurements have been introduced through the Head Observation function.

The level recordings of four of the pumping wells (Sñ-1, Sñ-2, Sñ-3 and Sñ-4) have been used, as well as two additional piezometers (Sñ-4 bis and Torreverde). The following table summarises the main characteristics of the piezometric points, the information for which has been provided by the company Hidralia S.A.

Table 3.1-7 Piezometers.

Piezo.	Use	X UTM	Y UTM	Z (m a.s.l.)	Prof. (m)	Data period	Owner	Concessionaire comp.
Torreverde	Piezometer	327558	4041421	18	59	2000-2022	Marbella City Council	Hidralia, S.A.
Sñ1	Extraction /injection	327465	4041812	27	103			
Sñ 2	Extraction /injection	327469	4041663	26	114			
Sñ 3	Extraction /injection	327567	4041669	21	110			
Sñ 4	Injection	327478	4041735	26	92			

This project has received funding from the European Union's Horizon Europe research and innovation programme under grant agreement No GA 101082048

Funded by the European Union

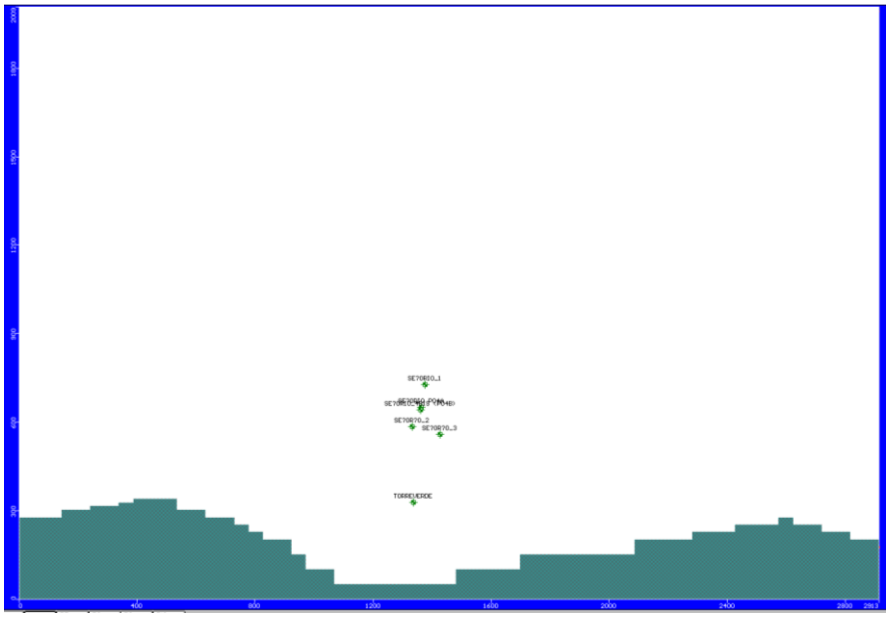

Figure 3.1-20 Location of the control piezometers.

3.1.3.5 CONCENTRATION

In order to have a first approximation of the propagation of seawater towards the aquifer, a type of boundary has been defined along the coastline that simulates an inflow of water at an altitude of 0 m a.s.l. with a chloride concentration of 19,000 mg/l, typical of seawater.

In the second stage, the total entry of seawater (40,000 mg/l) through the coastline has been simulated.

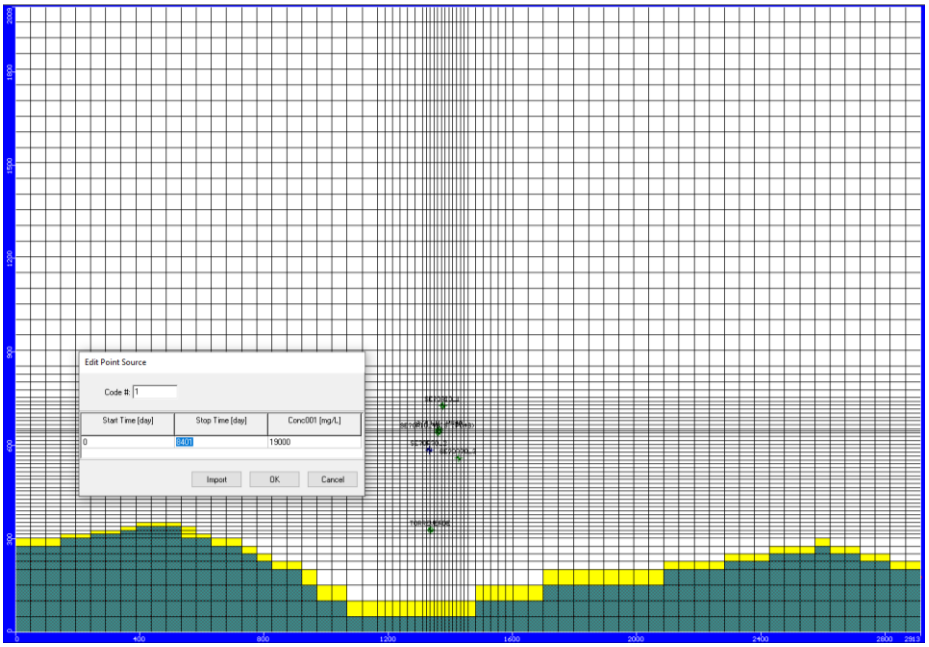

Figure 3.1-21 In yellow, coastline with a concentration of 19,000 mg/l of chlorides.

This project has received funding from the European Union's Horizon Europe research and innovation programme under grant agreement No GA 101082048

Funded by the European Union

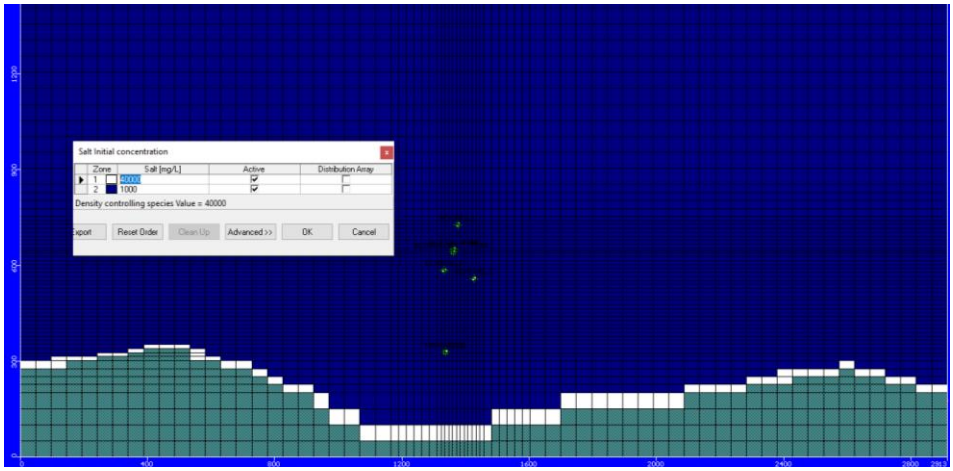

Figure 3.1-22 Concentrations of fresh and salt water assigned to the model.

3.1.4 TEMPORARY DISCRETIZATION

The aim of steady-state calibration is to obtain an initial starting piezometry from which the transient model is launched, which does not mean that this initial piezometry cannot be obtained directly with the transient simulation.

Thus, the lack of temporal coincidence in the exploitation/injection of the boreholes has led to the calibration of the model being carried out directly in a transitional regime based on an initial piezometry that allows a good fit (simulated/observed piezometry) at the time when there are control data.

On the other hand, it should be taken into account that in the simulated series (2000-2022) there is only piezometric control data from 2011 to 2017, in the case of Señorío 1, 2 and 3 wells, and from 2020 to 2022, in Señorío 4 wells.

Therefore, in this case, it is considered that, due to the scarcity of data in the modelled series, the calibration of the model should be based exclusively on the adjustment of the measured piezometric data with the simulated data, without forgetting the coherence of the hydraulic parameters assigned to the terrain.

3.1.5 LINKS BETWEEN DATA SETS AND MOD-REACH

The input data used for the development of the MOD-REACH and the results provided are summarised in the following table.

Table 3.1-8 Links between datasets and MOD-REACH.

TOOL COMPONENT	INPUT DATA	MODEL/METHODOLOGY	OUTPUT
MOD-REACH	Aquifer characteristics	Geometry boundaries	Initial data to run the model
MOD-REACH	Rainfall data	Data obtained by Red Hidrosur Network	Initial data to run the model
MOD-REACH	Pumping wells	Data obtained from Hidralia S.A.	Initial data to run the model

This project has received funding from the European Union's Horizon Europe research and innovation programme under grant agreement No GA 101082048
Funded by the European Union

TOOL COMPONENT	INPUT DATA	MODEL/METHODOLOGY	OUTPUT
MOD-REACH	Piezometer data	Data obtained from Hidralia S.A.	Initial data to run the model
MOD-REACH	Salinity concentration	Salinity prediction	Initial data to run the model

3.2 DATA-REACH

The methodology utilised in the two components of this approach is outlined below. It's important to emphasise that while this work details the results derived from applying this methodology to the Spanish demonstration site, it can be perfectly replicated at any other site, provided certain prerequisites such as the quality and availability of necessary data are met.

3.2.1 RETROSPECTIVE CLIMATE ANALYSIS

To achieve the study objectives, several activities were conducted.

3.2.1.1 DATA COLLECTION

Firstly, a bibliographic review was carried out, encompassing the search for scientific works related to geology, hydrogeology, and the functioning of the water supply system in the study area. Additionally, meteorological, hydrogeological, chemical status and cartographic data were collected from various sources, such as governmental databases and water management organisations.

Meteorological data (rainfall and temperature) from specific stations in the study area were obtained through unrestricted access to databases from SAIH, IFAPA, and RAIF as well as from the AEMET secondary network.

The hydrogeological data used in this study comprised piezometric levels from 28 points (Appendix A). Fifteen of these points were sourced from the web portal provided by the Ministry for Ecological Transition in the piezometric monitoring network, while the remaining 13 were provided by HIDRALIA.

Data regarding the chemical status of the groundwater body under study were obtained from the Andalusian Regional Government portal, using the query form for analytical results from the Red DMA.

A significant portion of the shapefile archives generated for the development and representation of maps in this work were created from files downloaded from DERA, established by the Andalusian Regional Government. The National Geographic Institute (IGN) Download Centre was also utilised.

3.2.1.2 DATA ANALYSIS AND PROCESSING

QGIS software was used for map creation, providing numerous tools for geographic information processing, editing, publishing, and design. Google Earth Pro was used to generate the piezometric network layer, facilitating the location of each piezometer and retrieval of their corresponding coordinates.

The analysis of climatic data began with data completion and subsequent processing using the Trasero 2.0 program (Padilla and Delgado, 2013). This program was also employed to calculate potential evapotranspiration using the Hargreaves method

This project has received funding from the European Union's Horizon Europe research and innovation programme under grant agreement No GA 101082048
Funded by the European Union

(Hargreaves and Samani, 1985), based on completed and corrected precipitation and temperature series. Six representative stations in the study area were selected.

Two climatic indices, SPI (Mckee et al., 1993) and SPEI (Vicente-Serrano et al., 2010), were used for this study. The former considers only precipitation, while the latter also incorporates temperature, specifically potential evapotranspiration.

Calculation of SPI

The SPI calculation is based on long-term precipitation records for a specific period, which are adjusted to a probability distribution and transformed into a normal distribution so that the mean SPI for a given location and period is zero. Positive SPI values indicate above-median precipitation, while negative values indicate below-median precipitation. Normalisation allows for the representation of both wet and dry climates.

SPI can be calculated for different time scales, from 1 month to 72 months. In this study, the 12-month SPI (SPI12) was used. Daily rainfall data from stations were converted to monthly increments to calculate the monthly SPI.

Calculation of SPEI

SPEI is calculated similarly to SPI but incorporates a climatic water balance, including temperature. It is computed using a monthly or weekly series of the difference between precipitation and potential evapotranspiration (PET) as input. The calculation involves a water balance at different time scales. One challenge in PET calculation is the requirement for various parameters such as air humidity and radiation. However, the authors proposed using the Thornthwaite method for SPEI calculation, which only requires monthly mean temperature and latitude. The SPEI index was calculated using the SPEI Calculator software provided by the authors, developed in 2009 and published in 2010 along with the article on the index (Vicente-Serrano et al., 2010).

Calculation of Granger causality test

Additionally, the Granger causality test has been applied to comprehend the predictive relationships between certain variables. The Granger causality test is a statistical hypothesis test for determining whether one-time series is useful in forecasting another. Named after the economist Sir Clive Granger, this test is based on the idea that if a variable X "Granger-causes" (or is a cause of) a variable Y, then past values of X should contain information that helps predict Y above and beyond the information contained in past values of Y alone. It's important to note that Granger causality is not to be confused with traditional causality. Instead, it's a useful statistical tool for understanding predictive relationships between variables in time series data.

In order to apply this test, the first condition is that the input series must be stationary. A stationary time series has a constant mean, variance, and autocorrelation over time. However, most of the time series data we encounter in real-world applications, such as stock prices or weather patterns, are non-stationary, exhibiting trends or seasonality. To test whether they are stationary or not, we apply two tests, the Augmented Dickey-Fuller Test along the Kwiatkowski–Phillips–Schmidt–Shin Test. If both agree that the tested series is non-stationary, then we must process it to obtain a stationary series. Differencing is applied to make a time series stationary. Differencing helps to remove the systematic patterns over time, making the series stationary and thus more suitable for analysis and forecasting.

This project has received funding from the European Union's Horizon Europe research and innovation programme under grant agreement No GA 101082048

Funded by the European Union

Once the input series are prepared, we check the Granger Causality of all possible combinations of the time series. The result is a table where the rows are the response variable, and the columns are predictors. The values in the table are the P-Values. P-Values less than the significance level (0.05), imply that the Null Hypothesis that the coefficients of the corresponding past values are zero, that is, X does not cause Y, can be rejected.

3.2.2 PREDICTIVE MODELS

To accomplish the stated objective of generating monthly probabilistic predictions of piezometric levels, electrical conductivity and reservoir volume (target variables) using machine learning techniques, the typical stages of a supervised learning problem have been traversed: data collection and pre-processing, learning, evaluation, and prediction using the selected model.

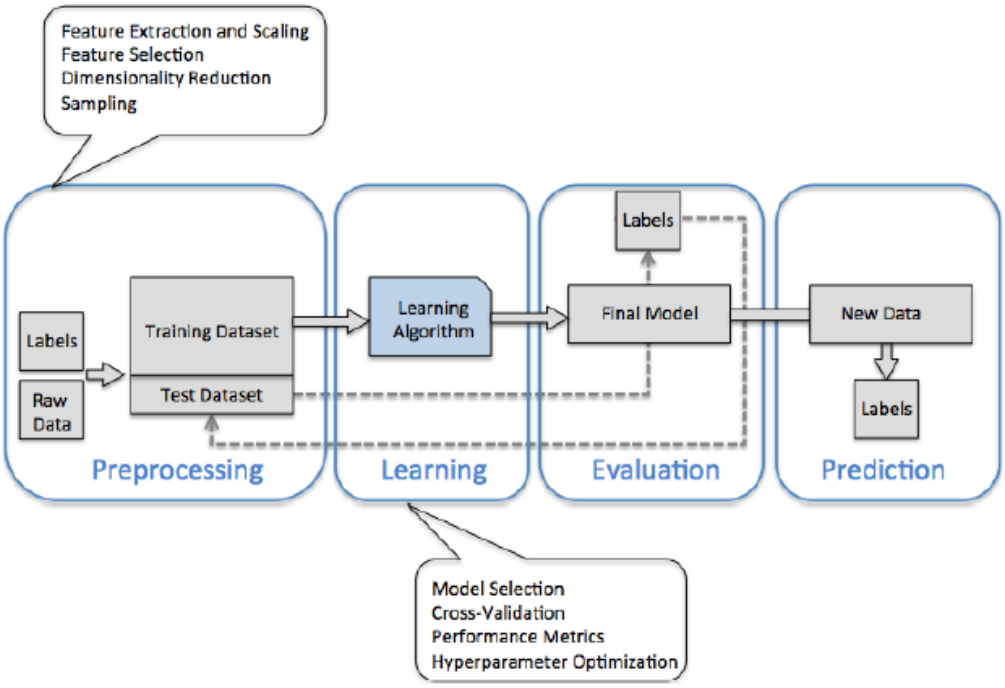

Figure 3.2-1 General methodology for developing Machine Learning models. (Lundberg, Scott M., and Su-In Lee. "A unified approach to interpreting model predictions." Advances in neural information processing systems 30 (2017)).

During the data collection stage, a search for historical data providing relevant information as input to predictive models has been conducted. For each point of interest, historical data of the target variable, as well as other identified explanatory variables (such as pumping, rainfall, etc.), have been compiled.

Specifically, over 20 years of data with monthly frequency have been extracted. Different data sources are distinguished in Figure 3.2-2.

This project has received funding from the European Union's Horizon Europe research and innovation programme under grant agreement No GA 101082048
Funded by the European Union

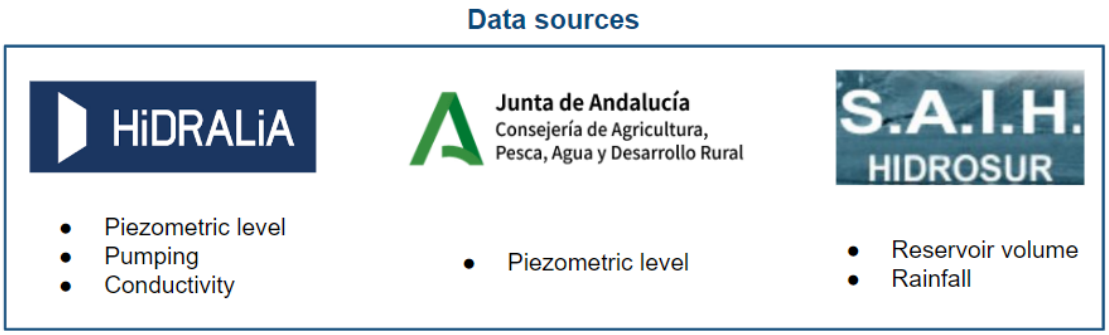

Figure 3.2-2 Different data sources and the data derived from each source.

These raw data may need to be processed by removing anomalous values and completing missing values. Subsequently, to obtain the monthly series, it may be necessary to process them for monthly aggregation based on the series type, using either cumulative (rainfall and pumping) or mean (piezometric level, volume and electrical conductivity) methods. Following this, the datasets are obtained for further analysis and their composition, start, and end dates can be seen in Table 3.2-1.

Table 3.2-1 Available data series.

Data Set	Target Variables	Explanatory Variables	Source	Start	End
Aloha	Piezometric level	Pumping Rainfall	Hidralia SAIH	April 2000	May 2023
Cable Ski	Piezometric level	Pumping Rainfall	Hidralia SAIH	April 2000	February 2024
Guadaiza	Piezometric level	Rainfall	Junta de Andalucía SAIH	April 2000	February 2024
Guadalmansa	Piezometric level	Rainfall	Junta de Andalucía SAIH	April 2000	February 2024
Guadalmina	Piezometric level	Pumping Rainfall	Hidralia SAIH	January 2002	February 2024
Rio Verde MB	Piezometric level	Pumping Rainfall	Hidralia SAIH	April 2000	February 2024
Rio Verde NA	Piezometric level	Pumping Rainfall	Hidralia SAIH	April 2000	February 2024
San Pedro	Piezometric level	Pumping Rainfall	Hidralia SAIH	April 2000	November 2023
Señorío (Pz level)	Piezometric level	Pumping Rainfall	Hidralia SAIH	April 2000	February 2024
Señorío (Conductivity)	Electrical conductivity	Piezometric level Pumping Rainfall	Hidralia SAIH	April 2000	February 2024

This project has received funding from the European Union's Horizon Europe research and innovation programme under grant agreement No GA 101082048
Funded by the European Union

La Concepción	Reservoir volume	Rainfall	SAIH	April 2000	March 2024
Charco Redondo	Reservoir volume	Rainfall	SAIH	November 2000	March 2024
Guadarranque	Reservoir volume	Rainfall	SAIH	January 1997	March 2024

Once the information has been gathered, an analytical exploration of the obtained data series is carried out. This involves characterising the possible relationships between them and selecting those series with the greatest explanatory capacity for the trends and behavioural patterns of the target series.

The problem of forecasting values of the different variables under study is converted into a supervised learning problem, utilising autoregressive model techniques (such as sliding windows), to enable the application of machine learning algorithms.

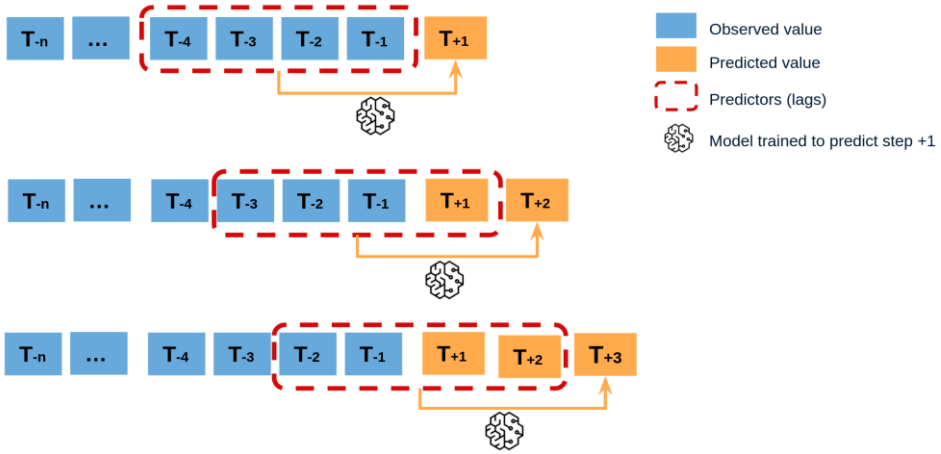

Figure 3.2-3 Diagram of the recursive multi-step forecasting. Source: https://skforecast.org/0.11.0/user_guides/autoregresive-forecaster.

The process of generating, calibrating, and validating the models begins with searching for and defining the model. A series of semi-automated experiments are then conducted to generate and compare various models based on specific metrics (MAE, RMSE, MDA) until those that provide the best validated predictive capability against historical data are identified. To select the model that best fits the objective, cross-validation is employed, a statistical method specifically designed for this purpose. This method involves randomly dividing the dataset into several folds, then training the model on all folds except one and testing the model on the remaining fold. These steps are repeated until the model has been tested on each fold, and its final metrics are the average of the scores obtained in each fold. This helps avoid overfitting and assesses the model's performance more robustly than simple training validation. In the case of time series, we cannot randomly choose samples and assign them to the validation or training set because we want to avoid using future data when training our model to preserve the temporal dependence between observations. Therefore, we start with a small subset of data for training, predict subsequent data, and then assess the accuracy of the predicted data. The same forecasted data are then included as part of the next training dataset, and subsequent data are forecasted.

This project has received funding from the European Union's Horizon Europe research and innovation programme under grant agreement No GA 101082048
Funded by the European Union

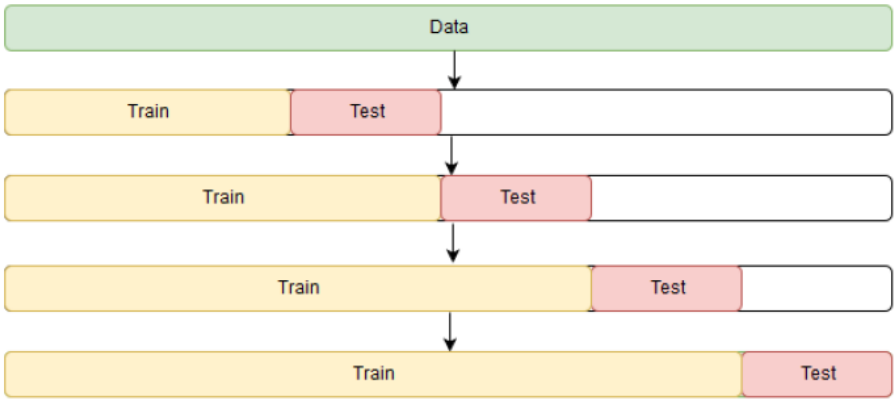

Figure 3.2-4 Time series cross-validation. Source: https://medium.com/@soumyachess1496/cross-validation-in-time-series-566ae4981ce4

The list of algorithms being evaluated includes, among others, the Huber Regressor, Support Vector Regression, Random Forest, XGBoost, CatBoost, Linear Regression, Ridge, Stochastic Gradient Descent Regression, ElasticNet, Lasso, LassoLars, Orthogonal Matching Pursuit, Bayesian ARD Regression, Bayesian Ridge Regression, Quantile Regressor, Passive Aggressive Regressor, and K-nearest Neighbors Regressor.

The main metrics used to evaluate the performance of the models are as follows:

- Mean Absolute Error (MAE): It's the average of the absolute difference between the observed value and the predicted values. The mean absolute error is linear, meaning that all individual differences are equally weighted in the average.

$$MAE = \frac{1}{n}\sum_{j=1}^{n} |y_j - \hat{y}_j|$$

- Root Mean Squared Error (RMSE): It's the average difference between the predicted values and the actual values, providing an estimate of how well the model can predict the target value. It represents the square root of the average squared distance between the actual value and the predicted value.

$$RMSE = \sqrt{\frac{1}{n}\sum_{j=1}^{n} (y_j - \hat{y}_j)}$$

- Mean Directional Accuracy (MDA): It's a metric that evaluates the model's ability to correctly predict the direction of movements in the data. It's calculated by dividing the number of times the actual change direction matches the predicted change direction by the model, by the total number of predictions.

$$MDA = \frac{1}{n}\sum_{j} 1_{sign(X_j - X_{j-1}) == sign(F_j - X_{j-1})}$$

- Symmetric Mean Absolute Percentage Error (sMAPE): It measures the relative accuracy of predictions by calculating the average absolute percentage

This project has received funding from the European Union's Horizon Europe research and innovation programme under grant agreement No GA 101082048
Funded by the European Union

difference between actual and predicted values. This metric will not be considered when the values fluctuate between -1 and 1 as it can lead to errors.

$$sMAPE = \frac{1}{n}\sum_{j=1}^{n} \frac{|\hat{y}_j - y_j|}{(|y_j| + |\hat{y}_j|)/2}$$

To validate the selected model, different training procedures and predictions are conducted at randomly selected moments over the past few years of data. This simulates the behaviour the model would have exhibited if it had been executed at a specific moment in the past.

To conclude the model selection process, it is important to understand why a model makes a specific prediction. However, the highest accuracy in large data sets is often achieved with complex models that even experts struggle to interpret. In response, several methods have recently been proposed to help users interpret the predictions of complex models, but it is often unclear how these methods relate to each other and when one method is preferable to another. To solve this problem, a unified framework for interpreting predictions, SHAP (SHapley Additive exPlanations), is used. SHAP assigns an importance value to each feature for a specific prediction. These are techniques that calculate a score for all input features for a given model; the scores simply represent the 'importance' of each feature. A higher score means that the specific feature will have a greater effect on the model used to predict a certain variable. SHAP is a game theory approach to explain the outcome of any machine learning model. It is based on Shapley values, which are used to assign meaning to the prediction of a model for each feature or feature value.

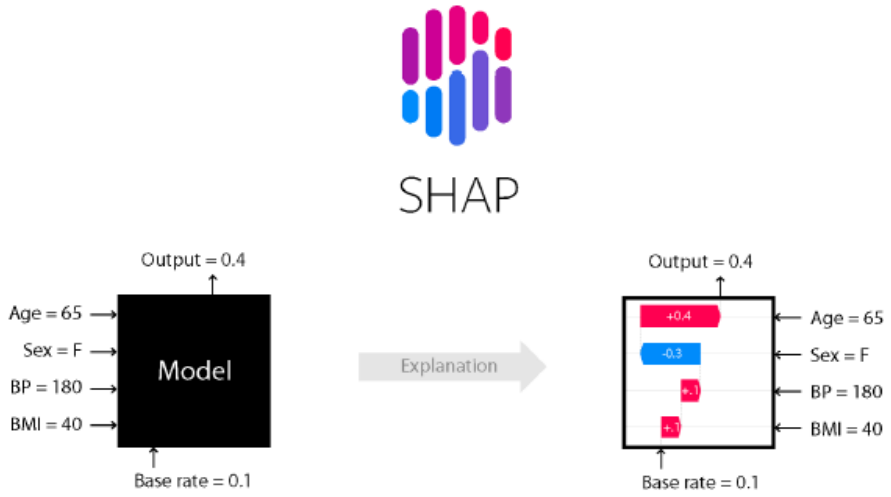

Figure 3.2-5 SHAP - Feature importance. Source: https://shap.readthedocs.io/en/latest/

With the final model selected based on different metrics, predictions are made for each of the target variables for the next 6 months, noting that the number of months to predict is not fixed and could be modified. The prediction results are accompanied by the corresponding prediction interval.

In inferential statistics, specifically in predictive inference, a prediction interval is an estimation of a range of values within which a future observation will fall with a certain probability, given what has already been observed. Prediction intervals are commonly used when making predictions based on regression models, as is the case with the work conducted. This probabilistic approach has a solid and robust scientific basis

This project has received funding from the European Union's Horizon Europe research and innovation programme under grant agreement No GA 101082048
Funded by the European Union

(Gneiting & Katzfuss, 2014; Todini, 2018). From this concept, another of the metrics that have been used to evaluate the different models is derived, the coverage range of each prediction, which assesses the number of actual values that fall within the prediction interval.

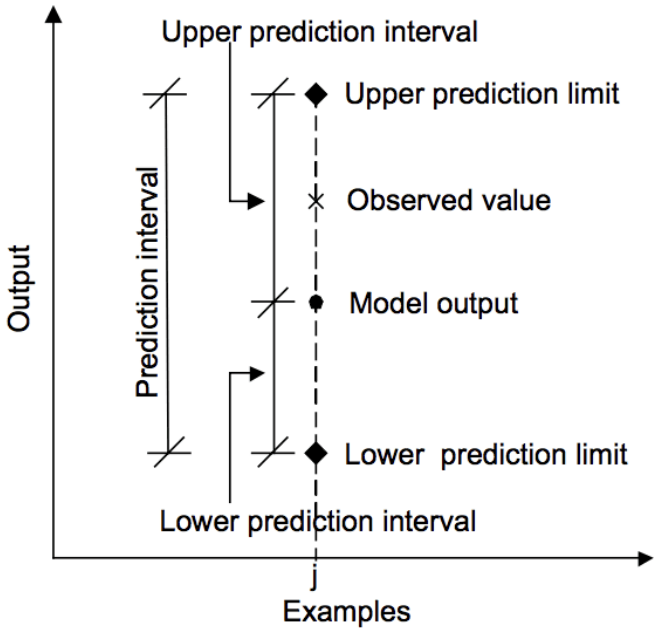

Figure 3.2-6 Conceptual framework illustrating the relationship between predicted values (model output) and actual values (observed value), as well as the prediction interval (prediction interval), with its corresponding upper prediction limit and lower prediction limit. Source: https://machinelearningmastery.com/prediction-intervals-for-machine-learning/

3.2.3 LINKS BETWEEN DATASETS AND DATA-REACH

The input data used for the development of the Data-Reach and the results provided are summarised in the following table.

Table 3.2-2 Links between datasets and DATA-REACH.

TOOL COMPONENT	INPUT DATA	MODEL/ METHODOLOGY	OUTPUT
DATA REACH - Retrospective analysis	Rainfall	Standardised Precipitation Index (Mckee et al., 1993)	12-month SPI
DATA REACH - Retrospective analysis	Rainfall Temperature	Standardised Precipitation Evapotranspiration Index (Vicente-Serrano et al., 2010)	12-month SPEI
DATA REACH - Retrospective analysis	Electrical conductivity Piezometric level Pumping Rainfall	Granger causality test	Predictive relationships between time series
DATA REACH - Predictive models	Piezometric level Pumping Rainfall	Monthly probabilistic predictions	Piezometric level prediction

This project has received funding from the European Union's Horizon Europe research and innovation programme under grant agreement No GA 101082048
Funded by the European Union

DATA REACH - Predictive models	Reservoir volume Rainfall	Monthly probabilistic predictions	Reservoir volume prediction
DATA REACH - Predictive models	Electrical conductivity Piezometric level Pumping Rainfall	Monthly probabilistic predictions	Electrical conductivity prediction

3.3 GIS-REACH

Risk has been defined by several specialists from many different points of view, but one of the simplest is "the probability of having social damages because of an extreme event" (Vías, 2005). Then, the risk of groundwater pollution is an outstanding social topic that must be addressed adequately, because millions of people in the world drink water coming from groundwater supply, including wells and springs, among other sources.

Groundwater pollution risk is a research field relatively new, but with some deficiencies because most of the authors assessed risk from the vulnerability and hazard perspective (Foster, 1987; Robins *et al*., 1994), which means they were only taking into account the physical parameters of the environment, and not the social perspective. Lately, Vías (2005) developed one of the most robust methodologies for groundwater risk assessment that considered the three components of risk assessment: vulnerability, hazard and exposure, coming from the conclusions of the COST Action 620 (Vulnerability and risk mapping for the protection of carbonated, karst aquifers) and Daly *et al*., 1997, 2002). Here, the author also considered the negative consequences of groundwater pollution on the population and groundwater-dependent activities. Other groundwater pollution risk assessment methodologies were developed by Alfors *et al*. (1973), Rowe (1977), Fournier (1979), Varnes (1984), Aller *et al*. (1987), Foster and Hirata (1988), Panizza (1988), Van Diseen and Mcverry (1994) and Mitchell (1990). Other recent EU projects, such as the PRIMA KARMA project, addressed vulnerability mapping of sensitive karstic areas around Europe and the Mediterranean coastal arc.

Due to the complexity that most of these methodologies have regarding the acquisition of spatially distributed, reliable, replicable and high-quality data, a new groundwater risk assessment methodology has been developed in the framework of this project, so it can be easily replicated in almost every groundwater body of Europe, with some exceptions that will be discussed later.

3.3.1 DEVELOPMENT OF A NEW RISK ASSESSMENT METHODOLOGY

The components of risk assessment for groundwater pollution that have been considered in this methodology are:

- Intrinsic **vulnerability** of the aquifer **(V)**. It takes into account the attenuation capacity of pollutants in the aquifer and the exposition of water resources to be polluted.
- Pollution **hazard (H)**. It comprises human activities and physical constraints to induce groundwater pollution.
- Human and environmental **exposure (E)**. It is composed of human and environmental elements that can be endangered because of groundwater pollution.

This project has received funding from the European Union's Horizon Europe research and innovation programme under grant agreement No GA 101082048
Funded by the European Union

Figure 3.3-1 summarises the groundwater pollution risk assessment developed in the framework of this project and all the used variables can be found in Appendix G, as well as an explanation of their characteristics and the way they have been elaborated.

3.3.1.1 DATA ANALYSIS AND PROCESSING

Multiple data sources have been used for the application of the abovementioned methodology, as referred to in Appendix G, which have been summarised in Table G-23 of this appendix. Spatial raster and vector data have been taken from several EU and international databases, so major replicability can be addressed throughout Europe. Also, as shown in Figure 3.3-1, earth observation data coming from satellites such as Sentinel-1, Sentinel-2 or the spatial mission Endeavour have been used for the Land Use and Land Subsidence variables.

This project has received funding from the European Union's Horizon Europe research and innovation programme under grant agreement No GA 101082048

Funded by the European Union

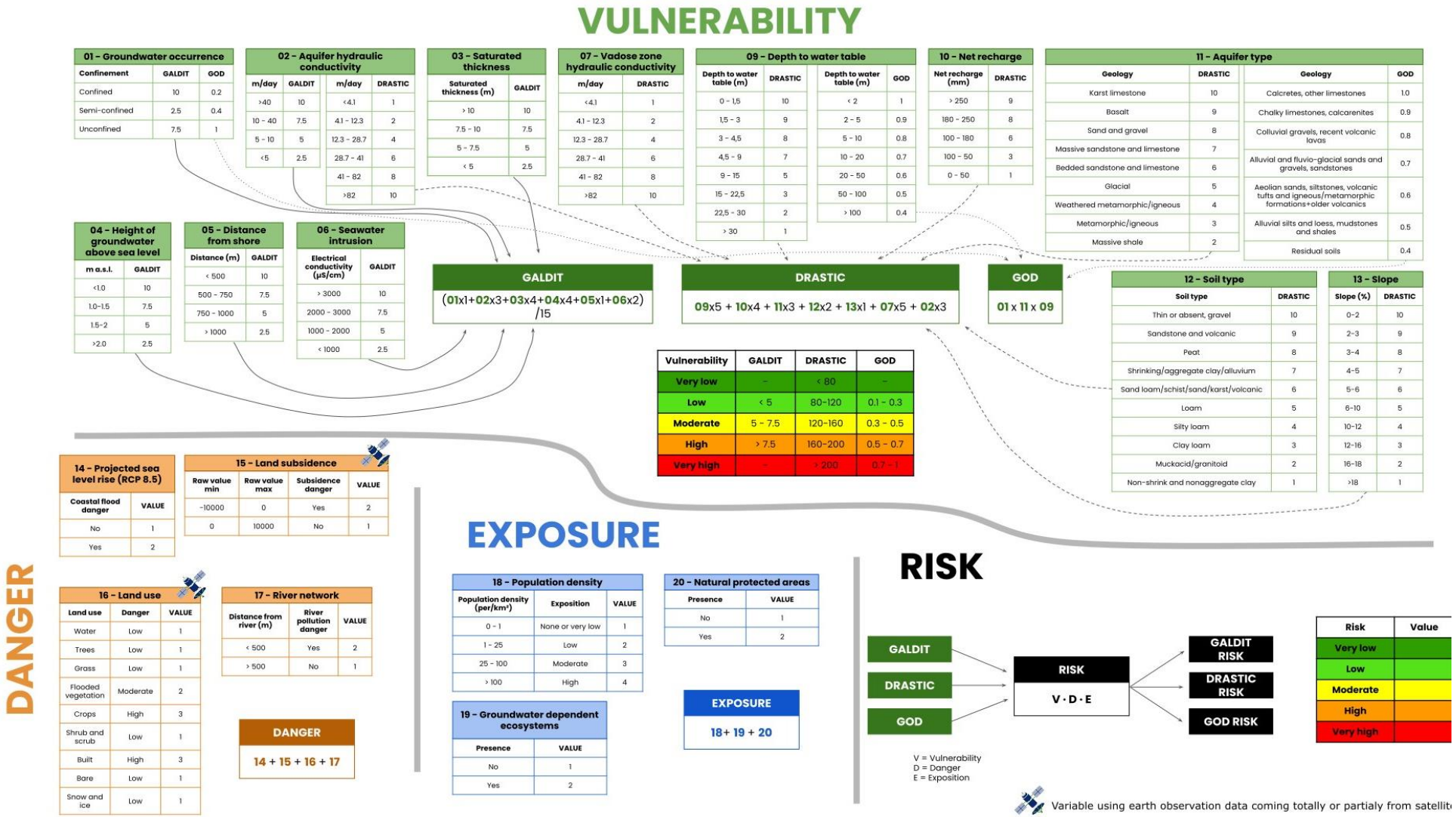

Figure 3.3-1 Groundwater pollution risk assessment methodology developed in the framework of the MAR2PROTECT project

This project has received funding from the European Union's Horizon Europe research and innovation programme under grant agreement No GA 101082048

Funded by the European Union

3.3.2 VULNERABILITY (V)

Several intrinsic vulnerability mappings to groundwater pollution of aquifers were considered at the beginning of the conceptualization: GALDIT, GALDIT-SUSI, DRASTIC, GOD, AVI, EPIC and COP. However, part of them require very specific and highly accurate data, which is out of the scope of the project. Nevertheless, GALDIT (Chachadi and Lobo-Ferreira, 2001), DRASTIC (Aller *et al.*, 1987) and GOD (Foster, 1987) methods met the requirements for replicability in different scenarios, while maintaining accuracy and scientific rigour. Table 3.3-1 shows the needed variables to apply these methodologies:

Table 3.3-1 Variables that are used to evaluate vulnerability to groundwater pollution using GALDIT, DRASTIC and GOD methods.

Variable	Code	GALDIT	DRASTIC	GOD
Groundwater occurrence (confinement)	01_confinement	x		x
Aquifer hydraulic conductivity	02_aquifer_hydraulic_cond	x	x	
Height of groundwater level above sea level	03_GW_height_masl = (08_DEM - 09_depth_to_GW)	x		
Distance from the shore	04_distance_from_shore	x		
Impact of existing status of seawater intrusion	05_seawater_intrusion	x		
Saturated thickness	06_saturated_thickness = (thickness - 03_GW_height_masl)	x		
Unsaturated zone characteristics	07_unsaturated_char		x	
Elevation	08_DEM		x	
Depth to the water table	09_depth_to_GW = (08_DEM - 03_GW_height_masl)		x	x
Net recharge	10_net_recharge		x	
Aquifer type	11_aquifer_type		x	x
Soil type	12_soil_type		x	
Slope	13_slope		x	

3.3.2.1 GALDIT method

The GALDIT model is a numerical ranking method based on overlay and index techniques, which considers six hydrogeological parameters with regard to significant seawater intrusion, and the name GALDIT is a combination of letters from the six parameters, being:

- Groundwater occurrence (G) - Weight = 1
- Aquifer hydraulic conductivity (A) - Weight = 3
- Height of groundwater level above sea level (L) - Weight = 4
- Distance from the shore (D) - Weight = 4
- Impact of the existing status of seawater intrusion (I) - Weight = 1
- Saturated aquifer thickness (T) - Weight = 2

The importance rating given to each parameter can be 2.5, 5, 7.5 or 10.

Finally, the index is calculated following the next equation:

This project has received funding from the European Union's Horizon Europe research and innovation programme under grant agreement No GA 101082048
Funded by the European Union

$$GALDIT\ Index\ = \frac{\sum_{i=1}^{6} \left(W_i \times R_i\right)}{\sum_{i=1}^{6} W_i}$$

3.3.2.2 DRASTIC method

The approach considers seven parameters, whose first letters compose the name of the method. Each of the seven parameters is ranked from 1 to 10 and is assigned to a multiplication factor that increases from 1 to 5 according to the importance of the parameter for the vulnerability estimate. These parameters are:

- Depth to water table (D) - Weight = 5
- Net recharge (R) - Weight = 4
- Aquifer type (L) - Weight = 3
- Soil type (S) - Weight = 2
- Topography (slope) (T) - Weight = 1
- Unsaturated zone characteristics (I) - Weight = 5
- Aquifer hydraulic conductivity (C) - Weight = 3

Finally, the index is calculated following the next equation:

$$DRASTIC\ Index\ = \sum_{i=1}^{7} W_i \times R_i$$

3.3.2.3 GOD method

This method was originally formulated for use in areas with limited data availability. The GOD scheme considers three parameters:

- Groundwater occurrence (G)
- Aquifer type (O)
- Depth to groundwater table (D)

Finally, the index is calculated following the next equation:

$$GOD\ Index\ = G_R \times O_R \times D_R$$

3.3.3 HAZARD (H)

Hazard has been assessed based on human activities and physical (human-induced) phenomena that can produce groundwater pollution in permeable systems. Several parameters, such as projected sea level rise (seawater intrusion increase), land subsidence (depletion of water resources), land use (dangerous activities such as urban or industrial) and river network proximity (pollution caused by flooding) have been used to estimate the hazard of a groundwater pollution event in the MAR2PROTECT demo sites.

3.3.4 EXPOSURE (E)

To assess the exposure to groundwater pollution both social and environmental elements have been taken into account. In this sense, population density is considered the main social exposure, as highly densely populated areas can be more exposed if their water supply is coming partially or completely from groundwater. On the other hand, groundwater pollution can affect ecosystems that are in great part dependent on groundwater, so both groundwater-dependent ecosystems (rivers,

This project has received funding from the European Union's Horizon Europe research and innovation programme under grant agreement No GA 101082048
Funded by the European Union

wetlands, marsh, etc.) and natural protected areas were considered sensitive systems to groundwater pollution.

3.3.5 RISK (R)

Once vulnerability, hazard and exposure have been calculated, risk can be assessed. However, calculations must be done using the raw values of each component, before its reclassification in classes (low, moderate...).

So, for each vulnerability index, the risk can be calculated using this equation:

$$RISK = V \times H \times E$$

Being:

V = vulnerability,

H = hazard,

E = exposure.

After that, the reclassifications shown in **Error! Reference source not found.**, **Error! Reference source not found.** and **Error! Reference source not found.** must be applied.

Table 3.3-2 Parameter reclassification for risk of groundwater pollution using DRASTIC as vulnerability index.

RISK DRASTIC			
Min raw value	**Max raw value**	**New value**	**RISK**
0	5000	1	Very low
5000	15000	2	Low
15000	25000	3	Moderate
25000	35000	4	High
35000	100000	5	Very high

Table 3.3-3 Parameter reclassification for risk of groundwater pollution using GALDIT as vulnerability index.

RISK GALDIT			
Min raw value	**Max raw value**	**New value**	**RISK**
0	500	1	Very low

This project has received funding from the European Union's Horizon Europe research and innovation programme under grant agreement No GA 101082048

Funded by the European Union

RISK GALDIT			
Min raw value	**Max raw value**	**New value**	**RISK**
500	1,000	2	Low
1,000	1,500	3	Moderate
1,500	2,000	4	High
2,000	100,000	5	Very high

Table 3.3-4 Parameter reclassification for risk of groundwater pollution using GOD as vulnerability index.

RISK GOD			
Min raw value	**Max raw value**	**New value**	**RISK**
0	40	1	Very low
40	80	2	Low
80	120	3	Moderate
120	160	4	High
160	10,000	5	Very high

For the next steps of these developments in the framework of the project, a normalisation of values for risk reclassification will be done because some differences can be detected when interpreting the risk using the above-mentioned vulnerability methodologies. E.g.: areas with higher risk using one vulnerability method while having higher vulnerability values using another method.

3.3.6 LINKS BETWEEN DATASETS AND GIS-REACH

The input data used for the Risk assessment and the results provided are summarised in the following table.

Table 3.3-5 Links between datasets and GIS-REACH.

This project has received funding from the European Union's Horizon Europe research and innovation programme under grant agreement No GA 101082048

Funded by the European Union

TOOL COMPONENT	INPUT DATA	MODEL/METHODOLOGY	OUTPUT
GIS-REACH	Groundwater occurrence (confinement)	Risk assessment (V)	Risk and vulnerability maps
GIS-REACH	Aquifer hydraulic conductivity	Risk assessment (V)	Risk and vulnerability maps
GIS-REACH	Height of groundwater level above sea level	Risk assessment (V)	Risk and vulnerability maps
GIS-REACH	Distance from the shore	Risk assessment (V)	Risk and vulnerability maps
GIS-REACH	Impact of existing status of seawater intrusion	Risk assessment (V)	Risk and vulnerability maps
GIS-REACH	Saturated thickness	Risk assessment (V)	Risk and vulnerability maps
GIS-REACH	Unsaturated zone characteristics	Risk assessment (V)	Risk and vulnerability maps
GIS-REACH	Elevation	Risk assessment (V)	Risk and vulnerability maps
GIS-REACH	Depth to the water table	Risk assessment (V)	Risk and vulnerability maps
GIS-REACH	Net recharge	Risk assessment (V)	Risk and vulnerability maps
GIS-REACH	Aquifer type	Risk assessment (V)	Risk and vulnerability maps
GIS-REACH	Soil type	Risk assessment (V)	Risk and vulnerability maps
GIS-REACH	Slope	Risk assessment (V)	Risk and vulnerability maps
GIS-REACH	Projected sea level rise	Risk assessment (H)	Risk and vulnerability maps
GIS-REACH	Land subsidence	Risk assessment (H)	Risk and vulnerability maps
GIS-REACH	Land use	Risk assessment (H)	Risk and vulnerability maps
GIS-REACH	River network	Risk assessment (H)	Risk and vulnerability maps
GIS-REACH	Population density	Risk assessment (E)	Risk and vulnerability maps

This project has received funding from the European Union's Horizon Europe research and innovation programme under grant agreement No GA 101082048

Funded by the European Union

3.4 CLIMATE PROJECTIONS

Climate projections are essential for understanding the impact of global climate change. However, inherent biases in these projections can compromise their accuracy. To overcome this challenge, a robust and efficient methodology for bias correction has been developed, utilising the Climadjust tool. This tool facilitates access to climate data and uses local observations to ensure a more precise evaluation of regional effects.

Regional Climate Models (RCMs) provide detailed information for smaller geographical areas, deriving boundary conditions from Global Climate Models (GCMs) or reanalysis products. Through the Climadjust platform, two types of simulations (or "experiments") can be conducted: historical simulations or scenarios (using GCMs and Representative Concentration Pathways (RCPs)).

Setting up an "experiment" requires the definition of a series of parameters and steps as detailed below.

3.4.1 Enter the initial data

In the first step, the user is prompted to enter the initial data for the experiment: the experiment title and the input data to use. The title will later appear in the file with the results. The input data is the "real" data through which the bias correction will be made. These data can be pre-loaded or selected from the public data provided by the system. For studies of specific regions, local data from observations within the study area is preferred, ideally comprising daily time series spanning a minimum of 30 years. In cases where there are less than 30 years of data, local observations are lacking (more than 20 %) or the station is too far from the study area, it is preferable to employ bias correction using the ERA5-Land data package.

3.4.2 Select the projection dataset

In this second step, the user can select the dataset to be used for projection. Depending on the area under study, there are three types of projections to use: two global (CMIP6, CMIP5) and one for Europe (EuroCordex). These projections contain the climate model packages that can later be used for simulations.

3.4.3 Choose the variable to adjust

In this step, the variable to be corrected is selected, whether it be maximum or minimum temperature, precipitation, etc.

3.4.4 Define the geographical coverage of the experiment

In this step, the user can define the area for which the experiment will be run. This can be done by either pasting a WKT code for a specific area or by drawing the desired area on the map displayed on the screen. It is important to ensure that the drawn polygon is within the range of the climatological station and the projection area (Europe, Global, etc.).

3.4.5 Set the temporal range and the RCP scenarios

In this step, the user can select the temporal range (the years for which the experiment will be run) and the RCP scenarios to be simulated. This defines the desired outcome, which can be historical or RCP climate scenarios.

3.4.6 Select the climate models to run in the experiment

The selection of the model to be used will determine the series of calculations and mathematical operations to process the simulation. Depending on the selected mathematical model, an experiment will perform one type of Earth's climate

This project has received funding from the European Union's Horizon Europe research and innovation programme under grant agreement No GA 101082048
Funded by the European Union

simulation or another for the study area. The number of available models depends on the type of projection selected. The only model package that already contains a pre-selection is the CMIP6. For the others, it is recommended that in case of uncertainty, as many models as possible should be used.

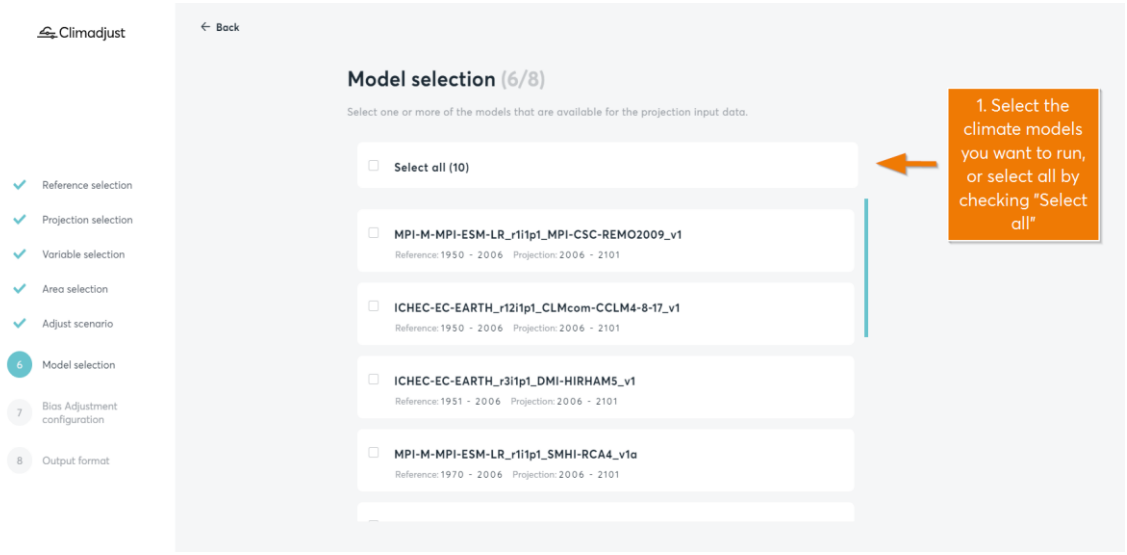

Figure 3.4-1 Model selection. Source: https://climadjust.com/app/documentation/help

The regional climate models and scale reduction methods contained in Climadjust follow the configuration below.

Example: MOHC-HadGEM2-ES_r1i1p1_CLMcom-CCLM4-8-17

- The name of the institution that developed the climate model: MOHC refers to the Met Office Hadley Centre (UK).
- The name of the climate model: HadGEM2-ES.
- A specific member within a set (ensemble) of simulations performed with a climate model. r1i1p1 indicates the first realisation of the first ensemble member.
- Scale reduction method and model: CLMcom-CCLM4-8-17. CLMcom refers to the limited area climate modelling community. CCLM4-8-17 is a specific version of the regional climate model CCLM (COSMO-CLM), developed for high-resolution climate simulations in Europe. It implicitly includes who developed the method. It also determines the geographical focus of the method, the configuration and parameterization.

3.4.7 Choose the Bias Adjustment and Validation method to apply

The Bias Adjustment method is a statistical technique that allows for the correction of bias between climate simulation and data obtained from weather station observations. The effectiveness of the adjustments can vary depending on the type of variable being studied. The table below provides a summary of methods that are better suited to certain types of variables. At this stage, there is also the option to select the desired validation to be applied, an additional process performed by the tool to calibrate the bias adjustment.

This project has received funding from the European Union's Horizon Europe research and innovation programme under grant agreement No GA 101082048
Funded by the European Union

Table 3.4-1 Summary of method types for variable Bias correction.

Variable	Bias Adjustment method
Precipitation	Scaling multiplicative, PQM, GPQM, EQM, ISIMIP3, QDM, PTR
Extreme Temperatures (max or min)	Scaling additive, EQM, DQM, QDM, ISIMIP3

3.4.8 Aggregate data on different spatial and temporal levels

The final step involves selecting the output format for the experiment. This includes options for temporal resolution, allowing for the output data to be aggregated on a daily, monthly, or yearly basis. The spatial resolution can either mirror the input data (native) or be aggregated, which is achievable by uploading a GeoJson file. There is also the choice of spatial aggregation type to apply to the variable, such as Mean, Sum, Maximum, or Minimum. The selection of temporal resolution will dictate the calculation of the resulting data, typically on a daily basis. The spatial resolution can also be set, typically as "Native". It should be noted that bias adjustment is always conducted at a daily level. If "Monthly" is selected, supplementary monthly data will be provided.

4 RESULTS

4.1 MOD-REACH

4.1.1 Calibration and adjustment

The calibration exercise consisted of estimating the characteristic hydraulic properties of each of the Hydrogeological Units that make up the modelled aquifer system. In this exercise, the parameters that have been calibrated are the hydraulic conductivity and the storage coefficients of each of the zones that define the UH of the numerical model.

In this way, the stationary and transient models have been calibrated iteratively in such a way that the calibrated parameters obtained are univocal and coherent, allowing a good fit for both models. Specifically, a manual calibration has been carried out for the transitional regime.

4.1.1.1 Calibration indicators

The evaluation of the calibration result has been carried out by quantifying the main indicators used to evaluate the fit of a hydrogeological model. These indicators are:

- The mean square error (RMSE), which is a good parameter if the errors are normally distributed is defined by:

$$RMSE = \sqrt{\frac{1}{n}\sum_{i=1}^{n} (h_i^{obs} - h_i^{sim})^2}$$

Where h^{obs} and h^{sim} are the observed and measured levels, respectively, and n is the total number of measurements.

- Mean absolute error (MAE), defined by:

This project has received funding from the European Union's Horizon Europe research and innovation programme under grant agreement No GA 101082048
Funded by the European Union

$$MAE = \frac{1}{n}\sum_{i=1}^{n} \left|h_i^{obs} - h_i^{sim}\right|$$

These indicators are usually evaluated as a percentage with respect to the difference between the minimum () and the maximum () level measured in the simulation period, in this way they are evaluated:$h_{min}^{obs}\, h_{max}^{obs}$

- The normalized mean square error (nRMSE), is defined by:

$$nRME = RMSE\ x\ 100/\left(h_{max}^{obs} - h_{min}^{obs}\right)$$

- The normalized mean absolute error (nMAE), is defined by:

$$nMAE = MAE\ x\ 100/\left(h_{max}^{obs} - h_{min}^{obs}\right)$$

4.1.1.2 Calibration results

presented. The adjustment obtained for the nRMSE and nMAE is 9.89% and 7.37%, respectively.

Table 4.1-1 Indicators for stationary model calibration. (Source: Authors).

Indicator	Value
Number of wells	6
RMSE	2,44
nRMSE (%)	9,89
DUDE	1,82
nMAE (%)	7,37
Residual Mean	0,61
Sum of Squares	2115,69
RMSE	2,44

Figure 4.1-1 presents the histogram of residuals obtained for calibration. This histogram shows a symmetrical distribution cantered around zero. That is, low residuals predominate, i.e. the difference between the observed and calculated level is around zero.

This project has received funding from the European Union's Horizon Europe research and innovation programme under grant agreement No GA 101082048
Funded by the European Union

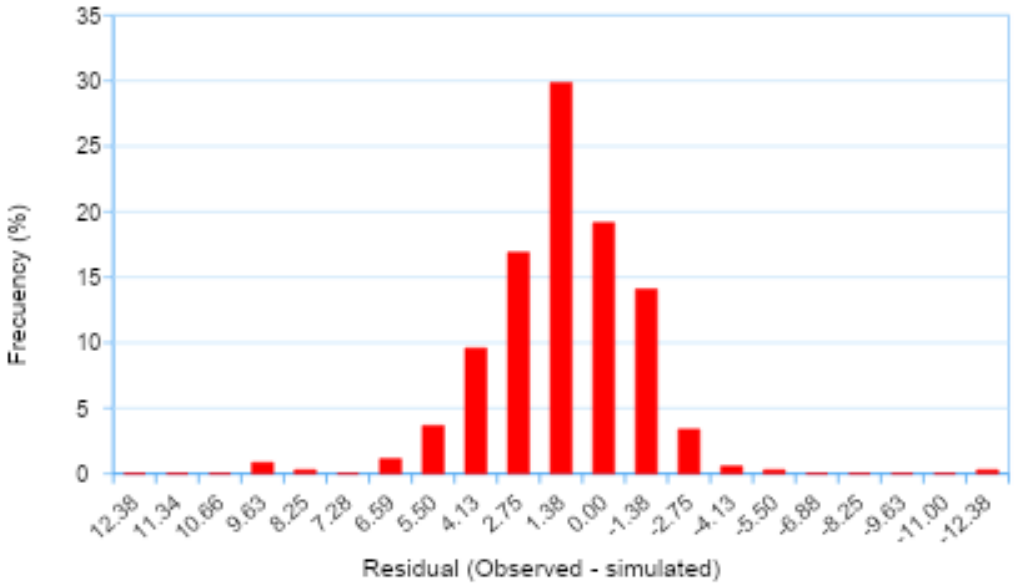

Figure 4.1-1 Histogram. Quantitative analysis of the calibration process. (Source: Authors).

The graphical representation of the adjustment between observed and measured levels is shown in Figure 4.1-2. As can be seen, except for a few isolated levels, most of the points represent a 1-1 trend between the observed levels and the levels calculated by the model.

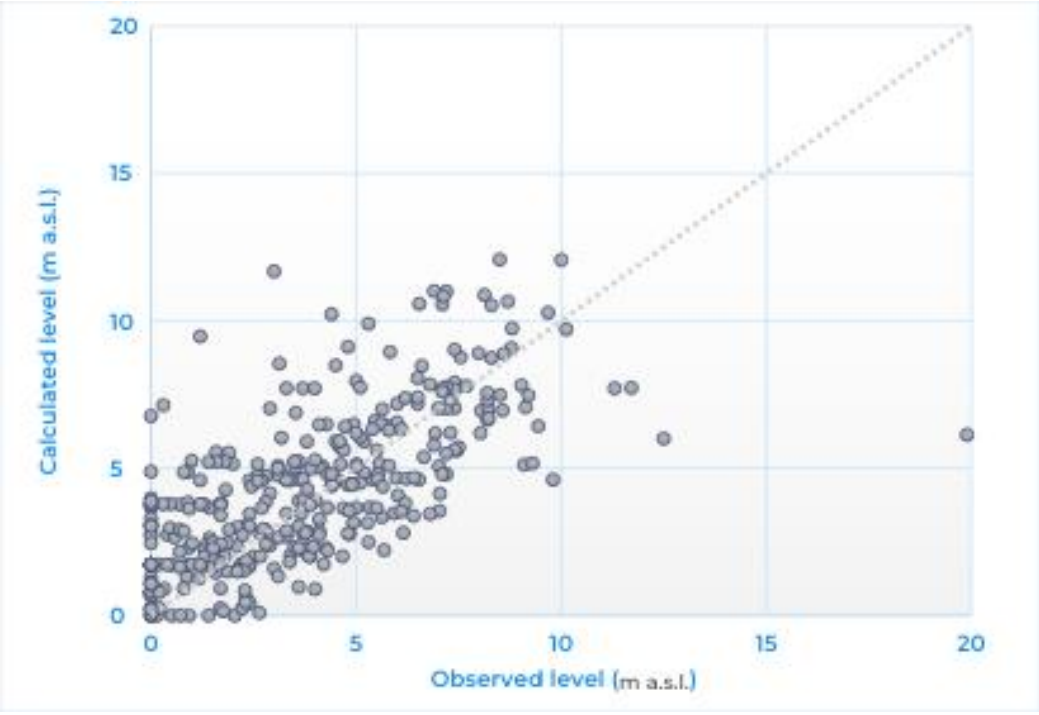

Figure 4.1-2 Relationship of observed and simulated levels. (Source: Authors).

As mentioned above, the validation of the model is carried out by the most reliable calibration source, the adjustment of the observed piezometric evolution with the calculated one.

The results obtained are presented from Figure 4.1-3 to Figure 4.1-8 where it is observed that there is a great coincidence of the piezometric values measured with

This project has received funding from the European Union's Horizon Europe research and innovation programme under grant agreement No GA 101082048
Funded by the European Union

those observed. In general, the specific cases, with the least adjustment, have a maximum difference of about 3 meters, the most common being that this difference is between 1 and 2 meters.

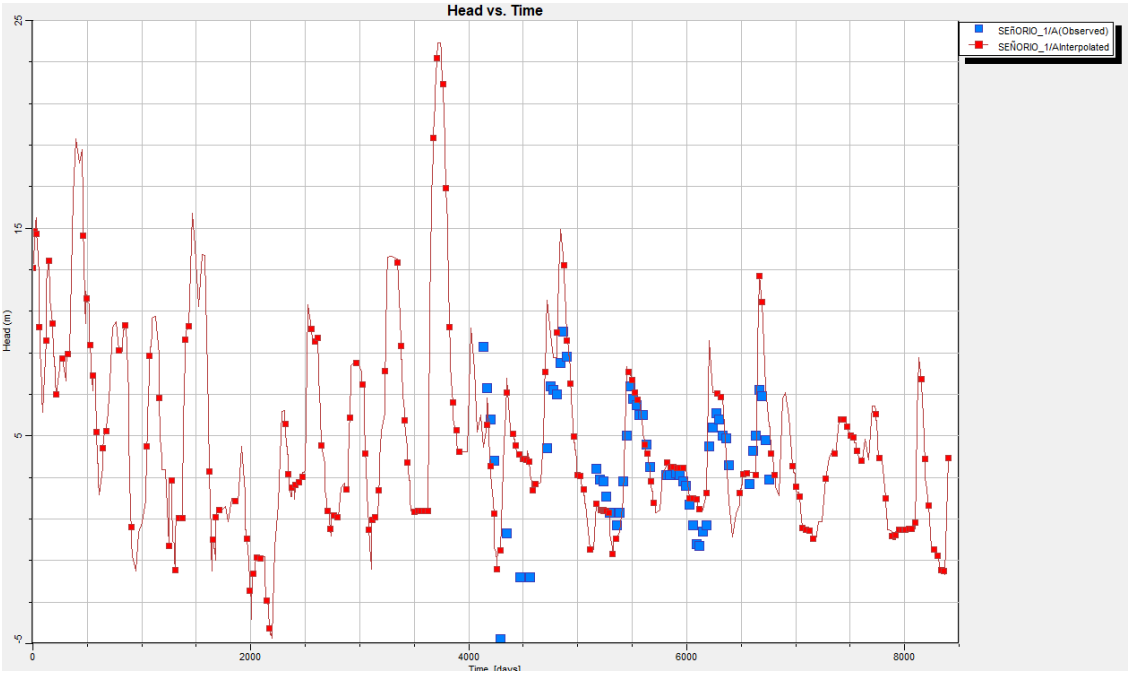

Figure 4.1-3 Comparison of the simulated (in red) and observed (in blue) piezometric evolution of well Sñ1 (2000-2023).

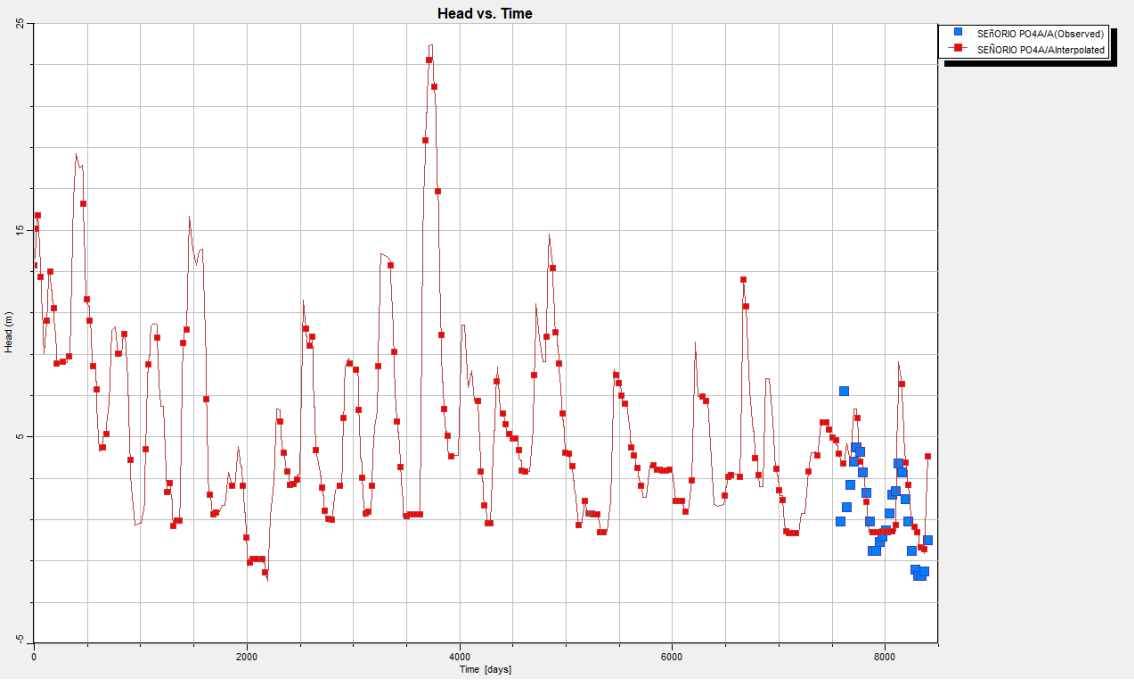

Figure 4.1-4 Comparison of the simulated (in red) and observed (in blue) piezometric evolution of the Sñ4A well (2000-2023).

This project has received funding from the European Union's Horizon Europe research and innovation programme under grant agreement No GA 101082048
Funded by the European Union

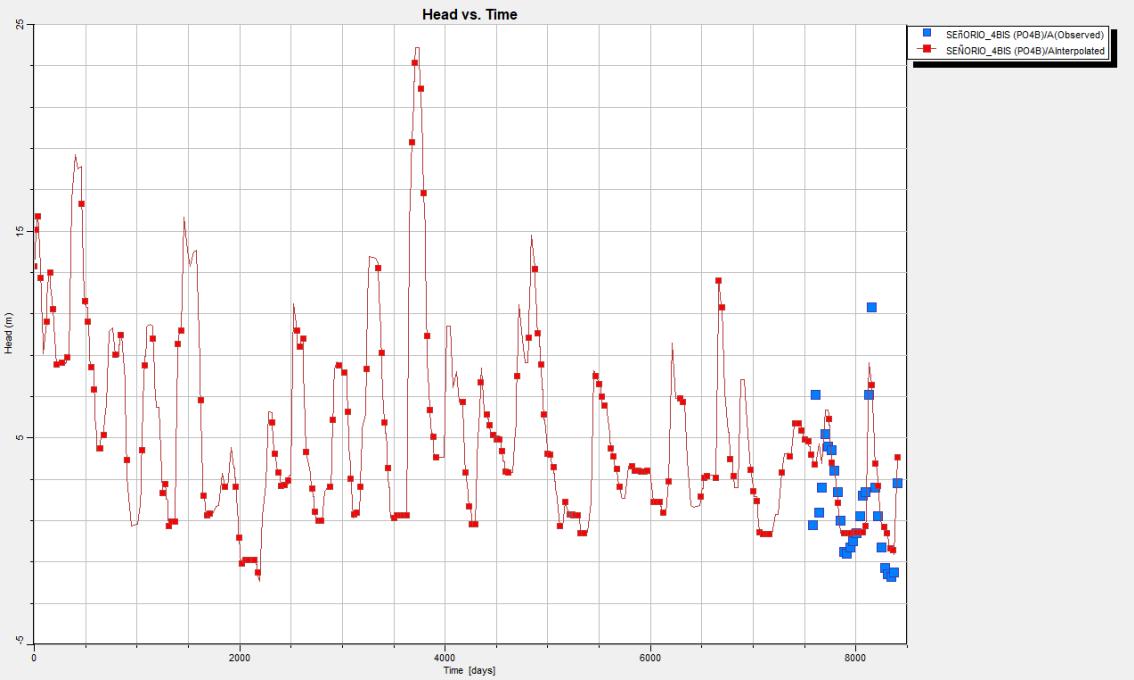

Figure 4.1-5 Comparison of the simulated (in red) and observed (in blue) piezometric evolution of the Sñ4B well (2000-2023).

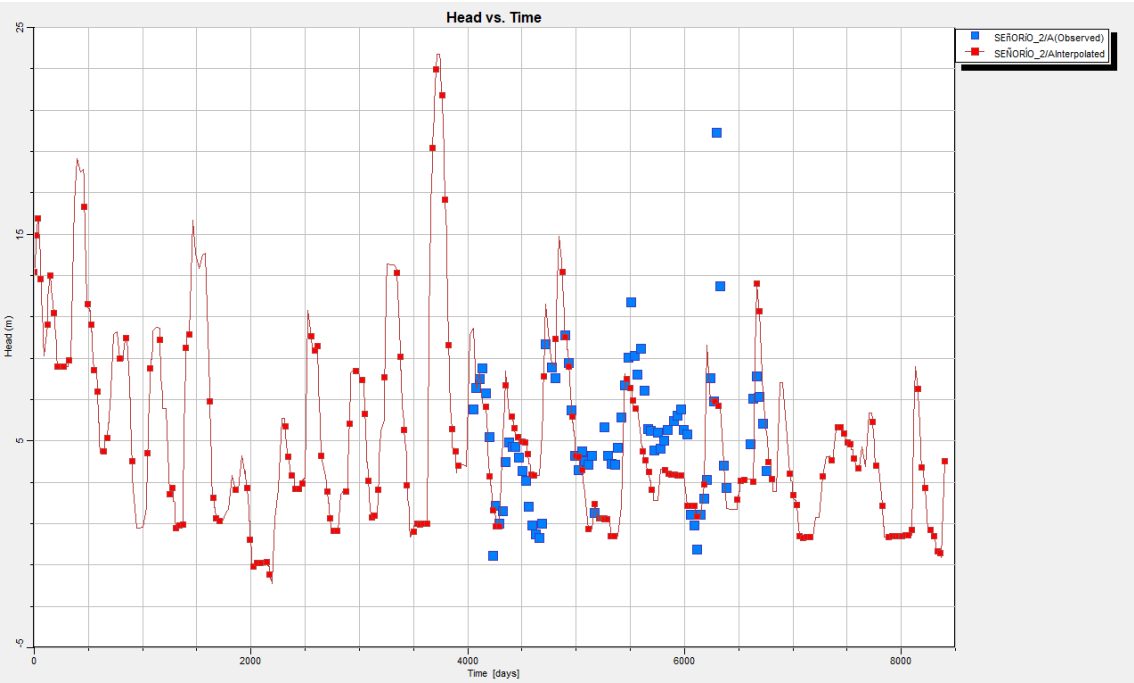

Figure 4.1-6 Comparison of the simulated (in red) and observed (in blue) piezometric evolution of the Sñ2 well (2000-2023).

This project has received funding from the European Union's Horizon Europe research and innovation programme under grant agreement No GA 101082048

Funded by the European Union

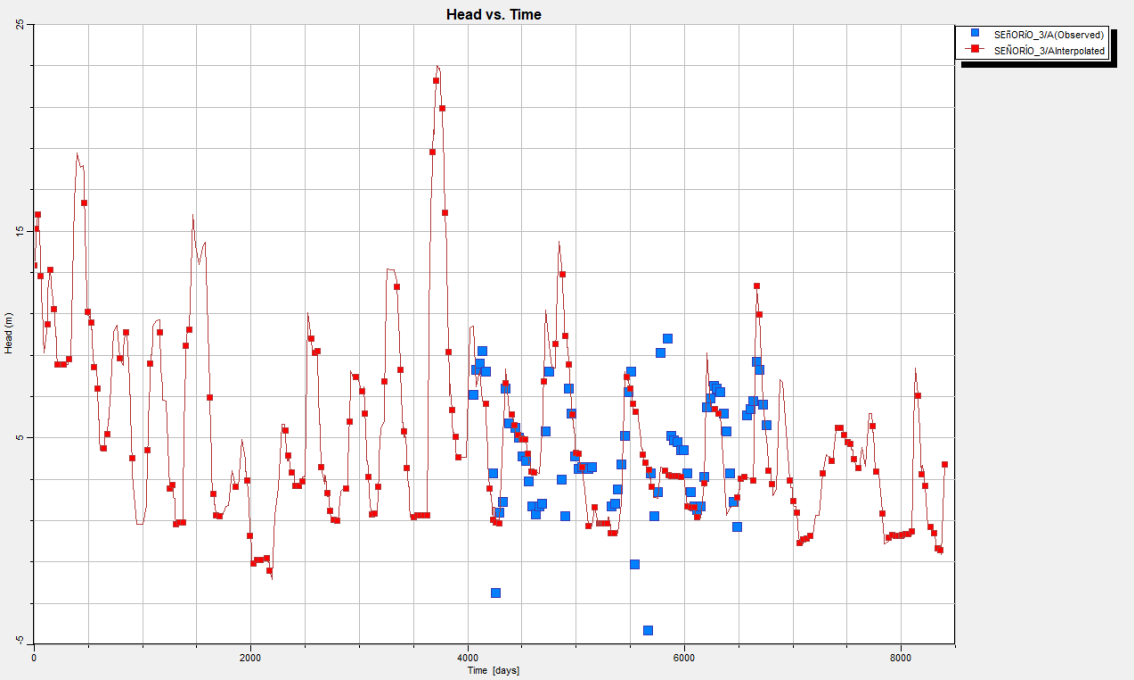

Figure 4.1-7 Comparison of the simulated (in red) and observed (in blue) piezometric evolution of the Sñ3 well (2000-2023).

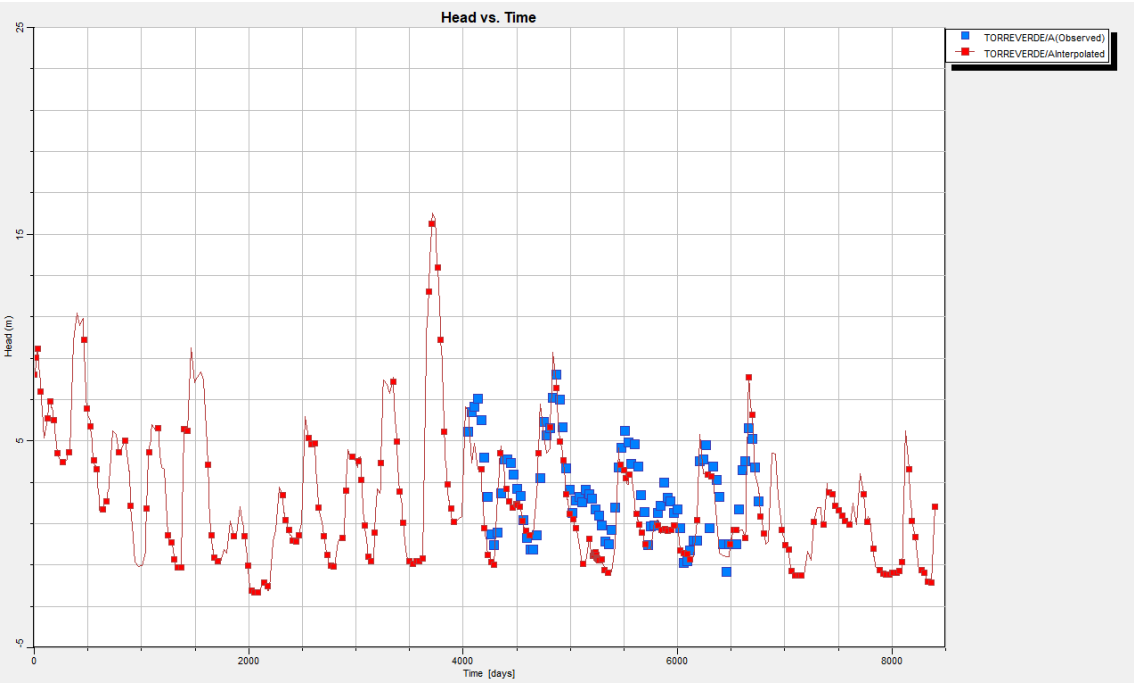

Figure 4.1-8 Comparison of the simulated (red) and observed (blue) piezometric evolution of the Torreverde well (2000-2023).

This project has received funding from the European Union's Horizon Europe research and innovation programme under grant agreement No GA 101082048

Funded by the European Union

4.1.1.3 Validation period 2011-2022

The simulation for the period 2011-2022 is carried out to obtain a second validation of the model, for coinciding dates, avoiding calculation errors. In this case, the piezometry observed is compared with the simulated piezometry, during the period 2011-2017, in the Sñ1, Sñ2 and Sñ3 and Torreverde wells.

The trends of the observed levels versus the levels calculated for this validation period are shown in Figure 4.1-9, Figure 4.1-10, Figure 4.1-11, and Figure 4.1-12.

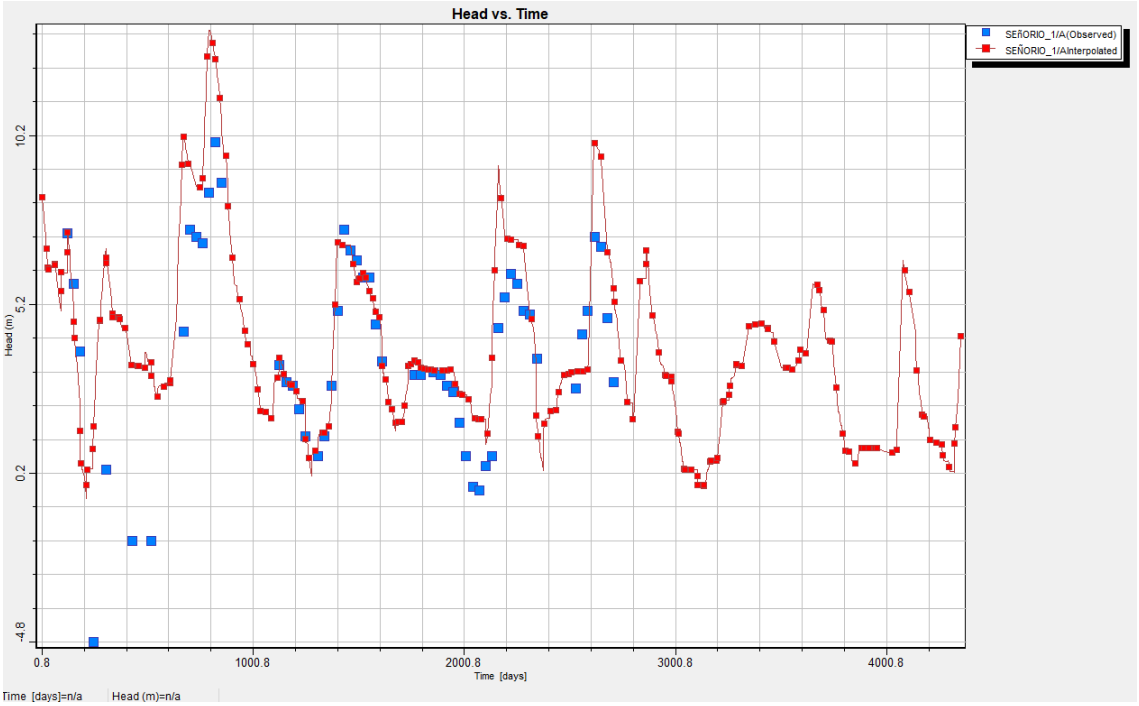

Figure 4.1-9 Comparison of the simulated (in red) and observed (in blue) piezometric evolution of the Sñ1 well period (2011-2022).

This project has received funding from the European Union's Horizon Europe research and innovation programme under grant agreement No GA 101082048

Funded by the European Union

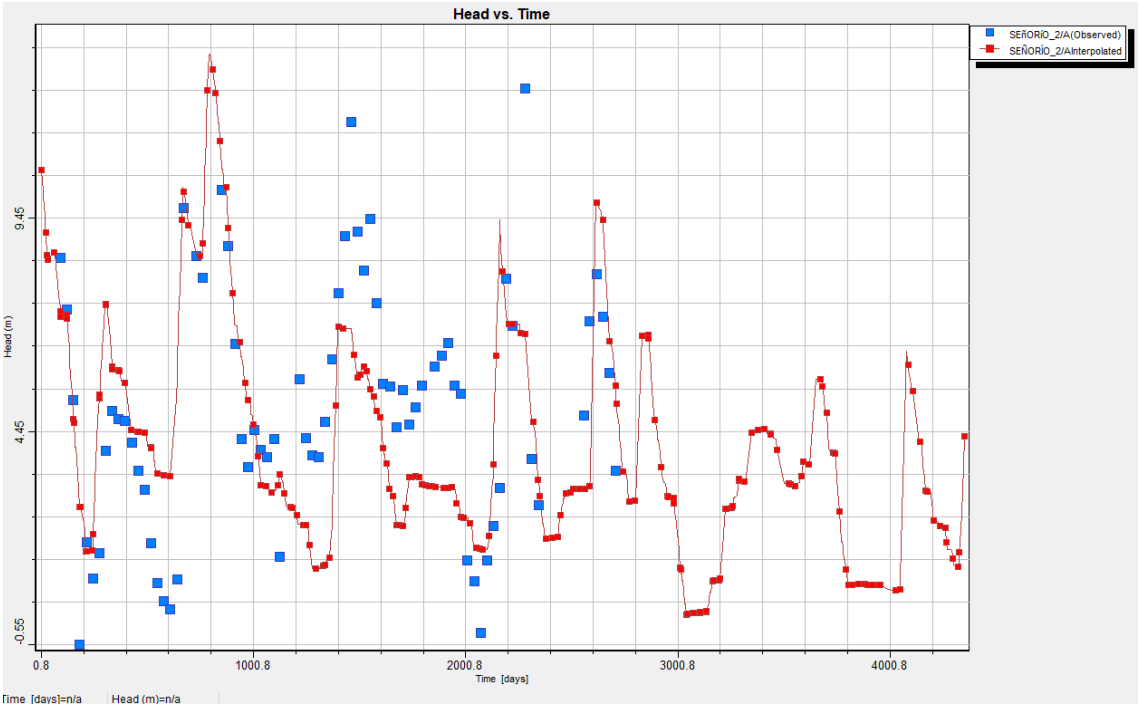

Figure 4.1-10 Comparison of the simulated (in red) and observed (in blue) piezometric evolution of the Sñ2 well period (2011-2022).

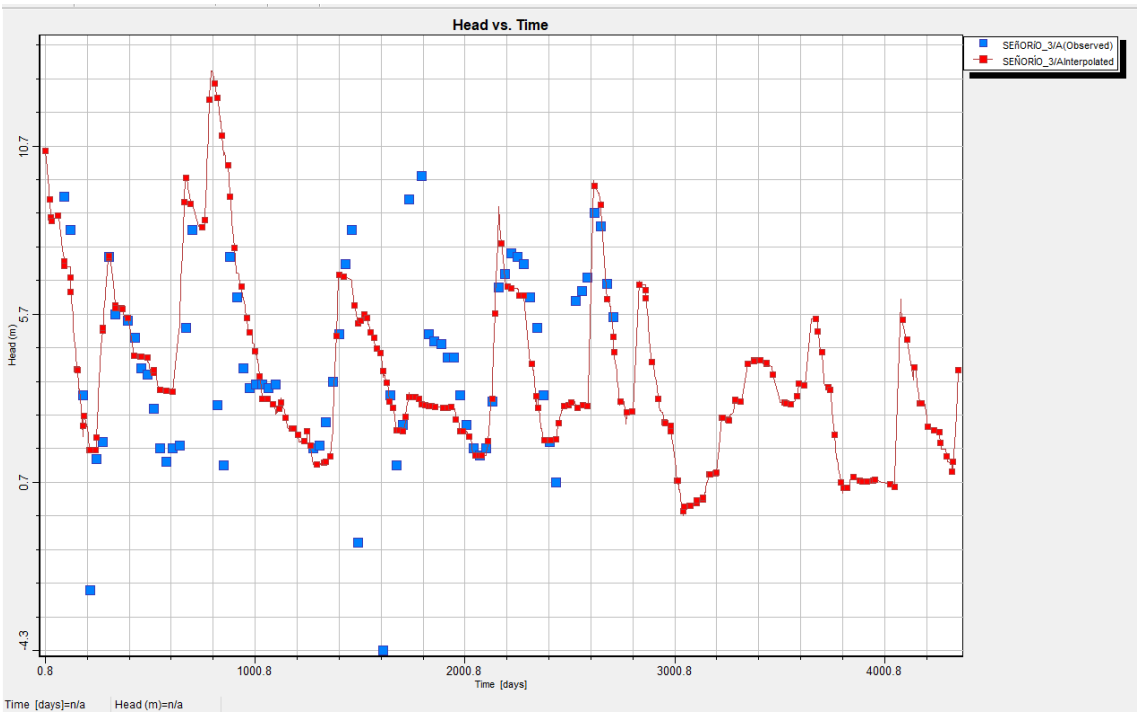

Figure 4.1-11 Comparison of the simulated (in red) and observed (in blue) piezometric evolution of the Sñ3 well period (2011-2022).

This project has received funding from the European Union's Horizon Europe research and innovation programme under grant agreement No GA 101082048

Funded by the European Union

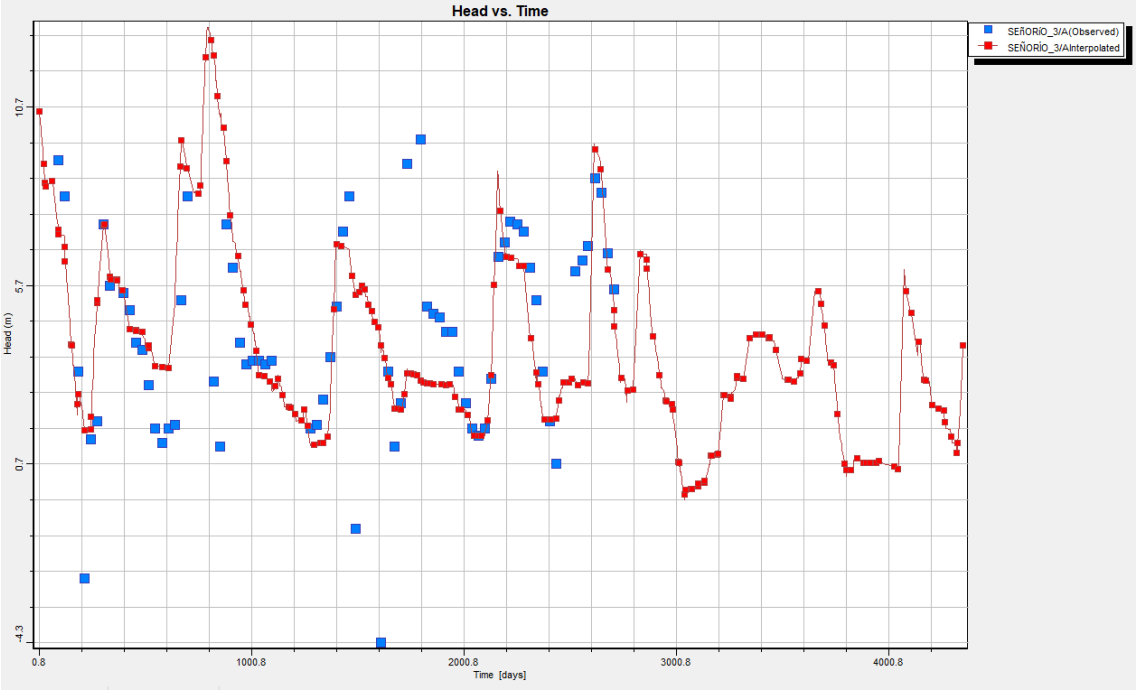

Figure 4.1-12 Comparison of the simulated (in red) and observed (in blue) piezometric evolution of the Torreverde well.

4.1.2 Calibrated hydraulic parameters

The hydraulic parameters considered are hydraulic conductivity and storage coefficient. As for the former, this is defined as the greater or lesser ease with which the medium allows water to pass through it per unit area transverse to the direction of flow. It is measured in meters per day (m/d). The second corresponds to the volume of water released by a vertical prism of the aquifer of a section equal to the unit and height equivalent to the saturated thickness of the aquifer when there is a unit decrease in the piezometric level. It is a dimensionless value.

The Señorío aquifer is mainly made up of Pliocene conglomerates, sands and sandy silts, of high permeability, being confined in its southern half. The tasks of reviewing technical studies included an exhaustive compilation of hydraulic parameters of the materials involved. This task focused both on technical studies by various Organisations and on the pumping analysis carried out by associated companies. The following tables summarise the sources consulted.

Table 4.1-2 Databases consulted.

Type of information	Database	Source
Distribution of permeability values and storage coefficient	Hydrogeological Atlas of the Province of Malaga	IGME-UMA Associated Unit "Advanced Hydrogeological Studies"
Distribution of permeability values and storage coefficient	Lithostratigraphic, permeability and hydrogeological map	Geological and Mining Institute of Spain (IGME)
Distribution of permeability values and storage coefficient	Hydrogeological map of Spain at a scale of 1:50,000	Geological and Mining Institute of Spain (IGME)

This project has received funding from the European Union's Horizon Europe research and innovation programme under grant agreement No GA 101082048
Funded by the European Union

Distribution of permeability values and storage coefficient	Water Point Database	Geological and Mining Institute of Spain (IGME)
Pumping tests	Private database	Aquagest Andalucía
Pumping tests	Private database	Pozos Reunidos S.L., 1996

Table 4.1-3 Articles reviewed.

Title	Author/s	Year
Hydrogeology of carbonate aquifers in the Sierras Blancas and Mijas (Baetic Mountain Range, Southern Spain)	Andreo, B	1997
Hydrogeological characterization of carbonate aquifers in southern Spain based on their natural responses	Jimenez, JA	2010
Hydrogeological cartography of the Municipality of Marbella. Unpublished report.	AQUAGEST ON S.A. INGEMISA	1995

The pumping test carried out in Señorío 4 shows that the aquifer has a transmissivity of 1,995 m^2/day and a storage coefficient of $5.7 \cdot 10^{-3}$ (Pozos Reunidos S.L., 1996) in that place. Considering that the aquifer has about 100 meters of power, its permeability would be about 20 m/d, in the analysed sector.

After compiling and analysing the set of information related to hydraulic parameters, it was decided to assign the following ranges of values to each hydrogeological unit:

- Quaternary aquifer (0.5-0.01 m/d)
- Pliocene aquifer (5-50 m/d)
- Paleozoic Aquitard/Aquiclude (0.01–0.001 m/d)

Likewise, the spatial distribution of hydraulic parameters is reflected in the following figures:

This project has received funding from the European Union's Horizon Europe research and innovation programme under grant agreement No GA 101082048
Funded by the European Union

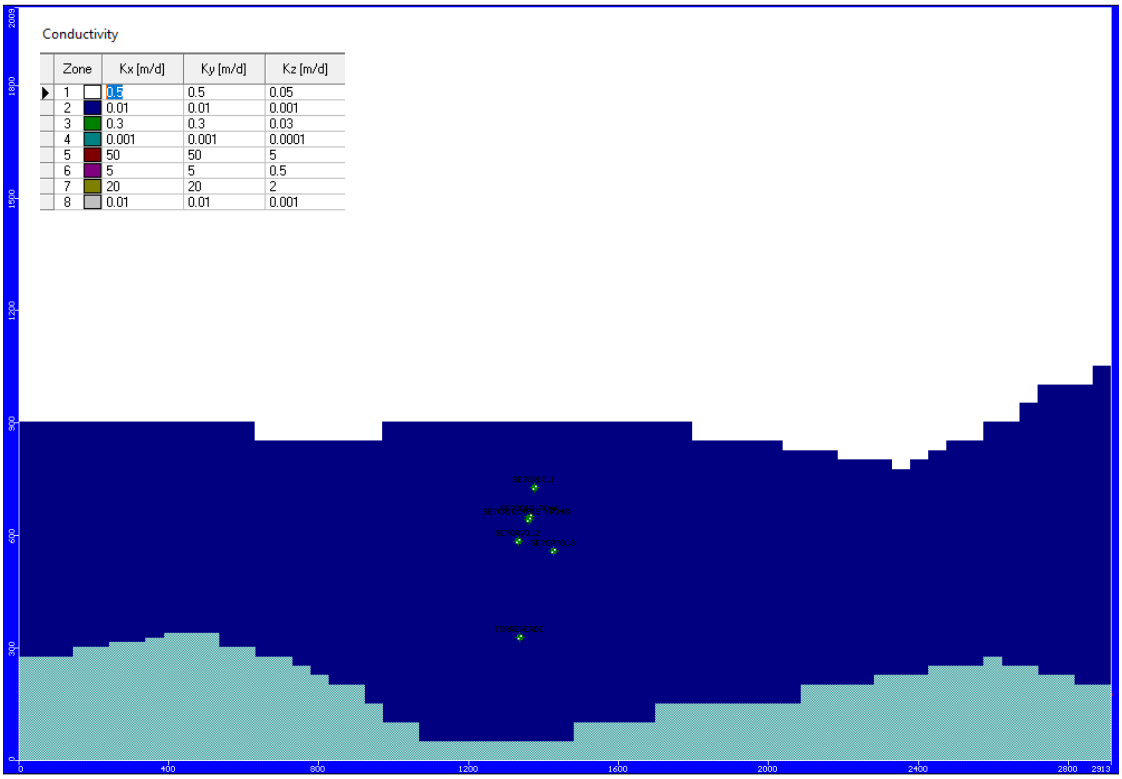

Figure 4.1-13 Permeability distribution in layer 1 (Quaternary).

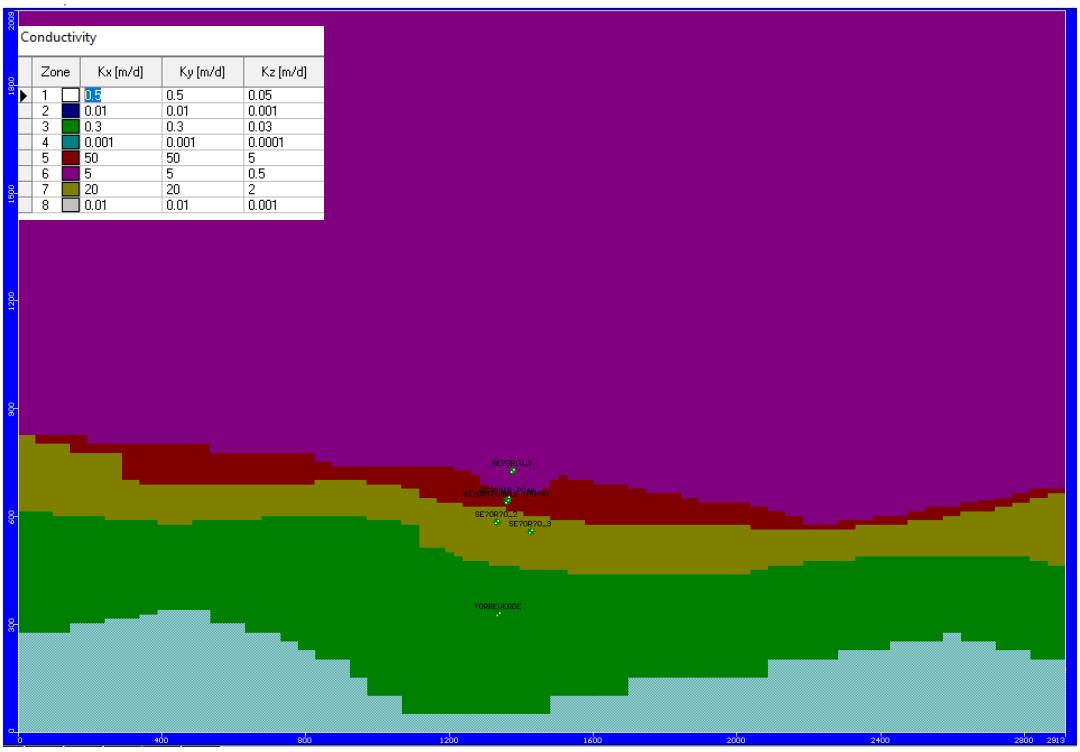

Figure 4.1-14 Permeability distribution in layer 2 (Pliocene).

This project has received funding from the European Union's Horizon Europe research and innovation programme under grant agreement No GA 101082048

Funded by the European Union

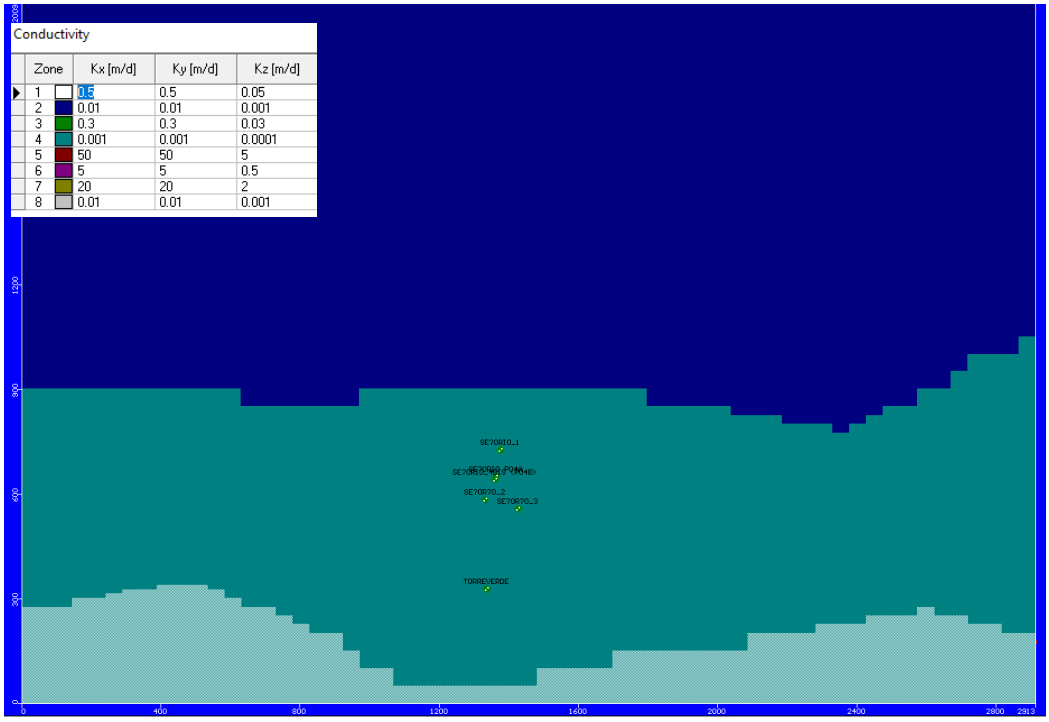

Figure 4.1-15 Permeability distribution in layer 3 (Paleozoic).

On the other hand, the ranges of storage coefficient values assigned to each hydrogeological unit are:

- Quaternary Aquifer (0.01)
- Pliocene Aquifer (0.01-0.05)
- Paleozoic Aquitard (0.001)

Its spatial distribution is as follows:

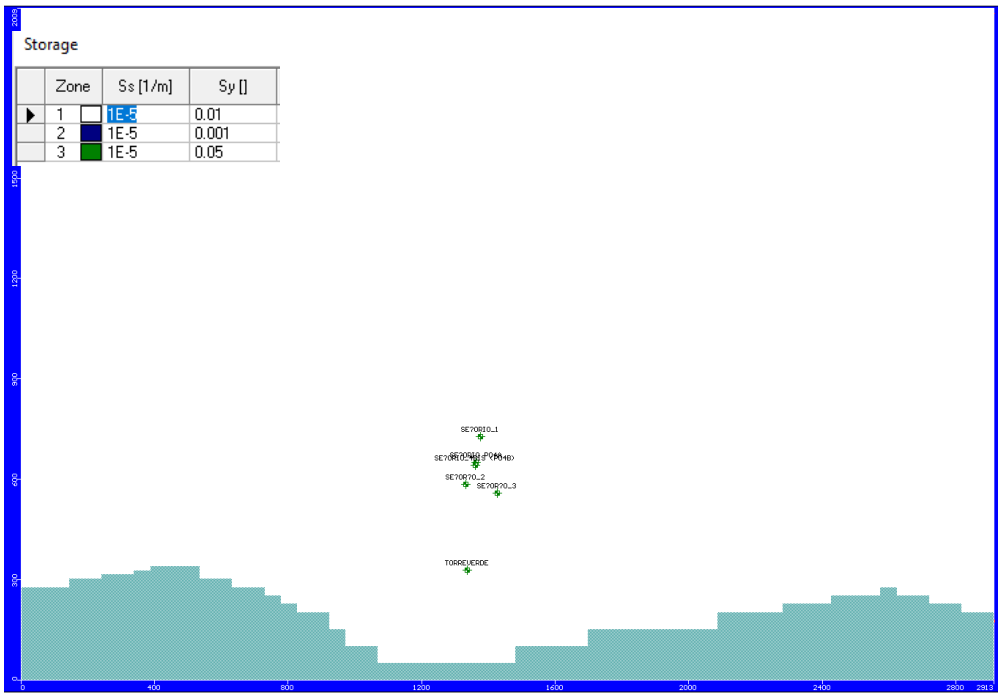

Figure 4.1-16 Storage coefficient distribution in layer 1 (Quaternary).

This project has received funding from the European Union's Horizon Europe research and innovation programme under grant agreement No GA 101082048
Funded by the European Union

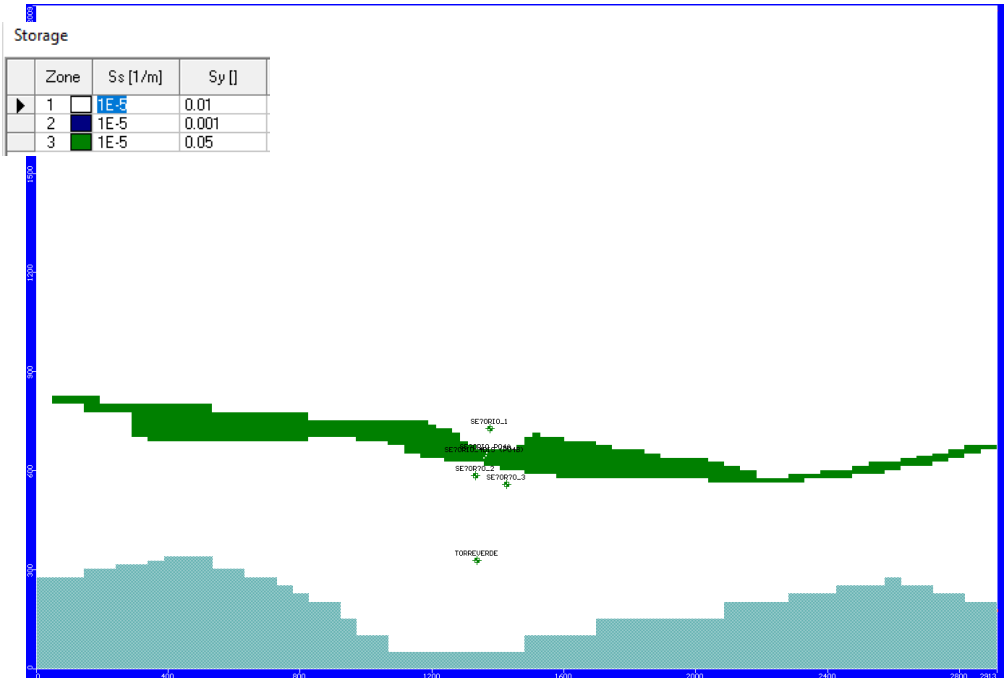

Figure 4.1-17 Storage coefficient distribution in layer 2 (Pliocene).

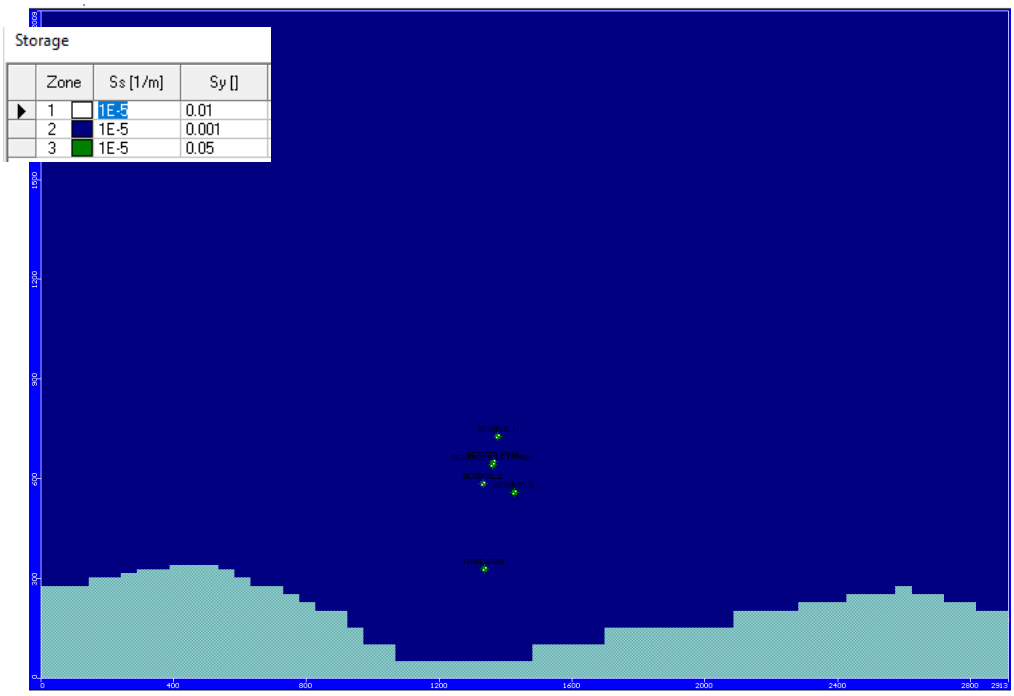

Figure 4.1-18 Distribution of the storage coefficient in layer 3 (Paleozoic).

4.1.3 Water balance

Below are the results of the water balance obtained for the simulated period 2000-2022, at an annual level.

This project has received funding from the European Union's Horizon Europe research and innovation programme under grant agreement No GA 101082048

Funded by the European Union

Table 4.1-4 Annual water balance in hm³/y. Simulation period 2000-2022.

YEAR	OUTPUTS				INPUTS		
	RIVERS	WELLS	CONSTANT HEAD	RECHARGE	RIVER	WELLS	CONSTANT HEAD
2000	0.19	1.13	1.19	1.32	0.01	0.10	0.15
2001	0.14	1.07	1.43	1.99	0.01	0.18	0.18
2002	0.10	1.04	0.84	1.52	0.01	0.10	0.31
2003	0.09	1.25	0.90	1.76	0.01	0.22	0.31
2004	0.10	1.32	1.10	1.51	0.01	0.24	0.28
2005	0.06	1.35	0.29	1.02	0.01	0.16	0.61
2006	0.06	1.19	0.53	1.86	0.01	0.27	0.44
2007	0.06	1.25	0.55	1.03	0.01	0.12	0.42
2008	0.07	1.32	0.81	2.15	0.01	0.51	0.33
2009	0.08	1.46	0.73	0.97	0.01	0.26	0.41
2010	0.14	1.64	1.79	3.57	0.01	0.33	0.18
2011	0.13	1.72	0.98	2.79	0.01	0.00	0.28
2012	0.09	1.18	0.68	1.31	0.01	0.03	0.37
2013	0.09	1.14	0.99	1.25	0.01	0.06	0.27
2014	0.05	1.09	0.30	1.47	0.01	0.01	0.58
2015	0.06	1.02	0.61	1.08	0.01	0.00	0.37
2016	0.04	1.00	0.38	1.02	0.01	0.02	0.50
2017	0.06	1.17	0.74	1.61	0.01	0.06	0.35
2018	0.07	1.15	0.85	2.14	0.01	0.01	0.32
2019	0.05	1.18	0.28	0.57	0.01	0.00	0.59
2020	0.05	0.90	0.60	1.43	0.01	0.01	0.38
2021	0.08	1.22	0.79	1.59	0.01	0.13	0.36
2022	0.08	1.22	0.77	1.60	0.01	0.13	0.37
AVERAGE	**0.08**	**1.22**	**0.79**	**1.59**	**0.01**	**0.13**	**0.36**

As entrances to the Señorío aquifer, there is an average recharge due to rainwater infiltration of 1.59 hm³/y, in addition, there is an entry through the coastline of 0.36 hm³ per year on average, the stream that crosses the aquifer would provide hardly any water (0.01 hm³/y). Artificially, an average injection of 0.13 hm³/y is produced through the Señorío wells.

Regarding the outflows, average extractions per pumping of 1.22 hm³/y are considered for the simulated period, and an average natural discharge to the sea of 0.79 hm³/y, while to the stream it would be 0.08 hm³/y.

This project has received funding from the European Union's Horizon Europe research and innovation programme under grant agreement No GA 101082048

Funded by the European Union

4.1.4 Piezometry

The following figures summarise the piezometry achieved over some periods of the simulation.

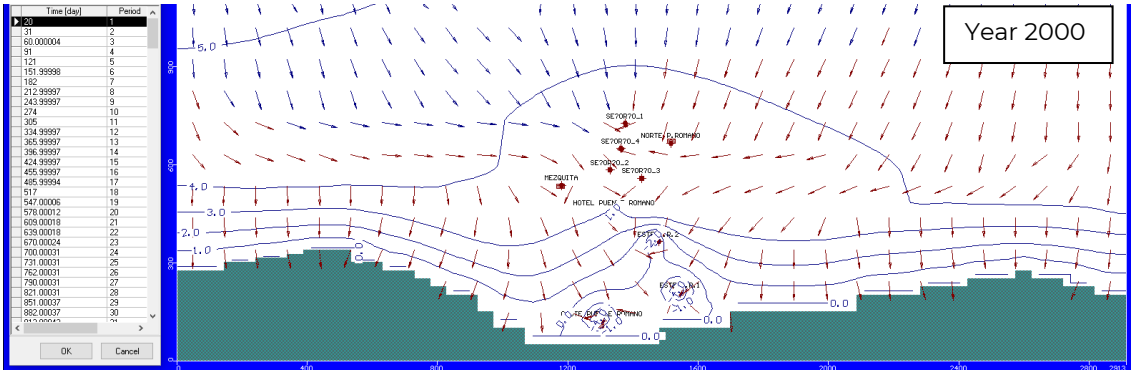

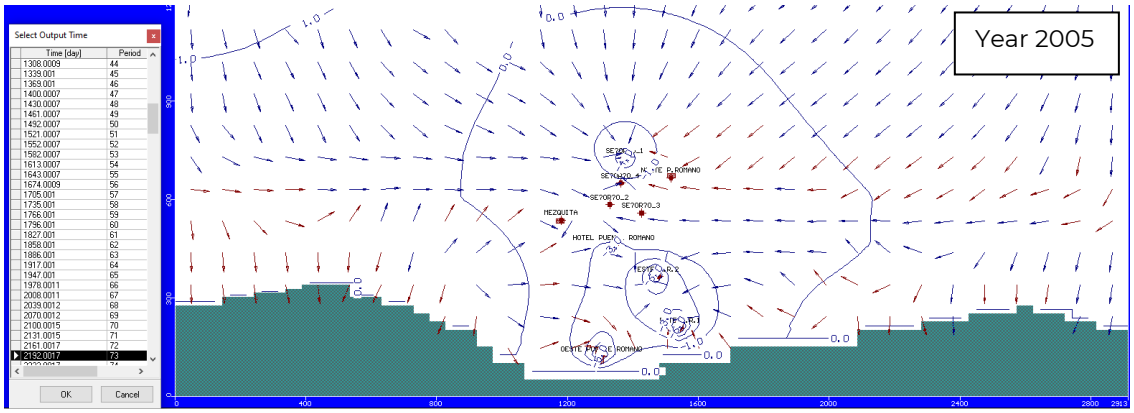

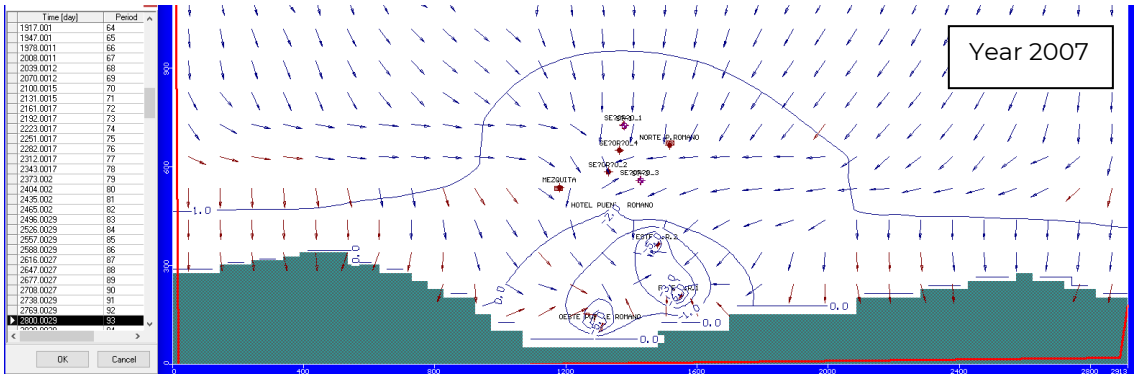

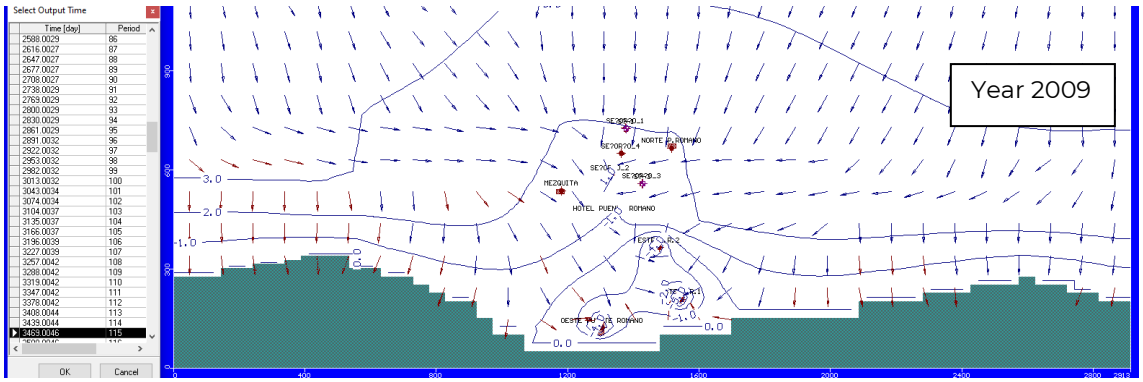

This project has received funding from the European Union's Horizon Europe research and innovation programme under grant agreement No GA 101082048

Funded by the European Union

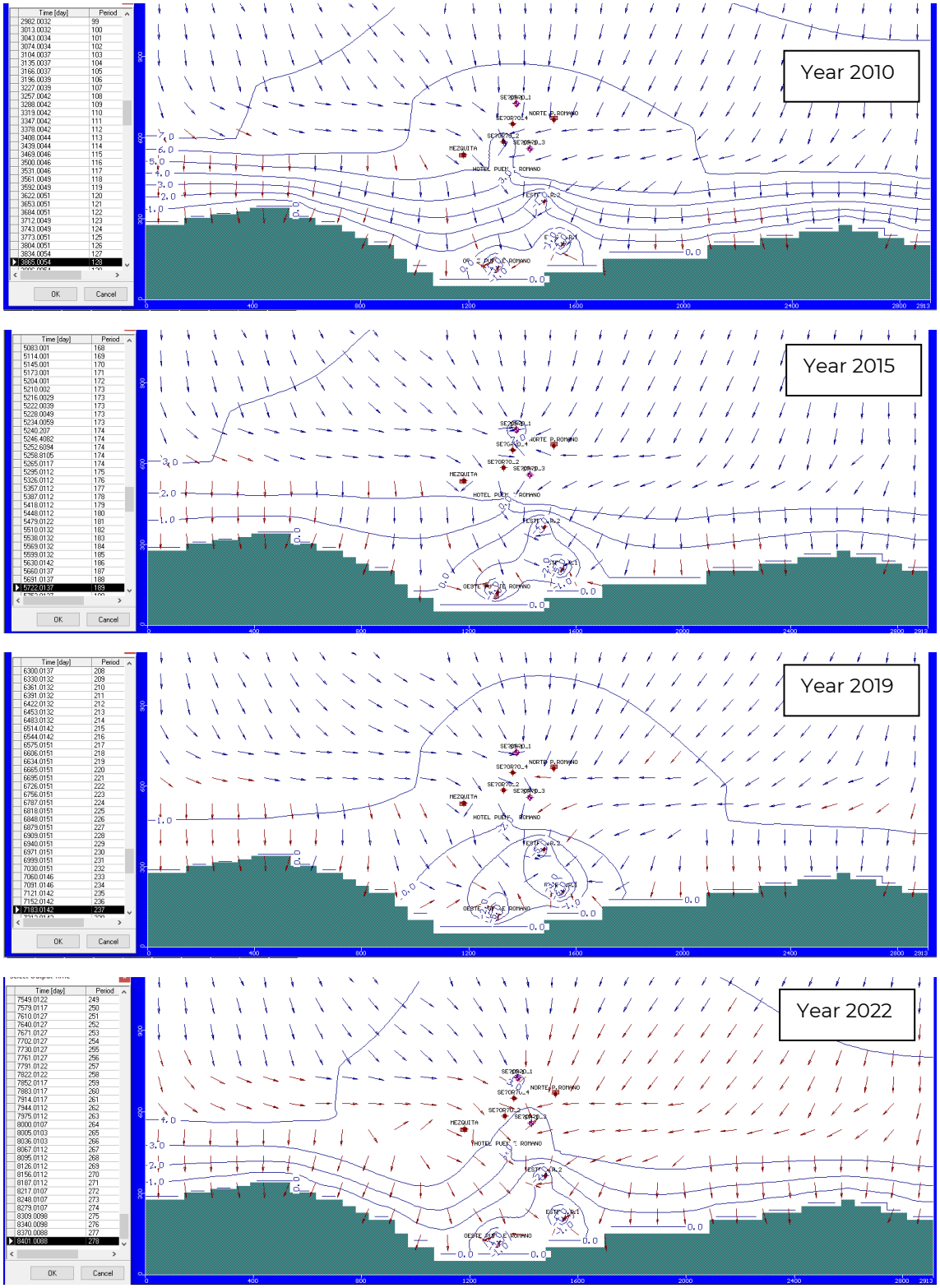

Figure 4.1-19 Piezometry distribution and flow direction over some simulation periods).

The direction and direction of the main flow is north-south, with a certain concentration towards the extraction points except in years when the farms exceed the annual average (1.22 hm^3/y) in which a concentric piezometry appears around the pumps, with inflows from the sea that represent average flows close to 0.36 hm^3/y, except on occasions where the infiltration of rainwater is 60% lower than the average (1 hm^3/y) in which maximum inflows from the sea of 0.61 hm^3/y could be reached.

This project has received funding from the European Union's Horizon Europe research and innovation programme under grant agreement No GA 101082048
Funded by the European Union

Logically, the inflows into the aquifer from the sea are conditioned not only by exploitation but also by the infiltration of rainwater and injection into boreholes.

The average annual piezometry around the Señorío boreholes is between 5-6 m a.s.l. and -4 to -6 m a.s.l.

However, in the simulated period, the outflows to the sea are twice as high as the inflows from the sea, although the piezometric reaches values below 0 m a.s.l., the flow of water comes from the aquifer (fresh water).

4.1.5 Numerical model uncertainties

As mentioned above, there is a certain degree of uncertainty regarding the withdrawals for private use considered in the model. Although the municipal wells of Señorío have periodic control of flows and piezometric levels, the same does not happen with the wells for private use.

In relation to the information reviewed, it has been observed that the wells have extracted an average flow of 0.65 hm^3/y, until the year 2000. From that year to the present, the exact volume of extraction and the pumping regime are unknown. Additionally, it has been observed that these wells are located in places with difficulty of access and mode of equipment, which has led to the absence of level measurements.

Due to the abovementioned, in the construction and calibration of the numerical model, average extractions have been considered for the entire period considering the historical extraction data measured until the year 2000. This extraction flow represents 53% of the total pumping of the aquifer (1.22 hm^3/y), which significantly influences the outputs of the numerical model (hydraulic parameters, piezometry and water balance). That is why the results obtained must be considered with caution.

On the other hand, it should be noted that, due to the uncertainty of the extraction flows of the modelled area, the initial level conditions from which to establish a robust steady-regime model are not exactly known.

4.1.6 Transport model results

From the edge condition imposed along the coastline, consisting of a chloride concentration of 19,000 mg/l, typical of seawater. The transport model indicates that the propagation of chlorides upstream of the aquifer would not affect the Señorío wells, even in the conditions where the greatest entry of seawater into the system occurs (the year 2005), remaining with values below the maximum concentration admissible for human consumption 250 mg/l (Royal Decree 140/2003).

However, there would be two wells, the wells closest to the coast (West and East of Puente Romano) that would reach concentrations much higher than 2,000 mg/l of chloride, specifically 10,639 mg/l in the West well of Puente Romano, and 4,903 mg/l in the East of Puente Romano 1.

This project has received funding from the European Union's Horizon Europe research and innovation programme under grant agreement No GA 101082048
Funded by the European Union

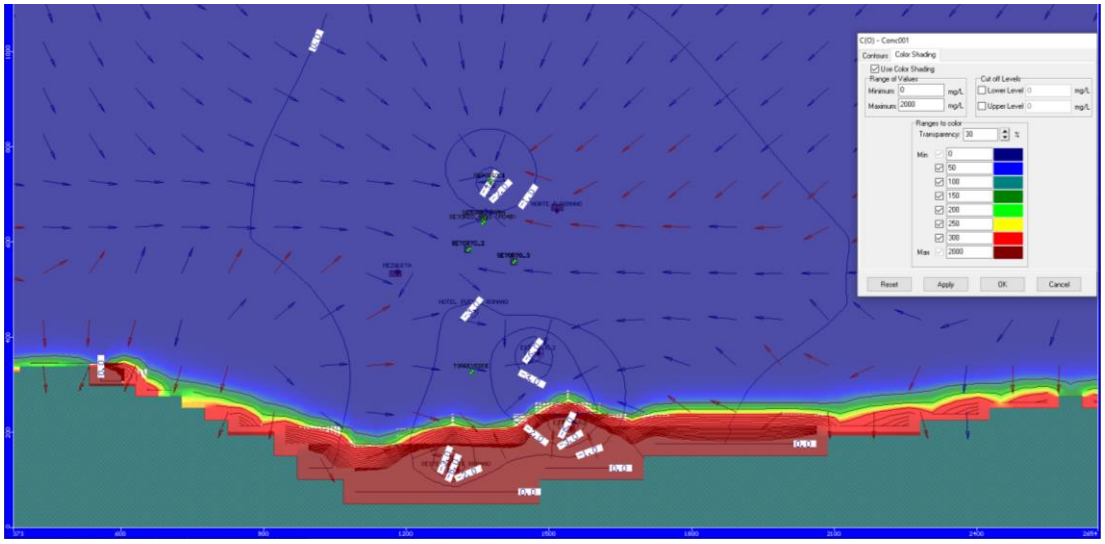

Figure 4.1-20 Detail of chloride propagation in 2005.

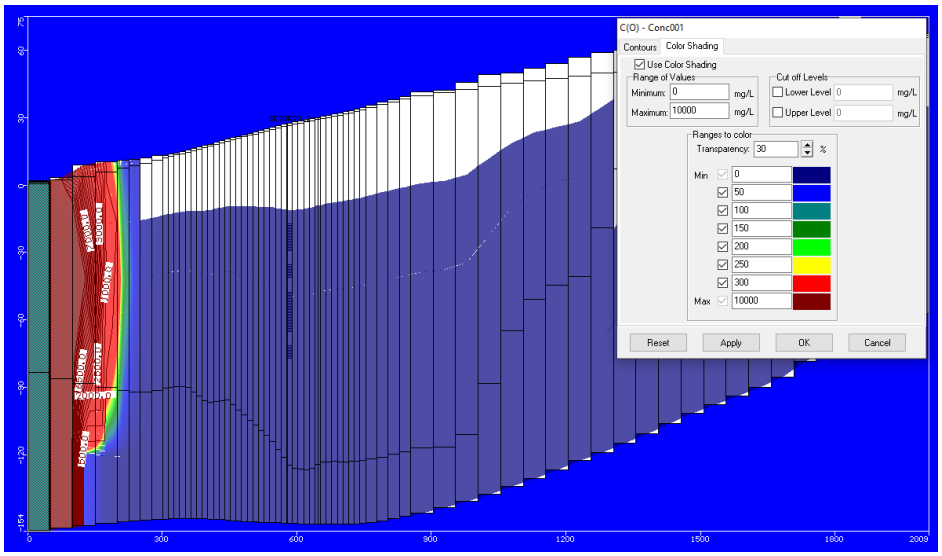

Figure 4.1-21 Detail of chloride propagation in an NS profile that crosses the Sñ-2 well (year 2005).

The lower permeability of the materials closest to the coast (0.5 m/d) favours the retention of the chloride ion in advance, even producing depression cones of up to -3 m a.s.l. (Hotel Puente Romano well) and -6 m a.s.l. (East Puente Romano 2 well).

4.1.6.1 Freshwater – saltwater simulation

On the other hand, in order to have a better approximation to reality, a second simulation has been carried out considering the difference in densities that exists between seawater and freshwater, in addition to their "typical" concentrations.

The greater density of seawater causes a wedge of saline intrusion in its displacement towards the aquifer that is located, due to a difference in densities, below the fresh water, leaving a transition zone or interface (mixture) between the two.

This project has received funding from the European Union's Horizon Europe research and innovation programme under grant agreement No GA 101082048

Funded by the European Union

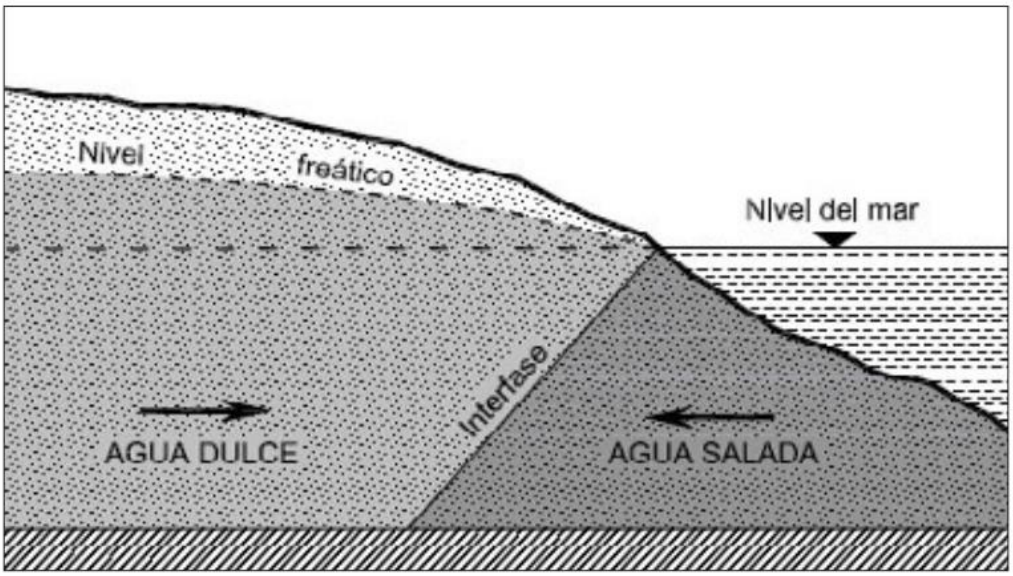

Figure 4.1-22 Schematic sketch of marine intrusion (López-Greta, J.A. & Gómez, Gómez, J.D, 2007)

For this reason, a new simulation has been carried out with the SEAWAT module, which establishes both the flow and transport models taking into account the difference in densities.

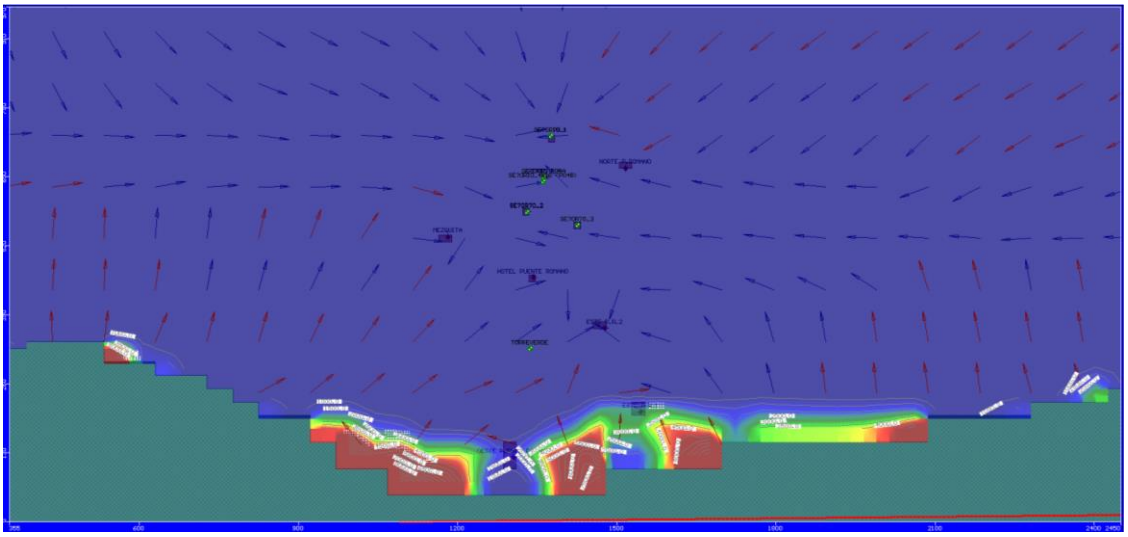

Figure 4.1-23 Detail of the marine intrusion in 2005.

In this case, the inflow of water is not carried out equally along the coastline but transition or mixing zones of between 1000 and 6000 mg/l are established at the surface that increase to at least 10,000 mg/l as the aquifer deepens.

In the following figures of concentration profiles, it can be seen that the highest concentration (brown) is located in the lowest area of the aquifer.

This project has received funding from the European Union's Horizon Europe research and innovation programme under grant agreement No GA 101082048

Funded by the European Union

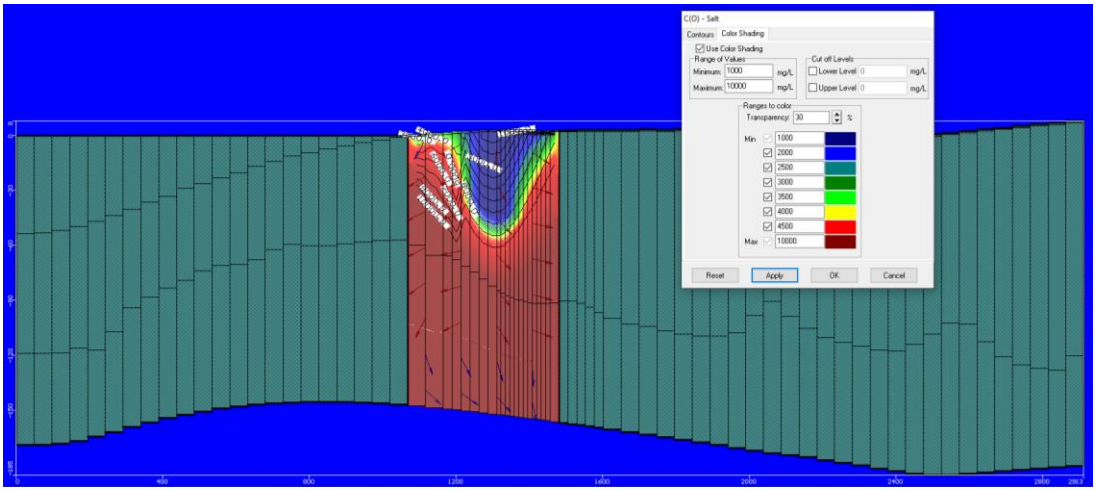

Figure 4.1-24 Detail of the marine intrusion in an EW profile that crosses the Puente Romano West sounding.

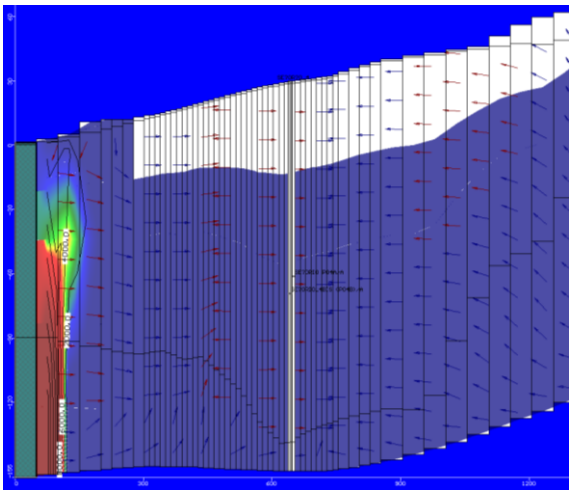

Figure 4.1-25 Detail of the marine intrusion in an NS profile that crosses the Sñ-2.

4.1.7 Simulation scenarios

4.1.7.1 Relationship of the Arroyo de Nagüeles with the aquifer

The introduction of the Nagüeles stream into the numerical model has been carried out considering its axis and the topography of the land. In addition, it has been assigned a conductance value that has made it possible to establish the transfer flow with the aquifer.

According to the data obtained, the stream, mainly in its initial section (to the north) clearly behaves as a winning section (0.08 hm^3/y), so that the aquifer cedes water to the stream, however, as it passes, this cession becomes less and less evident, due to the extraction of the Señorío wells that lower the piezometric level preventing the contribution of water to it. However, there is also a small transfer from the stream to the aquifer (0.01 hm^3/y).

This project has received funding from the European Union's Horizon Europe research and innovation programme under grant agreement No GA 101082048

Funded by the European Union

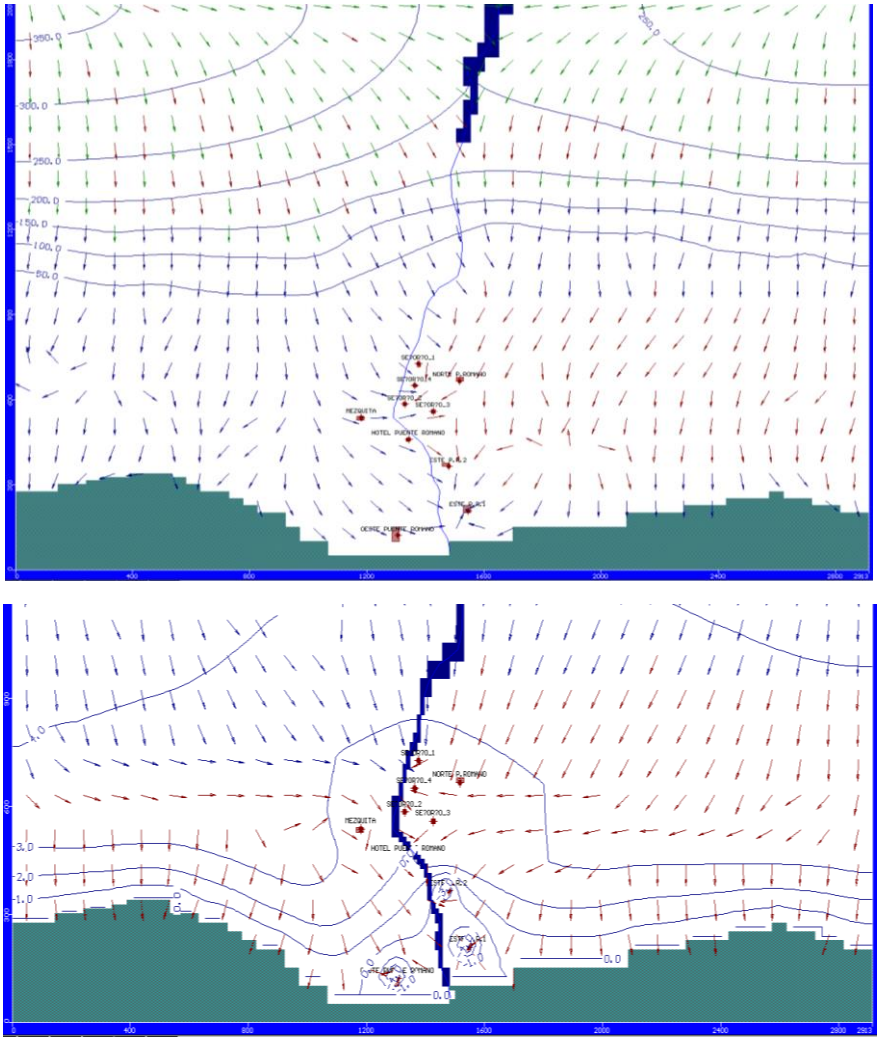

Figure 4.1-26 River-aquifer relationship.

4.2 DATA-REACH

4.2.1 RETROSPECTIVE CLIMATE ANALYSIS

A detailed analysis of the correlation between climatic indices and both chemical (physicochemical parameters) and quantitative status variables (piezometric levels) has been conducted. The main objective of this analysis is to identify signs of temporal deterioration of the Marbella-Estepona groundwater body.

To achieve this, an analysis of two climatic indices (SPI and SPEI) has been carried out at different points in the study area. Subsequently, droughts associated with these indices have been identified, and correlations between these indices and piezometry and water quality parameters have been obtained.

4.2.1.1 CALCULATION OF THE CLIMATIC INDICES

The registration period differs for both indices, as the one corresponding to temperature, required by the SPEI, is shorter than that of precipitation (Table 4.2-1). Thus, the SPI could be calculated from September 1995 (data from October 1994), and the SPEI from November 1999 (data from December 1998). This lag at the start of the registration period with the first value of the indices is because the SPI and SPEI are calculated on a 12-month time scale, and therefore the value of the first month of the

This project has received funding from the European Union's Horizon Europe research and innovation programme under grant agreement No GA 101082048
Funded by the European Union

series is calculated using the previous twelve-monthly data. The end of the registration period, however, is the same for all, May 2023.

Table 4.2-1 Climate indices calculated in this study and registration periods.

CLIMATE INDEX	DATA PERIOD	INDEX PERIOD
SPI	October-94 / May-23	September-95 / May-23
SPEI	December-98 / May-23	November-99 / May-23

Calculation of the Standardised Precipitation Index (SPI)

For the computation of the Standardised Precipitation Index (SPI) in the study area, climatic information has been gathered. In this instance, the recorded variable was precipitation, collected from the 10 selected pluviometric stations for the climatic analysis.

All of them have a recording period, previously completed and processed, of 27 years (01/10/1994 - 01/05/2023), with the exception of two stations, Manilva and Puerto Banús, which have a 32-year record (01/01/1990 - 01/05/2023). The decision was made to consider the SPI from the shorter record as valid, thereby simplifying and making more representative the comparison of the SPI across all 10 stations.

Figure 4.2-1 displays the generated SPI indices for the selected 10 stations. The SPI trends are very similar across all stations, allowing for the detection of alternating wet and dry periods throughout the study period.

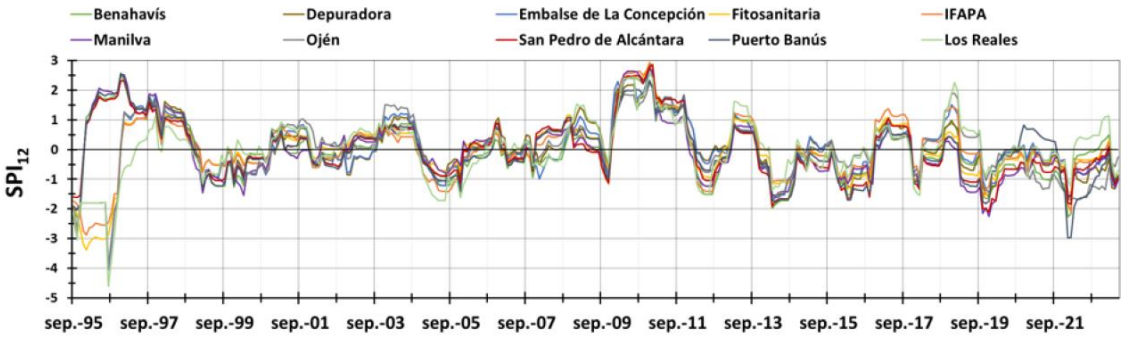

Figure 4.2-1 Evolution of the Standardised Precipitation Indices (SPI12) during the period 01/09/1995 - 01/05/2023 at the rain gauge stations in the study area.

In this large-scale comparison, it is worth noting the wettest period identified in the years 2009/10-2010/11, during which SPI values of up to 2.93 were reached at the IFAPA station in December 2010. The second wettest period detected is that of the year 1996/97, with a maximum SPI value of 2.57 at the Puerto Banús station.

Conversely, the driest period that can be identified spans from 2019 to the end of the record. During this period, values of up to 2.98 were recorded in January 2022 at the Puerto Banús station. It is important to highlight the presence of pronounced peaks corresponding to the very negative values reached in August 1996 at some stations: Los Reales, Embalse de la Concepción, Depuradora and Ojén, where the SPI reaches values of -4.7, -4.07, -3.97 and -3.93, respectively.

The significant disparity in the Standardised Precipitation Index (SPI) values for the month in question at these stations, compared to the others, has led to a review of the

This project has received funding from the European Union's Horizon Europe research and innovation programme under grant agreement No GA 101082048
Funded by the European Union

monthly precipitation series corresponding to these stations. In this analysis, it was observed that not a single millimetre of rain was recorded at these four stations from December 1994 to August 1996, after which rain values were recorded again. The complete absence of precipitation records in these series over a 20-month period explains the extremely negative SPI value generated for August 1996.

If we look at the source of the data for these stations, it is worth emphasising that they all belong to the SAIH network. In contrast, those that do not belong to this network do not present such a marked peak in that year. In fact, there is not even a negative value for the month of August 1996. This fact is highly significant and should be taken into account when choosing reference stations. The very negative values would indicate a very pronounced meteorological drought of great intensity, but it would then be unexplainable why the rest of the stations did not detect any drought period.

However, in addition to the SAIH stations, there are two stations, Fitosanitaria and IFAPA, which significantly differ in the first months of recording compared to the other stations. It is important to note that the first five years of recording at these stations lacked data, which required their completion. Although they could be completed by linear regression with the other stations, the fact that it is a period of several years implies that the data are not completely reliable.

For all these reasons, it has been decided to recalculate the SPI for all stations by reducing the recording period, thus eliminating the months in which it is considered that the SAIH stations have erroneous records and the other two stations reduce the number of years in which they lacked data at the beginning. This new calculation starts from data since August 1996 and therefore the start of the SPI values begins in July 1997. Figure 4.2-2 shows the SPI series calculated with the reduced period (Jul-97/May-23).

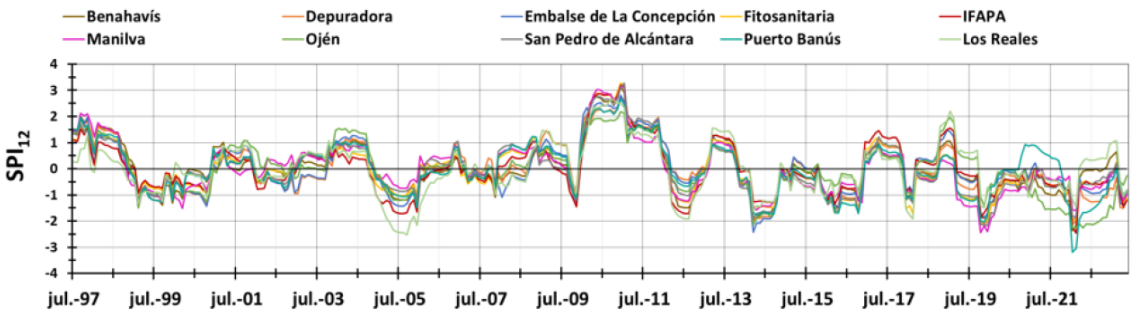

Figure 4.2-2 Evolution of the Standardised Precipitation Indices (SPI12) during the period 01/07/1997 - 01/05/2023 at the rain gauge stations in the study area.

Even after shortening the period, some discrepancies have been detected again for certain periods of specific stations (those belonging to the SAIH) and the monthly precipitation series have been analysed in greater detail. It has been found that some months contain inconsistent rainfall data, always less than expected compared to the stations from the other three data sources (AEMET, IFAPA and RAIF). For this reason, it has been decided to definitively eliminate the SAIH stations for the calculation of climate indices. The stations finally selected were Benahavís, Fitosanitaria, IFAPA, Manilva, San Pedro de Alcántara and Puerto Banús (Figure 4.2-3).

This project has received funding from the European Union's Horizon Europe research and innovation programme under grant agreement No GA 101082048
Funded by the European Union

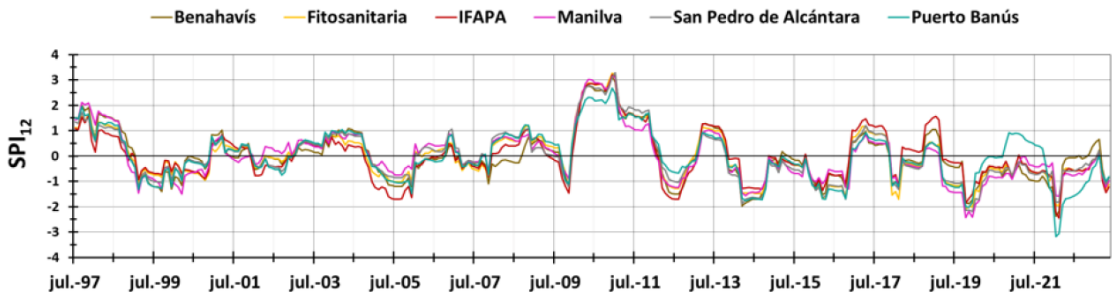

Figure 4.2-3 Evolution of the Standardised Precipitation Indices (SPI12) during the period 01/07/1997 - 01/05/2023 at the selected rain gauge stations in the study area.

A comparative analysis of the SPI of the different stations has been carried out, using the coefficient of determination (R^2) for the calculation period (Figure 4.2-4). All stations show high correlation values with each other, with a range between 0.75 (between the IFAPA station and the Puerto Banús station) and 0.95 (between the Fitosanitaria and San Pedro de Alcántara stations).

	Benahavís	Fitosanitaria	IFAPA	Manilva	San Pedro de Alcántara	Puerto Banús
Benahavís	1					
Fitosanitaria	0,88	1				
IFAPA	0,86	0,89	1			
Manilva	0,83	0,91	0,77	1		
San Pedro de Alcántara	0,87	0,95	0,84	0,91	1	
Puerto Banús	0,76	0,83	0,75	0,78	0,85	1

Figure 4.2-4 Observed correlations (R2) of the SPI12 indices among the different rain gauge stations during the period from July 1997 to May 2023.

Calculation of the Standardised Precipitation Evapotranspiration Index (SPEI)

For the calculation of the Standardised Precipitation Evapotranspiration Index (SPEI) in the study area, climatic information has been gathered. In this case, the recorded variables were precipitation and temperature from the six selected pluviometric stations for the calculation of the aforementioned index.

The calculation period is reduced compared to the SPI because the temperature data have a shorter length than the precipitation data. Therefore, the index is restricted to the period between November 1999 and May 2023.

Given that not all stations have temperature recording data, the temperature data from the nearest stations that do have this meteorological variable have been assigned to these stations. In all these cases, the IFAPA station has been selected as the closest one to carry out this assignment (Table 4.2-2). It is worth noting that the Fitosanitaria station has not been considered for the temperature because irregularities have been identified in the completed data series of this station.

Table 4.2-2 Association of temperature with stations that do not present this meteorological variable. Stations where the temperature record of the same station has been used are represented with an equal sign (=).

STATION	CHOSEN TEMPERATURE
Benahavis	=

This project has received funding from the European Union's Horizon Europe research and innovation programme under grant agreement No GA 101082048
Funded by the European Union

Fitosanitaria	**IFAPA**
IFAPA	=
Manilva	**IFAPA**
San Pedro de Alcántara	**IFAPA**
Puerto Banús	=

The evolutions of the SPEI index at the different stations are shown in Figure 4.2-5.

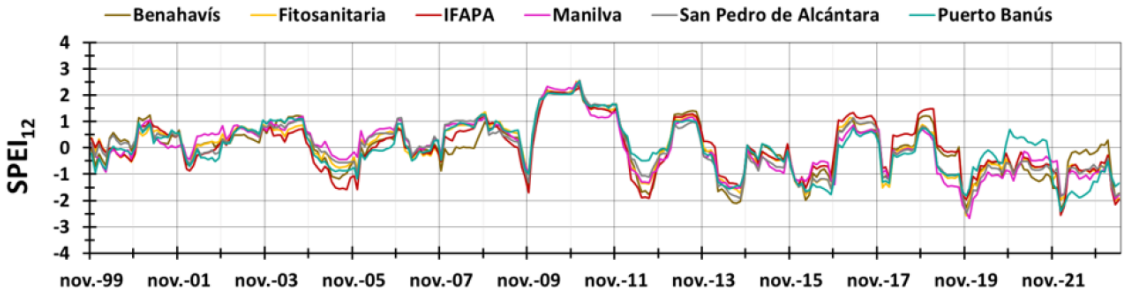

Figure 4.2-5 Evolution of the Standardised Precipitation Evapotranspiration Indices (SPEI12) during the period 01/11/1999 - 01/05/2023 at the selected rain gauge stations in the study area.

The evolutions of the SPEI, like those of the SPI, are very similar and also allow the detection of alternating wet and dry periods at all stations throughout the study period. The wettest period identified is that of the year 2009/10 and the driest corresponds to the period from 2019 to the end of the record.

A comparative analysis of the SPEI for the different stations has been carried out, using the coefficient of determination (R^2) for the calculation period (Figure 4.2-6). All stations show high correlation values among them, with a range between 0.73 and 0.95, very similar to that obtained with the SPI (0.75 and 0.95). With the SPEI, the lowest correlation occurs between the Benahavís and Puerto Banús stations. The highest correlation coincides with that obtained for the SPI, between the Fitosanitaria and San Pedro de Alcántara stations.

	Benahavís	Fitosanitaria	IFAPA	Manilva	San Pedro de Alcántara	Puerto Banús
Benahavís	1					
Fitosanitaria	0,87	1				
IFAPA	0,86	0,88	1			
Manilva	0,78	0,92	0,77	1		
San Pedro de Alcántara	0,86	0,95	0,84	0,92	1	
Puerto Banús	0,73	0,84	0,74	0,77	0,84	1

Figure 4.2-6 Evolution of the Standardised Precipitation Evapotranspiration Indices (SPEI12) during the period 01/11/1999 - 01/05/2023 at the selected rain gauge stations in the study area.

This project has received funding from the European Union's Horizon Europe research and innovation programme under grant agreement No GA 101082048
Funded by the European Union

4.2.1.2 RELATIONSHIP BETWEEN INDICES AND QUANTITATIVE STATUS

The stations used in the calculation of SPI and SPEI for correlation with quality data will be those of IFAPA, San Pedro de Alcántara, and Puerto Banús. Therefore, these will be the ones selected for the analysis with piezometry.

Despite selecting piezometric control points with the most extensive record series, it has been observed that most of them have a record that is shorter than that obtained for SPI and SPEI. This complicates the analysis of the evolution of these indices with the evolution of piezometric levels.

In the evolution of piezometric levels of the control points analysed with the climatic indices calculated at the IFAPA station, no apparent relationships between the piezometric levels and the indices have been identified. That is, the piezometry at these control points does not clearly identify periods of drought and wet periods that the SPI and SPEI indices have been able to detect (Figure 4.2-7). It is true that the drought identified from the climatic indices, from 2019 to the present, is somewhat reflected in the piezometric maximums, which tend to be increasingly lower. Both piezometers mainly capture the Pliocene aquifer of Estepona.

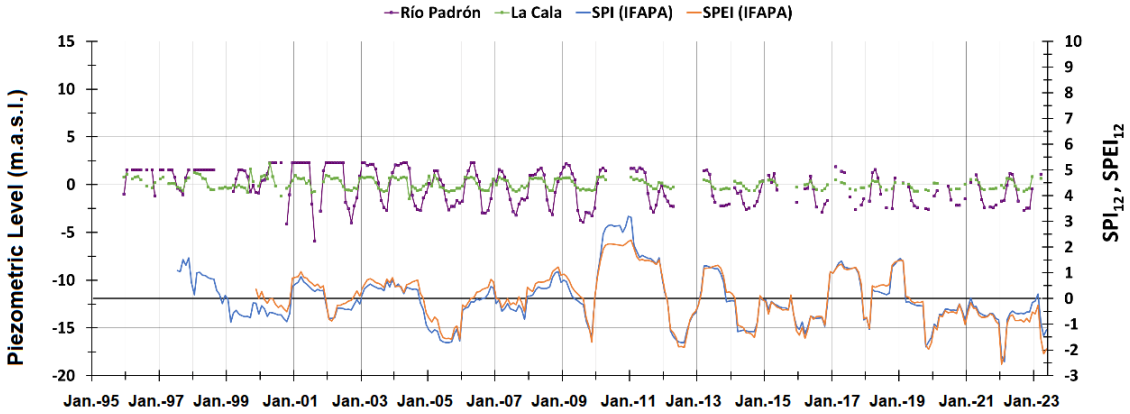

Figure 4.2-7 Evolution of the piezometric series of points P-2 and P-3 and the SPI and SPEI indices of the IFAPA station for the study period.

In the case of the evolution of piezometric levels of the points related to the indices of the San Pedro de Alcántara station, there does appear to be some correlation with the climatic indices (Figure 4.2-8). When these detected the drought of 1998/99, the piezometric level of Pz-2 (P-7) dropped significantly. Furthermore, the wet period of 2009/10-2010/11 detected by both indices is also reflected in the piezometric maximums reached by the piezometry of point C.Sky1 (P-17) for those years. On the other hand, the drought detected from 2019 to the end of the record can also be seen in the maximum values of both piezometric evolutions, with a trend for these values to be increasingly lower. The P-17 borehole is located in the Pliocene materials of San Pedro de Alcántara, where exploitation is carried out during the recharge months.

This project has received funding from the European Union's Horizon Europe research and innovation programme under grant agreement No GA 101082048
Funded by the European Union

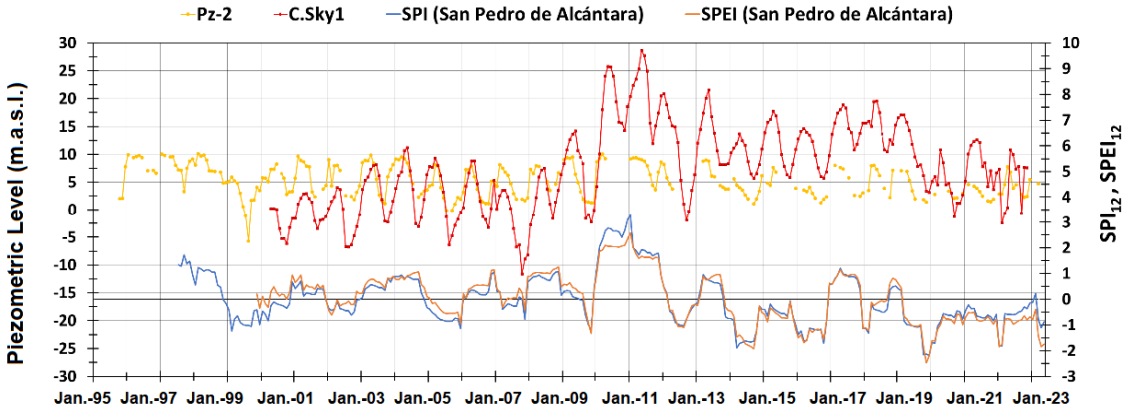

Figure 4.2-8 Evolution of the piezometric series of points P-7 and P-17 and the SPI and SPEI indices of the Pedro station for the study period.

Finally, in the case of the piezometric evolutions of the points analysed with the indices at the Puerto Banús station, certain relationships can also be observed (Figure 4.2-9). Señorío 2 (P-24) reflects the drought detected by the SPI in 1998/99, as the piezometric levels significantly decreased. For the wet year 2009/10, a piezometric peak is also detected. Similar to the previous figure, a general downward trend of the piezometric peaks is observed as the dry period begins in 2019. For the other two control points, Real Zaragoza (P-15) and RVMB3 (P-21), these are not as evident, especially in the latter due to its discontinuity in the record.

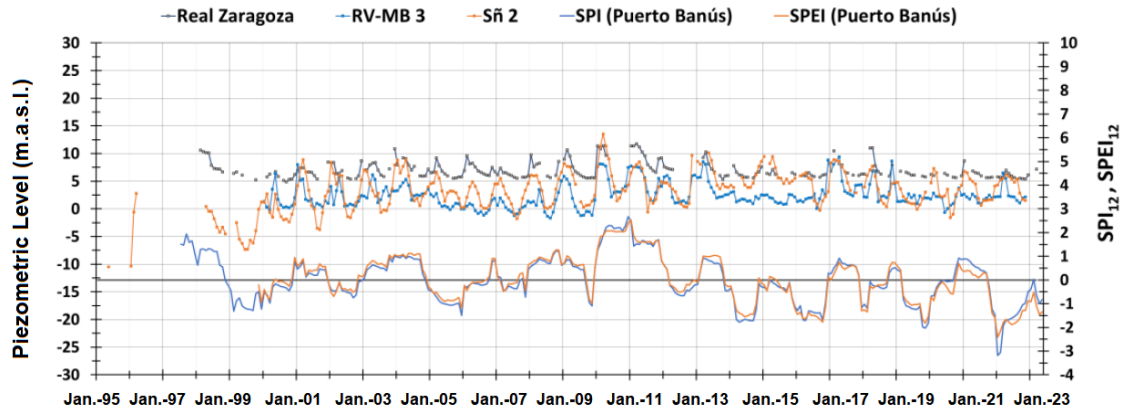

Figure 4.2-9 Evolution of the piezometric series of points P-15, P-21 and P-24 and the SPI and SPEI indices of the Puerto station for the study period.

Despite the potential relationships identified, there is a factor to consider. Some control points of the Marbella-Estepona groundwater body, such as Señorío 2, have been used for the artificial recharge of the Señorío de Marbella aquifer since 2000. Therefore, piezometric rises may not be exclusively related to rainy periods, but also to artificial recharge events.

Moreover, most of these aquifers are subject to intense exploitation of their resources, adding another layer of complexity to their analysis. The extraction of groundwater can cause piezometric declines not necessarily related to dry periods. On the other hand, the fact that some control points are springing in certain years, like the Río Padrón well, further complicates the interpretation of piezometric levels in relation to climatic indices, especially during wet periods.

Therefore, the information provided by the piezometric evolutions should be cross-referenced with subsequent research on artificial recharge events and the

This project has received funding from the European Union's Horizon Europe research and innovation programme under grant agreement No GA 101082048
Funded by the European Union

exploitation of aquifers by pumping, both by distribution companies and individuals, as these practices may be altering the natural climatic signal.

4.2.1.3 RELATIONSHIP BETWEEN INDICES AND CHEMICAL STATUS

The indices calculated in this study, SPI and SPEI, have been related to different quality parameters of the groundwater body under study to try to identify correlations between them.

In the analysis of temporal deterioration due to drought events, 15 hydrochemical parameters have been compiled from each of the six sampling points, distributed throughout the Marbella-Estepona groundwater body. The data comes from a selection of the 34 existing parameters that were initially available (Figure 4.2-10), but which have been discarded due to the high absence of data or their lack of relevance to the study.

		Nº samples per control point						
		Monterroso	Río Verde	Río Padrón	Señorío	Atalaya	Elviria	Total nº samples
Parameters	Alkalinity	8	4	9	5	8	8	42
	Ammonium	37	11	33	15	12	12	120
	Bicarbonates	23	11	19	15	12	12	92
	Calcium	10	5	11	7	10	10	53
	Dissolved Calcium	13	6	0	0	0	0	19
	Carbonates	8	4	9	5	8	8	42
	TOC	10	5	11	7	10	10	53
	Chlroides	37	11	33	15	12	12	120
	Total Coliforms	8	4	0	0	0	0	12
	Conductivity in situ (20°C)	37	11	33	14	12	12	119
	Escherichia Coli	4	2	0	0	0	0	6
	Fluorides	37	11	33	15	12	12	120
	Phosphates	35	10	31	15	10	10	111
	Magnessium	10	5	11	7	10	10	53
	Dissolved Magnessium	27	6	22	8	2	2	67
	Total Magnessium	14	0	14	0	0	0	28
	Organic Matter	2	1	2	0	2	2	9
	Nitrates	74	22	66	30	26	26	244
	Nitrites	37	11	33	15	12	12	120
	Total Nitrogen	1	0	0	0	0	0	1
	Piezometric level	1	6	0	0	0	0	7
	Piezometric level (monitored)	2	0	0	0	0	0	2
	Dissolved Oxygen (in situ)	10	4	34	6	14	9	77
	PAHs D. 75/440/CEE Max Sum	6	3	7	4	6	6	32
	PAHs D. 75/440/CEE Min Sum	6	3	7	4	6	6	32
	pH	0	0	0	1	0	0	1
	pH (in situ)	37	11	33	14	12	12	119
	Potassium	10	5	0	0	0	0	15
	Dissolved Potassium	13	6	0	0	0	0	19
	Sodium	10	5	11	7	10	10	53
	Dissolved Sodium	13	6	8	8	2	2	39
	Suspended solids	8	4	0	0	0	0	12
	Sulphates	36	11	33	15	12	12	119
	Temperature (in situ)	37	11	33	15	12	12	120

Figure 4.2-10 Number of existing samples of each parameter at each sampling station during the historical record.

A detailed analysis of the periodicity of sample collection has been conducted to aid in the simplification of selected parameters, which can be summarised in Figure 4.2-11.

The correlations between the selected parameters and the indices of this study are shown in

Figure 4.2-12 - Figure 4.2-16. Values in red tones represent a negative correlation and those in green tones, a positive correlation. Significant correlations (moderate and high) are identified with a Pearson correlation limit of $r > 0.5$ and $r < -0.5$, and low magnitude correlations with $r > 0.3$ and $r < -0.3$. A significance level of 0.05 has been used for the calculation of correlations.

This project has received funding from the European Union's Horizon Europe research and innovation programme under grant agreement No GA 101082048
Funded by the European Union

It is worth noting the limited availability of samples. In this study, only parameters with a total number of observations equal to or greater than 10 samples have been considered, as with a lower number the result is hardly representative.

	Control point	Start	End	Frequency	N° samples
Alkalinity	Monterroso	08/03/2011	27/10/2015	2 / year	8
	Río Verde	08/03/2011	29/04/2015	1 / year	4
	Río Padrón	08/03/2011	29/10/2015	2 / year	9
	Señorío	21/05/2013	08/10/2015	2 / year	5
	Atalaya	08/03/2011	29/10/2015	2 / year	8
	Elviria	08/03/2011	18/11/2015	2 / year	8
Ammonium	Monterroso	08/03/2011	17/02/2023	2 / year	37
	Río Verde	08/03/2011	22/02/2023	1 / year	11
	Río Padrón	08/03/2011	16/02/2023	2 / year	33
	Señorío	24/05/2012	18/03/2022	2 / year	15
	Atalaya	08/03/2011	18/10/2017	2 / year	12
	Elviria	08/03/2011	18/10/2017	2 / year	12
Bicarbonates	Monterroso	08/03/2011	17/02/2023	2 / year	23
	Río Verde	08/03/2011	22/02/2023	1 / year	11
	Río Padrón	08/03/2011	16/02/2023	2 / year	19
	Señorío	24/05/2012	18/03/2022	2 / year	15
	Atalaya	08/03/2011	18/10/2017	2 / year	12
	Elviria	08/03/2011	18/10/2017	2 / year	12
Calcium	Monterroso	08/03/2011	27/10/2015	2 / year	10
	Río Verde	08/03/2011	29/04/2015	1 / year	5
	Río Padrón	08/03/2011	29/10/2015	2 / year	11
	Señorío	24/05/2012	08/10/2015	2 / year	7
	Atalaya	08/03/2011	29/10/2015	2 / year	10
	Elviria	08/03/2011	18/11/2015	2 / year	10
Dissolved Calcium	Monterroso	23/03/2017	17/02/2023	2 / year	13
	Río Verde	23/03/2017	22/02/2023	1 / year	6
	Río Padrón	-	-	-	0
	Señorío	-	-	-	0
	Atalaya	-	-	-	0
	Elviria	-	-	-	0

	Control point	Start	End	Frequency	N° samples
Carbonates	Monterroso	08/03/2011	27/10/2015	2 / year	8
	Río Verde	08/03/2011	29/04/2015	1 / year	4
	Río Padrón	08/03/2011	29/10/2015	2 / year	9
	Señorío	21/05/2013	08/10/2015	2 / year	5
	Atalaya	08/03/2011	29/10/2015	2 / year	8
	Elviria	08/03/2011	18/11/2015	2 / year	8
TOC	Monterroso	08/03/2011	27/10/2015	2 / year	10
	Río Verde	08/03/2011	29/04/2015	1 / year	5
	Río Padrón	08/03/2011	29/10/2015	2 / year	11
	Señorío	24/05/2012	08/10/2015	2 / year	7
	Atalaya	08/03/2011	29/10/2015	2 / year	10
	Elviria	08/03/2011	18/11/2015	2 / year	10
Chlorides	Monterroso	08/03/2011	17/02/2023	2 / year	37
	Río Verde	08/03/2011	22/02/2023	1 / year	11
	Río Padrón	08/03/2011	16/02/2023	2 / year	33
	Señorío	24/05/2012	18/03/2022	2 / year	15
	Atalaya	08/03/2011	18/10/2017	2 / year	12
	Elviria	08/03/2011	18/10/2017	2 / year	12
Total Coliforms	Monterroso	08/03/2011	27/10/2015	2 / year	8
	Río Verde	08/03/2011	29/04/2015	1 / year	4
	Río Padrón	-	-	-	0
	Señorío	-	-	-	0
	Atalaya	-	-	-	0
	Elviria	-	-	-	0
Cond. in situ 25°C	Monterroso	08/03/2011	17/02/2023	2 / year	37
	Río Verde	08/03/2011	22/02/2023	1 / year	11
	Río Padrón	08/03/2011	16/02/2023	2 / year	33
	Señorío	24/05/2012	18/03/2022	2 / year	14
	Atalaya	08/03/2011	18/10/2017	2 / year	12
	Elviria	08/03/2011	18/10/2017	2 / year	12

	Control point	Start	End	Frequency	N° samples
E Coli	Monterroso	08/03/2011	23/10/2012	2 / year	4
	Río Verde	08/03/2011	29/05/2012	1 / year	2
	Río Padrón		-	-	0
	Señorío	-	-	-	0
	Atalaya	-	-	-	0
	Elviria	-	-	-	0
Fluorides	Monterroso	08/03/2011	17/02/2023	2 / year	37
	Río Verde	08/03/2011	22/02/2023	1 / year	11
	Río Padrón	08/03/2011	16/02/2023	2 / year	33
	Señorío	24/05/2012	18/03/2022	2 / year	15
	Atalaya	08/03/2011	18/10/2017	2 / year	12
	Elviria	08/03/2011	18/10/2017	2 / year	12
Phosphates	Monterroso	24/05/2012	17/02/2023	2 / year	35
	Río Verde	29/05/2012	22/02/2023	1 / year	10
	Río Padrón	23/05/2012	16/02/2023	2 / year	31
	Señorío	24/05/2012	18/03/2022	2 / year	15
	Atalaya	23/05/2012	18/10/2017	2 / year	10
	Elviria	28/05/2012	18/10/2017	2 / year	10
Magnesium	Monterroso	08/03/2011	27/10/2015	2 / year	10
	Río Verde	08/03/2011	29/04/2015	1 / year	5
	Río Padrón	08/03/2011	29/10/2015	2 / year	11
	Señorío	24/05/2012	08/10/2015	2 / year	7
	Atalaya	08/03/2011	29/10/2015	2 / year	10
	Elviria	08/03/2011	18/11/2015	2 / year	10

	Control point	Start	End	Frequency	N° samples
Dissol. Magnesium	Monterroso	23/03/2017	17/02/2023	2 / year	27
	Río Verde	23/03/2017	22/02/2023	1 / year	6
	Río Padrón	23/03/2017	16/02/2023	2 / year	22
	Señorío	21/03/2017	18/03/2022	2 / year	8
	Atalaya	23/03/2017	18/10/2017	2 / year	2
	Elviria	21/03/2017	18/10/2017	2 / year	2
Total Magnesium	Monterroso	20/09/2021	06/07/2022	7 / year	14
	Río Verde	20/09/2021	06/07/2022	7 / year	0
	Río Padrón	-	-	-	14
	Señorío	-	-	-	0
	Atalaya	-	-	-	0
	Elviria	-	-	-	0
Organic Matter	Monterroso	08/03/2011	17/08/2011	2 / year	2
	Río Verde	08/03/2011	08/03/2011	1	1
	Río Padrón	08/03/2011	17/08/2011	2 / year	2
	Señorío	-	-	-	0
	Atalaya	08/03/2011	17/08/2011	2 / year	2
	Elviria	08/03/2011	17/08/2011	2 / year	2

Figure 4.2-11 Recording period and approximate frequency for each parameter and station. It is represented with a dash where there is no data.

For the specific case of the "Atalaya" sampling point, significant correlations have been identified between certain variables (

Figure 4.2-12). The correlations of the indices, both SPI and SPEI, with the variables are very similar. The highest significant correlations correspond to chloride, electrical conductivity (EC), sodium, temperature and sulphate, all of them also with statistical significance (SS) except for the latter. The mentioned correlations are negative, meaning that higher climatic index values (episodes without prolonged drought) are associated with lower values of the mentioned variables and vice versa. The first case

This project has received funding from the European Union's Horizon Europe research and innovation programme under grant agreement No GA 101082048
Funded by the European Union

could be explained by the dilution effect of groundwater by rainwater infiltration. There are other variables with lower magnitude correlations, such as calcium, fluorides and nitrates. It is worth noting that the only positive correlation is that of nitrates, and this could be explained by the fact that, during rain events, there is a drag of nutrients (soil washing) and these finally penetrate the aquifer.

The fact that EC and the contents of chloride and sodium, related to marine intrusion processes, are lower in wet periods could also be explained by the extrusion of saltwater towards the sea due to the recharge of the aquifers during these periods.

	SPI (Pedro)	SPEI (Pedro)	N° samples
Bicarbonates	-0.20	-0.16	12
Calcium	-0.39	-0.33	10
TOC	-0.30	-0.28	10
Chlroides	-0.6 (SS)	-0.58 (SS)	12
Conductivity in situ (20°C)	-0.76 (SS)	-0.73 (SS)	12
Fluorides	-0.48	-0.45	12
Phosphates	0.18	0.15	10
Magnessium	-0.29	-0.29	12
Nitrates	0.42	0.37	14
Dissolved Oxygen (in situ)	Insufficient amount of data		7
pH (in situ)	-0.27	-0.27	12
Potassium	Insufficient amount of data		0
Sodium	-0.65 (SS)	-0.63 (SS)	12
Sulphates	-0.52	-0.50	12
Temperature (in situ) (20°C)	-0.64 (SS)	-0.6 (SS)	12

Figure 4.2-12 Existing correlations between the two climate indices calculated and the chemical status variables (physicochemical parameters) of the sampling point 'Atalaya'.

In the case of the "Elviria" sampling station, the highest correlations have been detected in bicarbonates, also with statistical significance (Figure 4.2-13). Other variables that also present moderate and high correlations are calcium, total organic carbon and sodium. Among the low-magnitude correlations is EC. All the mentioned correlations are negative. As in the Atalaya station, the correlations obtained are very similar for the SPI and the SPEI. This may be due to the high correlation between both indices.

	SPI (Puerto)	SPEI (Puerto)	N° samples
Bicarbonates	-0.79 (SS)	-0.78 (SS)	12
Calcium	-0.59	-0.61	10
TOC	-0.50	-0.46	10
Chlroides	-0.19	-0.22	12
Conductivity in situ (20°C)	-0.40	-0.39	12
Fluorides	0.16	0.18	12
Phosphates	0.00	0.08	10
Magnessium	0.12	0.07	12
Nitrates	-0.12	-0.02	14
Dissolved Oxygen (in situ)	Insufficient amount of data		4
pH (in situ)	0.17	0.15	12
Potassium	Insufficient amount of data		0
Sodium	-0.62	-0.62	10
Sulphates	-0.21	-0.22	12
Temperature (in situ) (20°C)	-0.02	-0.04	12

This project has received funding from the European Union's Horizon Europe research and innovation programme under grant agreement No GA 101082048

Funded by the European Union

Figure 4.2-13 Existing correlations between the two climate indices calculated and the chemical status variables (physicochemical parameters) of the sampling point 'Elviria'.

At the "Monterroso" sampling point, the highest correlations have been detected in calcium (negative) and potassium (positive) (Figure 4.2-14). Although the calcium with the SPEI is the only one that exceeds r < -0.5, statistical significance has been detected in all. Low magnitude correlations have also been detected in chloride, magnesium, EC, sodium and sulphates, the last three only with one index, but with both close to 0.3. In this case, the correlations of all the mentioned variables, except for calcium, EC and magnesium, are positive, meaning that with lower index values (drier period) the values of the variables are lower, and vice versa.

	SPI (IFAPA)	SPEI (IFAPA)	N° samples
Bicarbonates	-0.19	-0.27	23
Calcium	-0.47 (SS)	-0.53 (SS)	23
TOC	-0.24	-0.23	10
Chlroides	0.32	0.33	32
Conductivity in situ (20°C)	-0.30	-0.38 (SS)	32
Fluorides	0.25	0.27	32
Phosphates	0.18	0.21	30
Magnessium	-0.31	-0.34	32
Nitrates	0.21	0.24	32
Dissolved Oxygen (in situ)	Insufficient amount of data		5
pH (in situ)	0.13	0.12	32
Potassium	0.49 (SS)	0.47 (SS)	23
Sodium	0.31	0.29	23
Sulphates	0.27	0.32	32
Temperature (in situ) (20°C)	0.06	0.04	32

Figure 4.2-14 Existing correlations between the two climate indices calculated and the chemical status variables (physicochemical parameters) of the sampling point 'Monterroso'.

At the "Río Verde" sampling point, there is a significant correlation (r > 0.5) in pH using the SPI, which is positive (Figure 4.2-15). Low magnitude correlations have also been detected in TOC and temperature, with a negative sign, and for sulphate, negatively for both indices. The SPEI has detected a low magnitude negative correlation of bicarbonates, where the SPI has not detected any. On the other hand, the SPI detected a significant correlation of pH and the SPEI did so but of low magnitude.

	SPI (Puerto)	SPEI (Puerto)	N° samples
Bicarbonates	-0.16	-0.33	11
Calcium	-0.10	-0.22	11
TOC	-0.37	-0.38	5
Chlroides	0.17	0.18	11
Conductivity in situ (20°C)	-0.04	-0.17	11
Fluorides	0.05	0.13	11
Phosphates	0.01	0.09	10
Magnessium	-0.10	-0.24	11
Nitrates	0.16	0.05	11
Dissolved Oxygen (in situ)	Insufficient amount of data		2
pH (in situ)	0.53	0.42	11
Potassium	0.16	0.00	11
Sodium	0.07	-0.05	11
Sulphates	0.34	0.47	11
Temperature (in situ) (20°C)	-0.32	-0.34	11

This project has received funding from the European Union's Horizon Europe research and innovation programme under grant agreement No GA 101082048

Funded by the European Union

Figure 4.2-15 Existing correlations between the two climate indices calculated and the chemical status variables (physicochemical parameters) of the sampling point 'Río Verde'.

At the "Río Padrón" sampling point, very few but significant correlations have been detected for nitrates and pH, with both indices (Figure 4.2-16), and positive, meaning that higher index values correspond to higher variable values. As was the case at the "Atalaya" point, the correlation of nitrates may be due to soil washing during rain episodes. A low-magnitude negative correlation of sodium with the SPI has also been detected.

	SPI (IFAPA)	SPEI (IFAPA)	N° samples
Bicarbonates	0.03	-0.06	17
Calcium	Insufficient amount of data		9
TOC	Insufficient amount of data		9
Chlroides	-0.12	-0.10	25
Conductivity in situ (20°C)	-0.25	-0.23	25
Fluorides	0.11	0.18	25
Phosphates	0.09	0.13	23
Magnessium	-0.26	-0.24	25
Nitrates	0.59 (SS)	0.62 (SS)	25
Dissolved Oxygen (in situ)	Insufficient amount of data		0
pH (in situ)	0.51 (SS)	0.52 (SS)	25
Potassium	Insufficient amount of data		0
Sodium	-0.31	-0.29	17
Sulphates	-0.08	-0.04	25
Temperature (in situ) (20°C)	0.18	0.18	25

Figure 4.2-16 Existing correlations between the two climate indices calculated and the chemical status variables (physicochemical parameters) of the sampling point 'Río Padrón'.

Finally, at the "Señorío" sampling point, no significant correlations (limit: Pearson correlation r > 0.5 and r < -0.5) have been identified between the different variables (Figure 4.2-17). However, several low magnitude correlations (r > +/- 0.3) have been detected, some of them close to the 0.5 limit, representative of moderate correlations (e.g., pH for the SPI). Other low-magnitude correlations are those of magnesium and EC for both indices and chloride for the SPEI.

	SPI (Puerto)	SPEI (Puerto)	N° samples
Bicarbonates	-0.10	-0.18	15
Calcium	Insufficient amount of data		7
TOC	Insufficient amount of data		7
Chlroides	-0.26	-0.31	15
Conductivity in situ (20°C)	-0.36	-0.34	14
Fluorides	-0.23	-0.11	15
Phosphates	-0.12	-0.07	15
Magnessium	-0.41	-0.36	15
Nitrates	0.23	0.20	15
Dissolved Oxygen (in situ)	Insufficient amount of data		0
pH (in situ)	0.43	0.30	14
Potassium	Insufficient amount of data		0
Sodium	-0.04	-0.01	15
Sulphates	-0.13	-0.11	15
Temperature (in situ) (20°C)	0.26	0.24	15

Figure 4.2-17 Existing correlations between the two climate indices calculated and the chemical status variables (physicochemical parameters) of the sampling point 'Señorío'.

This project has received funding from the European Union's Horizon Europe research and innovation programme under grant agreement No GA 101082048

Funded by the European Union

Having described all the correlations found between the selected parameters and the SPI and SPEI indices at the sampling stations, a more detailed study has been carried out to analyse the most significant correlations. Each station has been analysed for the specific dates on which the samples were taken and their corresponding SPI and SPEI values.

A generalised pattern can be observed in terms of the behaviour of the variables in relation to the values of the indices. Generally, on dates when there are high values of SPI and SPEI (related to wet years) such as 2011, belonging to the wettest period detected during the study period, or 2017, belonging to the second wettest year (if 1998/99 or 2003/04 are not taken into account, as there are no record data until 2011), lower values of the following variables have been detected: chlorides, electrical conductivity, sulphate, sodium, temperature, bicarbonates (only in Elviria) and calcium. This may be due to the fact that during these wet periods, the aquifer is recharged and as a result, there is a dilution effect of the mentioned ions, mineralisation and EC decrease. The decrease in temperature may be the result of the entry of rainwater (colder than the one remaining in the aquifer) causing the mixed water to reduce its temperature.

For dry periods, such as the years 2011/12, 2013/14, or the last dry period of the study period, which begins in 2019 and continues until the end of the record, it has been observed that, generally, in the years 2011, 2012, 2019 and 2022 the opposite occurs to what was explained for wet periods. In these cases, the ions increase their concentration, and mineralisation and EC increase.

On the other hand, it has been observed that both in “Atalaya” and in “Río Padrón” there is a positive correlation between nitrates and the SPI and SPEI. In 2011, a wet period, a higher concentration of nitrates was noted. This may be related to the fact that when there is a rain event, there is a drag of nutrients (soil washing) and they reach the aquifer. These two sampling points are the ones closest to the rivers, Padrón and Guadalmina, respectively. The influence can be significant if there is some connection between the river and the aquifer, which could explain the higher concentration of nitrates. The nitrates could be dragged by the river and end up in the aquifer during certain periods.

Below are some figures in which several patterns mentioned at the “Atalaya” sampling point can be observed (Figure 4.2-18). Figure 4.2-18 shows how in the wettest periods (2011, 2017) there are lower concentrations of calcium, sulphate, chloride and sodium, which results in a lower EC. In addition, the temperature of the aquifer water is lower, due to the colder entry of rainwater. On the other hand, for drier periods (2013-2016), these ions increase their concentration, and therefore the EC also increases. The temperature in this case increases. This may be due to the fact that in wet episodes the water dilutes the ions and in dry episodes, this dilution does not occur. Moreover, the increase in cations such as sodium or anions such as chloride may indicate processes of marine intrusion, as when there are periods of drought, the rainwater is not sufficient to recharge the aquifer and the advance of the salt wedge is more likely.

In other stations, the generalised pattern is not so clear. This is the case, for example, of the Elviria well (Figure 4.2-19), where "anomalies" can be seen for specific months in chloride or sulphate for May 2012. As for nitrate, it follows the pattern mentioned above, although for June 2015 the concentration rose and even exceeded that of the wet year 2011.

It's important to note that comparing water points with each other is not a straightforward task, given the discrepancy in sampling dates for each one, even

This project has received funding from the European Union’s Horizon Europe research and innovation programme under grant agreement No GA 101082048
Funded by the European Union

though in some cases these dates may coincide. The divergence in sampling times contributes to the joint analysis lacking full reliability and representativeness.

In addition to the conditioning factor of sample availability, the complexity of these aquifers is added. These are small coastal aquifers, most of which are subject to intensive exploitation. This makes it complex to discern the origin of salinity in the aquifer at certain periods, as it can be caused by several factors: intensive pumping, the advance of seawater towards the mainland, or a decrease in aquifer recharge due to the presence of dry climatic periods in which rainfall decreases significantly, or even a combination of all these factors.

The evolutions of quality parameters and climatic indices from the rest of the sampling points are shown in Appendix C.

This project has received funding from the European Union's Horizon Europe research and innovation programme under grant agreement No GA 101082048

Funded by the European Union

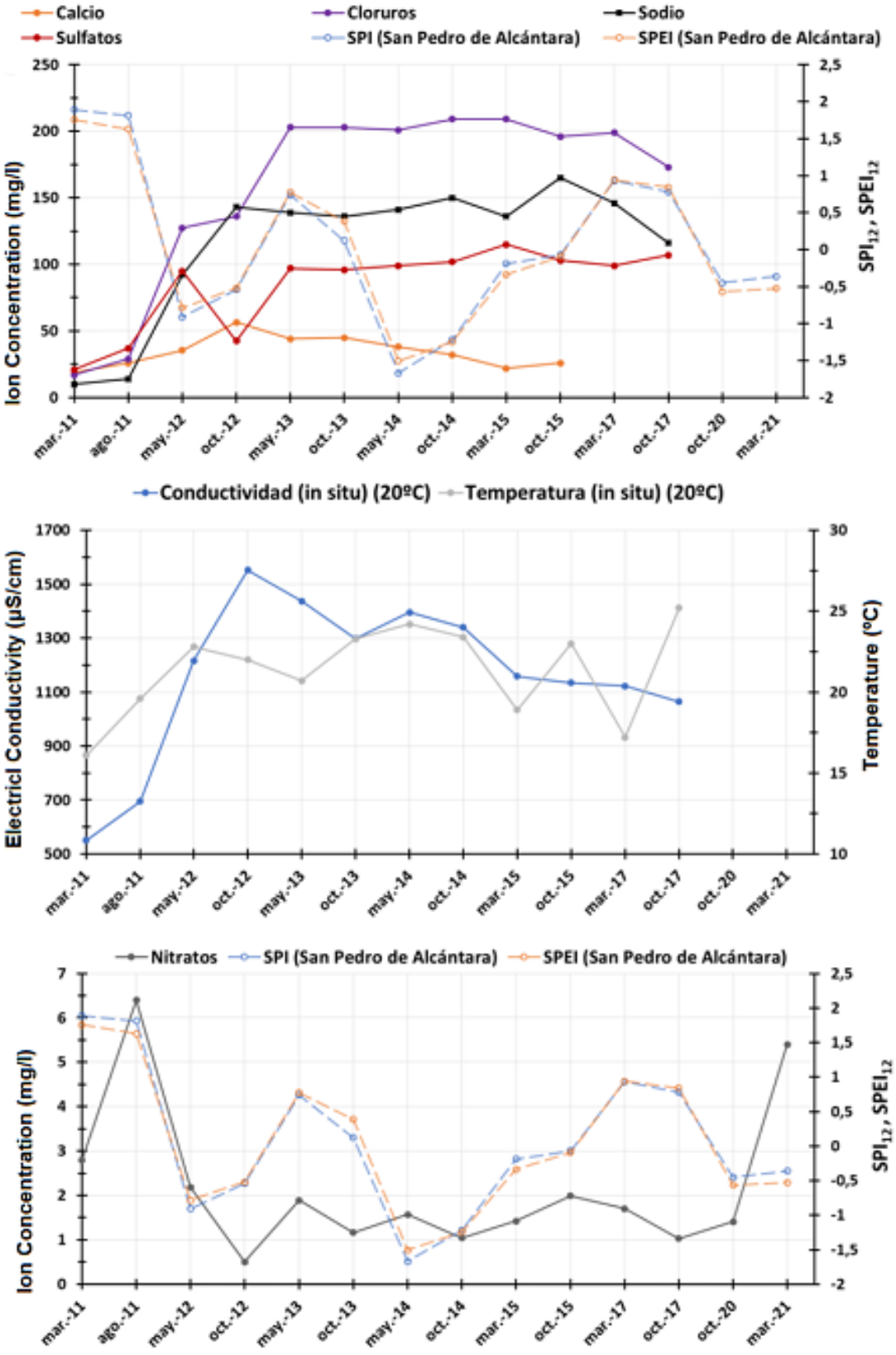

Figure 4.2-18 Monthly evolution of the main physicochemical parameters of the water samples from the 'Atalaya' sampling station, along with the representation of the SPI and SPEI for the sampling dates.

This project has received funding from the European Union's Horizon Europe research and innovation programme under grant agreement No GA 101082048

Funded by the European Union

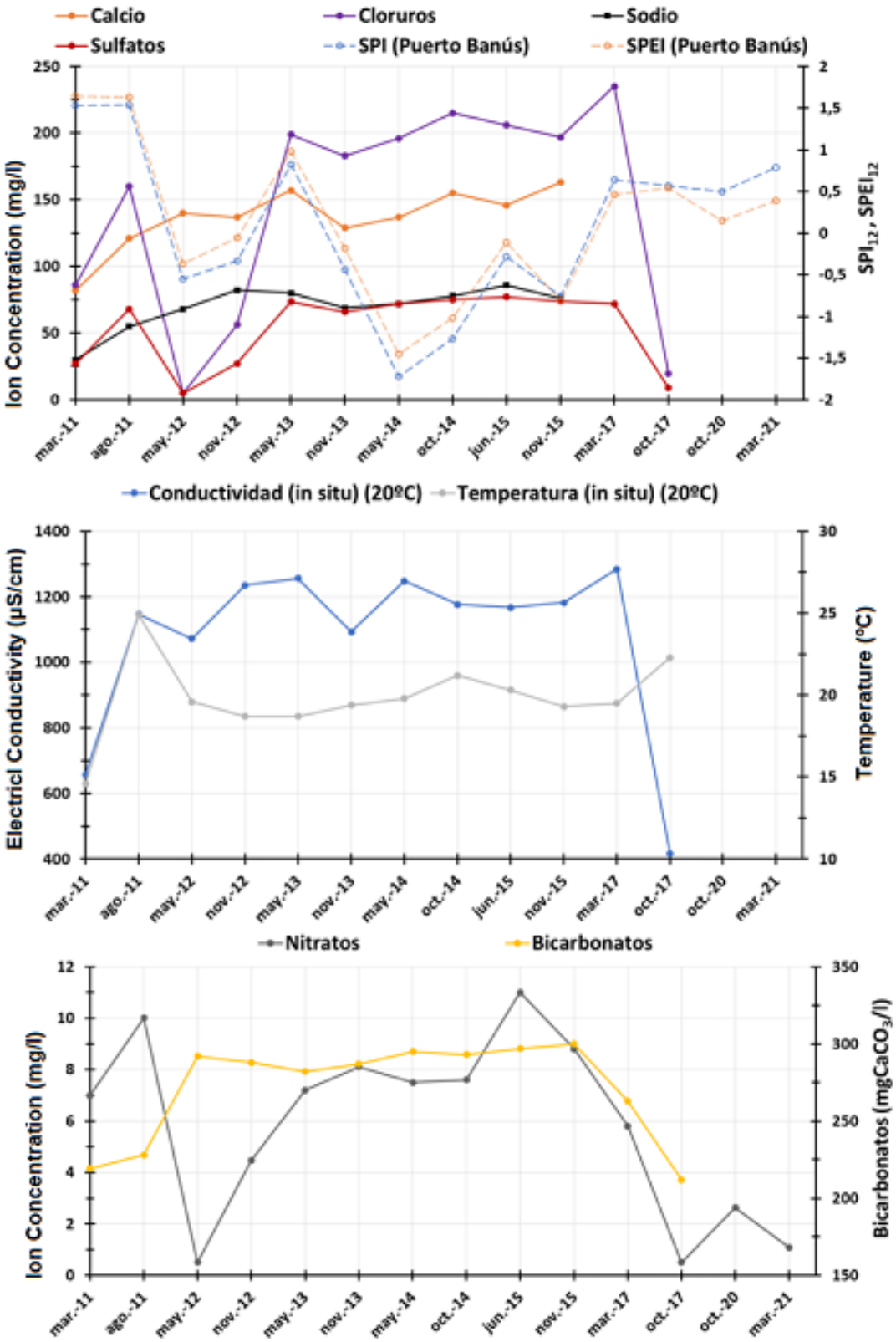

Figure 4.2-19 Monthly evolution of the main physicochemical parameters of the water samples from the 'Elviria' sampling station, along with the representation of the SPI and SPEI for the sampling dates.

This project has received funding from the European Union's Horizon Europe research and innovation programme under grant agreement No GA 101082048

Funded by the European Union

4.2.1.4 GRANGER CAUSALITY TEST

Lastly, the Granger causality test has been applied at the sampling point of El Señorío to understand the predictive relationships among its variables. This is the point where we had the most variables available, which are: electrical conductivity, piezometric level, pumping, and precipitation. As a result, the following table is obtained:

Table 4.2-3 Granger causality test results at the Señorío sampling point.

Target	EC_x	pz_level_x	pump_x	prec_x
EC_y	1	0.0004	0.026	0.017
pz_level_y	0.2727	1	0	0
pump_y	0.0052	0	1	0
prec_y	0.1272	0	0.0001	1

- **EC**: electrical conductivity at the Señorío sampling point
- **pz_level**: the piezometric level at the Señorío sampling point
- **pump**: water extractions at the Señorío sampling point
- **prec**: precipitation collected in the area

Table 4.2-3 shows the p-values for the hypothesis that the row variable is not Granger-caused by the column variable. A low p-value (typically ≤ 0.05) indicates strong evidence against the null hypothesis, leading to the rejection of the null hypothesis. Conversely, a high p-value (> 0.05) indicates weak evidence against the null hypothesis, thus the null hypothesis is not rejected.

For instance, if one intends to predict electrical conductivity, attention should be paid to the EC_y row, the p-values suggest that it is Granger-caused by pz_level_x, pump_x and prec_x as all these p-values are less than 0.05 (a common significance level).

In the case of wanting to predict the piezometric level, the p-values suggest that it is Granger-caused by pump_x and prec_x, as all these p-values are less than 0.05. However, it is not Granger-caused by EC_x, as the p-value is greater than 0.05.

4.2.2 PREDICTIVE MODELS

4.2.2.1 VALIDATION PROCESS

In order to validate the selected model for each point of interest, predictions for the next 6 months have been carried out at 10 random moments during the last 10 years of data. The outcome consists of 60 predictions across different months of the period selected.

In some instances, a date has appeared more than once among the 10 randomly selected dates. To maintain the randomness and avoid considering the same date twice, the decision has been made to remove the duplicate date without replacing it with an additional, different date.

In addition to the resulting metrics from comparing the actual values with the predicted values for each point, a representative graph of the set of predictions used in the validation is also provided.

This project has received funding from the European Union's Horizon Europe research and innovation programme under grant agreement No GA 101082048
Funded by the European Union

The results for one of the study points are presented below, while the outcomes of the validation process for the remaining points can be found in Appendix D.

Table 4.2-4 Validation process metrics in the Cable Ski well.

DATE	SMAPE (%)	MDA	MAE	Coverage
2014-01-01	16.29	80	1.93	100
2016-01-01	5.11	80	0.69	100
2016-05-01	10.31	100	0.94	100
2016-11-01	29.8	100	4.04	50
2017-04-01	9.61	80	1.51	100
2017-05-01	19.82	80	2.92	100
2017-07-01	15.75	80	2.11	100
2017-11-01	9.21	60	1.46	100
2019-01-01	8.8	80	1.36	100
2019-04-01	4.55	80	0.51	100
AVERAGE	**12.92**	**82**	**1.75**	**95**

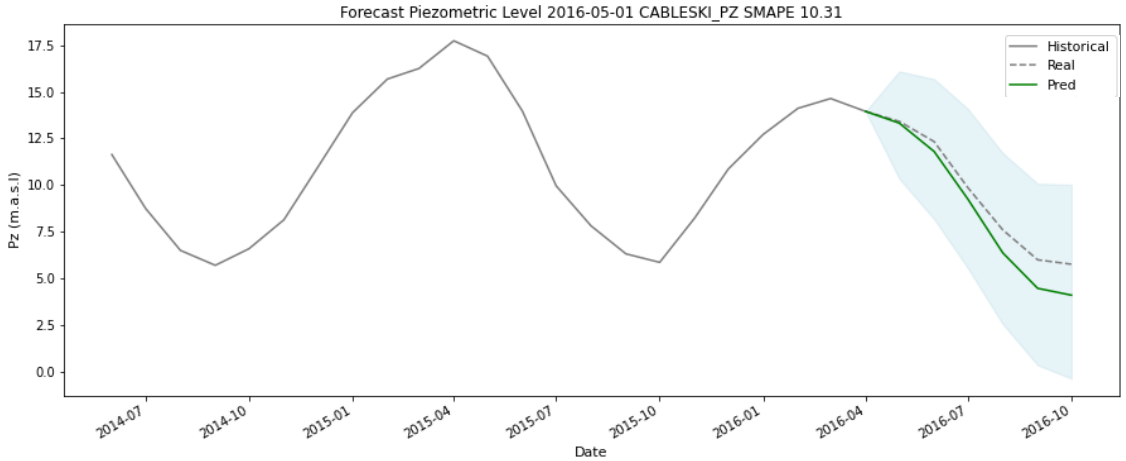

Figure 4.2-20 Prediction of piezometric level (m.a.s.l.) in the Cable Ski well on one of the random dates used for the validation process. The blue shading refers to the prediction interval.

4.2.2.2 FEATURE IMPORTANCE

To assist the user in interpreting the predictions of the selected models, some plots have been generated using the unified framework for prediction interpretation, SHAP (SHapley Additive exPlanations).

For each point of interest, two plots will be provided:

This project has received funding from the European Union's Horizon Europe research and innovation programme under grant agreement No GA 101082048
Funded by the European Union

- Bar plot (left): the mean absolute value of the SHAPE values for each feature is simply taken to produce a standard bar chart, indicating which variables are most significant in the prediction.
- Beeswarm plot (right): provides an overview of which features are most important for a model by plotting the SHAP values of each feature for each sample. The above chart arranges the features by the sum of the magnitudes of the SHAP values across all samples and uses the SHAP values to show the distribution of the impact of each feature on the model's outcome. The colour represents the feature value (high in red, low in blue).

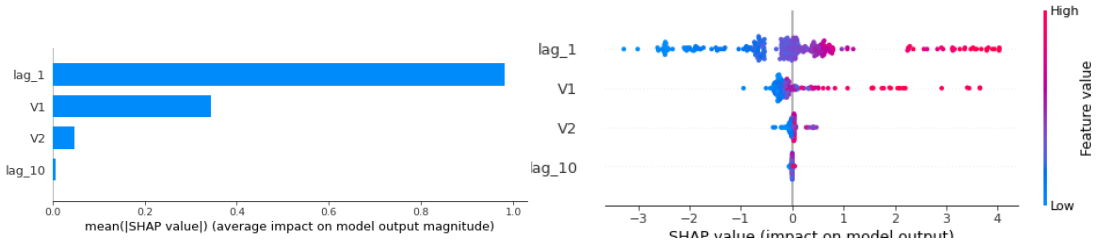

Figure 4.2-21 Río Verde MB Shap's values Summary.

This is the result of the two plots for Río Verde MB, the rest of the plots can be seen in Appendix E.

4.2.2.3 PREDICTIONS

In this section, future predictions are presented for the modelled points of piezometric level (m.a.s.l.), electrical conductivity (µS/cm), and reservoir volume (hm^3) for the 6 months following the last recorded data in each case.

Aloha: Piezometric level

Table 4.2-5 Prediction values and prediction interval for Aloha well in the period June 2023 - November 2023.

DATE	PREDICTION	LOWER BOUND	UPPER BOUND
2023-06-01	1.68	-0.73	4.05
2023-07-01	0.96	-1.62	3.34
2023-08-01	0.73	-1.70	3.60
2023-09-01	0.96	-1.52	3.40
2023-10-01	1.81	-0.86	4.58
2023-11-01	2.77	-0.16	5.41

This project has received funding from the European Union's Horizon Europe research and innovation programme under grant agreement No GA 101082048
Funded by the European Union

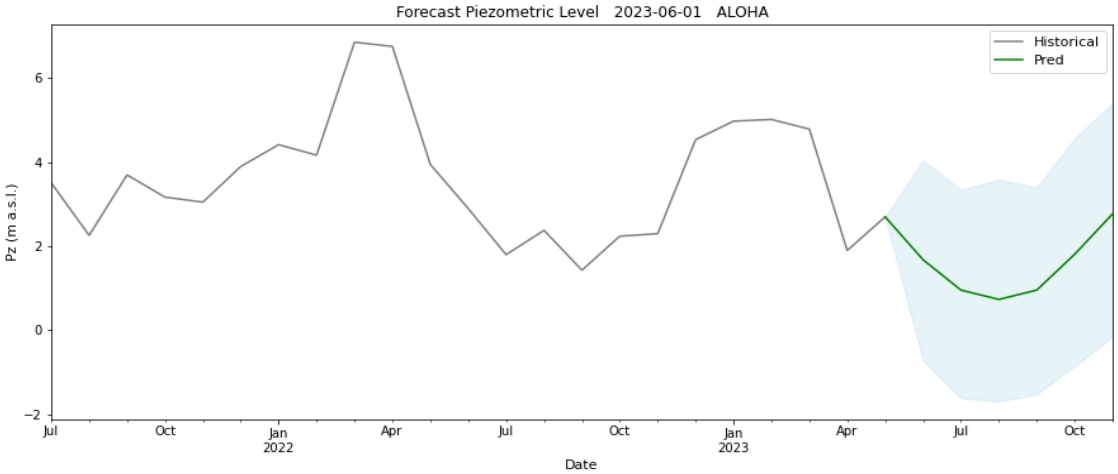

Figure 4.2-22 Prediction for Aloha well in the period June 2023 - November 2023. The blue shading refers to the prediction interval.

Cable Ski: Piezometric level

Table 4.2-6 Prediction values and prediction interval for Cable Ski well in the period March 2024 - August 2024.

DATE	PREDICTION	LOWER BOUND	UPPER BOUND
2024-03-01	-1.72	-5.38	1.17
2024-04-01	-1.91	-6.79	1.95
2024-05-01	-1.45	-7.24	3.02
2024-06-01	-1.86	-7.50	3.78
2024-07-01	-1.88	-8.27	4.28
2024-08-01	-2.72	-9.22	3.88

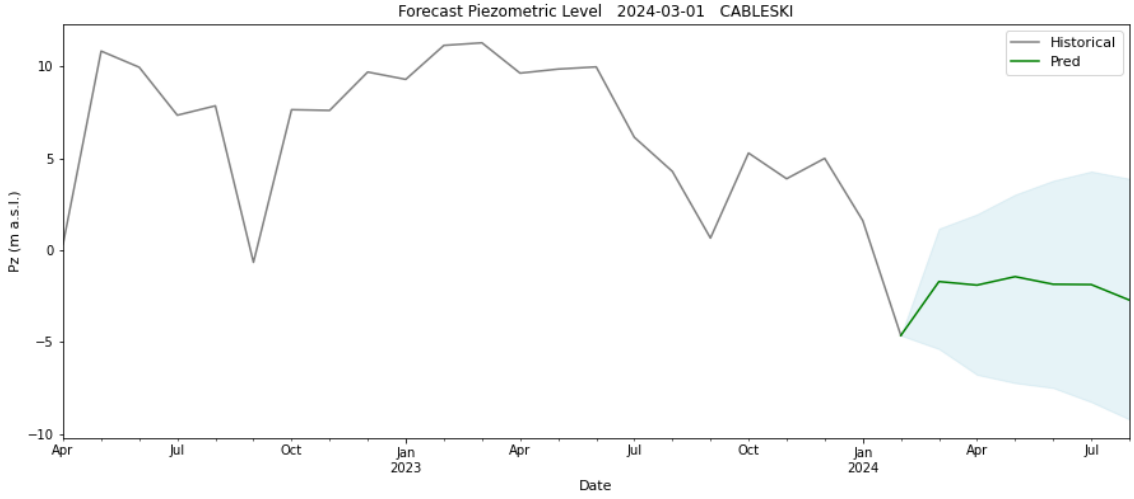

Figure 4.2-23 Prediction for Cable Ski well in the period March 2024 - August 2024. The blue shading refers to the prediction interval.

This project has received funding from the European Union's Horizon Europe research and innovation programme under grant agreement No GA 101082048

Funded by the European Union

Guadaiza: Piezometric level

Table 4.2-7 Prediction values and prediction interval for Guadaiza well in the period March 2024 - August 2024.

DATE	PREDICTION	LOWER BOUND	UPPER BOUND
2024-03-01	8.53	7.72	9.89
2024-04-01	8.42	7.58	9.68
2024-05-01	7.90	6.86	9.10
2024-06-01	7.50	6.69	8.91
2024-07-01	7.17	6.13	8.66
2024-08-01	7.05	6.29	8.45

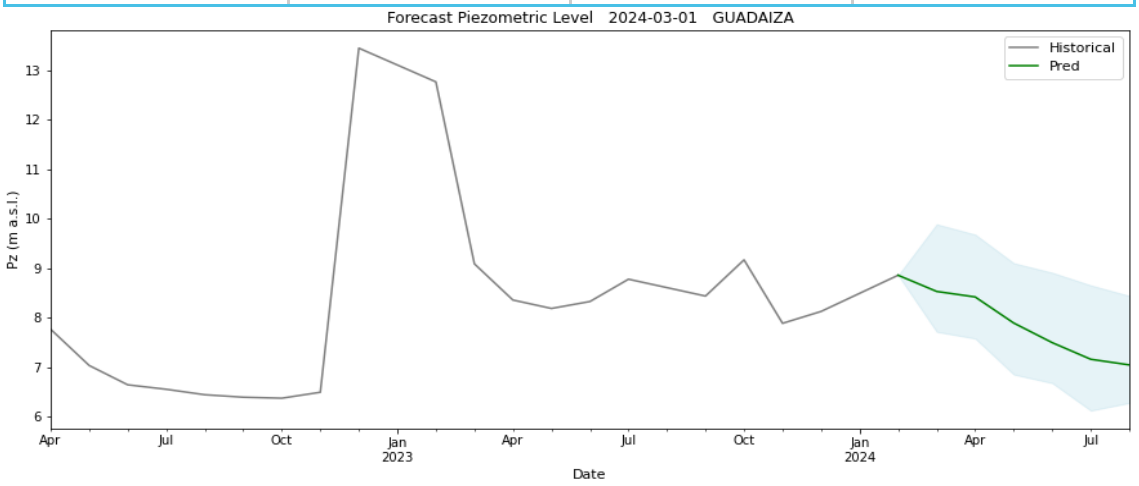

Figure 4.2-24 Prediction for Guadaiza well in the period March 2024 - August 2024. The blue shading refers to the prediction interval.

Guadalmansa: Piezometric level

Table 4.2-8 Prediction values and prediction interval for Guadalmansa well in the period March 2024 - August 2024.

DATE	PREDICTION	LOWER BOUND	UPPER BOUND
2024-03-01	3.79	1.58	6.47
2024-04-01	4.19	1.65	7.23
2024-05-01	4.01	1.28	7.12
2024-06-01	3.57	0.81	7.11
2024-07-01	2.92	-0.05	6.61
2024-08-01	2.33	-0.67	6.07

This project has received funding from the European Union's Horizon Europe research and innovation programme under grant agreement No GA 101082048
Funded by the European Union

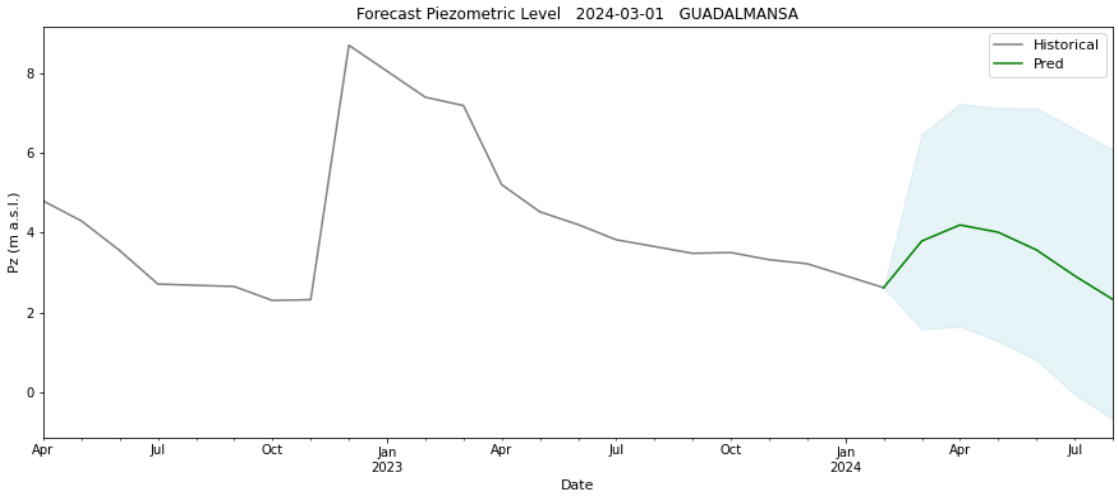

Figure 4.2-25 Prediction for Gaudalmansa well in the period March 2024 - August 2024. The blue shading refers to the prediction interval.

Guadalmina: Piezometric level

Table 4.2-9 Prediction values and prediction interval for Guadalmina well in the period March 2024 - August 2024.

DATE	PREDICTION	LOWER BOUND	UPPER BOUND
2024-03-01	17.63	16.15	19.73
2024-04-01	18.19	15.79	20.78
2024-05-01	18.35	15.79	20.99
2024-06-01	18.01	15.57	20.99
2024-07-01	17.62	15.26	20.11
2024-08-01	17.29	14.80	19.82

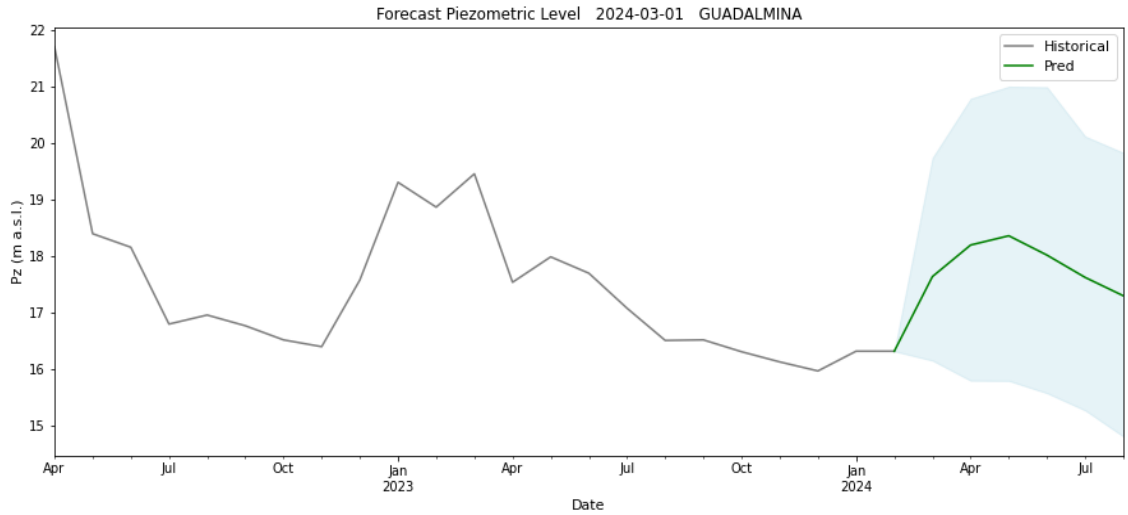

Figure 4.2-26 Prediction for Guadalmina well in the period March 2024 - August 2024. The blue shading refers to the prediction interval.

This project has received funding from the European Union's Horizon Europe research and innovation programme under grant agreement No GA 101082048

Funded by the European Union

Rio Verde MB: Piezometric level

Table 4.2-10 Prediction values and prediction interval for Río Verde MB well in the period March 2024 - August 2024.

DATE	PREDICTION	LOWER BOUND	UPPER BOUND
2024-03-01	0.45	-1.72	2.86
2024-04-01	0.97	-1.60	3.54
2024-05-01	1.63	-1.74	3.96
2024-06-01	2.16	-1.08	4.49
2024-07-01	2.25	-1.20	4.48
2024-08-01	2.27	-1.08	4.03

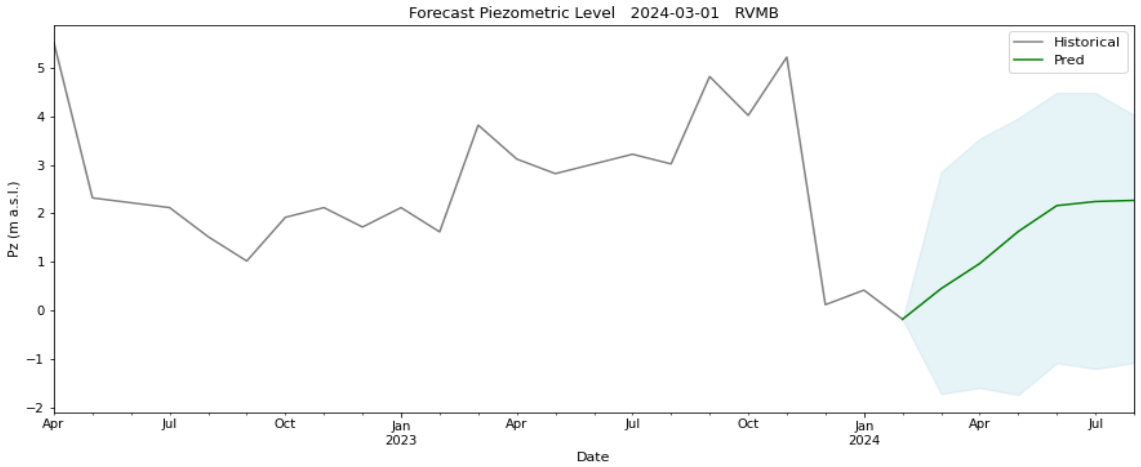

Figure 4.2-27 Prediction for Río Verde MB well in the period March 2024 - August 2024. The blue shading refers to the prediction interval.

Rio Verde NA: Piezometric level

Table 4.2-11 Prediction values and prediction interval for Río Verde NA well in the period March 2024 - August 2024.

DATE	PREDICTION	LOWER BOUND	UPPER BOUND
2024-03-01	0.91	-0.06	2.15
2024-04-01	0.85	-0.04	2.24
2024-05-01	0.82	-0.12	2.14
2024-06-01	0.82	-0.21	2.40
2024-07-01	0.83	-0.27	2.15
2024-08-01	0.88	-0.33	2.14

This project has received funding from the European Union's Horizon Europe research and innovation programme under grant agreement No GA 101082048
Funded by the European Union

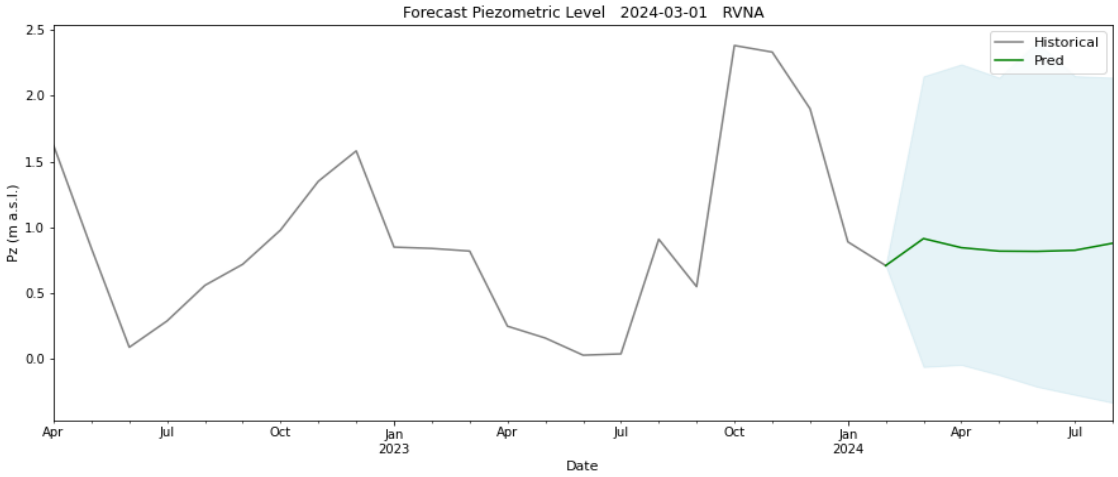

Figure 4.2-28 Prediction for Río Verde NA well in the period March 2024 - August 2024. The blue shading refers to the prediction interval.

San Pedro: Piezometric level

Table 4.2-12 Prediction values and prediction interval for San Pedro well in the period December 2023 - May 2024.

DATE	PREDICTION	LOWER BOUND	UPPER BOUND
2023-12-01	12.75	6.10	20.23
2024-01-01	12.80	4.98	21.31
2024-02-01	13.18	4.38	23.35
2024-03-01	13.32	2.47	27.36
2024-04-01	13.77	3.26	26.40
2024-05-01	13.36	2.60	28.08

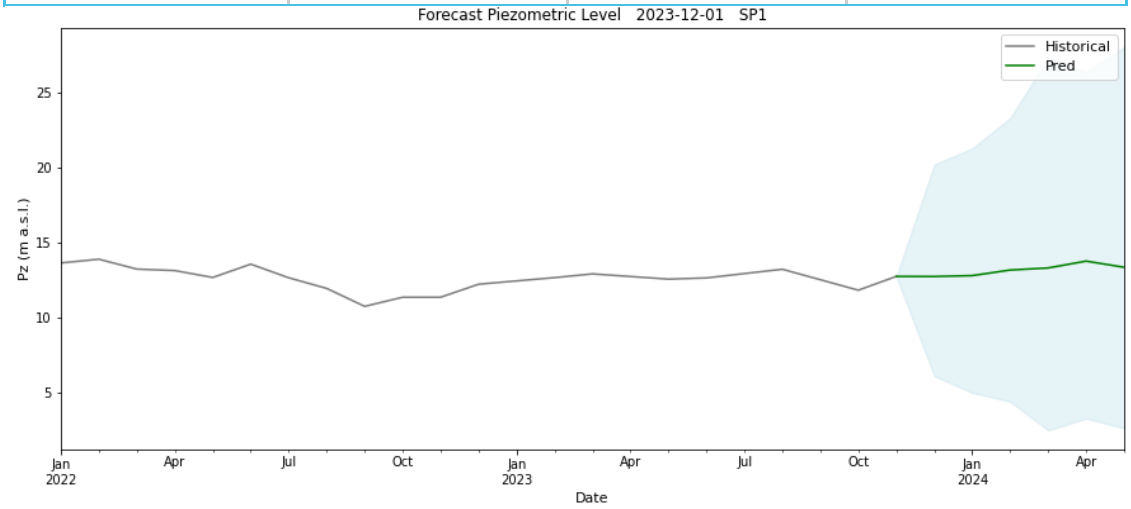

Figure 4.2-29 Prediction for San Pedro well in the period December 2023 - May 2024. The blue shading refers to the prediction interval.

This project has received funding from the European Union's Horizon Europe research and innovation programme under grant agreement No GA 101082048

Funded by the European Union

Señorío: Piezometric level

Table 4.2-13 Prediction values and prediction interval for Señorío well in the period March 2024 - August 2024.

DATE	PREDICTION	LOWER BOUND	UPPER BOUND
2024-03-01	1.41	-0.02	2.95
2024-04-01	1.87	-0.36	3.89
2024-05-01	1.65	-1.08	4.03
2024-06-01	1.14	-1.57	3.75
2024-07-01	0.46	-2.48	3.13
2024-08-01	-0.17	-2.94	2.58

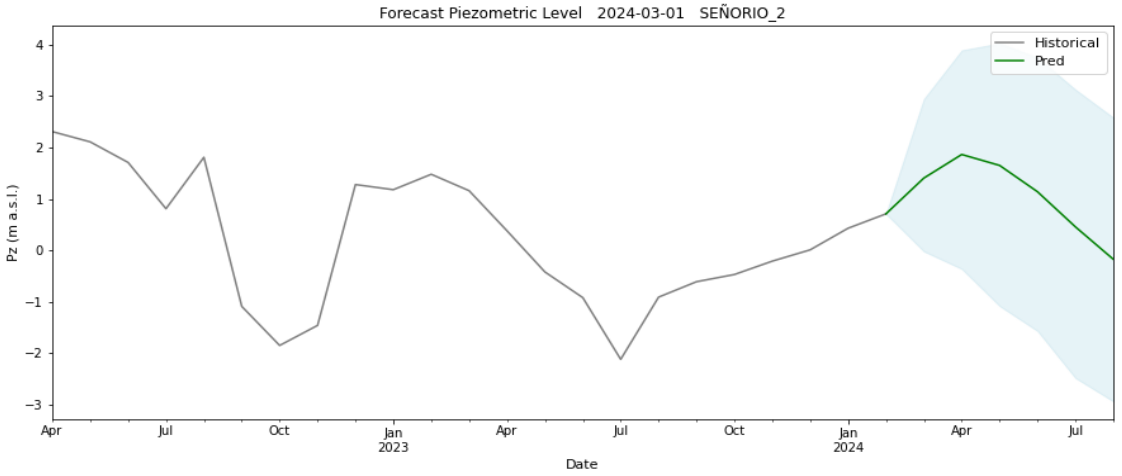

Figure 4.2-30 Prediction for Señorío well in the period March 2024 - August 2024. The blue shading refers to the prediction interval.

Señorío: Electrical Conductivity

Table 4.2-14 Prediction values and prediction interval for Señorío well in the period March 2024 - August 2024.

DATE	PREDICTION	LOWER BOUND	UPPER BOUND
2024-03-01	1047.83	783.15	1235.49
2024-04-01	1037.65	677.31	1318.24
2024-05-01	1033.64	634.32	1367.99
2024-06-01	1029.87	592.07	1464.08
2024-07-01	1030.16	638.99	1504.77
2024-08-01	1031.17	638.32	1550.35

This project has received funding from the European Union's Horizon Europe research and innovation programme under grant agreement No GA 101082048
Funded by the European Union

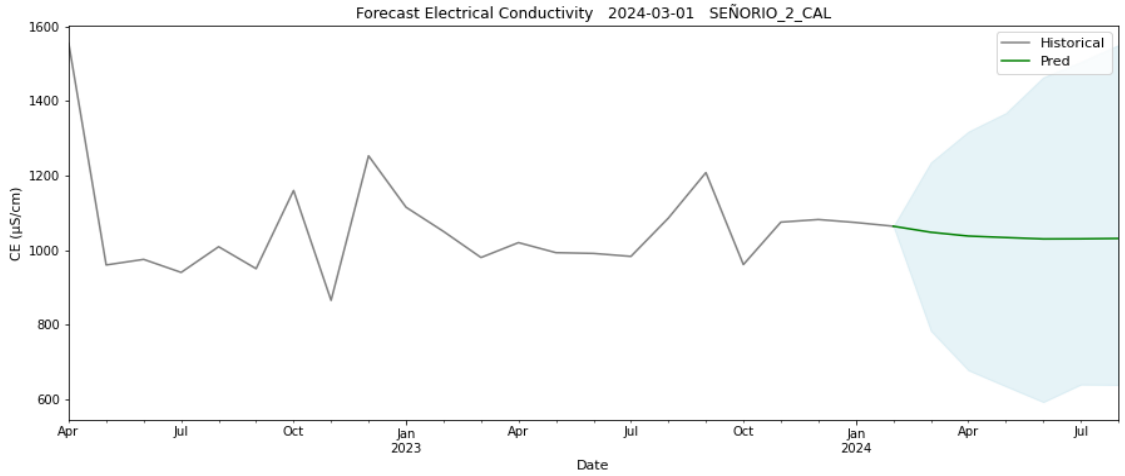

Figure 4.2-31 Prediction for Señorío well in the period March 2024 - August 2024. The blue shading refers to the prediction interval.

La Concepción: Reservoir volume

Table 4.2-15 Prediction values and prediction interval for the reservoir of La Concepción in the period April 2024 - September 2024.

DATE	PREDICTION	LOWER BOUND	UPPER BOUND
2024-04-01	29.87	27.12	33.38
2024-05-01	45.15	40.12	49.76
2024-06-01	49.05	43.91	56.21
2024-07-01	49.75	42.17	57.54
2024-08-01	47.34	37.40	56.00
2024-09-01	43.07	32.30	52.69

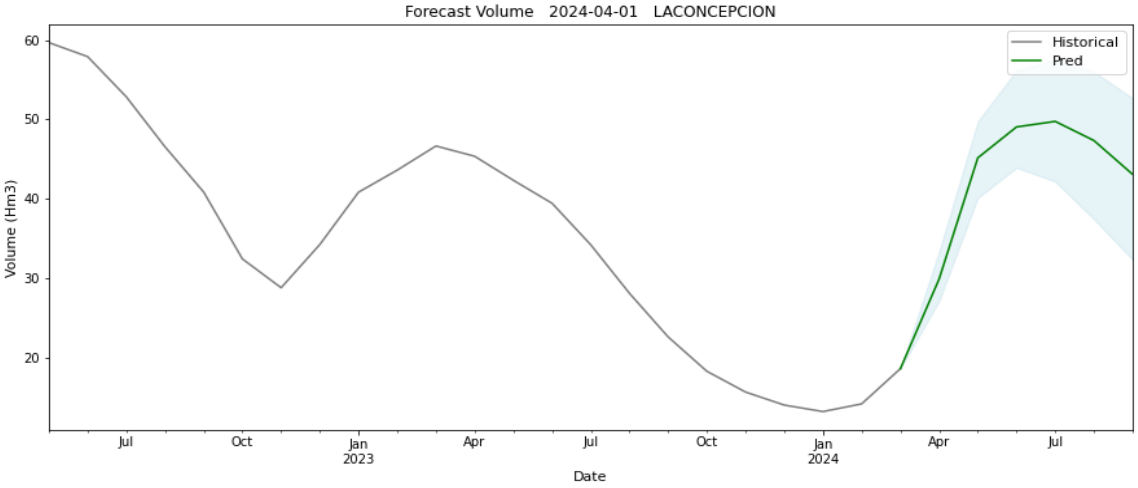

Figure 4.2-32 Prediction for the reservoir of La Concepción in the period April 2024 - September 2024. The blue shading refers to the prediction interval.

This project has received funding from the European Union's Horizon Europe research and innovation programme under grant agreement No GA 101082048
Funded by the European Union

Charco Redondo: Reservoir volume

Table 4.2-16 Prediction values and prediction interval for the reservoir of Charco Redondo in the period April 2024 - September 2024.

DATE	PREDICTION	LOWER BOUND	UPPER BOUND
2024-04-01	24.86	20.90	30.70
2024-05-01	24.59	18.80	32.62
2024-06-01	23.89	17.62	33.30
2024-07-01	22.74	14.94	33.57
2024-08-01	21.33	13.54	33.20
2024-09-01	20.02	10.23	31.86

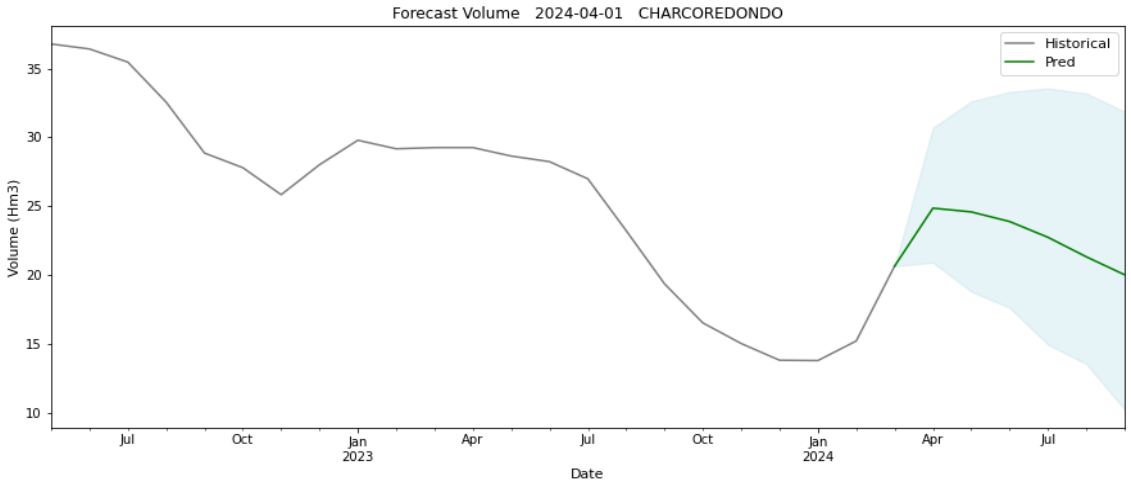

Figure 4.2-33 Prediction for the reservoir of Charco Redondo in the period April 2024 - September 2024. The blue shading refers to the prediction interval.

Guadarranque: Reservoir volume

Table 4.2-17 Prediction values and prediction interval for the reservoir of Guadarranque in the period April 2024 - September 2024.

DATE	PREDICTION	LOWER BOUND	UPPER BOUND
2024-04-01	36.47	31.78	40.31
2024-05-01	37.97	32.05	43.92
2024-06-01	34.77	28.25	40.13
2024-07-01	32.31	24.90	40.05
2024-08-01	29.08	22.98	36.35
2024-09-01	27.95	22.17	34.94

This project has received funding from the European Union's Horizon Europe research and innovation programme under grant agreement No GA 101082048
Funded by the European Union

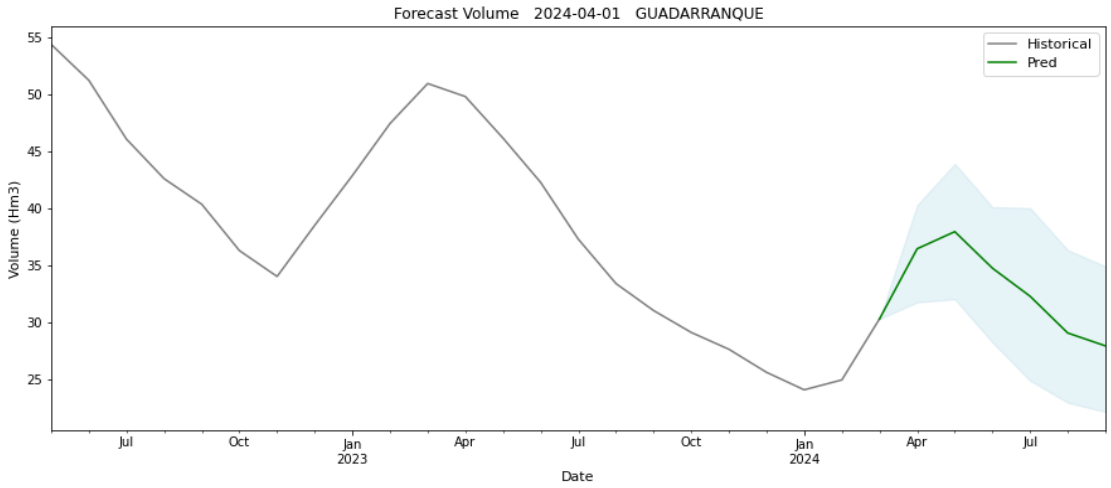

Figure 4.2-34 Prediction for the reservoir of Guadarranque in the period April 2024 - September 2024. The blue shading refers to the prediction interval.

4.2.3 CALIBRATION, VALIDATION AND UNCERTAINTIES

Model calibration is carried out through semi-automated experiments that generate and compare various models based on specific metrics (MAE, RMSE, MDA) using cross-validation. This process is detailed in the "3.2.2. PREDICTIVE MODELS" section.

Following calibration, the validation of the selected model is conducted through various training procedures and predictions at randomly selected moments over the past few years of data, simulating the behaviour the model would have exhibited at a specific moment in the past. This process is described in the "3.2.2. PREDICTIVE MODELS" section, while the "4.2.2.1. VALIDATION PROCESS" section presents the resulting metrics by comparing the actual values with the predicted values for each point of interest. It is observed that the different models are capable of reproducing the dynamics of the various variables as they present sMAPE errors between 10% and 20%.

Uncertainties are managed through the prediction interval, which is an estimate of a range of values within which a future observation will fall with a certain probability. This concept is explained in the "3.2.2. PREDICTIVE MODELS" section. It presents good uncertainty with coverage values normally exceeding 80% in the validation phase. Additionally, to assist in interpreting the predictions of the selected models and understanding the associated uncertainties, graphs generated with the unified framework for prediction interpretation, SHAP (SHapley Additive exPlanations), are used. These graphs indicate which variables are most significant in the prediction and provide an overview of which features are most important for a model.

4.3 GIS-REACH

Vulnerability, hazard and exposure mapping of each demo site allows to elaborate of risk maps of groundwater pollution to evaluate which areas or the territory are more sensitive to pollution events and, therefore, to address actions to prevent and mitigate it. In the next pages, we present the main results of the groundwater pollution risk mapping assessment, but all the intermediate results can be found in Appendix H.

4.3.1 DEMO SITE 3 - FRIELAS (PORTUGAL)

The vulnerability has been mapped through the DRASTIC, GALDIT and GOD methods. In general, the DRASTIC method (Appendix H Figure H-1) looks to show more detail when representing vulnerability, due to the higher amount of parameters taken into account. GALDIT method (Appendix H Figure H-2) highlights the vulnerability in the

This project has received funding from the European Union's Horizon Europe research and innovation programme under grant agreement No GA 101082048
Funded by the European Union

coastal area, as it is focused on it, so the vulnerability of inner areas should not be considered. On the other hand, the GOD method (Appendix H Figure H-3) shows rough results, as it only takes into account three parameters. Moderate vulnerability is present in most of the demo site area, while the GOD method calculated high vulnerability in an important part of the demo site.

Hazard mapping of the Frielas demo site (Appendix H Figure H-4) permits to check that the majority of the territory has a low hazard for groundwater pollution but is very conditioned by land use. Also, an important estuary area in the south is subjected to sea level rise hazard, but just a few metres of shoreline are affected.

High to moderate values of exposure to groundwater pollution in the Frielas demo site (Appendix H Figure H-5) can be found mostly in populated areas (close to the Tejo estuary).

Finally, risk mapping to groundwater pollution of the Frielas demo site (Figure 4.3-1) allows to distinguish that the most populated areas, as well as where the most permeable materials are located, are the areas with moderate to very high levels of risk. On the other hand, not populated areas, with natural land uses and low-permeability geological materials, show low to very low values of risk.

This project has received funding from the European Union's Horizon Europe research and innovation programme under grant agreement No GA 101082048

Funded by the European Union

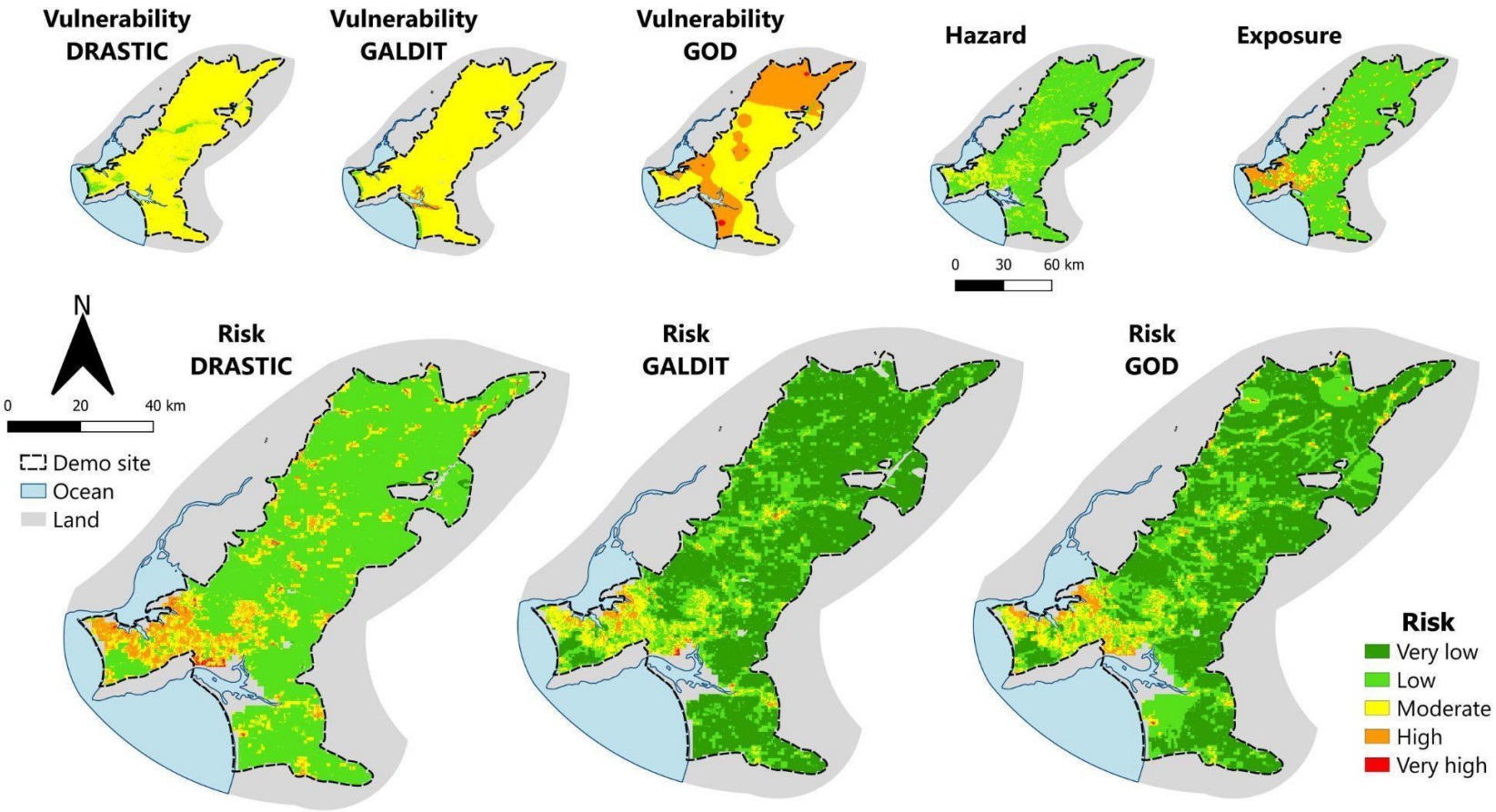

Figure 4.3-1 Risk to groundwater pollution of the Frielas demo site.

This project has received funding from the European Union's Horizon Europe research and innovation programme under grant agreement No GA 101082048

Funded by the European Union

4.3.2 DEMO SITE 4 - EMILIA-ROMAGNA (ITALY)

Vulnerability maps of the demo site of Emilia-Romagna show remarkable differences between methods. DRASTIC method (Appendix H Figure H-6) presents a great area of low to moderate vulnerability values, very conditioned by the unsaturated zone characteristics. On the other hand, the GALDIT method (Appendix H Figure H-7) only shows low and moderate values, being the last ones more present on the shoreline. Finally, the GOD method (Appendix H Figure H-8) highlights very high vulnerability values in the coastal area, where groundwater levels are shallower and where unconfinement is present.

The hazard to groundwater pollution in Emilia-Romagna (Appendix H Figure H-9) is well conditioned by land use and sea level rise, as well as the river network. Sea level rise estimates are very remarkable, with areas that could suffer flooding up to 50 km far from the coast, due to the very low topography of the demo site. Moderate hazard zones are predominant in the middle east part of the demo site, while low hazard zones are shown mostly in the western part. Besides, close to the shoreline, the river network marks high-hazard areas, as they join with sea level rise hazards.

Groundwater-dependent ecosystems and natural protected areas slightly condition the exposure of the demo site to groundwater pollution (Appendix H Figure H-10). The great part of the mapping area is covered by moderate and high exposure areas, as this is a very populated part of Italy.

Groundwater pollution risk maps of Emilia-Romagna (Figure 4.3-2) clearly show that the northeastern part of the demo site, close to the Po River mouth, is the riskiest due to the higher vulnerability values (better hydrogeological properties), with moderate to very high-risk values. This fact is more remarkable using DRASTIC and GOD vulnerability methods. Risk assessment using DRASTIC also shows a moderate to very high risk in the southern part of the demo site, due to the moderate vulnerability given.

This project has received funding from the European Union's Horizon Europe research and innovation programme under grant agreement No GA 101082048
Funded by the European Union

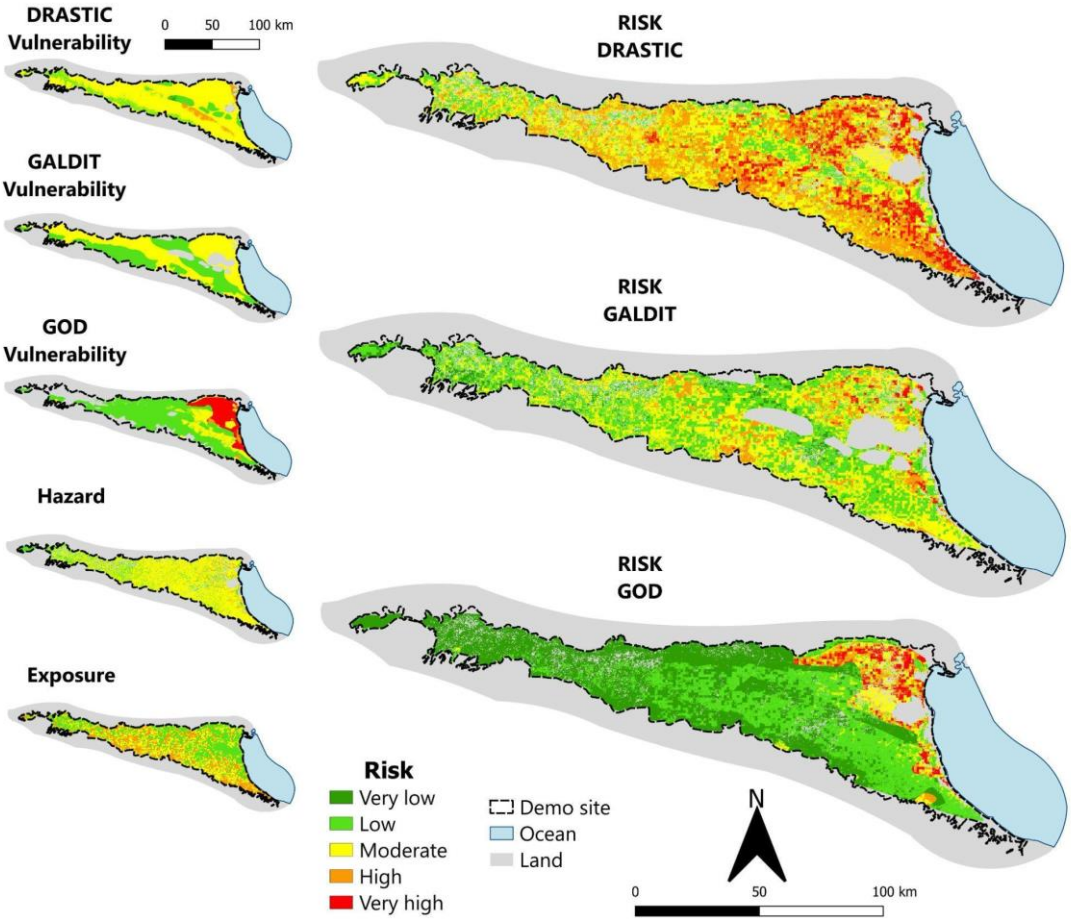

Figure 4.3-2 Risk to groundwater pollution of the Emilia-Romagna demo site.

4.3.3 DEMO SITE 5 - CAPE FLATS (SOUTH AFRICA)

Cape Flats demo site data has been taken from several of the abovementioned sources, but also from local data. This is important, as the spatial availability of data conditions the spatial mapping of each index. In this case, some of the maps have a partial representation due to the spatial availability of groundwater depth measurements.

DRASTIC vulnerability of the Cape Flats demo site (Appendix H Figure H-11) shows that most of the area is covered by low vulnerability values, while presenting moderate values in those parts coinciding with the most permeable lithologies, as alluvial sediments or aeolian sands, among others.

The GALDIT vulnerability map (Appendix H Figure H-12), however, only presents a very thin band of moderate values close to the shoreline, because of the distance parameter, maintaining low values in all the rest of the demo site.

Finally, the GOD vulnerability method (Appendix H Figure H-13) shows moderate to high values.

Hazard to groundwater pollution in the Cape Flats demo site (Appendix H Figure H-14) is majorly conditioned by land use, but also by land subsidence probability, which covers close to one-third of the surface because of groundwater abstraction and the existence of buildings.

This project has received funding from the European Union's Horizon Europe research and innovation programme under grant agreement No GA 101082048
Funded by the European Union

Exposure levels in Cape Flats (Appendix H Figure H-15) are mainly high, mainly because of the high population density, which is lower in the northern and the eastern parts of the demo site.

Groundwater pollution risk assessment in the Cape Flats demo site (Figure 4.3-3) is only shown for those areas limited to the spatial availability of data (groundwater depth in this case). Remarkable high to very high-risk values can be found in the western part of the represented area because of the higher vulnerability values and higher exposure. On the other hand, lower risk values can be found in the eastern part of the demo site.

This project has received funding from the European Union's Horizon Europe research and innovation programme under grant agreement No GA 101082048

Funded by the European Union

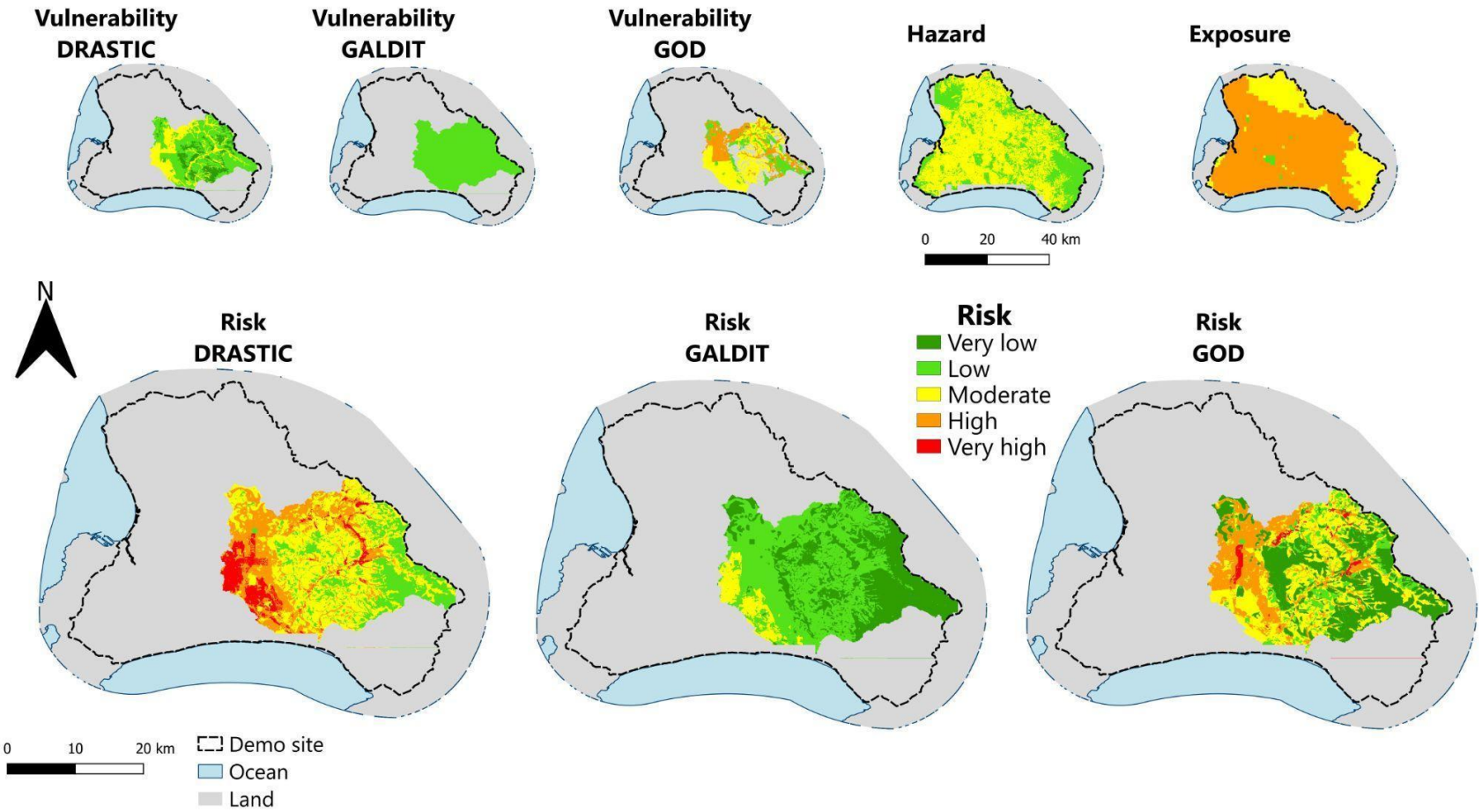

Figure 4.3-3 Risk to groundwater pollution of the Cape Flats demo site.

This project has received funding from the European Union's Horizon Europe research and innovation programme under grant agreement No GA 101082048

Funded by the European Union

4.3.4 DEMO SITE 6 - MARBELLA (ES)

Due to the availability and testing with more accurate, local data, of the Spanish demo site of Marbella, these vulnerability maps have been done without considering some of the general, replicable data that have been taken into account in the previous demo sites.

All DRASTIC (Appendix H Figure H-16), GALDIT (Appendix H Figure H-17) and GOD (Appendix H Figure H-18) vulnerability mapping of the Marbella demo site shows the common pattern of higher values coinciding with the most permeable geological materials, which are gravels and sands located around the network of short rivers that end in the Mediterranean Sea. Very low or low values are uncommon and are only found in the northern parts of the demo site, because of the more impervious behaviour of geology. The GALDIT method remarks moderate vulnerability values in the shoreline.

Hazard evaluation of groundwater pollution (Appendix H Figure H-19) is mainly conditioned by land use because no sea level rise or subsidence hazard is present. Besides, land use only gives low to moderate hazard values in some little areas of the demo site.

Higher population density areas of the Marbella demo site are behind moderate to high exposure values (Appendix H Figure H-20). Low exposure values are predominant in the rest of the area.

Finally, groundwater pollution risk mapping of the Marbella demo site (Figure 4.3-4) shows remarkable differences between the vulnerability methods chosen. So, DRASTIC-based risk mapping presents very high values in some parts of the demo site, when combined with hazard and exposure. On the other hand, GALDIT-based and GOD-based risk mapping show a major part of the demo site as very low to low risk, while maintaining some little areas (mainly due to higher exposure values) with high to very high-risk values.

This project has received funding from the European Union's Horizon Europe research and innovation programme under grant agreement No GA 101082048
Funded by the European Union

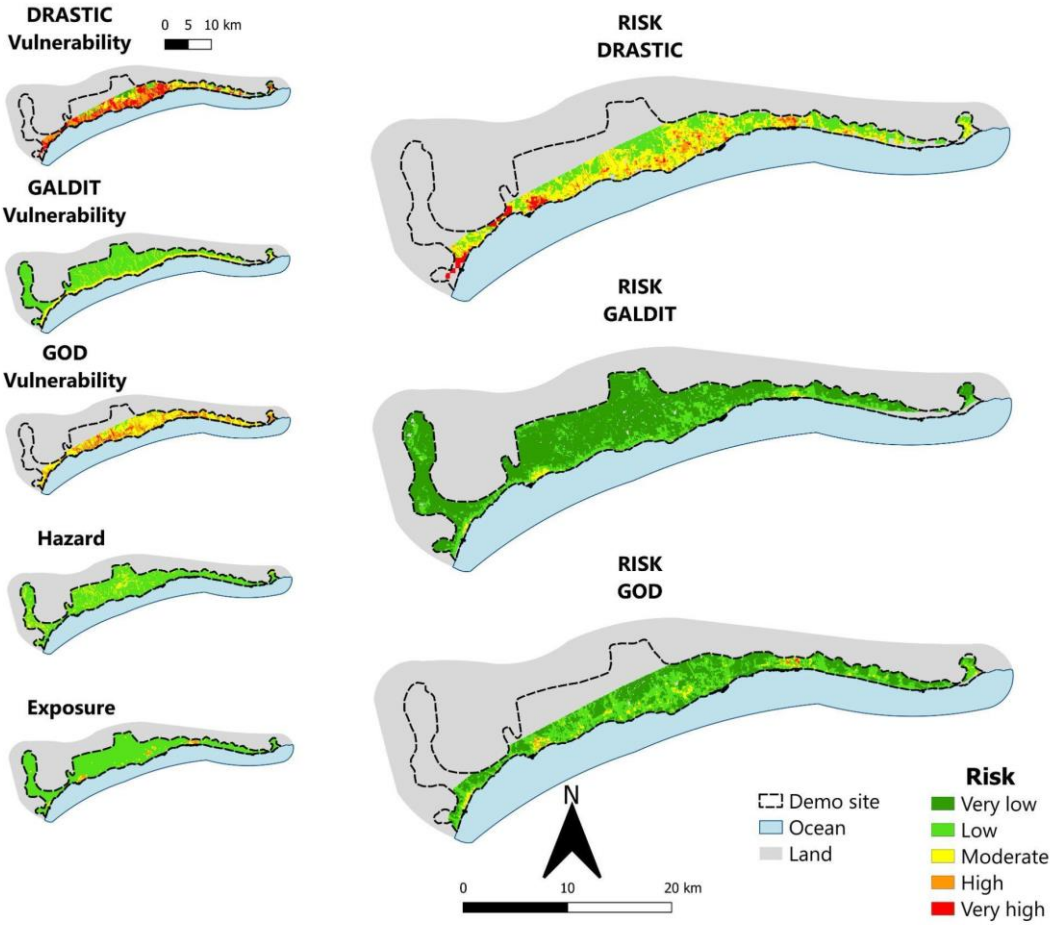

Figure 4.3-4 Risk to groundwater pollution of the Marbella demo site.

4.3.5 UNCERTAINTIES AND VALIDATION

Some uncertainties regarding the risk mapping to groundwater pollution can be described after elaborating and applying the above-mentioned methodology, which applies to all the methodologies: the resolution of the spatial data used.

In this way, when more accurate data, with better resolution, is available, more precise results will be obtained in theory. For example, hydrogeology layers (e.g. aquifer hydraulic conductivity) are based on the IHME1500 (International Hydrogeological Map of Europe), whose scale is 1:1.500.000, which introduces a clear uncertainty in where the limits of the aquifers are located, that sometimes can include or exclude critical information. So, as shown in DS6, where better layers are available, more spatially detailed results are obtained that can reduce these uncertainties. Nevertheless, some studies revealed that a higher spatial resolution does not necessarily improve the quality of the results (Mark and Aronson, 1984; Rosso et al., 1991; Gupta et al., 2007; Wörman et al. 2007; Reinecke et al., 2020).

Also, as some relative assertions are made with some layers, so the methodology can be widely replicable all throughout EU countries, uncertainties regarding the precision of the information can be done.

Although these mentioned uncertainties, the methodology can be reasonably validated from the former layers themselves.

This project has received funding from the European Union's Horizon Europe research and innovation programme under grant agreement No GA 101082048
Funded by the European Union

Vulnerability assessment shows remarkable differences between the DRASTIC, GALDIT and GOD methods. DRASTIC and GOD methods are clearly conditioned by the presence and type of aquifers, and therefore their hydraulic properties, so more permeable materials (higher hydraulic conductivity) will coincide with higher vulnerabilities, which is very logical regarding the real field conditions. The GALDIT method is strongly conditioned by the coastal fringe and its hydrogeological characteristics, which determines the final result of maps (higher vulnerabilities in those areas closer to the sea).

Hazard evaluation of groundwater pollution is very conditioned by land use in most of the demo sites, as the presence of crops and towns is considered a major source of pollutants, as reflected in all the results. Also, in coastal areas where there exists a significant increase in predicted sea level, the hazard is consistently higher.

Regarding the exposure variable of the risk evaluation, the presence of populated areas is the main driver of the results, as are the places more exposed to groundwater pollution effects, apart from the naturally protected (or not protected) areas receiving groundwater fluxes.

Finally, the risk mapping to groundwater pollution assessment shows results coinciding with the mentioned parameters. In this sense, higher risk values will be present in those places with higher hydraulic conductivities (or permeable materials), crop existence and higher population densities, being lower on the contrary.

4.4 CLIMATE PROJECTIONS

This part of the tool is focused on generating daily climate projections for seven demonstration sites. These projections encompassed precipitation, minimum temperature, and maximum temperature. While attempts were made to utilise real data from nearby stations, the majority of the data was sourced from the ERA5-Land data package. This was due to the fact that the obtained series did not reach 30 years of data, had more than 20% missing data, or deviated excessively from the study area.

The Coupled Model Intercomparison Project Phase 6 (CMIP6) was employed as the projection dataset for all experiments. CMIP6 is a global collaborative initiative aimed at enhancing our understanding of Earth's climate systems. It focuses on the evaluation and comparison of coupled climate models, which simulate the interaction between the atmosphere, oceans, cryosphere, and other terrestrial components. These models are crucial for projecting future climate changes and understanding the impacts of global warming, thus providing vital information for policy formulation and adaptation/mitigation strategies.

The experiments were conducted under two future climate scenarios: SSP2 and SSP5. The SSP2 scenario represents a world with moderate economic and population growth rates, with a balanced focus on climate change mitigation and adaptation. In contrast, the SSP5 scenario describes a future characterised by rapid economic and technological development, high greenhouse gas emissions, and a prolonged reliance on fossil fuels.

Given that CMIP6's historical records extend up to 2014, the projections span from 2015 to 2100. Five models from the CMIP6 preselection were chosen for the study:

- GFDL-ESM4_r1i1p1f1
- IPSL-CM6A-LR_r1i1p1f1
- MPI-ESM1-2-HR_r1i1p1f1
- MRI-ESM2-0_r1i1p1f1

This project has received funding from the European Union's Horizon Europe research and innovation programme under grant agreement No GA 101082048

Funded by the European Union

- UKESM1-0-LL_r1i1p1f2

The bias correction method selected for use in the different experiments at each demo site was ISIMPI3. This method involves transferring the simulated climate change signals to historical observations for each quantile, accompanied by time series detrending to recover the trends. It also includes the replacement of values exceeding thresholds with random numbers, as well as the adjustment of marginal distributions for each variable.

Finally, the spatial resolution was set to "Native", and the output was in NetCDF format. This data was subsequently processed using different Python libraries to generate the graphs displaying the obtained results. For clarity, the results for each case are presented in both a daily graph (original output) and a graph with annual grouping (annual accumulation for precipitation and annual average for temperature). Also, each graph includes a first-degree polynomial line to indicate the trend of the predicted series. This provides a clear visual representation of the overall direction of the data, aiding in the interpretation of the results and the identification of any significant trends or patterns.

The following presents the results from one of the models, covering all three variables and both scenarios. The outcomes from the remaining models are included in Appendix F, and some graphic examples of minimum temperature, maximum temperature and precipitation are shown in Figure 4.4-1, Figure 4.4-2 and Figure 4.4-3, respectively.

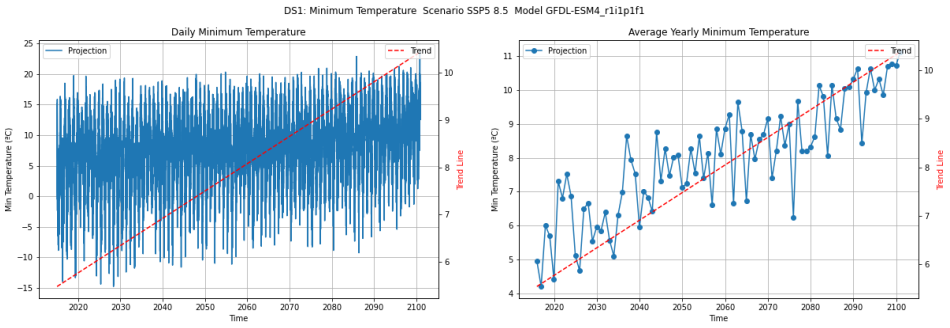

Figure 4.4-1 GFDL-ESM4_r1i1p1f1 model projections of minimum temperature in DEMO SITE 1.

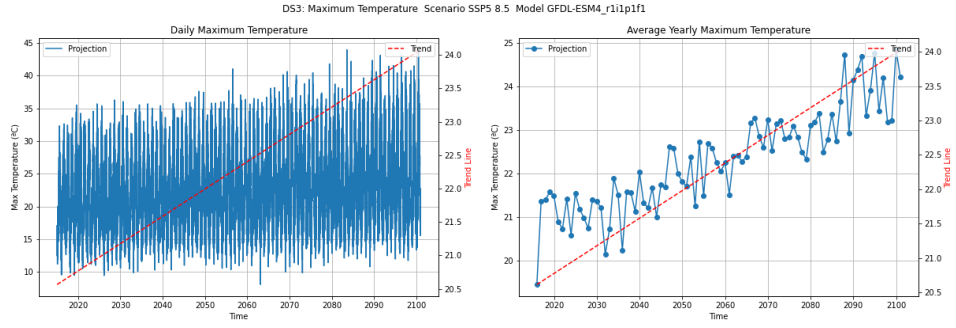

Figure 4.4-2 GFDL-ESM4_r1i1p1f1 model projections of maximum temperature in DEMO SITE 3.

This project has received funding from the European Union's Horizon Europe research and innovation programme under grant agreement No GA 101082048
Funded by the European Union

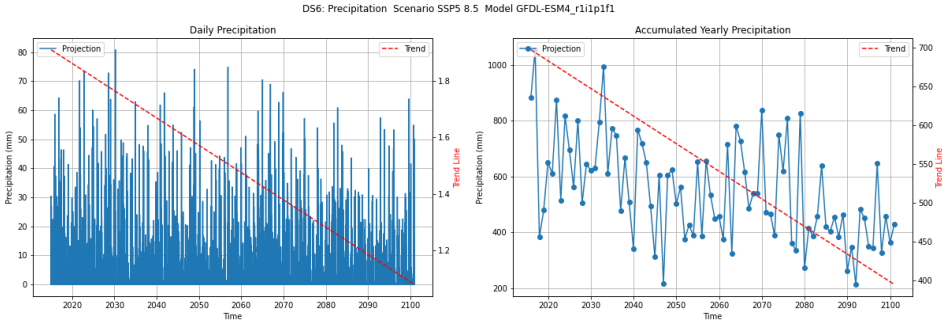

Figure 4.4-3 GFDL-ESM4_r1i1p1f1 model projections of precipitation in DEMO SITE 6.

4.4.1. DEMO SITE 1 - VALKENBURG LAKE (NETHERLANDS)

Precipitation modelled values for the Valkenburg Lake demo site show apparent ascending trends for daily and accumulated yearly precipitation for the SSP2 scenario, while slight descending trends are detected for the SSP5 scenario. Both minimum and maximum temperature projections for SSP2 and SSP5 allow to discern remarkable ascending trends, with values of almost 2 degrees for the SSP5 over the SSP2 scenario.

4.4.2. DEMO SITE 2 - OUED SOUHIL, NABEUL (TUNISIA)

Climate projections for the Tunisian demo site (DS2) are showing the most relevant effects of climate change in the Mediterranean region, as decreasing precipitation values, but concentrated in less time, as well as an increase in the minimum and maximum temperature. In this case, very high daily precipitation rates can be observed for SSP2 and SSP5 scenarios, being higher in the last one. Also, accumulated yearly precipitation values are very alarming, with values under 300 mm/year. Both yearly averages of minimum and maximum temperatures show increments of +2°C for SSP2 and +4°C for SSP5, while daily trends have a slight ascending slope.

4.4.3. DEMO SITE 3 - FRIELAS (PORTUGAL)

As well as for the DS2 in Tunisia, the Frielas demo site (Portugal) climate projections are showing significant descending trends in both daily and yearly precipitation for SSP2 and SSP5 scenarios, respectively. On the other hand, ascending trends are also distinguishable in the minimum and maximum temperature modelling. However, the magnitude of the increase in temperatures is lower than in the Tunisian case.

4.4.4. DEMO SITE 4 - EMILIA-ROMAGNA (ITALY)

Remarkable descending trends of yearly precipitation for the SSP5 scenario in the Emilia-Romagna demo site are visible, with more than 200 mm/year less precipitation by the end of the century. Special attention deserves the high values that daily precipitation can achieve not only in the SSP5 scenario but also in SSP2, which can be translated into important flooding in the Po basin.

4.4.5. DEMO SITE 5 - CAPE FLATS (SOUTH AFRICA)

Previously it has been mentioned that the Mediterranean region is going to be more sensitive to Climate Change impacts, but also those other regions with Mediterranean climate in the World, such as South Africa. In this demo site, noticeable descending trends of precipitation show a high affection for Climate Change, reducing in some cases by half the current values. This is more remarkable when analysing SSP5 scenarios. Temperature extremes also show ascending trends, like in all the other demo sites, with slight increases regarding minimum values and higher ones regarding maximum temperatures. Remarkable increases of more than 3.5°C can be achieved by 2100.

This project has received funding from the European Union's Horizon Europe research and innovation programme under grant agreement No GA 101082048
Funded by the European Union

4.4.6. DEMO SITE 6 - MARBELLA (SPAIN)

Climate Change projections for the Marbella demo site (Spain) are one of the best examples of the impact in Mediterranean areas. Important decreases in the annual precipitation, as well as increased daily accumulated precipitation, in the form of flash storms and floods, will decrease the resilience of the territory, which is more noticeable under the SSP5 scenario. Temperature values also show increases, being more than 2°C and 4°C in the case of minimum and maximum values, respectively, for both SSP2 and SSP5 scenarios.

4.4.7. DEMO SITE 7 - LIMA RIVER ESTUARY (PORTUGAL)

The same behaviour that was described for demo site 3, in Frielas (Portugal), can be observed in the Lima River Estuary demo site (Portugal), but with different magnitudes of values. An important decrease of more than 1000 mm/year of rainfall in some years, as well as a high number of strong rainy days, are shown. This can be interpreted as a switch from an Atlantic climate to a Mediterranean climate in this area. Minimum and maximum temperatures also show remarkable increases (> 2°C and > 4°C, respectively), being always higher under the SSP5 scenario.

5 CONCLUSIONS AND NEXT STEPS

5.1 MOD-REACH

Regarding the numerical model of the El Señorío aquifer, we can summarise the conclusions obtained in the following points:

- The geometry of the model is based on the geophysical campaign collected in the report “Increase of the available resource through the improvement of the knowledge of the limits and geometry of the aquifers of Marbella” (GEOMAR PROJECT), 2017, which has been processed for its arrangement in 3D.
- There are 3 hydrogeological units: Quaternary, Pliocene, and Paleozoic. The Quaternary is very thin (around 1 metre in of Señorío wells and Torreverde) so it barely intervenes in the model, the Pliocene has an average thickness of 100 metres and a high conductivity, and the Paleozoic constitutes the "waterproof" base of the Señorío aquifer. Quaternary and Pliocene are of detrital nature, waterproof, and metapelitic.
- There is a channel that crosses the aquifer from north to south (Nagüeles stream) with which there is hydraulic transfer. The model's adjustment mainly defines it as a winning stream, the aquifer mainly gives it water in its initial section. However, the amount of circulating water would be less than 0.1 hm^3/a (274 m^3/d).
- The hydraulic parameters assigned to the model come from a pumping test carried out in the Señorío 4 well, from previous studies and the calibration of the numerical model. The achieved values are:

Table 5.1-1 Hydraulic parameters assigned to the model.

LAYER	CONDUCTIVITY (m/d)	STORAGE
QUATERNARY	0.5-0.01	0.01
PLIOCENE	0.3-50	0.01-0.05
PALEOZOIC	0.01-0.001	0.001

This project has received funding from the European Union’s Horizon Europe research and innovation programme under grant agreement No GA 101082048
Funded by the European Union

- There are 12 control points (wells/observation heads), 6 of them are municipal, are in operation and are perfectly controlled in terms of flow and levels, although 2 of them act exclusively as observation heads. The remaining 6 wells are privately owned, so it is not known exactly if throughout the simulated period, they continue in operation with the pumping they were doing before the year 2000 (the period in which they were controlled).

Table 5.1-2 Coordinates, the use and flow of the 12 control points.

WELL	UTM X	UTM Y	Z (m a.s.l)	USE (*)	FLOW (hm^3/a)
Señorío 1	327465	4041811	27	P-I-H	0.56-0.13
Señorío 2	327469	4041662	26	P-I-H	
Señorío 3	327567	4041668	21	P-I-H	
Señorío 4A	327478	4041734	26	I-H	
Señorío 4B	327480	4041726	26	H	0
Torreverde	327558	4041421	18	H	0
Norte Puente Romano	327619	4041800	26	P	0.65
Mezquita	327343	4041570	24	P	
Hotel Puente Romano	327520	4041549	20	P	
Este Puente Romano 1	327793	4041375	10	P	
Este Puente Romano 2	327679	4041502	16	P	

(*) P=Pumping well I=Injection well H=Head observation

- The initial simulation comprises the period 2000-2022, although the head observation appears from the year 2011. A second simulation is carried out for the period 2011-2023, with the objective of calculating the calibration error (RMSE).
- The inputs to the system correspond to the infiltration of rainwater, injection through wells and intrusion from the sea and to a very small extent from the Nagüeles stream. The outputs occur mainly by pumping, and towards the sea, and in a small proportion towards the stream.
- The model is validated with the most reliable source, which is the head, starting from hydraulic parameters consistent with previous studies/tests

This project has received funding from the European Union's Horizon Europe research and innovation programme under grant agreement No GA 101082048
Funded by the European Union

carried out in the area. The error (RMSE) reached is close to 10 % (2.625 m). It is considered that the lack of adjustment in some periods is due to the uncertainty about the exploitation regime of the private surveys, which has not been controlled since 2000.

- The average annual water balance corresponds to:

Table 5.1-3 Average annual water balance.

INPUTS		**OUTPUTS**	
RECHARGE	1.59	WELLS	1.22
WELLS	0.13	RIVER	0.08
RIVER	0.01	SEA	0.79
SEA	0.36		
TOTAL	**2.09**	**TOTAL**	**2.09**

The sea outputs are slightly more than double the marine water inputs into the aquifer.

- The simulated piezometry shows a predominant flow direction from north to south, with some concentration towards the extraction wells, in which there are minimums of up to - 6 metres above sea level, around the private use wells near the coastline (Este Puente Romano 1, 2 and Oeste Puente Romano), and -4 metres above sea level, at the Señorío 1 well. The Señorío 2, 3 and 4 wells are very close to -1 metre above sea level. The maximums reached correspond to the year 2010, where the recharge by precipitation (3.57 hm^3/a) exceeds 60% of the average, as does the injection by wells (0.33 hm^3/a), in this situation, punctual levels of 23 m above sea level are reached in the Señorío wells and 15 metres above sea level, in Torreverde.
- The transport model predicts that with an input of chlorides through the coastline concentration equal to 19,000 mg/L, there will be an advancement of about 200 m towards the aquifer, significantly affecting the Oeste Puente Romano well (>10,000 mg/L) and Este Puente Romano 1 (5,000 mg/L approx.). Beyond that distance, the concentration of chlorides would not pose a risk to the potable water supply to the municipality (<250 mg/L, according to RD 140/2003).
- Considering the variable density module (SEAWAT), the sea intrusion would cause an impact around the coastline, with a gradual increase as it goes deeper into the aquifer. However, the risk of contamination would disappear from about 200 metres upstream of it.
- For a better understanding of the aquifer's hydrodynamics and adjustment of the numerical model, it is recommended:
    - Carry out differential measurements along the Nagüeles stream to determine the river-aquifer relationship more accurately.
    - Investigate the updated extraction of private-use wells and if possible take some piezometric level measures in order to reduce uncertainty and achieve a better calibration of the model.

This project has received funding from the European Union's Horizon Europe research and innovation programme under grant agreement No GA 101082048

Funded by the European Union

- Improve the calculation of the recharge by infiltration of rainwater from the aquifer.

5.2 DATA-REACH

5.2.1 RETROSPECTIVE CLIMATE ANALYSIS

The hydrometeorological analysis conducted in the study area has identified a certain interannual climate variability concerning precipitation, characterised by wet, dry, and average periods. In such a climate, it is crucial to understand the environment and manage resources effectively to meet demands during dry periods and utilise surplus resources during wet periods. This study aimed to identify dry and wet periods using two climate indices, the SPI (Standardised Precipitation Index) and the SPEI (Standardised Precipitation Evapotranspiration Index). Correlations were then made between these indices and quantitative (piezometric levels) and chemical (physicochemical parameters of water) variables to detect potential temporal deterioration of the Marbella-Estepona groundwater body (060.040) due to drought events.

The comparative analysis of SPI and SPEI showed that both indices allowed the identification of dry and wet periods throughout the study period. However, these indices have numerous limitations, including discrepancies in the length of records for calculating both indices, resulting in an overestimation of drought events by the SPI (longer record). The type of dry periods identified varied depending on the seasons and indices used. However, considering the percentage of dry months throughout the study period, a general trend was observed in most stations to detect a higher percentage of months categorised as "extremely dry" using the SPEI.

In general, no uniform pattern was observed regarding the indices in different stations. Therefore, it was not conclusively determined which of the two indices more accurately reflects the climatic reality in the study area. The relationships of these indices with the piezometry of some representative points in the study area indicate that the piezometric evolutions of most points do not clearly show the droughts identified by the indices. However, certain points with a more extended record period did reflect some more relevant dry and wet periods, such as 1998/99 and 2009/10, respectively.

The results of the correlations between the climate indices and the physicochemical parameters sometimes showed high correlations for some parameters. A more detailed analysis of these correlations revealed that there are certain changes in parameter values when rainy and dry episodes occur. However, a significant limitation was detected regarding the small number of samples and, above all, the periodicity with which they are taken. Not all compared samples are taken on the same date, making a precise analysis even more complex.

Consequently, there is a clear need to improve the quantitative and chemical sampling network in the Marbella-Estepona water body by the Andalusian Government, regarding sampling points and periodicity in sample collection. Additionally, improving the record of control meteorological stations is suggested. During this study, it was found that a high number of missing data in the series of meteorological variables, particularly precipitation and temperature, significantly affects analyses using climate indices. For this reason, greater attention to the quality and continuity of meteorological records is recommended, especially if predictions related to climate change in the study area are to be made.

This project has received funding from the European Union's Horizon Europe research and innovation programme under grant agreement No GA 101082048
Funded by the European Union

Apart from the limitations found in the correlation analysis between the climate indices and the status variables, both chemical and quantitative, in relation to the data scarcity and the periodicity of the samples, especially in the case of the physicochemical parameters, several factors add complexity to this analysis in the study area. The analysis of drought indices based on a natural signal such as climatology does not present a good fit for the Marbella-Estepona groundwater body. In the Mediterranean climate context, droughts should not be counted below the year, and even less below the month, as is the case with the indices studied.

Despite these limitations, an attempt was made to analyse to what extent the aquifer sectors of this groundwater body are marked by the climate signal from these indices. Although some relationships of these indices in the evolutions of piezometric levels and physicochemical parameters have been detected, the study area presents certain complexity, as the aquifers that make up the groundwater body are coastal and small, mostly subject to intensive exploitation. All this contributes to the difficulty of affirming that the decrease in piezometric levels and the deterioration of water quality is a consequence of the climate signal (detection of drought periods) rather than the influence of pumping or sea intrusion given the proximity to the sea.

Therefore, this study suggests the need to contrast the information from the correlations obtained with subsequent research on the influence of pumping, sea intrusion, and artificial recharge on the quantitative and chemical status of the waters, in addition to trying to analyse the influence of the climate signal. Additionally, an improvement in climate indices is proposed, as these are used in most organisations that manage water resources and do not always accurately reflect the climate context.

5.2.2 PREDICTIVE MODELS

Piezometric levels predictive models are very capable of reproducing the hydrogeological dynamics (seasonal fluctuations with lower values during Summer and higher values during Winter and Spring) of the studied aquifers with remarkably low uncertainty and high similarity with the real behaviour of groundwater level variations. The average sMAPE value of all models is 23.7 %, while MDA (Mean Directional Accuracy) is around 71 %, which means a very nice reproduction of the variability of groundwater level in the modelled wells. The coverage value of 89.4 shows a very nice accuracy of the predictions.

An exception can be made when analysing the Río Verde MB results (Appendix D Figure D-5), as it shows the highest sMAPE values (40.98 %), as well as the lowest MDA (51.1 %). Nevertheless, the predictive model still is able to reproduce Summer descending levels and a slight increase during the Autumn of the simulated period.

The predictive model carried out for the electrical conductivity of the Señorío well (Appendix D Figure D-9) presents a very nice coverage (100 %), but also a very low sMAPE (5.8%) and a 52% of MDA. The predicted values are very close to the real ones, both in values and trend, as they clearly represent the slight increase of electrical conductivity in groundwater of coastal aquifers when sufficient rainfall is not taking place, so then an increase of saline intrusion can occur.

Predictive models of storage volume in the three analysed reservoirs show very high consistency and accuracy, as sMAPE values range from 10.28 % to 13.91%, MDA ranges between 58% and 73.33%, and coverage ranges from 65% to 87.04%. These models represent with noticeable fidelity the descending levels of storage volume in the reservoirs, considering months with the absence of precipitation.

This project has received funding from the European Union's Horizon Europe research and innovation programme under grant agreement No GA 101082048

Funded by the European Union

It is important to take into account that stored water predictions use only one explainable variable (precipitation), and that the reservoirs may have other additional parameters. La Concepción reservoir (Appendix D Figure D-10) shows higher sMAPE and lower coverage values, as it has a lower capacity of storage, and therefore its hydrological response when it receives inputs from rainfall or rivers, or when water is taken for other uses, is faster. On the other hand, Charco Redondo and Guadarranque (Appendix D Figure D-11 and D-12, respectively) reservoirs have more storage volume (+ 20 hm^3), so their hydrological responses are smoother and, therefore, predicted volumes are more accurate.

In the forthcoming months, a UNIBO student will be based at Cetaqua to attempt to assess the efficacy of two different tools, DRONE and REACH, in forecasting the impacts of climate change on the Spanish demo site (Marbella). The DRONE model will be applied to the Spanish context, providing insights into its adaptability. The outcomes from both models will be compared, highlighting their respective strengths and potential areas for improvement. The possibility of synergies between the two will also be explored. Lastly, a managed aquifer recharge simulation may be carried out to evaluate the potential of human intervention in reducing saline water intrusion.

5.3 GIS-REACH

A groundwater pollution risk mapping methodology has been developed in the framework of this project, based on existing knowledge but also incorporating breaking new spatial information such as land subsidence and near-real-time land use data, as well as projected sea level rise, among others.

Selected variables for mapping vulnerability, hazard and exposure to groundwater pollution have been adapted to be applied in almost every aquifer throughout Europe's borders. Of course, there exist several parameters, such as groundwater depth, that require local information or inputs. Nevertheless, if a replication site has the availability of more precise data, it can also be used while adapting the format of the spatial data.

Risk mapping of groundwater pollution has been assessed in 4 demo sites, located in Portugal (Frielas - DS3), Italy (Emilia-Romagna - DS4), South Africa (Cape Flats - DS5) and Spain (Marbella - DS6). Among the three components of risk, vulnerability maps show remarkable differences between the applied methods (GALDIT, DRASTIC, GOD), with being DRASTIC the most accurate one in terms of spatial resolution.

In general, less populated areas with the presence of natural type land uses, coinciding with low permeability geological features, present lower values of risk of groundwater pollution. On the other hand, populated areas, regions with predominant urban and agricultural landscapes, and optimal hydrogeological characteristics for groundwater flow and pollutant transport are the ones showing higher risk values. Also, when assessing risk using the GALDIT vulnerability method, the shoreline of coastal aquifers is always showing the highest risk values.

5.4 CLIMATE PROJECTIONS

This methodology offers a flexible tool for users to access and analyse climate projection data over time, integrating data from various sources for a comprehensive understanding of potential or historical climate changes in specific regions. However, users must interpret these results carefully, considering the models, assumptions, and data quality involved. Factors like local topography and regional climatic influences should also be considered. Despite providing valuable insights, these projections are

This project has received funding from the European Union's Horizon Europe research and innovation programme under grant agreement No GA 101082048
Funded by the European Union

not definitive predictions and should be viewed with scepticism, especially when used for decision-making in policy, planning, or resource management.

The results primarily highlight a trend towards decreased precipitation and increased temperatures across all cases and scenarios (with an exception). This suggests a future with less rainfall and higher temperatures, which not only has significant implications for policy formulation and adaptation/mitigation strategies but also further enhances our understanding of the potential impacts of climate change.

Impacts of climate change projections previously analysed can lead to quantitative and qualitative impacts on both surface water and groundwater resources, which empower the need for regional mitigation and adaptation strategies such as Managed Aquifer Recharge (MAR).

So, an overall decrease of accumulated precipitation in almost all the demo sites, as well as very concentrated daily rainfall, are going to put urban and agricultural uses in danger, as well as the ecosystem's survival. This impact will be higher as temperature rises and, therefore, evapotranspiration values will be higher.

MAR strategies can contribute to mitigate this issue by storing and accumulating surface water coming from recent precipitation in the aquifers, so it can be used after in other demanding periods, such as Summer, when no rainfalls are taking place and usually reservoirs have lower storage. Also, MAR actions would help the conservation of the groundwater resource by acting as a filter for raw pollution coming from surface water and cleaning the existing groundwater (by pumping and injection).

All these climate projections will be shared with the technical partners of the consortium, particularly, focusing on DRONE and RAINREC digital tools.

5.5 INSIGHTS ON THE USEFULNESS OF REACH TOOL FOR FOSTERING MANAGED AQUIFER RECHARGE IN THE CONTEXT OF CLIMATE CHANGE

The versatility and functional diversity of the different components of the REACH tool give it the following attributes:

- The construction of a physical model for the simulation of groundwater functioning (e.g., **MOD-REACH**) allows the generation of 'what-if' scenarios to evaluate the impacts and benefits of new MAR schemes. These scenarios provide key information to foster one or another type of MAR scheme.
- The use of AI-based techniques programmed in the open language (Python) gives data-driven models (**DATA-REACH**) a high potential for replication and transferability in other geographical, climate, and hydrogeological contexts.
- These AI-based techniques (**DATA-REACH**) have been applied to a wide range of variables (stored water in reservoirs, groundwater levels and electrical conductivity), and all of them need to be considered to establish specific and optimised MAR regimes. MAR performance depends on current but also future 'water boundary' conditions (e.g., predicted stored water in a reservoir linked to a MAR operation scheme). Such risk management strategies will be defined in **deliverable D4.6**.
- The methodology used for the predictive models (**DATA-REACH**) developed on the current **D4.3** can be applied to other time series/variables directly related to MAR operation (water levels in infiltration basins, clogging risk in boreholes, ...), promoting the performance and effectiveness on the short, mid and long-terms.

This project has received funding from the European Union's Horizon Europe research and innovation programme under grant agreement No GA 101082048
Funded by the European Union

- The retrospective climate analysis (**DATA-REACH**) can contribute to the identification of groundwater areas more vulnerable to climate change impacts (e.g., statistical correlation between historical decreasing drought trends and groundwater body status), and, in consequence, be good candidates to implement MAR systems.
- The module related to the geospatial analysis of vulnerability and risk to groundwater pollution (**GIS-REACH**), is crucial to identify areas of interest (AOI) in which MAR schemes are implemented. The combination of the risk pollution maps together with those related to MAR potential areas will provide a composite GIS result that will be deeply analysed in **deliverable D4.6**.
- Regarding seawater intrusion risk mapping (**GIS-REACH / GALDIT**), the identification of groundwater areas highly impacted by the saltwater interface can inform on the necessity to implement specific MAR schemes as seawater intrusion barriers. In the line of the previous bullet point, the combination of such a vulnerability mapping and MAR feasibility data will permit the study of potential recharge water to be used.
- The efforts done to conceptualise and develop a GIS methodology (**GIS-REACH**) fed by spatial data at the European level (as minimum data requirements) is a crucial added value proposition of the REACH Tool as a whole.

- The REACH tool's components (e.g., MOD-REACH, DATA-REACH, GIS-REACH) offer comprehensive simulation, risk assessment, and predictive modelling capabilities. This holistic approach supports optimised MAR implementation and risk management strategies across different contexts, especially useful when facing administrative and public perception barriers.

This project has received funding from the European Union's Horizon Europe research and innovation programme under grant agreement No GA 101082048

Funded by the European Union

6 REFERENCES

Alfors, J., Burnett, J.L. and Gay, T.E. (1973). Urban geology, Master Plan of California: the nature, magnitude and cost of geological hazards in California and recommendations for their mitigation. *Bulletin of California Division of Mines and Geology*, 198.

Aller, L., Bennet, T., Leer, J., Petty, J. and Hacket, G. (1987). *DRASTIC: A standardised system for evaluation groundwater pollution potential using hydrogeologic settings*. US Environmental Protection Agency. Ada. Oklahoma, 455 pp.

Argamasilla, M. (2017). *Desarrollo metodológico para la planificación y gestión del agua en áreas turísticas costeras sometidas a clima mediterráneo y a grandes variaciones estacionales de la demanda. Caso de la Costa del Sol Occidenta*l. Doctoral Thesis, Universidad de Málaga, 444 pp.

Chachadi, A.G. and Lobo-Ferreira, J.P. (2001). Sea water intrusion vulnerability mapping of aquifers using the GALDIT method. In *Proceedings of the UNESCO-IHP Workshop on Modelling in Hydrogeology*, Chennai, India, 3-7 December 2001.

Custodio, E. y Llamas, M.R. (1996). *Hidrología subterránea, tomo I (Groundwater Hydrology, Vol I)*. Ediciones Omega, Barcelona.

Daly, D., Dassargues, A., Drew, D., Dunne, S., Goldscheider, N., Neale, N., Popescu, C. and Zwahlen, F. (2002). Main concepts of the European Approach for (karst) groundwater vulnerability assessment and mapping. *Hydrogeological Journal*, 10(2), Heidelberg, 340-345.

Daly, D., Deporte, C., Hötzl, H., Neale, S. and Stournaras, G. (1997). *Definitions. Report of working ground 0*, meeting COST Action 620, Liege. 7 pp.

Darmendrail, D. (2001). *The French approach to contaminated-land management*. BRGM/RP-51098-FR, 150 p.

Ducci, D. (1999). GIS techniques for mapping groundwater contamination risk. *Natural Hazards*, 20, pp 279-294.

Foster, S. (1987). Fundamental Concepts in Aquifer Vulnerability, Pollution Risk and Protection Strategy. *International Conference, 1987, Noordwijk Aan Zee, the Netherlands Vulnerability of Soil and Groundwater to Pollutants*. Netherlands Organization for Applied Scientific Research, The Hague, 69-86.

Foster, S. and Hirata, R. (1988). *Groundwater pollution risk assessment: a methodology using available data*. WHO-PAHO-CEPIS Technical Report (Lima-Perú), 73 pp.

Fournier, E. (1979). Objectives of volcanic monitoring and prediction. *J. Geol. Soc.*, 136, 321-326.

Freeze, R.A. and Cherry, A.J. (1979). *Groundwater*. Prenctic Hall, Inc. Englewwod Cliffs. 604 pp.

Gneiting, T. and Katzfuss, M. (2014). Probabilistic forecasting. *Annual Review of Statistics and Its Application*, 1(1), 125–151. https://doi. org/10.1146/annurev-statistics-062713-085831.

This project has received funding from the European Union's Horizon Europe research and innovation programme under grant agreement No GA 101082048

Funded by the European Union

Hasan, M.F., Smith, R., Vajedian, S. et al. Global land subsidence mapping reveals widespread loss of aquifer storage capacity. *Nat Commun* 14, 6180 (2023). https://doi.org/10.1038/s41467-023-41933-z

Kopp, R.E., DeConto, R.M., Bader, D.A., Hay, C.C., Horton, R.M., Kulp, S., Oppenheimer, M., Pollar, D. and Strauss, B.H. (2017). Evolving Understanding of Antartic Ice-Sheet Physics and Ambiguity in Probabilistic Sea-Level Projections. *Earth's Future*, 5, 1217-1233.

López-Geta, J.A. and Gómez-Gómez J.D. (2007). La intrusión marina y su incidencia en los acuíferos españoles. Enseñanza de las Ciencias de la Tierra, 2007 (15.3), 266-273. I.S.S.N.: 1132-9157.

Mitchell, J.K. (1990). Human dimensions of environmental hazards, complexity, disparity and the search for guidance. In: A. Kirby (Ed), *Nothing to fear*. University of Arizona Press, Tucson. 131-175.

Panizza, M. (1988). *Geomorfologia applicata. Metodi di applicazione alla pianificazione territoriale e alla valutazione d'impato ambientale*. La nuova Italia Cientifica, Roma, 339 pp.

Perles, M.J., Vías J.M. and Andreo, B. (2004). Cartografía de vulnerabilidad y riesgo de contaminación en acuíferos carbonáticos. In B. andreo y J.J. Durán (eds), *investigaciones en sistemas kársticos españoles*. Spanish contribution to the Project 448 of the PICG of UNESCO, World Correlation of Karstic Ecosystems. IGME, Serie Hidrogeología y Aguas Subterráneas, 12, 247-273.

Raucher, R.L. (1983). A conceptual framework for measuring the benefits of groundwater protection. *Water Resources Research*, 19, 320-326.

Robins, N., Adams, B., Foster, S. and Palmer, R. (1994). Groundwater vulnerability mapping: The British perspective. *Hydrogeologie*, 3, 35-42.

Rowe, W. (1977). *An anatomy of risk*. John Wiley & Sons, New Jersey. 488 pp.

Sanz, E., Menéndez Pidal de Navascués, I. and Távara, C. (2011). Calculating the average natural recharge in large areas as a factor of their lithology and precipitation. *Hydrol. Earth Sust. Sci.*, 8, 4753-4788.

Shechter, M. (1985). Economic aspects in the investigation of groundwater contamination episodes. *Groundwater*, 23, 190-197.

Todini, E. (2018). Paradigmatic changes required in water resources management to benefit from probabilistic forecasts. *Water Security*, 3, 9–17.

Van Dissen, R. and Mcverry, G. (1994). Earquake hazard and risk in New Zealand. In: A.G. Hull and R. Coory (Eds). Proceedings of the Natural Hazards Management Workshop, Wellington. *Institute of Geological and Nuclear Sciences Information Series*, 31, 67-71.

Varnes, D.J. (1984). Landslide hazard zonation: a review of principles and practice. *Natural Hazards*, 3. UNESCO, 63 pp.

Vías, J. (2005). *Desarrollo metodológico para la estimación y cartografía del riesgo de contaminación de las aguas subterráneas mediante SIG. Aplicación en acuíferos del sur de España*. Doctoral Thesis, Universidad de Málaga. 458 pp.

This project has received funding from the European Union's Horizon Europe research and innovation programme under grant agreement No GA 101082048

Funded by the European Union

Zamrsky, D., Oude Essink, G. and Bierkens, M. (2017): Aquifer thickness along the global coastline: link to shape files [dataset]. *PANGAEA*, https://doi.org/10.1594/PANGAEA.880771

Zamrsky, D., Oude Essink, G. and Bierkens, M. (2018): Estimating the thickness of unconsolidated coastal aquifers along the global coastline. *Earth System Science Data*, 10(3), 1591-1603

This project has received funding from the European Union's Horizon Europe research and innovation programme under grant agreement No GA 101082048

Funded by the European Union

APPENDIX A. INVENTORY OF PIEZOMETRIC POINTS

Table A-1 Inventory of piezometric points.

Code	Point	Name	Start	End	Aquifer	Operated by	UTM coordinates	
							X	Y
P-1	P.06.48.001-S	Manilva Pz. 1	Mar-96	Mar-23	-	Junta	296.404	4.029.186
P-2	P.06.40.006-B	La Cala.	Dec-95	Mar-23	Pliocene	Junta	308.486,22	4.033.696,38
P-3	P.06.40.005-B	Padrón	Dec-95	Mar-23	Pliocene	Junta	311.178,63	4.034.676,92
P-4	P.06.40.004-B	Guadalmansa - Guadalmina	Feb-07	Mar-23	Quaternary	Junta	315.463	4.036.432
P-5	P06-40-003-S	Pz E-1	Aug-96	Mar-23	Quaternary	Junta	315.411	4.036.587
P-6	P06-40-004-S	Pz E-2	Aug-96	Mar-23	Quaternary	Junta	315.38	4.036.956
P-7	P.06.40.002-S	Pz-2	Oct-95	Mar-23	Plio-Quaternary	Junta	315.150,98	4.037.318,45
P-8	P.06.40.006-S	Guadlms. 1	Oct-03	Mar-23	Plio-Quaternary	Junta	315.185,52	4.037.653,65
P-9	P.06.40.007-S	Guadlms. 2	Feb-04	Mar-23	Plio-Quaternary	Junta	315.055,30	4.037.868,37
P-10	P.06.40.003-B	Guadlmn. Urb. Alh.	Feb-07	Apr-21	Quaternary	Junta	320.016,61	4.037.820,89
P-11	P.06.40.001-S	Guadz. Pz-1	Feb-98	Mar-23	Quaternary	Junta	323.112	4.039.953
P-12	P.06.40.002-B	R. Verde. Ramb. Mb. Istán	Feb-07	Mar-23	Quaternary	Junta	325.363,40	4.042.679,68
P-13	P.06.40.001-B	R. Real	Feb-07	Mar-23	Pliocene	Junta	335.087	4.041.633
P-14	P.06.40.012-S	Siete Revuelt. PZ. 1	Feb-98	Mar-23	-	Junta	337.231	4.041.600
P-15	P.06.40.011-S	Real Zarag. Pz. 1	Feb-98	Mar-23	-	Junta	340.032	4.040.906
P-16	P.R. Guadalmina	P. Guadalmina	Jan-02	Nov-22	Quaternary	Hidralia	319.728	4.039.543
P-17	Cable Sky 1	C.Sky1	Apr-00	Nov-22	Pliocene	Hidralia	320.623	4.040.117
P-18	San Pedro 1	S.P. 1	Jan-00	Nov-22	Pliocene	Hidralia	321.048	4.040.281
P-19	Aloha Alto	Aloha Alto	-	-	Pliocene	Hidralia	324.656	4.041.676
P-20	Aloha Bajo	Aloha Bajo	Jan-00	Nov-22	Pliocene	Hidralia	324.766	4.041.703
P-21	Río Verde Marbella 3	RV-MB 3	Jan-00	Nov-22	Quaternary	Hidralia	325.378	4.042.277

This project has received funding from the European Union's Horizon Europe research and innovation programme under grant agreement No GA 101082048

Funded by the European Union

P-22	Río Verde Nueva Andalucía 3	RV.NA4	Jan-00	Sep-22	Quaternary	Hidralia	325.332	4.041.795
P-23	Señorío 1	Sñ 1	Apr-11	Jun-18	Pliocene	Hidralia	327.452	4.041.808
P-24	Señorío 2	Sñ 2	May-95	Nov-22	Pliocene	Hidralia	327.478	4.041.667
P-25	Señorío 3	Sñ 3	Jan-00	Nov-22	Pliocene	Hidralia	327.566	4.041.670
P-26	Señorío 4	Sñ 4	-	-	Pliocene	Hidralia	327.480	4.041.736
P-27	Piez. 4B	4B	Sep-20	Mar-23	Pliocene	Hidralia	327.840	4.041.726
P-28	Torreverde	Torreverde	Jan-00	Nov-21	Pliocene	Hidralia	327.558	4.041.429

This project has received funding from the European Union's Horizon Europe research and innovation programme under grant agreement No GA 101082048

Funded by the European Union

APPENDIX B. WELLS AND WEATHER STATIONS CONSIDERED IN APPENDIX A

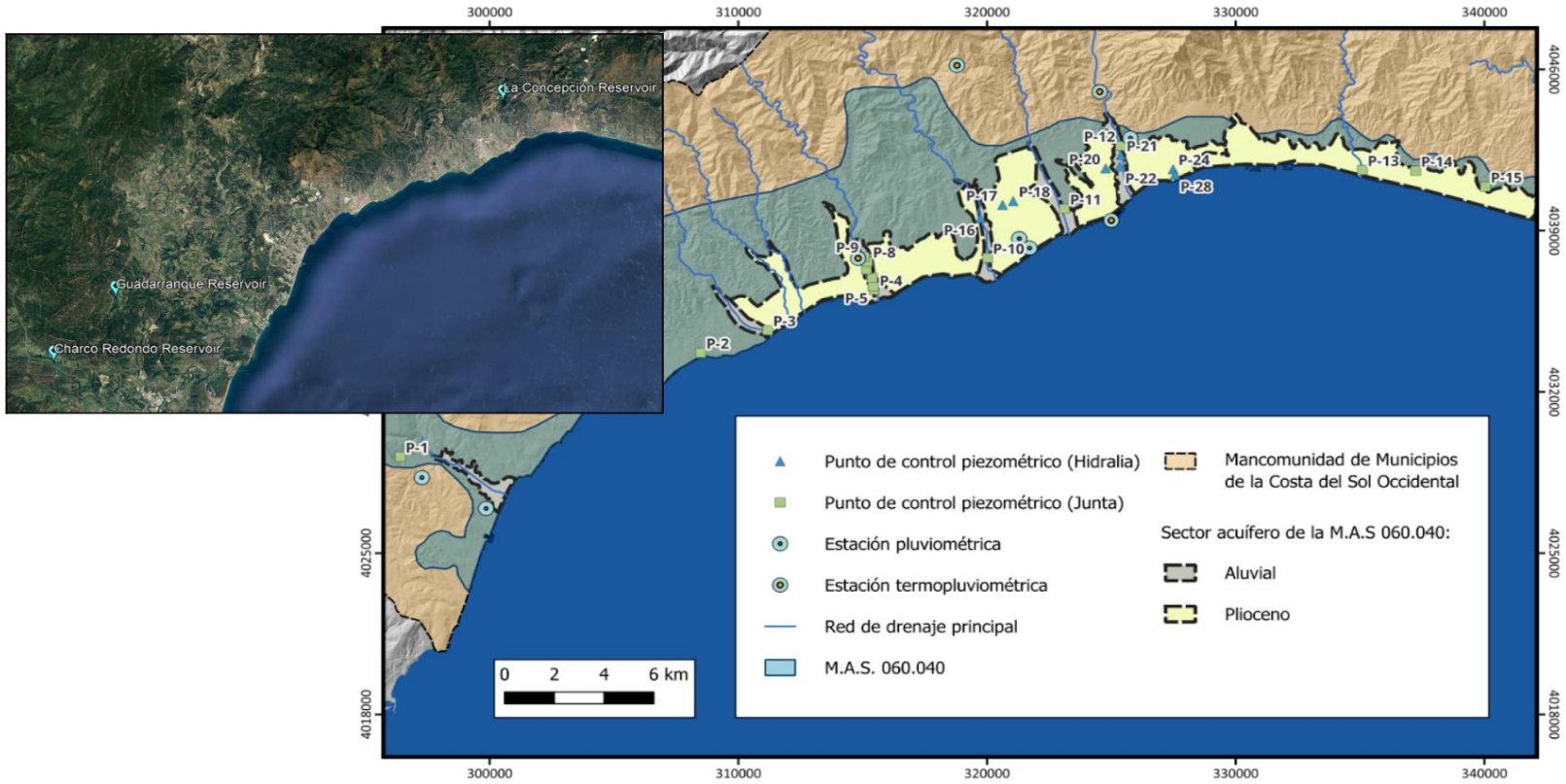

Figure B-1 Wells and weather stations considered in Appendix A Table A-1, as well as modelled reservoirs.

This project has received funding from the European Union's Horizon Europe research and innovation programme under grant agreement No GA 101082048

Funded by the European Union

APPENDIX C. EVOLUTION OF PHYSICOCHEMICAL PARAMETERS AT DIFFERENT SAMPLING POINTS

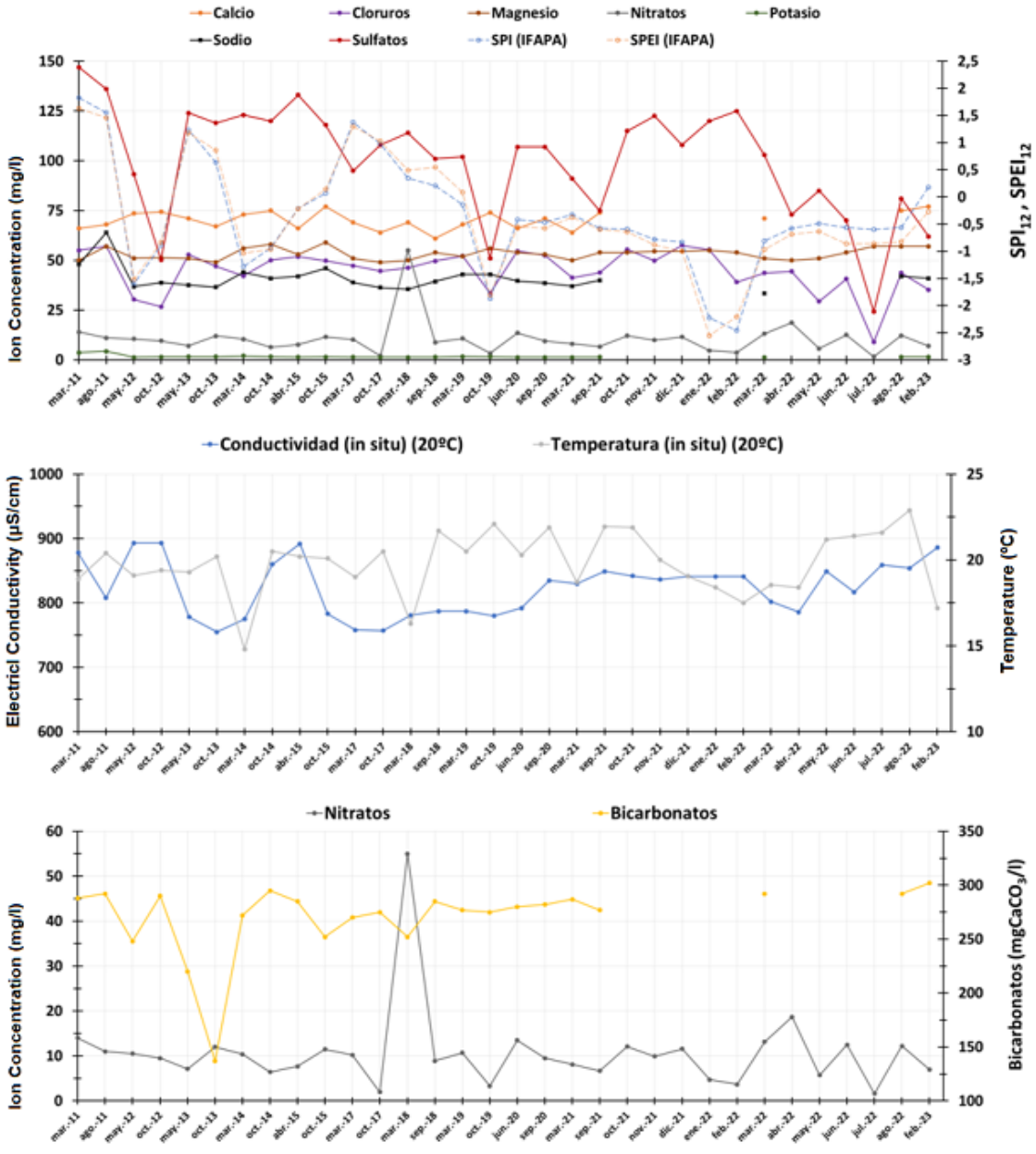

Figure C-1 Evolution of physicochemical parameters at the 'Monterroso' sampling point.

This project has received funding from the European Union's Horizon Europe research and innovation programme under grant agreement No GA 101082048

Funded by the European Union

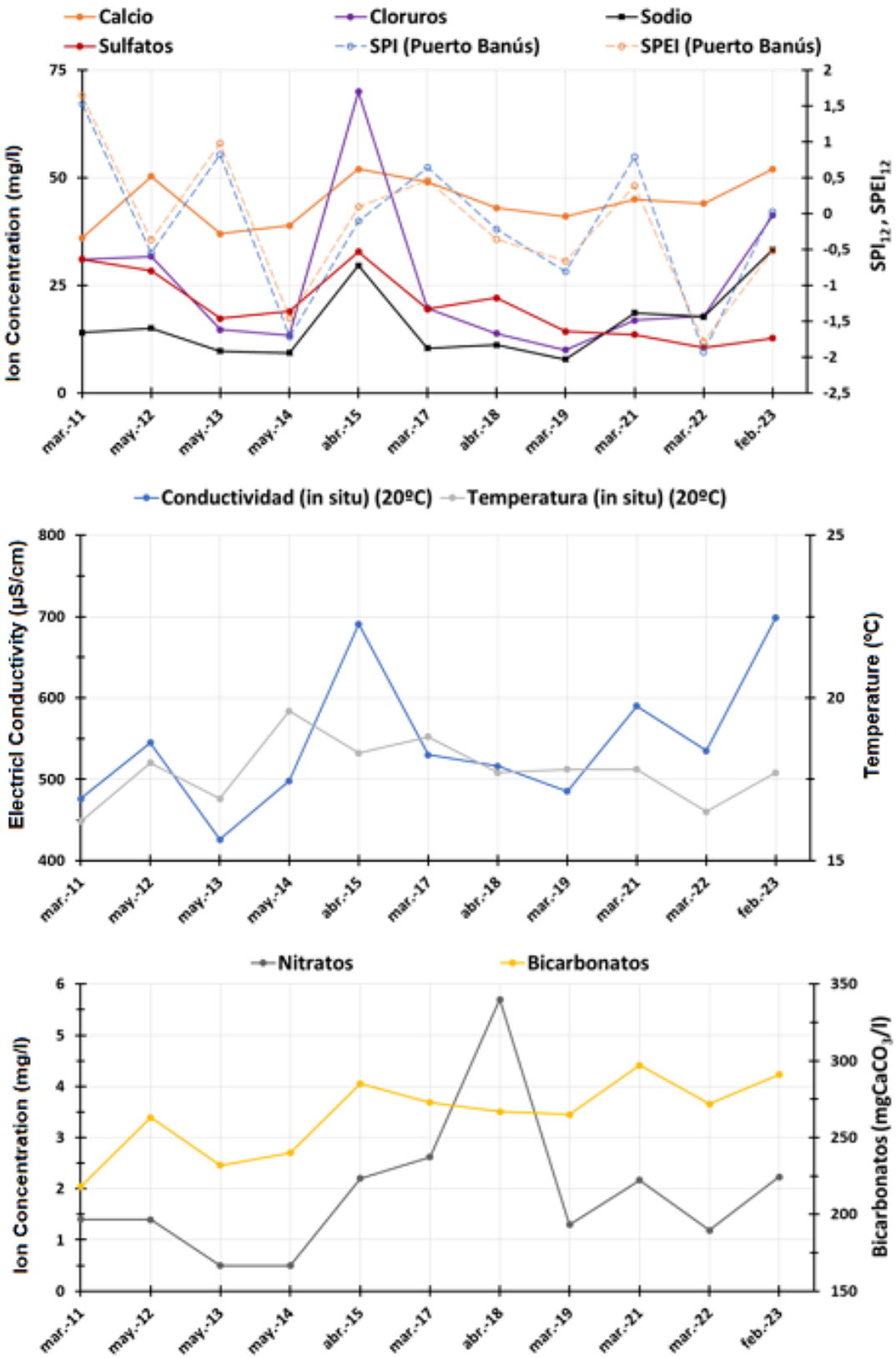

Figure C-2 Evolution of physicochemical parameters at the 'Río Verde' sampling point.

This project has received funding from the European Union's Horizon Europe research and innovation programme under grant agreement No GA 101082048

Funded by the European Union

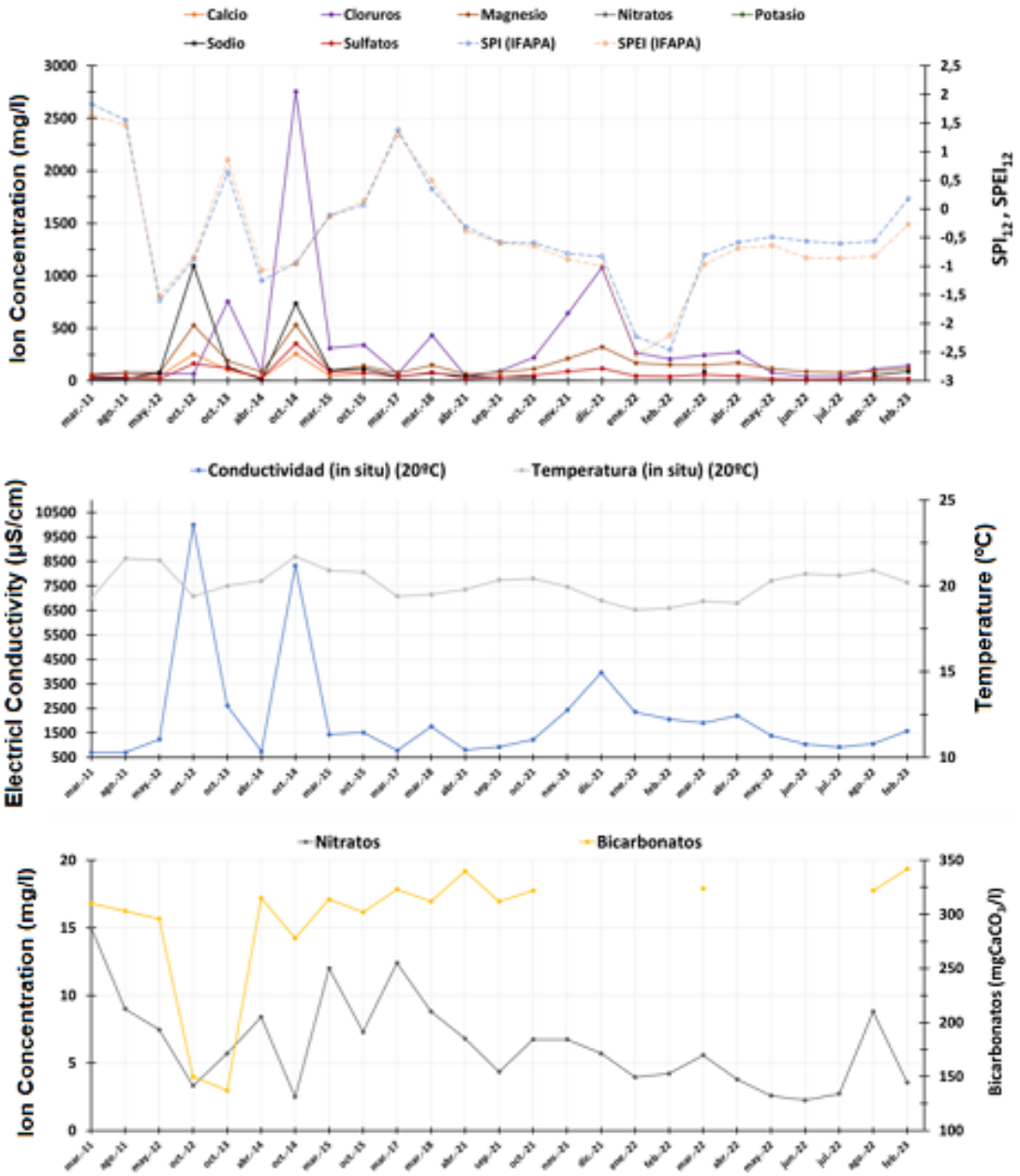

Figure C-3 Evolution of physicochemical parameters at the 'Río Padrón' sampling point.

This project has received funding from the European Union's Horizon Europe research and innovation programme under grant agreement No GA 101082048

Funded by the European Union

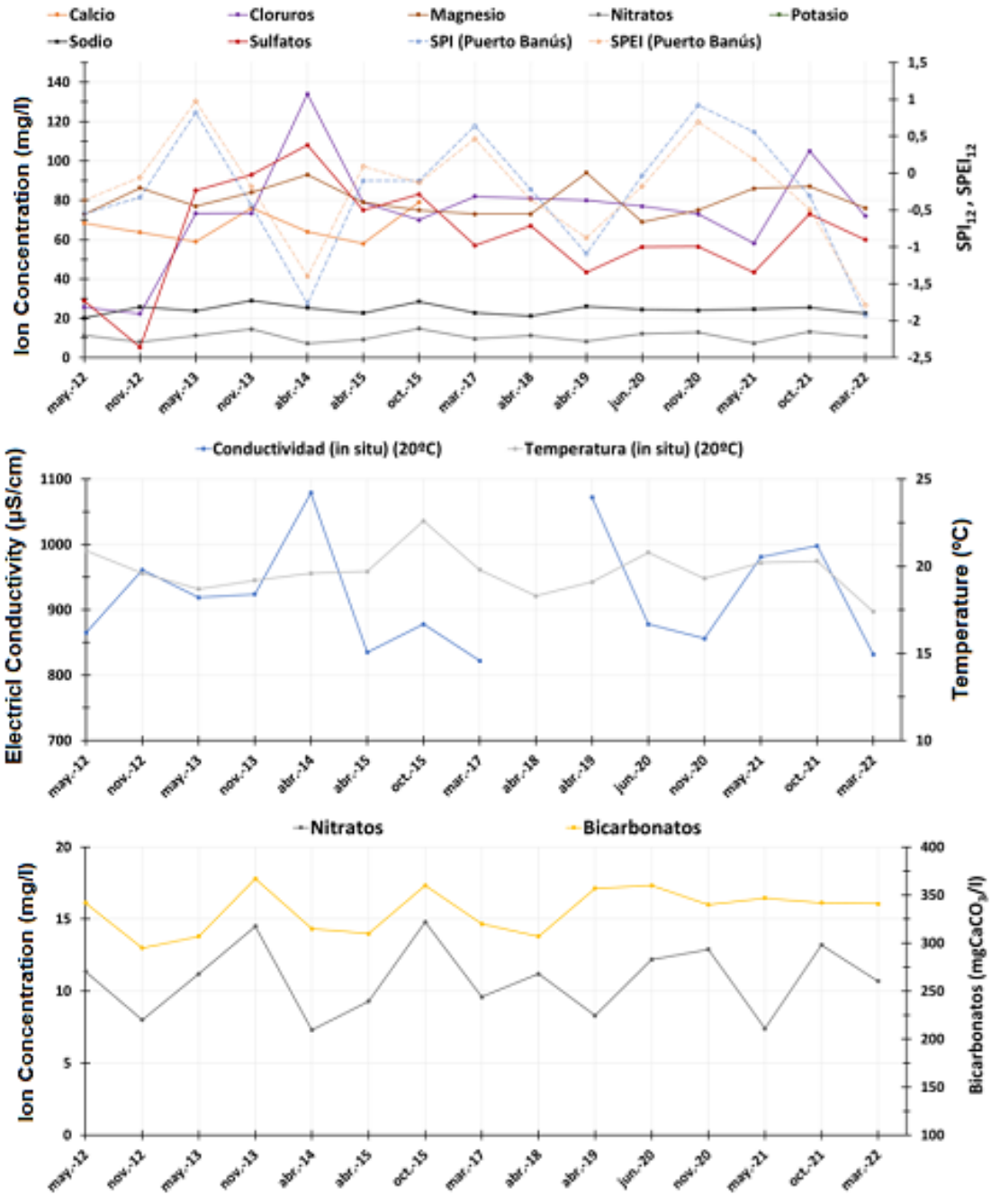

Figure C-4 Evolution of physicochemical parameters at the 'Señorío' sampling point.

This project has received funding from the European Union's Horizon Europe research and innovation programme under grant agreement No GA 101082048

Funded by the European Union

APPENDIX D. PREDICTIVE MODELS: VALIDATION PROCESS

Aloha: Piezometric level

Table D-1 Validation process metrics in the Aloha well.

DATE	SMAPE (%)	MDA	MAE	Coverage
2013-05-01	-	100	1.17	100
2013-07-01	-	80	1.45	100
2013-11-01	-	80	1.87	83.33
2014-03-01	-	80	2.03	66.67
2016-04-01	-	20	0.79	100
2017-02-01	-	100	3.18	33.33
2018-11-01	-	80	1.73	83.33
2019-01-01	-	60	0.83	100
MEAN	**-**	**75**	**1.63**	**83.33**

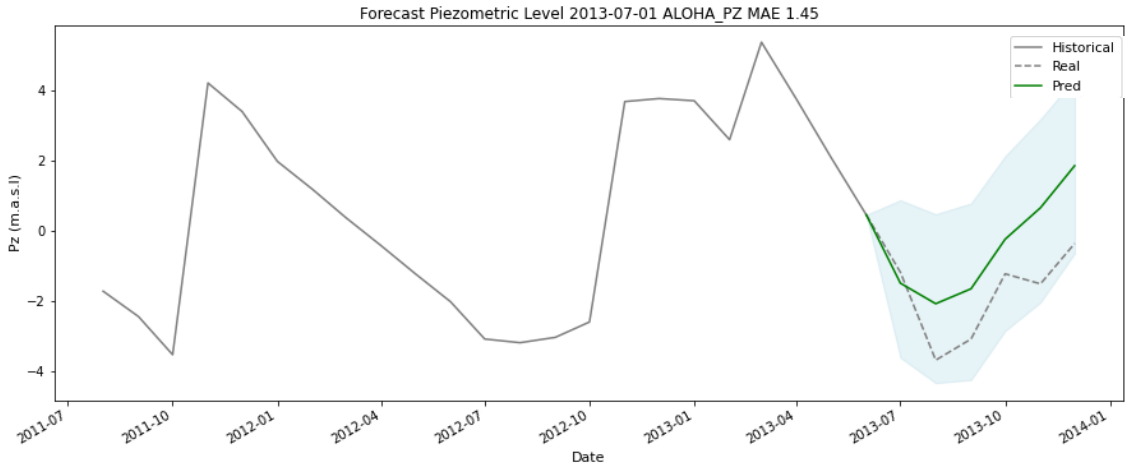

Figure D-1 Prediction of piezometric level (m.a.s.l.) in the Aloha well on one of the random dates used for the validation process. The blue shading refers to the prediction interval.

Guadaiza: Piezometric level

Table D-2 Validation process metrics in the Guadaiza well.

DATE	SMAPE (%)	MDA	MAE	Coverage
2015-03-01	1.83	100	0.14	100

This project has received funding from the European Union's Horizon Europe research and innovation programme under grant agreement No GA 101082048
Funded by the European Union

2015-12-01	11.35	80	0.82	83.33
2017-04-01	5.74	60	0.41	83.33
2017-05-01	6.22	60	0.43	83.33
2018-08-01	7.17	40	0.54	83.33
2019-09-01	6.16	20	0.46	100
2020-09-01	7.45	60	0.59	100
2020-12-01	9.57	80	0.77	83.33
MEAN	**6.94**	**62.5**	**0.52**	**89.58**

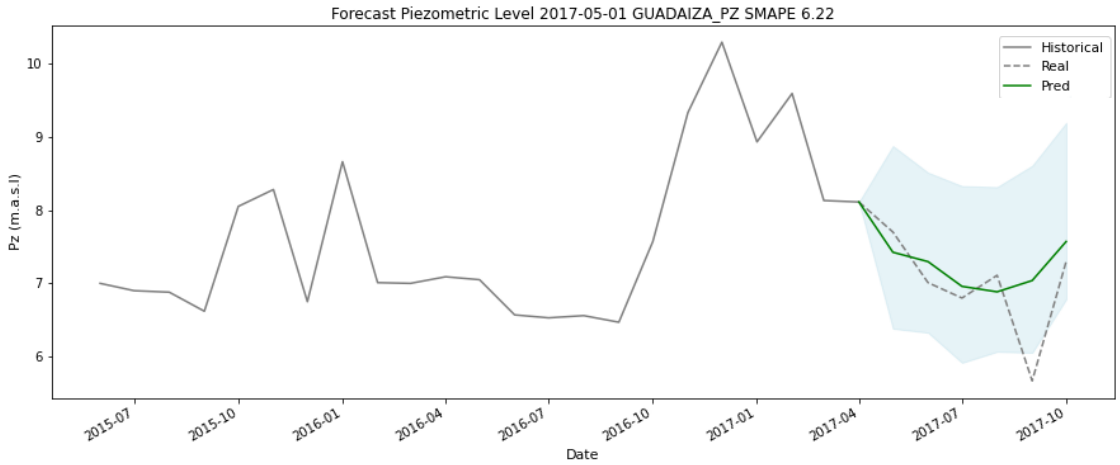

Figure D-2 Prediction of piezometric level (m.a.s.l.) in the Guadaiza well on one of the random dates used for the validation process. The blue shading refers to the prediction interval.

Guadalmansa: Piezometric level

Table D-3 Validation process metrics in the Guadalmansa well.

DATE	SMAPE (%)	MDA	MAE	Coverage
2013-01-01	30.77	80	2.1	100
2015-01-01	30.6	60	1.64	83.33
2015-05-01	22.75	80	0.8	100
2015-11-01	39.51	60	2.01	100
2016-04-01	14.7	60	0.42	100
2016-05-01	23.21	80	0.61	100
2016-07-01	25.24	80	0.67	100

This project has received funding from the European Union's Horizon Europe research and innovation programme under grant agreement No GA 101082048
Funded by the European Union

2016-11-01	42.24	40	2.84	50
2018-01-01	39.55	80	2.54	100
2018-04-01	21.85	100	1.2	100
MEAN	**29.04**	**72**	**1.48**	**93.33**

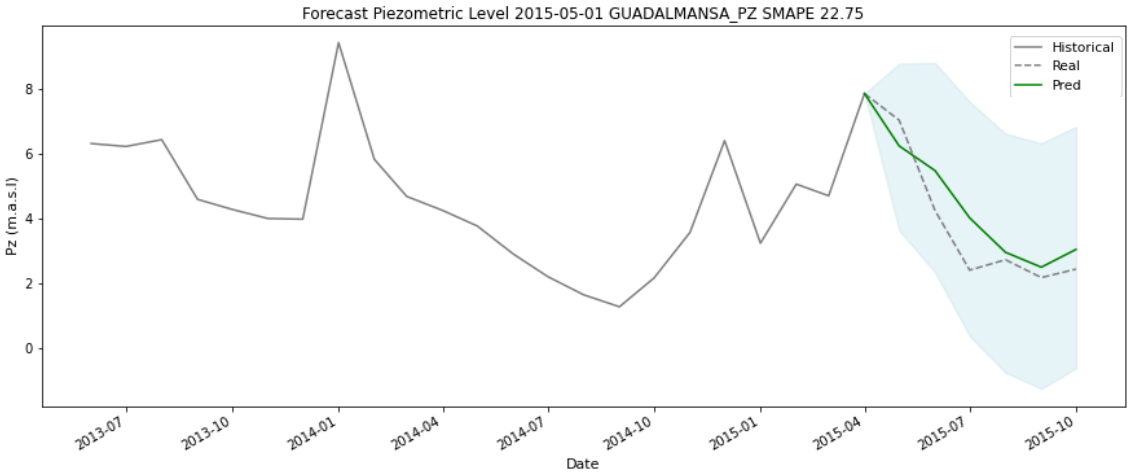

Figure D-3 Prediction of piezometric level (m.a.s.l.) in the Guadalmansa well on one of the random dates used for the validation process. The blue shading refers to the prediction interval.

Guadalmina: Piezometric level

Table D-4 Validation process metrics in the Guadalmina well.

DATE	SMAPE (%)	MDA	MAE	Coverage
2014-05-01	4.79	100	0.85	100
2014-07-01	2.86	60	0.51	100
2014-11-01	5.54	60	1.03	100
2015-03-01	5.6	60	1	100
2017-04-01	13.39	80	2.77	50
2018-02-01	1.5	100	0.28	100
2019-11-01	5	40	0.96	100
2020-01-01	5.64	60	1.08	100
MEAN	**5.54**	**70**	**1.06**	**93.75**

This project has received funding from the European Union's Horizon Europe research and innovation programme under grant agreement No GA 101082048
Funded by the European Union

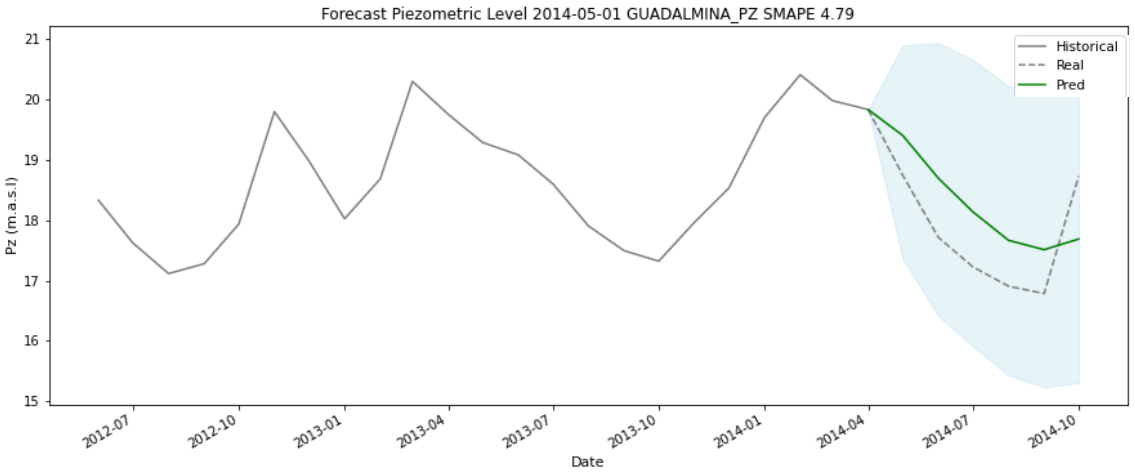

Figure D-4 Prediction of piezometric level (m.a.s.l.) in the Guadalmina well on one of the random dates used for the validation process. The blue shading refers to the prediction interval.

Rio Verde MB: Piezometric level

Table D-5 Validation process metrics in the Río Verde MB well.

DATE	SMAPE (%)	MDA	MAE	Coverage
2014-03-01	87.96	60	1.32	66.67
2014-09-01	31.64	60	0.65	100
2015-10-01	58.67	20	1.09	100
2016-03-01	46.28	40	0.74	100
2017-05-01	29.63	100	0.99	83.33
2019-02-01	17.3	40	0.32	100
2019-05-01	34.64	40	0.71	100
2019-11-01	26.88	20	0.57	100
2021-02-01	35.87	80	0.63	100
MEAN	**40.98**	**51.11**	**0.78**	**94.44**

This project has received funding from the European Union's Horizon Europe research and innovation programme under grant agreement No GA 101082048
Funded by the European Union

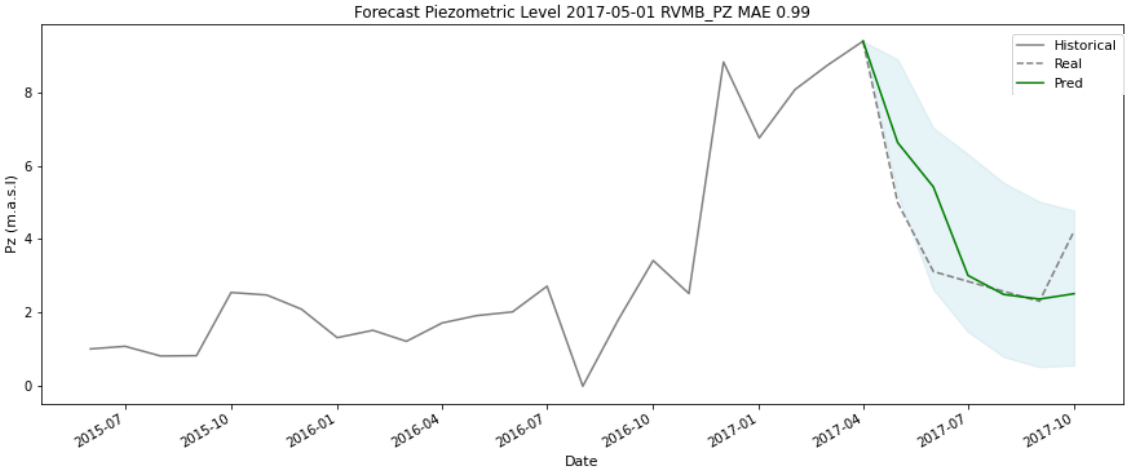

Figure D-5 Prediction of piezometric level (m.a.s.l.) in the Río Verde MB well on one of the random dates used for the validation process. The blue shading refers to the prediction interval.

Rio Verde NA: Piezometric level

Table D-6 Validation process metrics in the Río Verde NA well.

DATE	SMAPE (%)	MDA	MAE	Coverage
2016-03-01	23.3	60	0.19	100
2016-12-01	66.25	60	1.36	50
2018-04-01	29.37	80	0.41	100
2018-05-01	22.18	60	0.26	100
2019-08-01	23.34	80	0.34	83.33
2020-09-01	59.55	80	0.82	66.67
2021-09-01	11.98	60	0.16	100
2021-12-01	23.58	60	0.35	100
MEAN	**32.44**	**67.5**	**0.49**	**87.5**

This project has received funding from the European Union's Horizon Europe research and innovation programme under grant agreement No GA 101082048
Funded by the European Union

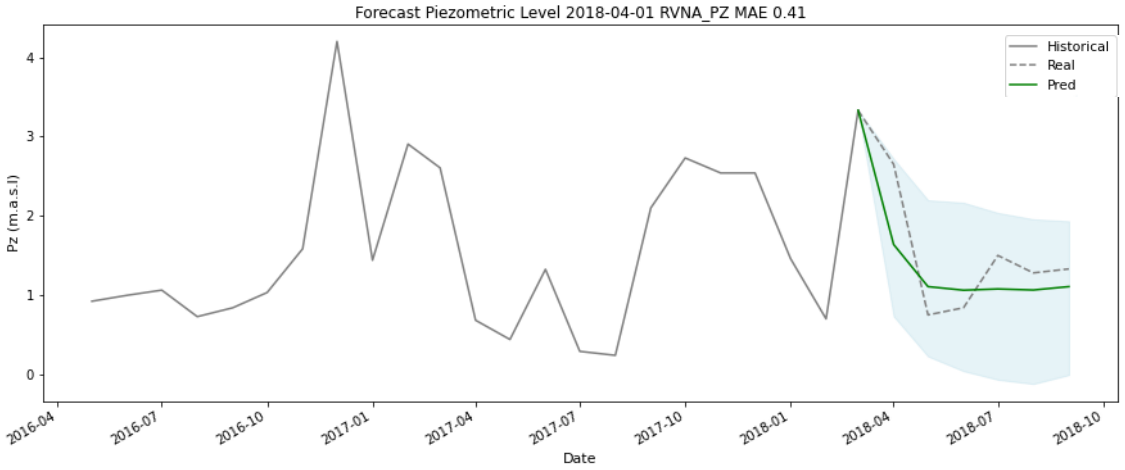

Figure D-6 Prediction of piezometric level (m.a.s.l.) in the Río Verde NA well on one of the random dates used for the validation process. The blue shading refers to the prediction interval.

San Pedro: Piezometric level

Table D-7 Validation process metrics in the San Pedro well.

DATE	SMAPE (%)	MDA	MAE	Coverage
2014-01-01	24.57	80	2.6	100
2014-03-01	44.88	80	3.99	100
2014-06-01	47.75	100	1.4	100
2014-10-01	28.36	100	1.75	100
2014-11-01	13.77	100	1.07	100
2015-01-01	10.02	80	1.21	100
2018-06-01	15.26	80	1.81	100
2018-11-01	17.84	60	3.03	83.33
2019-10-01	52.94	60	3.97	83.33
MEAN	**28.38**	**82.22**	**2.31**	**96.3**

This project has received funding from the European Union's Horizon Europe research and innovation programme under grant agreement No GA 101082048
Funded by the European Union

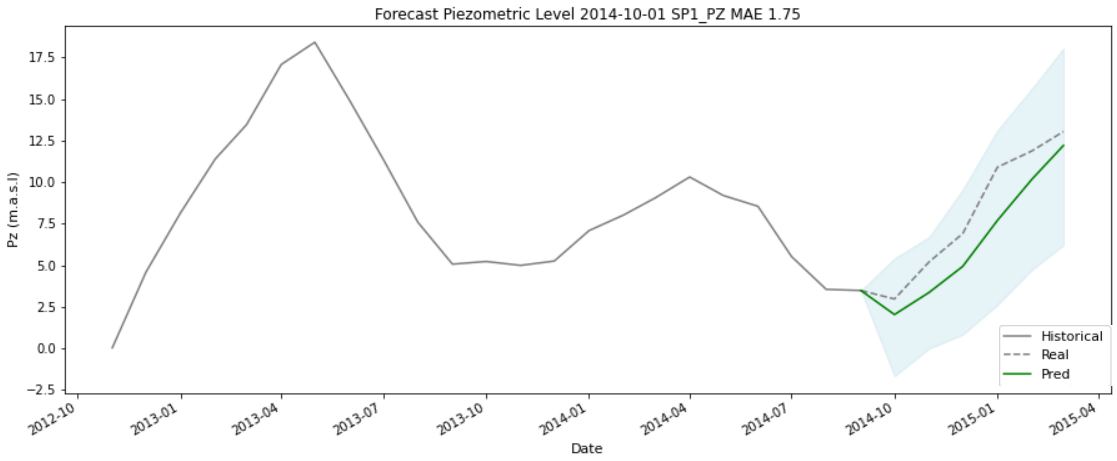

Figure D-7 Prediction of piezometric level (m.a.s.l.) in the San Pedro well on one of the random dates used for the validation process. The blue shading refers to the prediction interval.

Señorío: Piezometric level

Table D-8 Validation process metrics in the Señorío well.

DATE	SMAPE (%)	MDA	MAE	Coverage
2013-02-01	46.9	40	4.04	16.67
2013-03-01	51.27	60	4.09	16.67
2014-05-01	30.68	80	1.46	66.67
2015-04-01	18.04	100	1.14	83.33
2015-09-01	29.04	80	1.56	100
2016-10-01	44.87	80	2.45	50
2017-05-01	4.16	80	0.2	100
2017-09-01	24.37	80	0.93	100
2019-04-01	46.18	80	0.41	100
2019-12-01	36.37	80	1.64	83.33
MEAN	**33.19**	**76**	**1.79**	**71.67**

This project has received funding from the European Union's Horizon Europe research and innovation programme under grant agreement No GA 101082048

Funded by the European Union

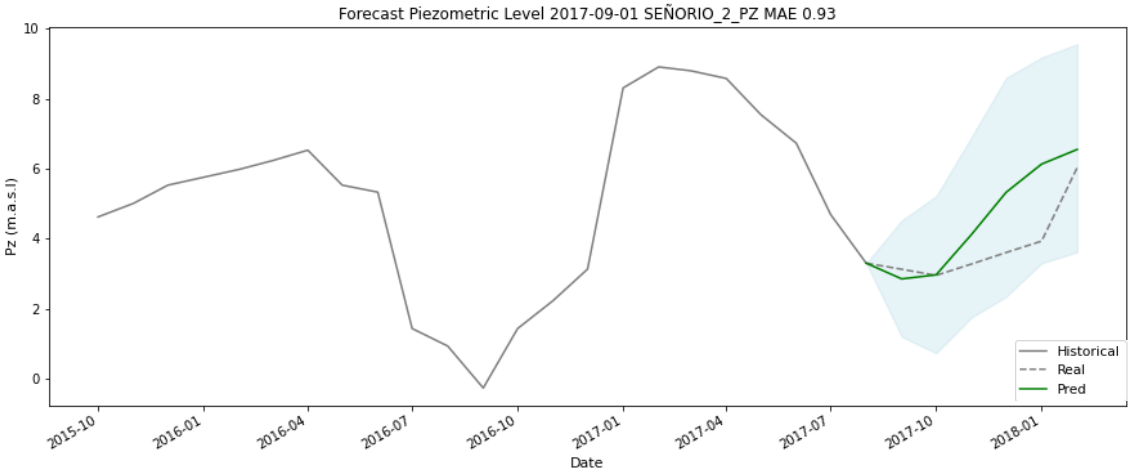

Figure D-8 Prediction of piezometric level (m.a.s.l.) in the Señorío well on one of the random dates used for the validation process. The blue shading refers to the prediction interval.

Señorío: Electrical Conductivity

Table D-9 Validation process metrics in the Señorío well.

DATE	SMAPE (%)	MDA	MAE	Coverage
2013-02-01	2.63	80	22.29	100
2013-03-01	4.11	100	35.5	100
2014-05-01	13.94	20	119.64	100
2015-04-01	2.65	40	22.49	100
2015-09-01	0.82	80	7.1	100
2016-10-01	6.7	40	61.36	100
2017-05-01	2.66	60	27	100
2017-09-01	8.87	0	92.7	100
2019-04-01	9.81	60	117.19	100
2019-12-01	6.52	40	65.8	100
MEAN	**5.87**	**52**	**57.11**	**100**

This project has received funding from the European Union's Horizon Europe research and innovation programme under grant agreement No GA 101082048

Funded by the European Union

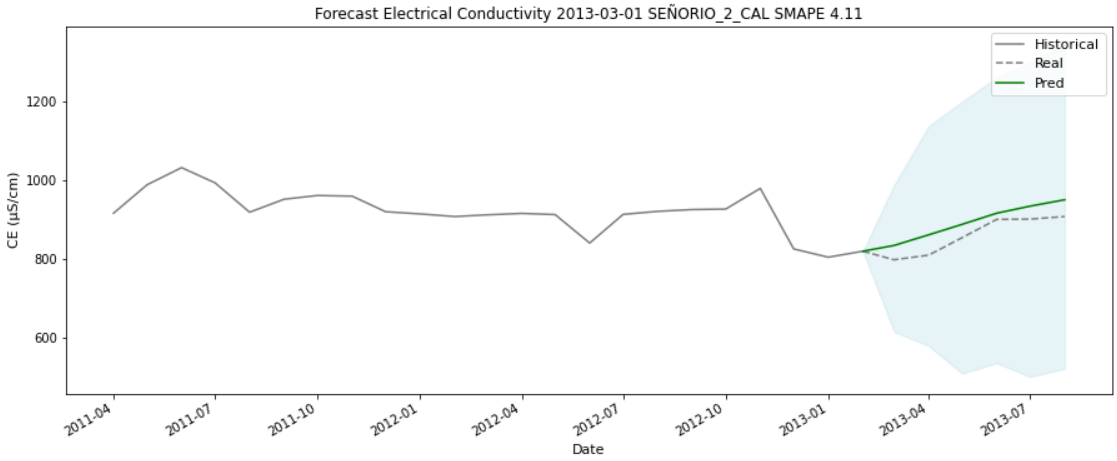

Figure D-9 Prediction of electrical conductivity (µS/cm.) in the Señorío well on one of the random dates used for the validation process. The blue shading refers to the prediction interval.

La Concepción: Reservoir volume

Table D-10 Validation process metrics in the reservoir of La Concepción.

DATE	SMAPE (%)	MDA	MAE	Coverage
2015-01-01	8.49	40	4.49	16.67
2015-04-01	9.34	80	4.51	66.67
2015-07-01	5.7	80	2.43	83.33
2016-06-01	19.09	60	8.69	100
2018-05-01	6.63	80	2.99	66.67
2019-09-01	30.85	80	10.28	50
2020-02-01	5.77	60	3.12	50
2020-12-01	7.5	80	3.75	100
2021-07-01	12.53	60	4.26	66.67
2021-09-01	33.19	20	12.17	50
MEAN	**13.91**	**64**	**5.67**	**65**

This project has received funding from the European Union's Horizon Europe research and innovation programme under grant agreement No GA 101082048

Funded by the European Union

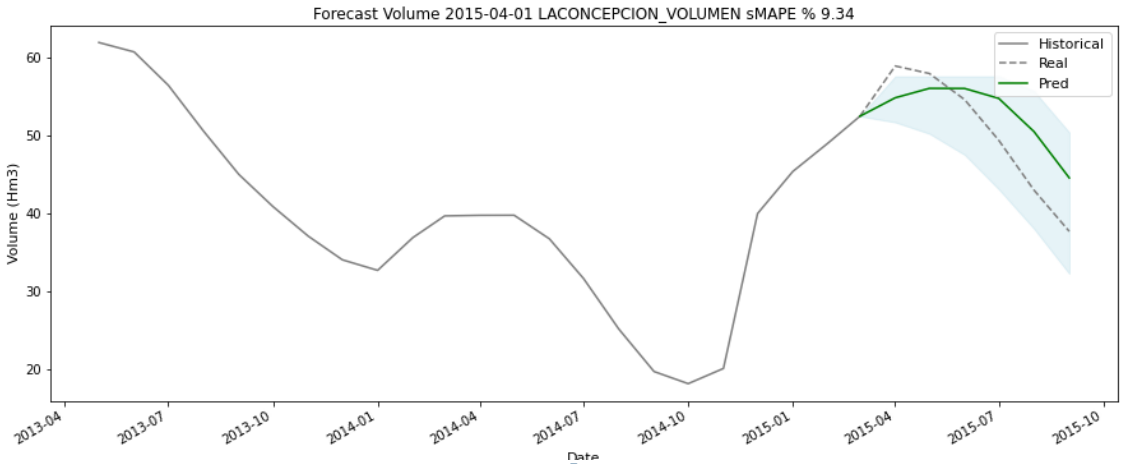

Figure D-10 Prediction of reservoir volume (Hm^3) in the reservoir of La Concepción on one of the random dates used for the validation process. The blue shading refers to the prediction interval.

Charco Redondo: Reservoir volume

Table D-11 Validation process metrics in the reservoir of Charco Redondo.

DATE	SMAPE (%)	MDA	MAE	Coverage
2015-01-01	9.91	60	4.81	66.67
2015-03-01	5.24	80	2.31	100
2015-06-01	13.65	100	5.69	100
2015-10-01	2.69	80	1.26	100
2015-11-01	2.96	80	1.4	100
2016-01-01	7.68	100	3.54	100
2019-06-01	8.63	80	3.88	100
2019-11-01	11.54	40	4.08	83.33
2020-10-01	30.2	40	6.12	33.33
MEAN	**10.28**	**73.33**	**3.68**	**87.04**

This project has received funding from the European Union's Horizon Europe research and innovation programme under grant agreement No GA 101082048

Funded by the European Union

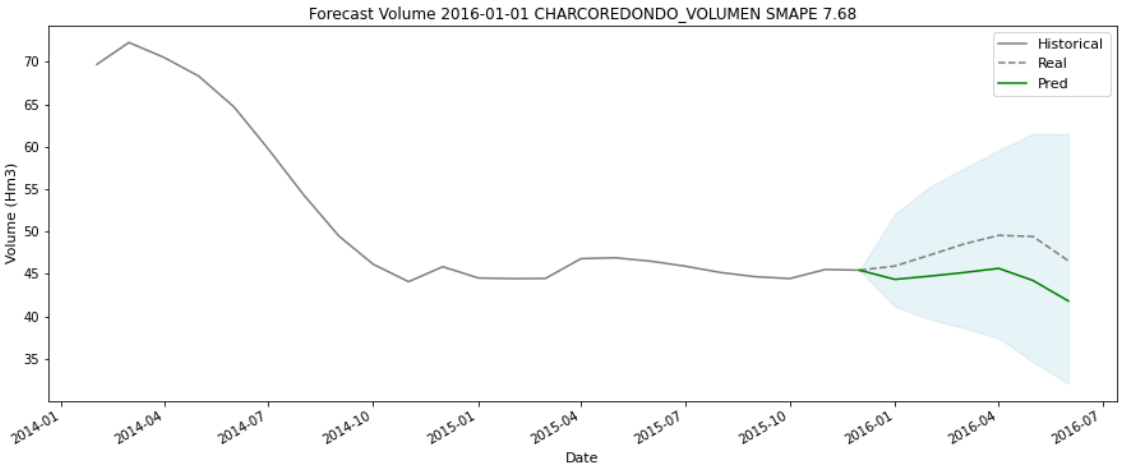

Figure D-11 Prediction of reservoir volume (Hm^3) in the reservoir of Charco Redondo on one of the random dates used for the validation process. The blue shading refers to the prediction interval.

Guadarranque: Reservoir volume

Table D-12 Validation process metrics in the reservoir of Guadarranque.

DATE	SMAPE (%)	MDA	MAE	Coverage
2015-02-01	3.94	80	2.92	83.33
2015-03-01	6.81	60	4.78	66.67
2016-05-01	15.45	40	4.88	50
2017-04-01	2.65	80	1.62	100
2017-09-01	18.3	40	8.92	33.33
2018-10-01	4.48	20	3.17	100
2019-05-01	6.69	100	3.46	83.33
2019-09-01	12.7	40	5.83	83.33
2021-04-01	6.1	80	2.77	83.33
2021-12-01	26.5	40	9.83	16.67
MEAN	**10.36**	**58**	**4.82**	**70**

This project has received funding from the European Union's Horizon Europe research and innovation programme under grant agreement No GA 101082048

Funded by the European Union

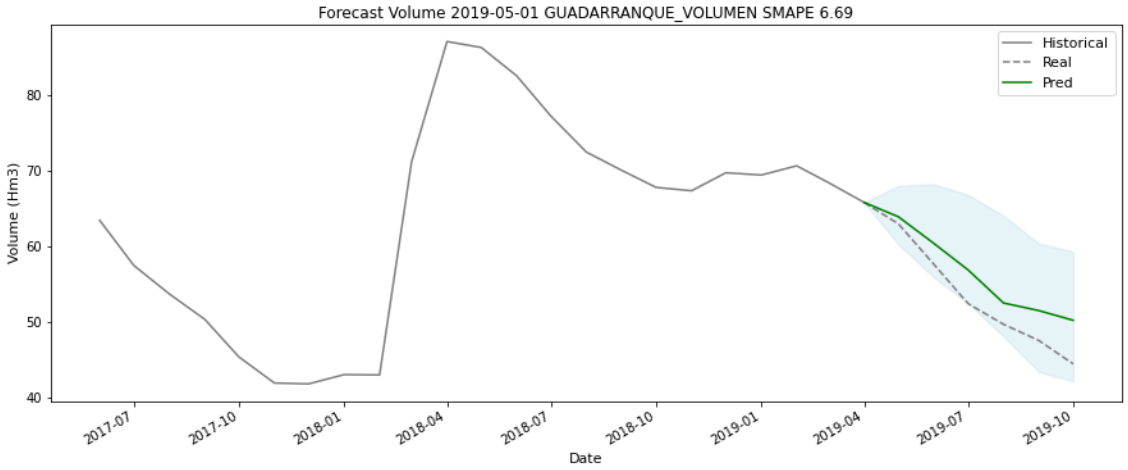

Figure D-12 Prediction of reservoir volume (Hm^3) in the reservoir of Guadarranque on one of the random dates used for the validation process. The blue shading refers to the prediction interval.

This project has received funding from the European Union's Horizon Europe research and innovation programme under grant agreement No GA 101082048

Funded by the European Union

APPENDIX E. PREDICTIVE MODELS: FEATURE IMPORTANCE

Aloha: Piezometric level

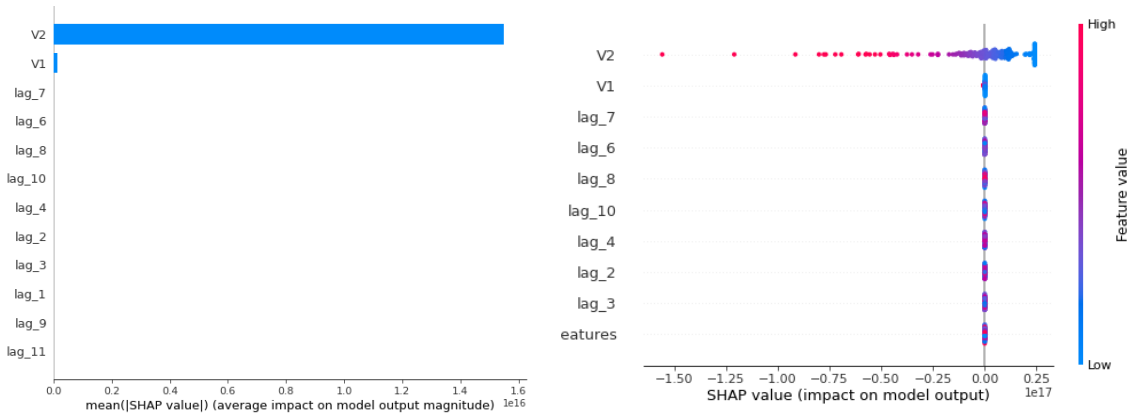

Figure E-1 Aloha Shap's values Summary.

Cable Ski: Piezometric level

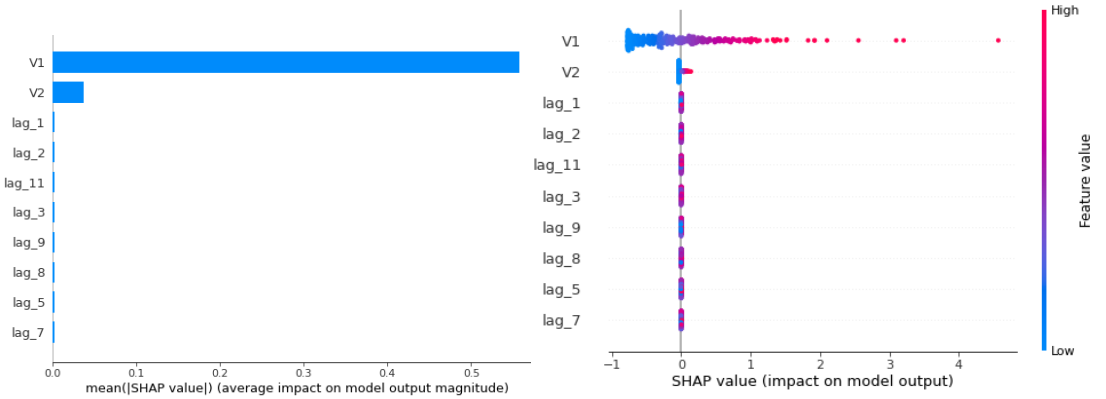

Figure E-2 Cable Ski Shap's values Summary.

Guadaiza: Piezometric level

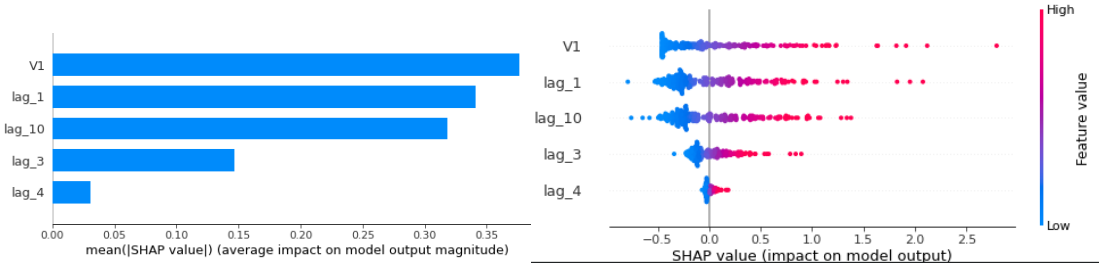

Figure E-3 Guadaiza Shap's values Summary.

Guadalmansa: Piezometric level

This project has received funding from the European Union's Horizon Europe research and innovation programme under grant agreement No GA 101082048

Funded by the European Union

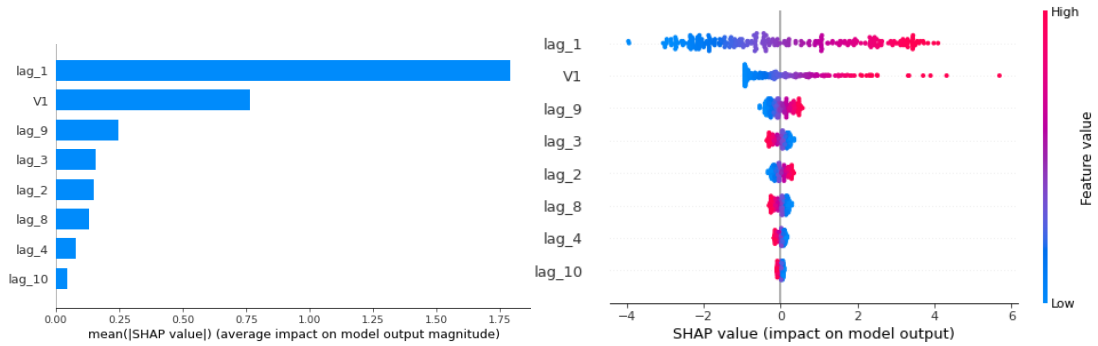

Figure E-4 Guadalmansa Shap's values Summary.

Rio Verde NA: Piezometric level

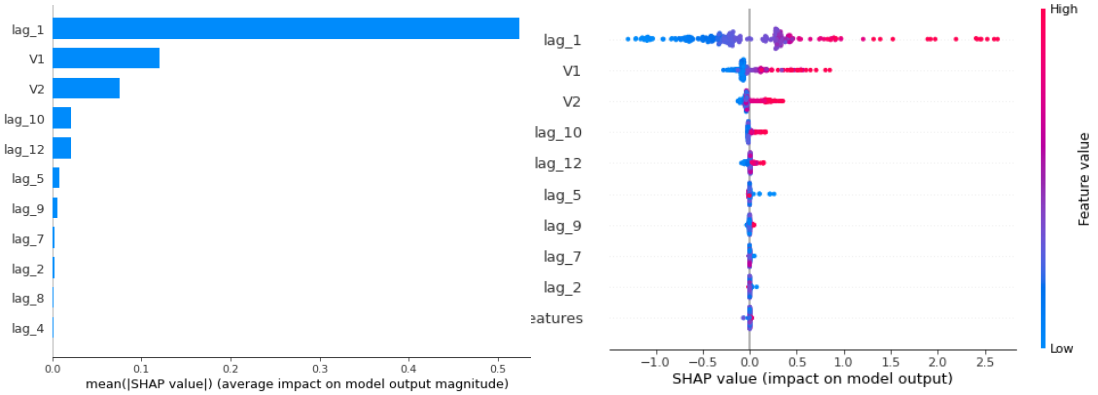

Figure E-5 Río Verde NA Shap's values Summary.

San Pedro: Piezometric level

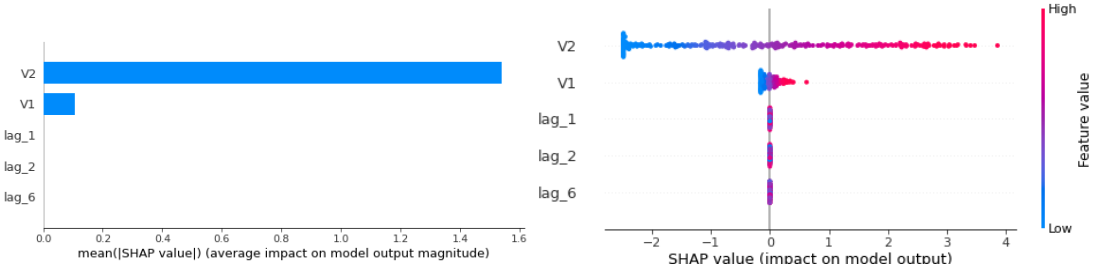

Figure E-6 San Pedro Shap's values Summary.

Señorío: Piezometric level

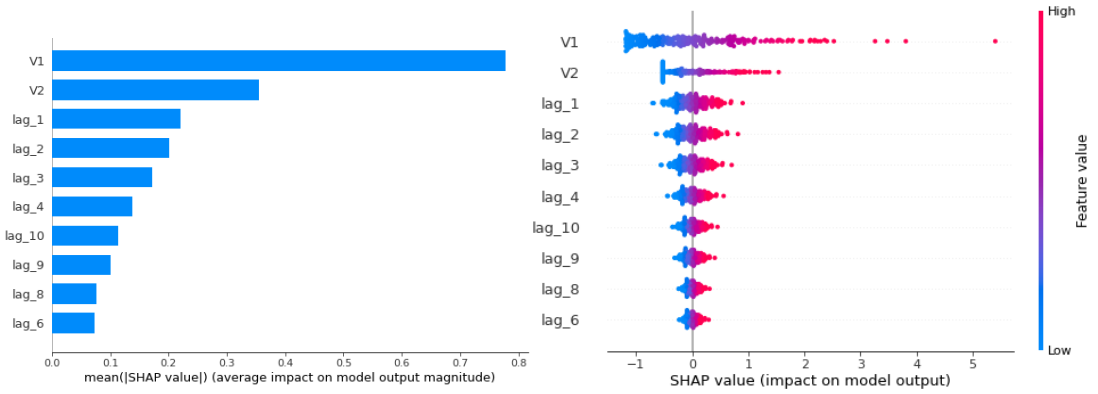

Figure E-7 Señorío Shap's values Summary (Pz level).

Señorío: Electrical Conductivity

This project has received funding from the European Union's Horizon Europe research and innovation programme under grant agreement No GA 101082048

Funded by the European Union

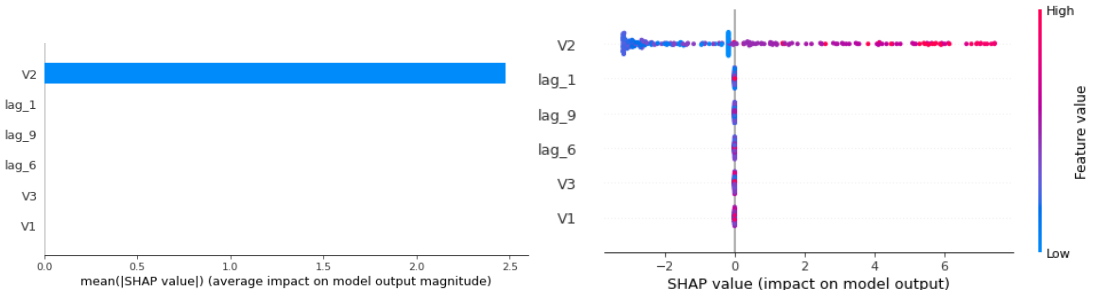

Figure E-8 Señorío Shap's values Summary (Electrical Conductivity).

La Concepción: Reservoir volume

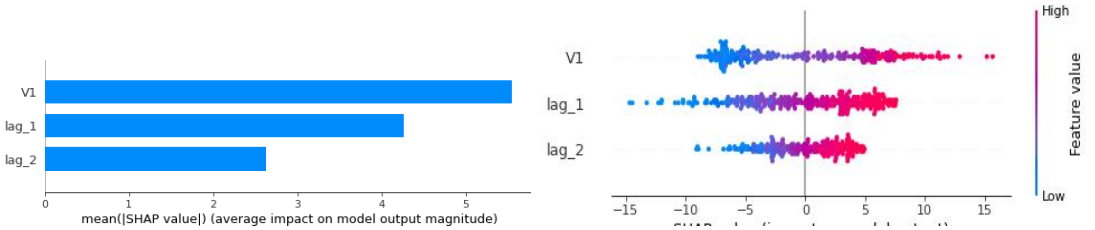

Figure E-9 La Concepción Shap's values Summary.

Charco Redondo: Reservoir volume

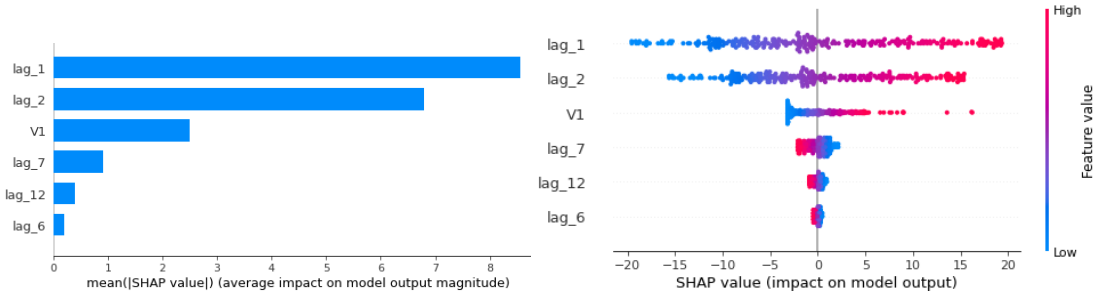

Figure E-10 Charco Redondo Shap's values Summary.

Guadarranque: Reservoir volume

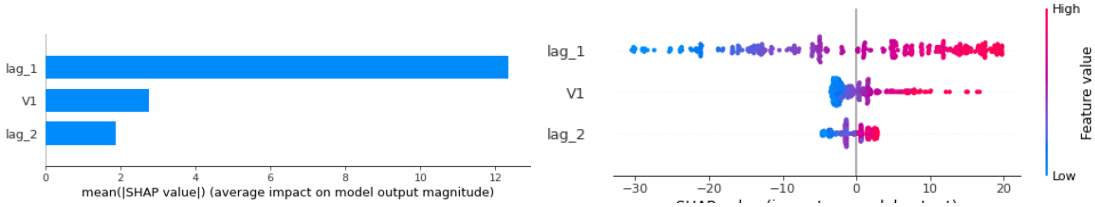

Figure E-11 Guadarranque Shap's values Summary.

This project has received funding from the European Union's Horizon Europe research and innovation programme under grant agreement No GA 101082048
Funded by the European Union

APPENDIX F. CLIMATE PROJECTIONS

Table F-1 Results of the climate projections for each demo site, variable and scenario.

Demo Site / Variable	Model	SCENARIO 4.5 - SSP2						SCENARIO 8.5 - SSP5					
		Daily Trend Slope	**Daily Min**	**Daily Max**	**Yearly Trend Slope**	**Yearly Min**	**Yearly Max**	**Daily Trend Slope**	**Daily Min**	**Daily Max**	**Yearly Trend Slope**	**Yearly Min**	**Yearly Max**
DS1 Prec	Mod 1	3.5E-06	0	58.81	0.43	678.06	1126.28	-2.7E-06	0	69.64	-0.39	671.68	1136.44
DS1 Prec	Mod 2	1.5E-06	0	55.39	0.17	602.65	1117.68	2.1E-06	0	68.67	0.25	624.95	1353.34
DS1 Prec	Mod 3	-8.1E-06	0	59.81	-1.11	575.29	1146.25	4.1E-07	0	53.71	0.03	618.45	1235.17
DS1 Prec	Mod 4	2.7E-06	0	74.51	0.31	624.17	1114.53	-3.3E-06	0	61.83	-0.49	552.25	982.09
DS1 Prec	Mod 5	-3.4E-06	0	91.04	-0.47	565.01	1251.9	-3.3E-06	0	151.21	-0.44	498.74	1155.66
DS1 Min Temp	Mod 1	4.6E-05	-14.37	21.98	0.02	5.37	10.22	1.6E-04	-14.78	23.64	0.06	4.19	11.13
DS1 Min Temp	Mod 2	9.7E-05	-17	22.29	0.03	5.46	10.34	2.4E-04	-17.68	26.09	0.09	4.73	13.34
DS1 Min Temp	Mod 3	4.1E-05	-13.45	22.06	0.01	4.62	8.53	1.2E-04	-15.5	23.79	0.04	4.94	10.5
DS1 Min Temp	Mod 4	3.7E-06	-16.23	22.1	0	5.54	8.48	5.9E-05	-15.76	22.68	0.02	5.75	9.89
DS1 Min Temp	Mod 5	1.5E-04	-14.35	26.42	0.05	4.31	12.23	2.8E-04	-14.06	27.31	0.1	5.73	15.18
DS1 Max Temp	Mod 1	5.5E-05	-6.25	35.1	0.02	12.11	16.93	1.6E-04	-7.22	36.36	0.06	11.46	18.83
DS1 Max Temp	Mod 2	9.0E-05	-10.05	36.45	0.03	12.67	17.09	2.3E-04	-10.11	40.86	0.08	11.91	20.48
DS1 Max Temp	Mod 3	5.1E-05	-6.79	39.22	0.02	11.6	16.06	1.3E-04	-7.12	40.38	0.04	11.65	17.72
DS1 Max Temp	Mod 4	1.1E-05	-6.75	37.88	0	12.89	15.52	6.5E-05	-6.83	38.19	0.02	13.12	17.14
DS1 Max Temp	Mod 5	1.4E-04	-7.61	40.91	0.05	11.76	19.01	2.8E-04	-7.45	42.64	0.1	13.27	22.63
DS2 Prec	Mod 1	-1.1E-05	0	129.75	-1.54	193.24	707.05	-5.5E-06	0	127.2	-0.74	131.66	700.23
DS2 Prec	Mod 2	-6.4E-06	0	126.05	-0.85	155.35	861.73	-2.6E-05	0	128.13	-3.41	155.13	1100.25
DS2 Prec	Mod 3	-9.8E-06	0	91.59	-1.32	159.6	607.96	-1.5E-05	0	101.02	-2.04	117.11	631.31
DS2 Prec	Mod 4	-1.1E-05	0	153.22	-1.54	179.41	849.9	-1.4E-05	0	109.85	-1.9	119.31	824.07
DS2 Prec	Mod 5	-4.0E-06	0	145.78	-0.56	168.51	811.62	-1.0E-05	0	194.06	-1.41	142.7	1301.17
DS2 Min Temp	Mod 1	4.3E-05	4.25	31.63	0.01	16.16	18.06	9.7E-05	2.85	33.49	0.03	16.11	19.59

This project has received funding from the European Union's Horizon Europe research and innovation programme under grant agreement No GA 101082048

Funded by the European Union

DS2 Min Temp	Mod 2	6.7E-05	3.23	30.62	0.02	16.26	19.43	1.8E-04	3.94	35.16	0.06	16.67	22.74
DS2 Min Temp	Mod 3	3.9E-05	3.21	30.49	0.01	16.13	18.16	1.0E-04	2.65	32.2	0.04	16.18	20.16
DS2 Min Temp	Mod 4	3.4E-05	1.96	30.6	0.01	16.19	18.37	7.2E-05	5.05	32.94	0.03	17.22	19.83
DS2 Min Temp	Mod 5	7.9E-05	4.61	32.05	0.03	16.71	20.02	1.7E-04	5.33	36.1	0.06	17.46	22.88
DS2 Max Temp	Mod 1	4.9E-05	6.65	43.13	0.02	22.12	24.43	1.0E-04	4.56	46.16	0.04	22.43	26.31
DS2 Max Temp	Mod 2	5.7E-05	9.4	43.11	0.02	22.51	25.44	1.5E-04	8.19	47.81	0.05	22.9	28.63
DS2 Max Temp	Mod 3	3.8E-05	5.79	42.3	0.01	22.29	24.2	1.0E-04	5.74	42.69	0.04	21.93	26.19
DS2 Max Temp	Mod 4	4.2E-05	6.83	42.21	0.01	22.13	24.85	8.3E-05	6.63	42.91	0.03	22.98	26.18
DS2 Max Temp	Mod 5	8.7E-05	7.16	42.66	0.03	22.61	26.45	1.7E-04	7.37	50.7	0.06	23.01	29.01
DS3 Prec	Mod 1	-9.7E-06	0	63.34	-1.32	307.73	1033.07	-1.6E-05	0	66.97	-2.2	216.03	935.88
DS3 Prec	Mod 2	-1.3E-05	0	97.4	-1.72	202.02	891.49	-2.8E-05	0	84.4	-3.78	121.69	823.14
DS3 Prec	Mod 3	-6.8E-06	0	65.68	-0.92	211.65	1035.73	-2.0E-05	0	80.03	-2.68	199.6	1066.95
DS3 Prec	Mod 4	-1.2E-05	0	71.34	-1.59	176.25	1516.4	-1.8E-05	0	66.03	-2.48	176.48	1200.76
DS3 Prec	Mod 5	-6.5E-06	0	69.7	-0.86	264.71	1154.4	-2.6E-05	0	82.03	-3.46	153.42	1393.33
DS3 Min Temp	Mod 1	2.8E-05	-1.2	27.49	0.01	13.95	15.81	6.5E-05	-0.06	30.57	0.02	13.88	16.8
DS3 Min Temp	Mod 2	5.4E-05	-2.86	30.36	0.02	13.79	16.26	1.4E-04	-0.49	33.56	0.05	13.99	18.76
DS3 Min Temp	Mod 3	3.4E-05	-0.29	29.38	0.01	13.33	15.43	7.7E-05	0.81	32.67	0.03	13.66	16.97
DS3 Min Temp	Mod 4	2.1E-05	1.96	27.52	0.01	13.1	15.29	6.7E-05	0.01	31.76	0.02	13.52	16.55
DS3 Min Temp	Mod 5	7.2E-05	1.74	29.19	0.03	13.54	17.03	1.6E-04	-0.06	31.73	0.06	13.89	19.24
DS3 Max Temp	Mod 1	5.1E-05	9.4	41	0.02	20.26	23.1	1.1E-04	8.09	43.97	0.04	19.45	24.85
DS3 Max Temp	Mod 2	8.2E-05	4.13	42.61	0.03	20.4	24.53	2.0E-04	9.41	47.82	0.07	20.57	27.98
DS3 Max Temp	Mod 3	4.7E-05	6.79	42.57	0.02	19.89	23.08	1.1E-04	8.06	46.37	0.04	19.83	25.23

This project has received funding from the European Union's Horizon Europe research and innovation programme under grant agreement No GA 101082048

Funded by the European Union

DS3 Max Temp	Mod 4	3.7E-05	7.87	41.18	0.01	19.7	22.67	8.7E-05	5.36	42.33	0.03	19.85	24.27
DS3 Max Temp	Mod 5	9.2E-05	9.06	41.14	0.03	19.67	24.98	2.0E-04	7.06	46.23	0.07	20.33	27.82
DS4 Prec	Mod 1	-7.9E-06	0	103.54	-1.1	402.6	1034.09	-1.6E-05	0	183.36	-2.13	406.87	1079.3
DS4 Prec	Mod 2	-1.0E-05	0	172.29	-1.39	472.04	1123.66	-3.1E-05	0	159.73	-4.14	293.37	1171.7
DS4 Prec	Mod 3	-1.1E-05	0	88.89	-1.46	339.22	1057.73	-2.7E-05	0	139.33	-3.67	277.9	1364.5
DS4 Prec	Mod 4	-6.7E-06	0	87.11	-0.93	459.12	1297.62	-1.4E-05	0	78.94	-1.87	358.71	1206.63
DS4 Prec	Mod 5	-1.1E-05	0	140.69	-1.51	414.69	1101.42	-2.7E-05	0	133.74	-3.62	355.05	1237.71
DS4 Min Temp	Mod 1	5.2E-05	-53.13	28.71	0.02	10.2	13.79	1.4E-04	-59.68	32.65	0.05	9.36	15.73
DS4 Min Temp	Mod 2	1.2E-04	-134.59	29.4	0.04	8.49	14.93	2.9E-04	-135.49	33.71	0.1	7.54	18.34
DS4 Min Temp	Mod 3	5.4E-05	-32.19	29.52	0.02	10.42	13.87	1.4E-04	-34.14	32.32	0.05	9.63	15.96
DS4 Min Temp	Mod 4	5.2E-05	-103.05	30.78	0.02	8.48	14.07	1.3E-04	-117.49	32.98	0.04	7.2	15.53
DS4 Min Temp	Mod 5	1.3E-04	-10.63	32.51	0.05	11.44	17.02	2.5E-04	-11.48	35.72	0.09	12.32	20.3
DS4 Max Temp	Mod 1	6.2E-05	-4.15	41.81	0.02	19.36	23.16	1.4E-04	-6.2	44.83	0.05	19.18	25.16
DS4 Max Temp	Mod 2	1.0E-04	-2.57	42.24	0.04	18.48	23.17	2.4E-04	-2.94	47.06	0.09	18.72	27.06
DS4 Max Temp	Mod 3	5.3E-05	-1.7	41.26	0.02	18.94	22.82	1.3E-04	-3.4	43.48	0.05	18.24	24.71
DS4 Max Temp	Mod 4	5.6E-05	-6.61	46.77	0.02	18.49	22.91	1.2E-04	-10.02	46.88	0.04	19.37	25.32
DS4 Max Temp	Mod 5	1.3E-04	-1.4	45.64	0.05	20.14	25.89	2.6E-04	-2.4	47.19	0.09	20.97	29.37
DS5 Prec	Mod 1	-1.1E-05	0	116.86	-1.55	417.16	938.47	-1.6E-05	0	146.75	-2.11	360.84	878.59
DS5 Prec	Mod 2	-7.2E-06	0	95.92	-0.98	437.01	1006.67	-2.2E-05	0	133.5	-2.94	338.11	1028.95
DS5 Prec	Mod 3	-1.0E-05	0	116.62	-1.4	335.02	963.44	-1.8E-05	0	99.03	-2.48	329.22	1020.98
DS5 Prec	Mod 4	-1.4E-06	0	122.66	-0.21	470.47	1092.26	-1.8E-05	0	116.89	-2.43	379.64	969.41
DS5 Prec	Mod 5	-1.9E-05	0	143.67	-2.55	337.07	1007.41	-1.9E-05	0	150.1	-2.61	255.97	959.9
DS5 Min Temp	Mod 1	2.3E-05	2.93	25.27	0.01	13.43	14.78	6.0E-05	3.15	26.45	0.02	13.64	16.2
DS5 Min Temp	Mod 2	3.9E-05	2.11	25.6	0.01	14.19	15.89	9.2E-05	2.7	27.51	0.03	14.79	18.12

This project has received funding from the European Union's Horizon Europe research and innovation programme under grant agreement No GA 101082048

Funded by the European Union

DS5 Min Temp	Mod 3	3.5E-05	3.66	26.22	0.01	12.82	14.75	7.1E-05	3.23	27.12	0.03	12.75	15.76
DS5 Min Temp	Mod 4	4.6E-05	3.02	27.78	0.02	12.48	14.75	1.0E-04	3.18	29.27	0.04	12.49	16.09
DS5 Min Temp	Mod 5	4.6E-05	0.12	26.63	0.02	13.73	16.2	1.2E-04	1.61	27.78	0.04	14.57	18.84
DS5 Max Temp	Mod 1	3.2E-05	9.07	39.12	0.01	21.28	23.52	9.2E-05	8.07	40.08	0.03	21.06	25.08
DS5 Max Temp	Mod 2	6.8E-05	4.63	41.89	0.03	21.35	24.88	1.6E-04	11.67	43.95	0.06	21.97	27.86
DS5 Max Temp	Mod 3	4.3E-05	8.28	41.03	0.02	20.67	23.21	8.4E-05	9.45	43.46	0.03	20.44	24.38
DS5 Max Temp	Mod 4	4.7E-05	9.58	39.97	0.02	20.75	23.29	1.1E-04	9.94	41.61	0.04	20.86	25.03
DS5 Max Temp	Mod 5	8.0E-05	9.19	42.56	0.03	21.04	24.85	1.5E-04	9.4	42.84	0.06	21.34	26.98
DS6 Prec	Mod 1	-2.1E-05	0	118.87	-2.86	242.87	1140.42	-2.6E-05	0	80.79	-3.55	212.98	1053.88
DS6 Prec	Mod 2	-2.0E-05	0	141.14	-2.73	209.78	1074.56	-3.7E-05	0	122.46	-4.94	177.2	1028.2
DS6 Prec	Mod 3	-1.4E-05	0	104.53	-1.9	152.31	1135.38	-3.3E-05	0	82.86	-4.46	163.05	1346.95
DS6 Prec	Mod 4	-1.9E-05	0	101.5	-2.54	121.11	1820.03	-2.7E-05	0	89.43	-3.7	174.37	1305.45
DS6 Prec	Mod 5	-1.8E-05	0	125.81	-2.35	185.58	1064.93	-3.8E-05	0	127.16	-5.12	62.41	1210.95
DS6 Min Temp	Mod 1	5.3E-05	-1.54	29.5	0.02	13.2	15.85	1.0E-04	-2.34	32.97	0.04	12.61	17.04
DS6 Min Temp	Mod 2	6.7E-05	-0.99	29.56	0.02	13.06	16.28	1.6E-04	0.64	33.63	0.06	13	18.52
DS6 Min Temp	Mod 3	5.1E-05	0.44	31.09	0.02	13.26	16.22	1.2E-04	0.12	32.87	0.04	13.32	17.63
DS6 Min Temp	Mod 4	3.3E-05	-0.45	30.8	0.01	13.38	15.18	9.6E-05	-1.49	34.86	0.03	13.16	16.99
DS6 Min Temp	Mod 5	8.4E-05	-0.82	29.22	0.03	13.23	16.93	2.1E-04	-0.37	32.42	0.08	13.11	20.61
DS6 Max Temp	Mod 1	5.9E-05	4.06	40.17	0.02	20.13	23.1	1.2E-04	4.78	43.16	0.04	19.6	24.59
DS6 Max Temp	Mod 2	7.1E-05	5.07	42.1	0.03	20.51	24.07	1.6E-04	4.55	45.14	0.06	20.35	26.27
DS6 Max Temp	Mod 3	4.9E-05	2.81	40.64	0.02	20.47	23.77	1.2E-04	4.89	41.86	0.04	19.98	25.33
DS6 Max Temp	Mod 4	4.8E-05	5.04	43.24	0.02	20.14	23	1.1E-04	5.23	45.39	0.04	20.28	24.86

This project has received funding from the European Union's Horizon Europe research and innovation programme under grant agreement No GA 101082048

Funded by the European Union

DS6 Max Temp	Mod 5	1.0E-04	3.93	41.37	0.04	20.43	25.7	2.3E-04	4.14	45.34	0.08	20.53	29.24
DS7 Prec	Mod 1	-5.5E-06	0	145.12	-0.81	906.28	2561.9	-3.3E-05	0	126.45	-4.48	915.16	2937.55
DS7 Prec	Mod 2	-2.0E-05	0	209.57	-2.68	815.52	2088.51	-4.7E-05	0	227.92	-6.3	646.27	2564.49
DS7 Prec	Mod 3	-1.7E-05	0	165.21	-2.28	790.07	2415.48	-3.7E-05	0	119.07	-4.91	604.8	2504.65
DS7 Prec	Mod 4	-1.2E-05	0	179.06	-1.65	779.98	3139.62	-3.0E-05	0	235.12	-4.15	637.45	2670.32
DS7 Prec	Mod 5	-9.0E-06	0	170.94	-1.16	823.86	2945.2	-6.3E-05	0	287.71	-8.44	393.59	3339.62
DS7 Min Temp	Mod 1	5.4E-05	-5.86	28.36	0.02	11.23	13.79	9.2E-05	-5.47	34.81	0.03	11.71	15.25
DS7 Min Temp	Mod 2	7.7E-05	-6.82	29.05	0.03	11.13	14.78	2.0E-04	-3.63	30.6	0.07	10.63	18.06
DS7 Min Temp	Mod 3	4.8E-05	-50.19	27.79	0.02	10.17	12.77	1.2E-04	-52.39	30.72	0.04	9.91	15.03
DS7 Min Temp	Mod 4	2.1E-05	-4.23	26.48	0.01	9.08	12.26	8.6E-05	-3.87	27.63	0.03	9.64	13.82
DS7 Min Temp	Mod 5	1.1E-04	-108.22	27.94	0.04	9.49	15.3	2.4E-04	-107.53	30.49	0.09	9.51	17.62
DS7 Max Temp	Mod 1	4.2E-05	0.7	40.89	0.01	18.77	21.65	1.1E-04	4.46	43.36	0.04	17.55	23.19
DS7 Max Temp	Mod 2	8.1E-05	4.3	42.22	0.03	19.44	23.84	2.0E-04	7.96	46.48	0.07	20.14	27.5
DS7 Max Temp	Mod 3	5.8E-05	4.92	43.2	0.02	18.16	21.83	1.3E-04	5.71	49.17	0.05	18.31	25.53
DS7 Max Temp	Mod 4	2.8E-05	3.15	39.67	0.01	17.55	20.74	9.0E-05	4.71	41.24	0.03	17.73	22.52
DS7 Max Temp	Mod 5	1.1E-04	7.14	38.76	0.04	17.87	23.92	2.4E-04	1.99	43.18	0.09	18.64	27.05

- Mod 1: GFDL-ESM4_r1i1p1f1
- Mod 2: IPSL-CM6A-LR_r1i1p1f1
- Mod 3: MPI-ESM1-2-HR_r1i1p1f1
- Mod 4: MRI-ESM2-0_r1i1p1f1
- Mod 5: UKESM1-0-LL_r1i1p1f2

This project has received funding from the European Union's Horizon Europe research and innovation programme under grant agreement No GA 101082048

Funded by the European Union

APPENDIX G. VARIABLES FOR GROUNDWATER POLLUTION RISK MAPPING

Vulnerability parameters

Groundwater occurrence - 01_confinement

Description: European groundwater body horizons delineated for the 2nd River Basin Management Plans under the Water Framework Directive.

Source:
https://sdi.eea.europa.eu/catalogue/srv/eng/catalog.search#/metadata/c5009a24-d30d-470d-bcb2-90dc70a0ce81

Adaptations to vulnerability indexes: a level of confinement is added to the GroundWaterBodyHorizon file (Table G-1) depending on the options shown in Figure G-1.

Table G-1 Parameter reclassification for groundwater occurrence.

Horizon	Confinement	01_GALDIT	01_GOD
3-19	Confined	10	0.2
2	Semi-confined	2.5	0.4
1	Unconfined	7.5	1

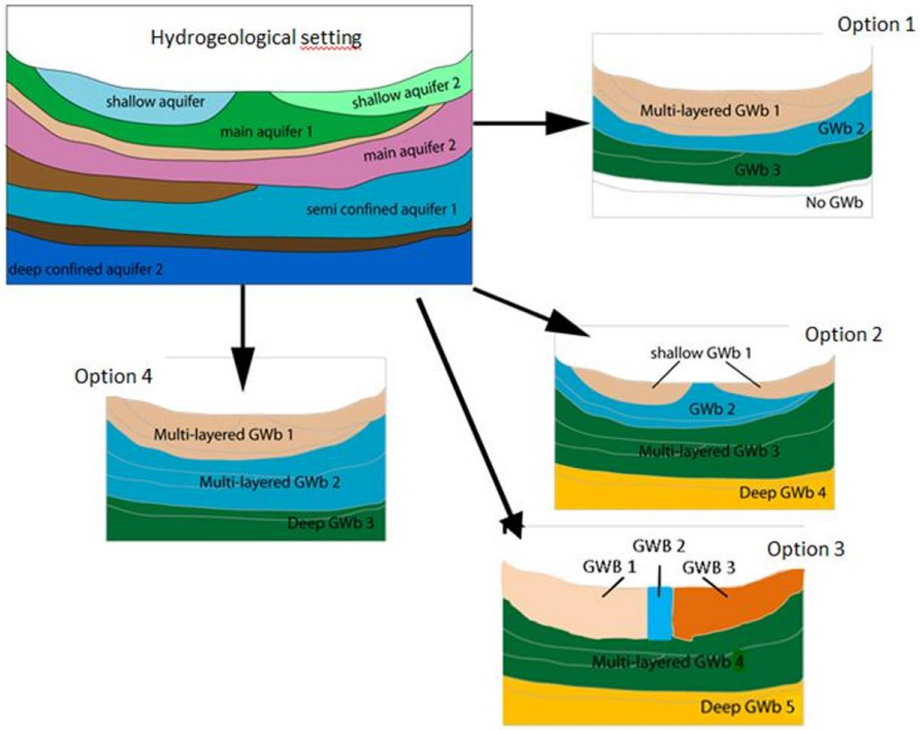

Source: European Commission. 2014: WFD Reporting Guidance 2016 Final V6.0.6

Figure G-1 Aquifer confinement options considered by the European Commission for Water Framework Directive.

This project has received funding from the European Union's Horizon Europe research and innovation programme under grant agreement No GA 101082048

Funded by the European Union

Aquifer hydraulic conductivity - 02_aquifer_hydraulic_cond

Description: International hydrogeological map of Europe 1:1,500,000.

Source: https://www.bgr.bund.de/EN/Themen/Wasser/Projekte/laufend/Beratung/Ihme1500/ihme1500_projektbeschr_en.html

Adaptations to vulnerability indexes: due to the lack of pan-European consistent hydrogeological data, more specifically hydraulic data, an association has been made associating rock types with hydraulic conductivity data.

To do this, rock types of the hydrogeological map of Europe were associated with standardised hydraulic conductivity values shown in Custodio and Llamas (1996), and later on converted to m/day using Freeze and Cherry (1979). Table G-2 summarises the reclassification of values:

Table G-2 Aquifer hydraulic conductivity values adapted from Custodio and Llamas (1996).

Rock	m/day	Rock	m/day
Volcanic rocks	0,03284847	Phyllites	0,00000325
Conglomerates	0,00325265	Claystones and clays	0,00003252
Limestones and marls	0,00325558	Sandstones and sands	0,00325265
Limestones and sands	0,00325558	Gravels	3255,57648662
Conglomerates and clays	0,00003252	Marlstones and sands	0,00325265
Limestones and clays	0,00325558	Quartzites	0,00000003
Shales	0,00000325	Marlstones and clays	0,00325265
Plutonic rocks	0,00000033	Snow field / ice field	0,03284847
Sands	32,52649395	Sandstones	0,00325265
Conglomerates and sands	0,00325265	Marls	0,00003252
Gneisses	0,00032526	Inland water	0
Silts	0,03252649	Clays	0,00003252
Marbles	32,52649395	Sandstones and clays	0,00325265
Schists	0,00000325	Marlstones and marls	0,00325558
Marlstones	32,52649395	Limestones	32,52649395
Sandstones and marls	0,00325265		

Later on, GALDIT and DRASTIC values were assigned as follows (Table G-3):

This project has received funding from the European Union's Horizon Europe research and innovation programme under grant agreement No GA 101082048

Funded by the European Union

Table G-3 Parameter reclassification for aquifer hydraulic conductivity.

m/day	02_GALDIT
>40	10
10 - 40	7.5
5 - 10	5
<5	2.5

m/day	02_DRASTIC
<4.1	1
4.1 - 12.3	2
12.3 - 28.7	4
28.7 - 41	6
41 - 82	8
>82	10

Height of groundwater level above sea level - 03_GW_height_masl

Description: spatial data representing groundwater level above sea level in unconfined aquifers.

Source: mostly local data, but in some places or Europe data can be found from the Digital Dataset of European Groundwater Resources 1:500,000.

- DS3 Frielas (PT): Sistema Nacional de Informacão de Recursos Hídricos
- DS4 Emilia Romagna (IT): Digital Dataset of European Groundwater Resources 1:500,000
- DS5 Cape Flats (SA): Local data provided by SU UNIVERSITY OF STELLENBOSCH.
- DS6 El Señorío (ES): Local data obtained from Argamasilla (2017).

Adaptations to vulnerability indexes Table G-4:

Table G-4 Parameter reclassification for the height of groundwater level above sea level.

Class	Range (m a.s.l.)	03_GALDIT
High	<1.0	10
Medium	1.0-1.5	7.5
Low	1.5-2	5
Very low	>2.0	2.5

Distance from the shore - 04_distance_from_shore

Description: Spatial data showing the existing distance from the shore using buffers of 500, 750 and 1000 m.

Source:
https://www.naturalearthdata.com/http//www.naturalearthdata.com/download/10m/physical/ne_10m_coastline.zip

Adaptations to vulnerability indexes: the shoreline is based on the "Coastline.shp" file from https://www.naturalearthdata.com/. Used the QGIS

This project has received funding from the European Union's Horizon Europe research and innovation programme under grant agreement No GA 101082048
Funded by the European Union

software to differentiate the buffer areas and classify them into Table G-5 values.

Table G-5 Parameter reclassification for distance from the shore.

Distance (m)	04_GALDIT
< 500	10
500 - 750	7.5
750 - 1,000	5
> 1,000	2.5

Impact of the existing status of seawater intrusion - 05_seawater_intrusion

Description: European groundwater bodies with electrical conductivity values, when available., obtained from the Water Framework Directive Database and the International hydrogeological map of Europe 1:1,500,000.

Source: WISE Water Framework Directive Database (europa.eu).

International hydrogeological map of Europe 1:1,500,000

Adaptations to vulnerability indexes: Electrical conductivity data for groundwater bodies has been extracted from the WFD database, from the SOW_GWB_gwPollutant table, taking the next fields: euGroundWaterBodyCode, gwPollutantCode, gwPollutantBackgroundLevelValue, gwPollutantBackgroundLevelUnit.

Units weren't unified, because some of them were expressed in µS/cm and others in S/m, so all of them were unified in µS/cm. Other values were corrected due to obvious mistakes in the original data input. Other values were deleted because of repeating values (-9999, -8888, -7777, etc.).

The remaining values were spatially joined with the GroundWaterBodyHorizon file. After this process, the GroundWaterBodyHorizon file was clipped using the 04_distance_from_shore layer, so only the coastal aquifers will be remaining. However, only a small amount of the European coastal aquifers had data, so another extra process was done.

Using the IHME1500 - International Hydrogeological Map of Europe 1:1,500,000 file named ihme1500__ec4060_v12_poly, the field SALININTRUS was taken. This field contains two values: 0 (no saline intrusion) and 1 (saline intrusion). So, due to the lack of data, a GALDIT value of 2.5 was assigned to SALININTRUS = 0 and a GALDIT value of 10 was assigned to SALININTRUS = 1. This file was clipped using 04_distance_from_shore.

Finally, a spatial join was done from GroundWaterBodyHorizon to ihme1500__ec4060_v12_poly, so all the coastal aquifers of Europe have an EC value and, therefore, a GALDIT value.

Assign values to the base groundwater bodies layer (Table G-6).

Table G-6 Parameter reclassification for the impact of the existing status of seawater intrusion.

This project has received funding from the European Union's Horizon Europe research and innovation programme under grant agreement No GA 101082048
Funded by the European Union

Ratio Cl-/HCO3	EC (µS/cm)	05_GALDIT
> 2	> 3000	10
1.5 - 2.0	2000 - 3000	7.5
1 - 1.5	1000 - 2000	5
< 1	< 1000	2.5

Saturated thickness - 06_saturated_thickness

Description: European coastal groundwater bodies with an estimation of aquifer thickness.

Source: WISE Water Framework Directive Database (europa.eu).

Zamrsky *et al.* (2017, 2018). https://doi.pangaea.de/10.1594/PANGAEA.880771

Adaptations to vulnerability indexes: Taking the sampling point network of the available spatial data from Zamrsky *et al.* (2017), a spatial join using the average of the nearest points was done to the European coastal groundwater bodies. Table G-7 shows the final GALDIT values.

Table G-7 Parameter reclassification for saturated thickness.

Saturated thickness (m)	06_GALDIT
> 10	10
7.5 - 10	7.5
5 - 7.5	5
< 5	2.5

Unsaturated zone characteristics - 07_unsaturated_char

This is the same information as 02_aquifer_hydraulic_cond.

DEM - 08_DEM

Description: Digital elevation dataset produced in the framework of the Shuttle Radar Topography Mission v4 (SRTM), with resolution ranging from 30 to 90 m. Data was downloaded using Google Earth Engine scripts. This data is used to produce the 09_depth_to_GW and the 13_slope layers.

Source: https://developers.google.com/earth-engine/datasets/catalog/CGIAR_SRTM90_V4#description

Depth to water table - 09_depth_to_GW

This project has received funding from the European Union's Horizon Europe research and innovation programme under grant agreement No GA 101082048

Funded by the European Union

Description: Spatial data showing the depth at which groundwater is located below the topographic surface.

Source: same as 03_GW_height_masl

Adaptations to vulnerability indexes: This layer comes from the difference between the DEM (08_DEM) and the groundwater height above sea level (03_GW_height_masl), in the next way. It can also come directly from point information about depth to groundwater:

09_depth_to_GW = [08_DEM] - [03_GW_height_masl]

Table G-8 shows the DRASTIC and GOD values coming from these data.

Table G-8 Parameter reclassification for depth to water table.

Depth to water table (m)	09_DRASTIC
0 - 1,5	10
1,5 - 3	9
3 - 4,5	8
4,5 - 9	7
9 - 15	5
15 - 22,5	3
22,5 - 30	2
> 30	1

Depth to water table (m)	09_GOD
< 2	1
2 - 5	0,9
5 - 10	0,8
10 - 20	0,7
20 - 50	0,6
50 - 100	0,5
> 100	0,4

Net recharge - 10_net_recharge

Description: Net recharge grid data in the 1981-2022 period.

Source: https://data.chc.ucsb.edu/products/CHIRPS-2.0/global_annual/

International hydrogeological map of Europe 1:1,500,000

Adaptations to vulnerability indexes: The net recharge is calculated from the precipitation data coming from the 1981-2022 CHIRPS global data.

First of all, the precipitation geotiff is clipped to the demo site. Secondly, the IHME1500 - International Hydrogeological Map of Europe 1:1,500,000 file named ihme1500__ec4060_v12_poly, is used to associate average European recharge data of aquifers to each geological formation (Table G-9), based on Sanz *et al.* (2011).

Table G-9 Percentage of precipitation destined to recharge. Based on Sanz et al. (2011).

This project has received funding from the European Union's Horizon Europe research and innovation programme under grant agreement No GA 101082048

Funded by the European Union

Geographics zones	1. Alluvials, sands and gravels	2. Conglomerates	3. Sandstones	4. Limestones and Dolomites	5. Marls, Silts and Clays
North	5.0	3.5	4.7	18.3	2.2
Center	4.6	3.4	4.1	20.7	2.1
South	5.3	3.2	4.5	21.9	1.9
Levante	5.0	3.3	4.3	20.7	2.2
Mean ($\bar{X}$)	5.0	3.4	4.4	20.7	2.0
σ^2	0.17	0.67	0.05	5.4	0.1
σ	0.4	0.8	0.2	2.3	0.3
$\sigma/\bar{x}$ (%)	8.2	23.5	5.1	11.2	15.1

After that, the geological data is also clipped to the demo site and rasterized, so it can be multiplied times the precipitation data, and divided by 100 (as recharge rates are expressed in percentages). Use the raster calculator with the rasterized aquifer recharge rate data as an extension. Table G-10 shows the DRASTIC values for this parameter.

Table G-10 Parameter reclassification for net recharge.

Net recharge (mm)	10_DRASTIC
> 250	9
180 - 250	8
100 - 180	6
100 - 50	3
0 - 50	1

Aquifer type - 11_aquifer_type

Description: Europe's aquifer spatial data coming from the International Hydrogeological Map of Europe 1:1,500,000.

Source: International hydrogeological map of Europe 1:1,500,000

Adaptations to vulnerability indexes: Lithology data of this layer was reclassified to meet the DRASTIC and GOD parameterization (Table G-11).

Table G-11 Parameter reclassification for aquifer type.

Geology	11_DRASTIC
Karst limestone	10
Basalt	9
Sand and gravel	8
Massive sandstone and limestone	7
Bedded sandstone and	6

Geology	11_GOD
Calcretes, other limestones	1.0
Chalky limestones, calcarenites	0.9
Colluvial gravels, recent volcanic lavas	0.8
Alluvial and fluvio-glacial sands and gravels, sandstones	0.7
Aeolian sands, siltstones, volcanic tufts	0.6

This project has received funding from the European Union's Horizon Europe research and innovation programme under grant agreement No GA 101082048

Funded by the European Union

limestone	
Glacial	5
Weathered metamorphic/igneous	4
Metamorphic/igneous	3
Massive shale	2

and igneous/metamorphic formations+older volcanics	
Alluvial silts and loess, mudstones and shales	0.5
Residual soils	0.4

Soil type - 12_soil_type

Description: Europe soil spatial distribution, based on the European Soil Database.

Source: European Soil Database

Adaptations to vulnerability indexes: Based on the European Soil Database file named sgdbe4_0.shp joined with the PARMADOM field from the stu_sgdbe.dbf file. After that, a manual reclassification of the DRASTIC values was done following Table G-12.

Table G-12 Parameter reclassification for soil type.

Soil type	12_DRASTIC
Thin or absent, gravel	10
Sandstone and volcanic	9
Peat	8
Shrinking/aggregate clay/alluvium	7
Sand loam/schist/sand/karst/volcanic	6
Loam	5
Silty loam	4
Clay loam	3
Muck acid/granitoid	2
Non-shrink and non aggregate clay	1

Slope - 13_slope

Description: Spatial raster data that shows the slope values (in percentage - %) of the demo site.

Source: same as 08_DEM.

Adaptations to vulnerability indexes: Based on 08_DEM. It has to be converted into projected coordinates (EPSG:4087 - WGS 84 / World

This project has received funding from the European Union's Horizon Europe research and innovation programme under grant agreement No GA 101082048
Funded by the European Union

Equidistant Cylindrical) to compute the slope function. Table G-13 shows the DRASTIC parameter values.

Table G-13 Parameter reclassification for slope.

Slope (%)	13_DRASTIC
0-2	10
2-3	9
3-4	8
4-5	7
5-6	6
6-10	5
10-12	4
12-16	3
16-18	2
>18	1

After the calculation of each index, raw values must be reclassified following Table G-14.

Table G-14 Parameter reclassification for each vulnerability index.

Vulnerability	GALDIT	DRASTIC	GOD
Very low	-	< 80	-
Low	< 5	80-120	0.1 - 0.3
Moderate	5 - 7.5	120-160	0.3 - 0.5
High	> 7.5	160-200	0.5 - 0.7
Very high	-	> 200	0.7 - 1

Hazard parameters

Projected sea level rise - 14_projected_SLR

Description: Data showing areas subjected to flooding associated with sea level rise under Representative Concentration Pathway (RCP) 8.5 in 2050, median 50.

Source: Kopp et al. (2017) - Supporting information

Adaptations to hazard indexes: Relative Sea Level (RSL) data were obtained from Kopp *et al.* (2017) using a corrected DP16 model under Representative

This project has received funding from the European Union's Horizon Europe research and innovation programme under grant agreement No GA 101082048
Funded by the European Union

Concentration Pathway (RCP) 8.5 in 2050, median of 50. These data were associated with 3078 sampling stations throughout the World and were interpolated.

Later, when working at the demo site scale, RSL is related to the digital elevation model (DEM) using the next formula: Pilot_site_DEM <= world RSL. The result is a binary layer marking with "1" all flooding areas, which must be reclassified using Table G-15 information and min <= value <= max condition.

Table G-15 Parameter reclassification for projected sea level rise.

Raw value min	Raw value max	New value	SLR_hazard
0	0	1	No
1	1	2	Yes

Land subsidence - 15_land_subsidence

Description: Land subsidence probability calculated by a global prediction model at high spatial resolution (~2 km) and resampled to 1 km grid size.

Source: Hasan *et al.* (2023).

GitHub repository

Google Earth Engine code

Adaptations to hazard indexes: Land subsidence probability data has been reclassified using min < value <= max condition as Table G-16 indicates.

Table G-16 Parameter reclassification for land subsidence.

Raw value min	Raw value max	New value	Subsidence_hazard
0	0.25	1	No
0.25	1	2	Yes

Land use - 16_land_use

Description: Near-real-time (NRT) land use/land cover (LULC) dataset coming from Dynamic World predictions using Sentinel-2 L1C collection from 2015 to the present, with revisiting frequency between 2-5 days.

Source: Google Earth Engine - Dynamic World v1

Adaptations to hazard indexes: firstly, a reclassification of land use values must be done (Table G-17), as no 0 values should exist in the raster data.

Table G-17 Parameter reclassification for land use (I).

Raw value min	Raw value max	New value	Land use
0	1	1	Water
1	2	2	Trees
2	3	3	Grass
3	4	4	Flooded vegetation

This project has received funding from the European Union's Horizon Europe research and innovation programme under grant agreement No GA 101082048

Funded by the European Union

4	5	5	Crops
5	6	6	Shrub and scrub
6	7	7	Built
7	8	8	Bare
8	9	9	Snow and ice

After that, a new reclassification was done to assign a hazard value to each land use (Table G-18).

Table G-18 Parameter reclassification for land use (II).

Raw value min	Raw value max	New value	Danger
1	2	1	Low
2	3	1	Low
3	4	1	Low
4	5	1	Low
5	6	3	High
6	7	1	Low
7	8	3	High
8	9	1	Low
9	10	1	Low

River network - 17_river_network

Description: River network 500 m buffer area

Source: HydroRIVERS

Adaptations to hazard indexes: this layer consists of a 500 m buffer of the river network of the demo site, which is reclassified as:

- 1 = no buffer areas (>500 m)
- 2 = buffer areas (<500 m)

Hazard calculation and reclassification

Once all these layers are available and pre-processed, the hazard index is calculated following the next equation:

$$Hazard = SRL \times 3 + LS \times 2 + LU \times 2 + R \times 1$$

Being:

SRL = projected sea level rise

LS = land subsidence

This project has received funding from the European Union's Horizon Europe research and innovation programme under grant agreement No GA 101082048

Funded by the European Union

LU = land use

R = river network

After the calculation, raw values must be reclassified using the next structure (Table G-19) and the min <= value < max condition:

Table G-19 Parameter reclassification for groundwater pollution hazard.

Raw value min	Raw value max	New value	Hazard
8	12	1	Low
12	16	2	Moderate
16	19	3	High

Exposure parameters

Population density - 18_pop_density

Description: Population density values for each country of the World. Data resolution depends on each country's data (city, municipality, county, province, state...).

Source: in general, for EU countries: GEOSTAT 2018. For the DS6 detailed mapping, the 250x250 m population density data were used. In the case of mapping population density outside Europe, World data can be found in SEDAC.

Adaptations to hazard indexes: Population density data is reclassified using the min < value <= max condition, as Table G-20 indicates.

Table G-20 Parameter reclassification for population density.

Raw value min	Raw value max	New value	Pop density exposure
0	1	1	None or very low
1	25	2	Low
25	100	3	Moderate
100	100,000	4	High

Groundwater dependent ecosystems - 19_GW_ecosystem

Description: The data show datasets presenting the ecosystem wetlands extent. This includes 20 wetland classes which, besides inland and coastal wetlands, include transitional ecosystems corresponding to wetlands such as riparian forests, wet grasslands, estuaries, or rice fields.

Source: European Environment Agency Datahub. "Extended wetland ecosystem layer 2018".

For sites outside the EU and in the Tropical and Subtropical regions, we use the Global Wetlands data (https://www2.cifor.org/global-wetlands/).

Adaptations to hazard indexes: The data has been reclassified using this criterion and "min <= value < max" (Table G-21).

Table G-21 Parameter reclassification for groundwater dependent ecosystems.

This project has received funding from the European Union's Horizon Europe research and innovation programme under grant agreement No GA 101082048

Funded by the European Union

Raw value min	Raw value max	New value	GW ecosystems exposure
0	1	1	No
1	21	2	Yes
21	100,000	1	No

Natural protected areas - 20_nat_prot_areas

Description: The data show all the natural protected areas included in the Natura 2000 database.

Source: Natura 2000 database

Adaptations to hazard indexes: Vector data has been rasterized with a value = 1. A Europe vector layer has been rasterized with a value = 1. Both layers have been coupled, so the Natural Protected Areas are shown with a value = 2.

Exposure calculation and reclassification

Once all these layers are available and pre-processed, the exposure index is calculated following the next equation:

$$Exposure = POP \times 4 + GW \times 2 + NAT \times 2$$

Being:

POP = population density

GW = groundwater dependent ecosystems

NAT = natural protected areas

After the calculation, raw values must be reclassified using the next structure (Table G-22) and the min <= value < max condition:

Table G-22 Parameter reclassification for groundwater pollution exposure.

Raw value min	Raw value max	New value	Exposure
8	13	1	Low
13	19	2	Moderate
19	25	3	High

Table G-22 Summary of the data sources used for the groundwater pollution risk mapping

Risk component	Variable	Data source with link	Specific information

This project has received funding from the European Union's Horizon Europe research and innovation programme under grant agreement No GA 101082048

Funded by the European Union

Vulnerability	Groundwater occurrence	WISE WFD groundwater body horizons reported under Water Framework Directive 2016 - PUBLIC VERSION - version 1.0, Jun. 2021	European groundwater body horizons delineated for the 2nd River Basin Management Plans under the Water Framework Directive.
Vulnerability	Aquifer hydraulic conductivity	IHME1500 - International Hydrogeological Map of Europe 1:1,500,000	The International Hydrogeological Map of Europe, scale 1:1,500,000 (IHME1500) is a series of general hydrogeological maps comprising 30 map sheets, partly with explanatory notes, covering nearly the whole European continent and parts of the Near East.
Vulnerability	Height of groundwater level above sea level	Mostly local data, but in some places or Europe data can be found from the Digital Dataset of European Groundwater Resources 1:500,000. ● DS3 Frielas (PT): Sistema Nacional de Informacão de Recursos Hídricos ● DS4 Emilia Romagna (IT): Digital Dataset of European Groundwater Resources 1:500,000 ● DS5 Cape Flats (SA): Local data provided by SU UNIVERSITY OF STELLENBOSCH. ● DS6 El Señorío (ES): Local data obtained from Argamasilla (2017).	Spatial data representing groundwater level above sea level in unconfined aquifers.
Vulnerability	Distance from the shore	Shoreline of the World	Spatial data showing the existing distance from the shore using buffers of 500, 750 and 1000 m using QGIS.
Vulnerability	Impact of existing status of seawater intrusion	WISE Water Framework Directive Database	European groundwater bodies with electrical conductivity values, when available., obtained from the Water Framework Directive Database and the International hydrogeological map of Europe 1:1,500,000.
Vulnerability	Saturated thickness	WISE Water Framework Directive Database and Zamrsky et al. (2017, 2018)	European coastal groundwater bodies (WISE) with an estimation of aquifer thickness (Zamrsky et al., 2017, 2018).

This project has received funding from the European Union's Horizon Europe research and innovation programme under grant agreement No GA 101082048

Funded by the European Union

Vulnerability	Unsaturated zone characteristics	IHME1500 - International Hydrogeological Map of Europe 1:1,500,000	The International Hydrogeological Map of Europe, scale 1:1,500,000 (IHME1500) is a series of general hydrogeological maps comprising 30 map sheets, partly with explanatory notes, covering nearly the whole European continent and parts of the Near East.
Vulnerability	DEM	SRTM Digital Elevation Data Version 4	Digital elevation dataset produced in the framework of the Shuttle Radar Topography Mission v4 (SRTM), with resolution ranging from 30 to 90 m. Data downloaded using Google Earth Engine scripts. This data is used to produce the 09_depth_to_GW and the 13_slope layers. Data coming from the Endeavour spatial mission (2000).
Vulnerability	Depth to water table	Mostly local data, but in some places or Europe data can be found from the Digital Dataset of European Groundwater Resources 1:500,000. ● DS3 Frielas (PT): Sistema Nacional de Informacão de Recursos Hídricos ● DS4 Emilia Romagna (IT): Digital Dataset of European Groundwater Resources 1:500,000 ● DS5 Cape Flats (SA): Local data provided by SU UNIVERSITY OF STELLENBOSCH. ● DS6 El Señorío (ES)	Spatial data showing the depth at which groundwater is located below the topographic surface.
Vulnerability	Net recharge	CHIRPS: Rainfall Estimates from Rain Gauge and Satellite Observations and IHME1500 - International Hydrogeological Map of Europe 1:1,500,000	Climate Hazards Group InfraRed Precipitation with Station data (CHIRPS) is a 35+ year quasi-global rainfall data set. Spanning 50°S-50°N (and all longitudes) and ranging from 1981 to near-present, CHIRPS incorporates our in-house climatology, CHPclim, 0.05° resolution satellite imagery, and in-situ station data to create gridded rainfall time series for trend analysis and seasonal drought monitoring. LINK TO SCIENTIFIC PAPER. CHIRPS uses the Tropical Rainfall Measuring Mission Multi-satellite Precipitation Analysis version 7 (TMPA 3B42 v7)7 to calibrate global Cold Cloud Duration (CCD)

This project has received funding from the European Union's Horizon Europe research and innovation programme under grant agreement No GA 101082048

Funded by the European Union

			rainfall estimates.
Vulnerability	Aquifer type	IHME1500 - International Hydrogeological Map of Europe 1:1,500,000	Europe's aquifer spatial data coming from the International Hydrogeological Map of Europe 1:1,500,000.
Vulnerability	Soil type	European Soil Database (ESDB) v2.0 - raster version	Europe soil spatial distribution, based on the European Soil Database.
Vulnerability	Slope	SRTM Digital Elevation Data Version 4	Spatial raster data that shows the slope values (in percentage - %) of the demo site. Slope calculated using QGIS.
Hazard	Projected sea level rise	Kopp et al. (2017)	Data showing areas subjected to flooding associated with sea level rise using a corrected DP16 model under Representative Concentration Pathway (RCP) 8.5 in 2050, median 50.
Hazard	Land subsidence	Hasan et al. (2023) GitHub repository Google Earth Engine code	Land subsidence probability calculated by a global prediction model at high spatial resolution (~2 km) and resampled to 1 km grid size. inSAR data coming from several literature sources, and processed using machine learning techniques by Hassan et al. (2023).
Hazard	Land use	Dynamic World v1	Near-real-time (NRT) land use/land cover (LULC) dataset coming from Dynamic World predictions using Sentinel-2 L1C collection (all bands used except B1, B8A, B9 and B10) from 2015 to present, with revisiting frequency between 2-5 days. Used bands were bilinearly upsampled to 10 m.
Hazard	River network	HydroRIVERS	River network 500 m buffer area using QGIS.
Exposure	Population density	In general, for EU countries: GEOSTAT 2018. For the DS6 detailed mapping, the 250x250 m population density data were used. In case of mapping population density outside Europe,	Population density values for each country of the World. Data resolution depends on each country's data (city, municipality, county, province, state...).

This project has received funding from the European Union's Horizon Europe research and innovation programme under grant agreement No GA 101082048

Funded by the European Union

		World data can be found in SEDAC.	
Exposure	Groundwater dependent ecosystems	European Environment Agency Datahub. "Extended wetland ecosystem layer 2018". For sites outside the EU and in the Tropical and Subtropical regions, we use the Global Wetlands data (https://www2.cifor.org/global-wetlands/).	
Exposure	Natural protected areas	Natura 2000 data - the European network of protected sites	The data show all the natural protected areas included in the Natura 2000 database.

This project has received funding from the European Union's Horizon Europe research and innovation programme under grant agreement No GA 101082048

Funded by the European Union

APPENDIX H. INTERMEDIATE RESULTS OF GROUNDWATER POLLUTION RISK MAPPING

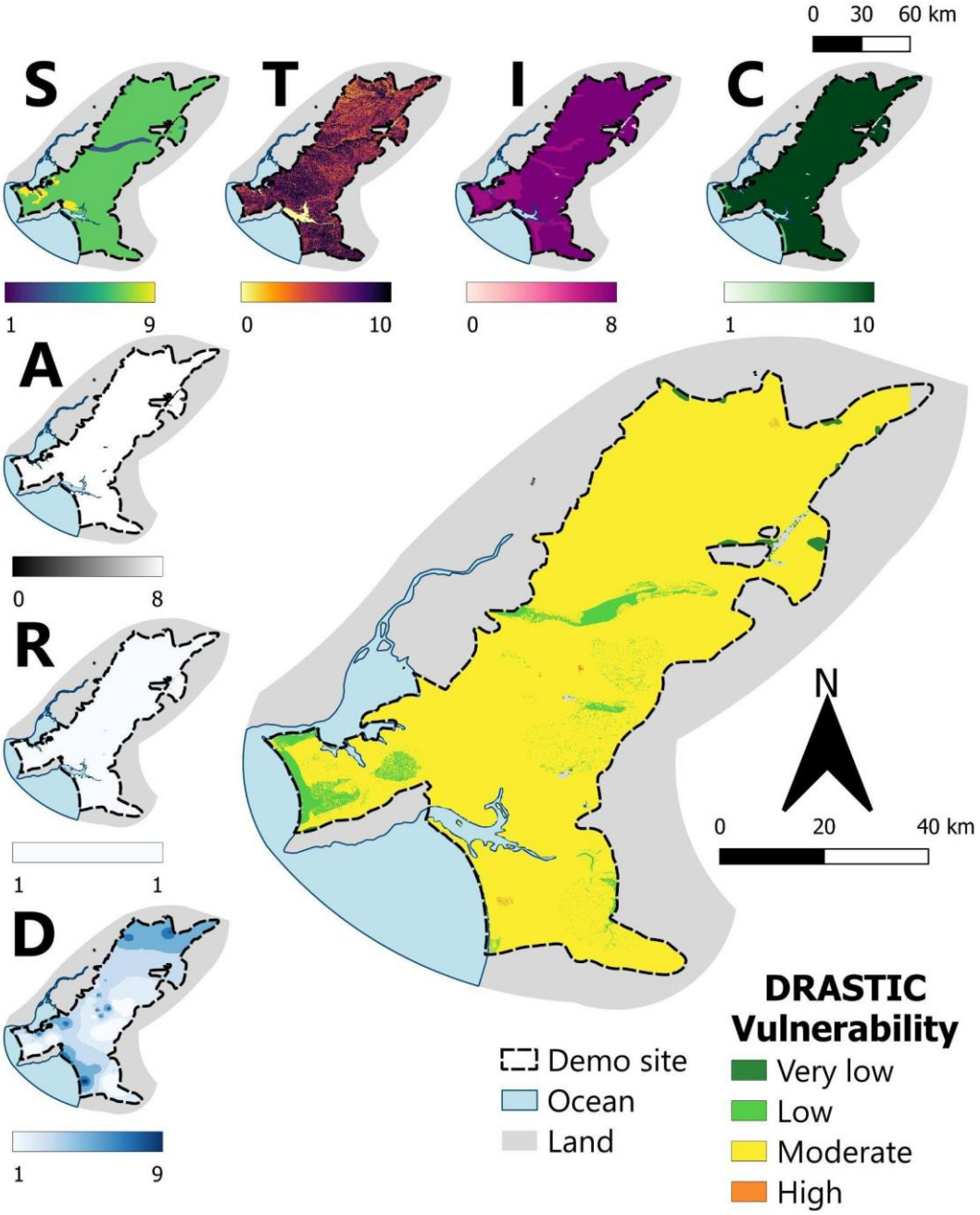

Figure H-1 Vulnerability to groundwater pollution of the Frielas demo site, calculated using the DRASTIC method.

This project has received funding from the European Union's Horizon Europe research and innovation programme under grant agreement No GA 101082048

Funded by the European Union

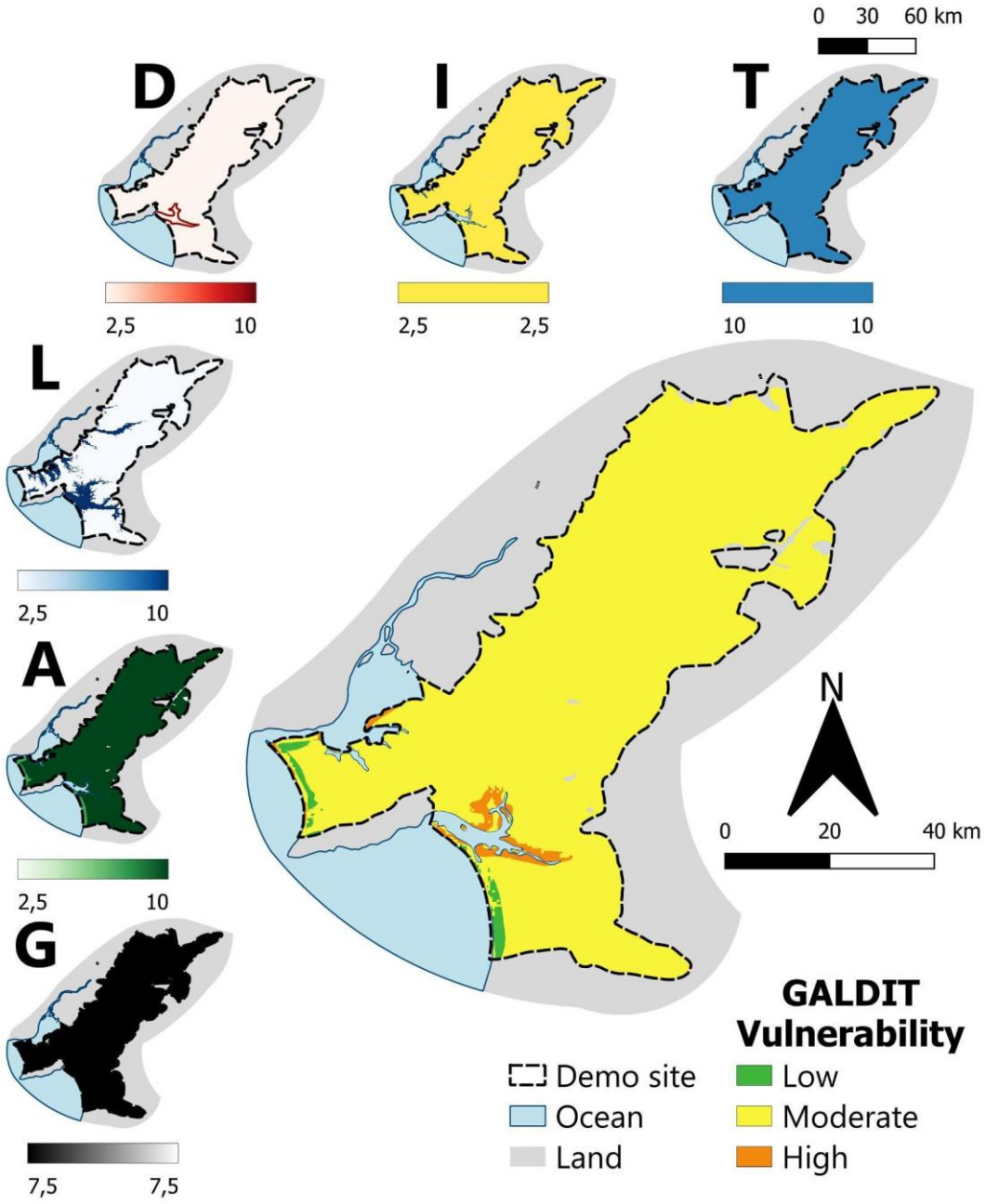

Figure H-2 Vulnerability to groundwater pollution of the Frielas demo site, calculated using the GALDIT method.

This project has received funding from the European Union's Horizon Europe research and innovation programme under grant agreement No GA 101082048

Funded by the European Union

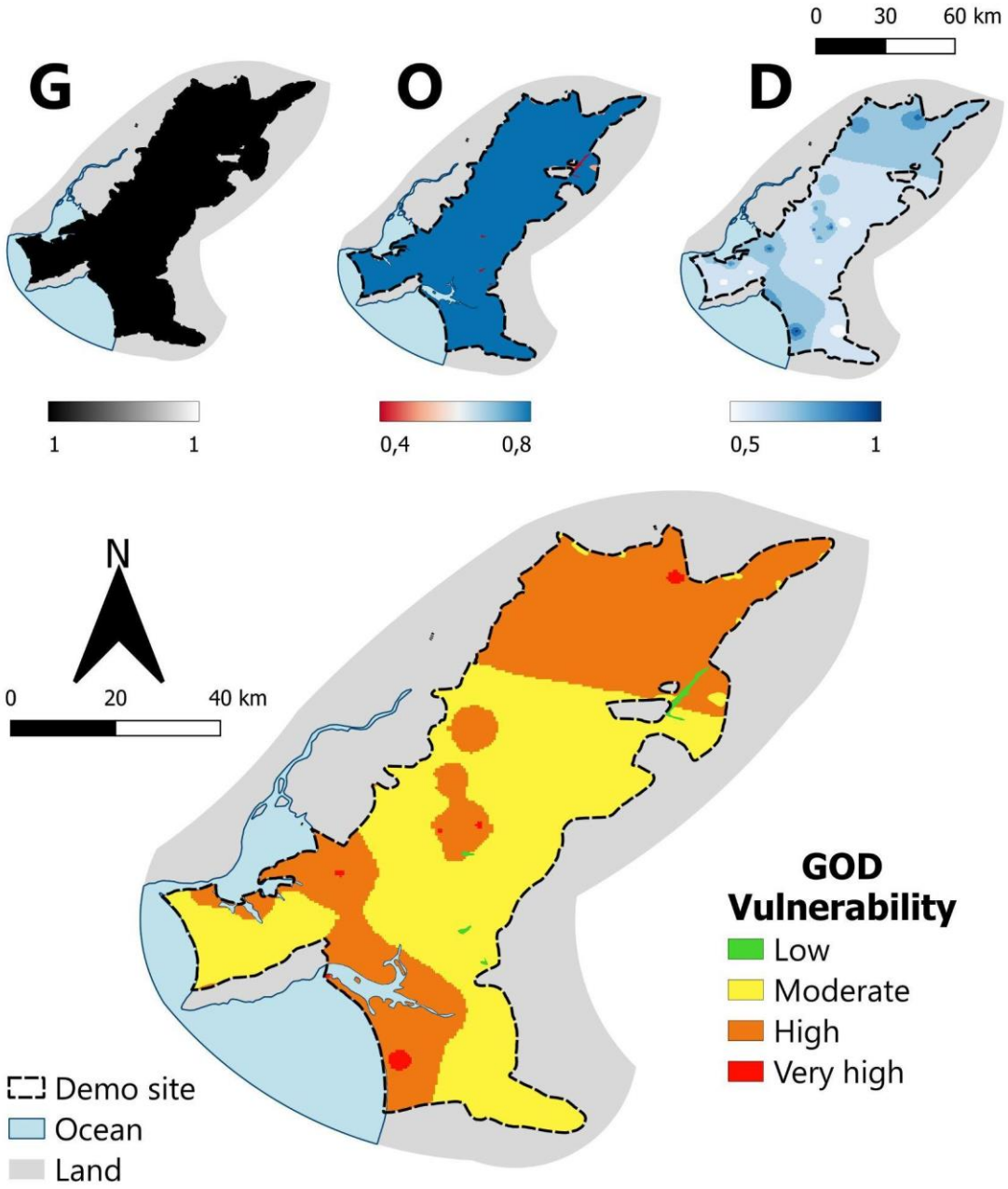

Figure H-3 Vulnerability to groundwater pollution of the Frielas demo site, calculated using the GOD method.

This project has received funding from the European Union's Horizon Europe research and innovation programme under grant agreement No GA 101082048

Funded by the European Union

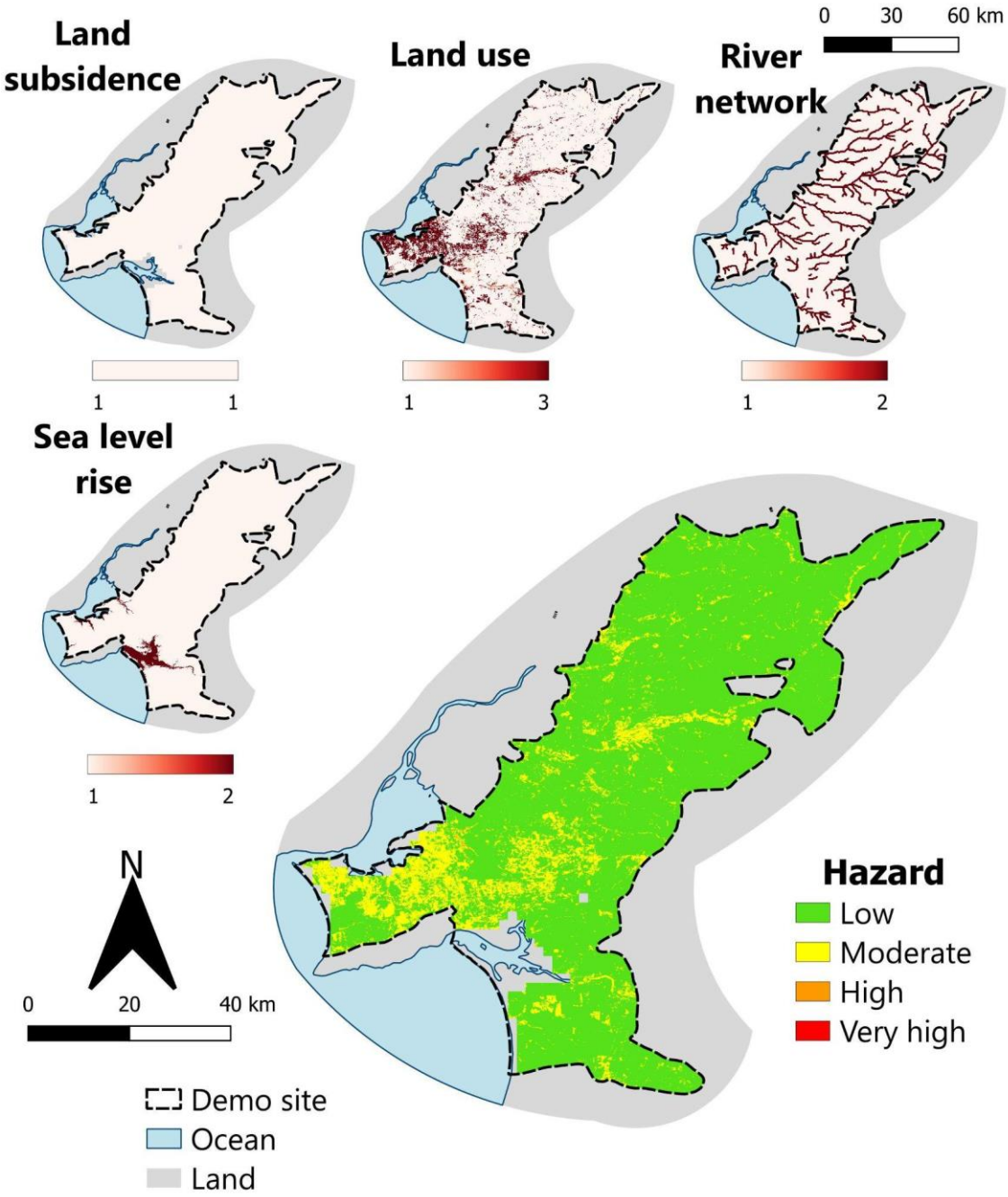

Figure H-4 Hazard to groundwater pollution of the Frielas demo site.

This project has received funding from the European Union's Horizon Europe research and innovation programme under grant agreement No GA 101082048

Funded by the European Union

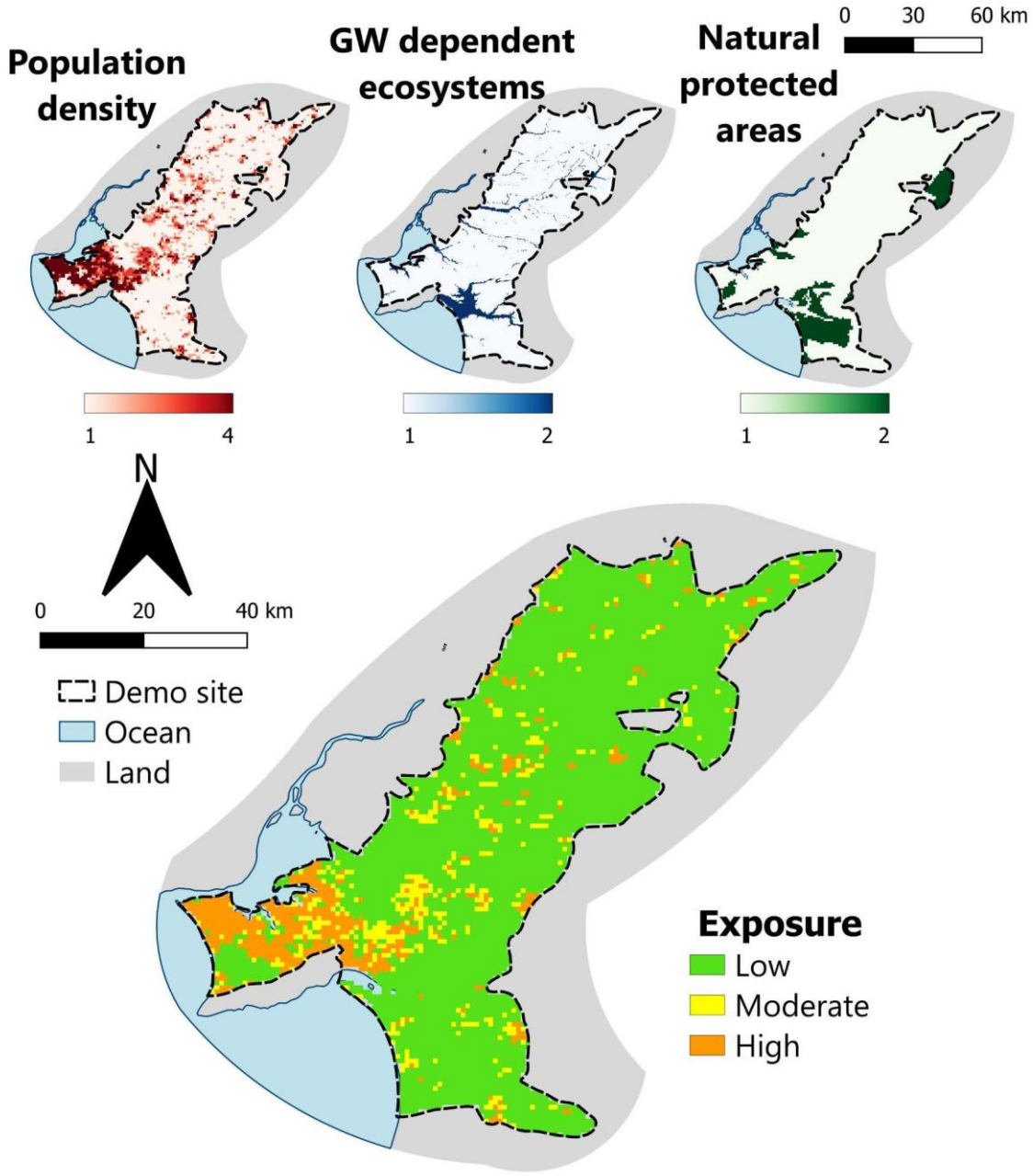

Figure H-5 Exposure to groundwater pollution of the Frielas demo site.

This project has received funding from the European Union's Horizon Europe research and innovation programme under grant agreement No GA 101082048

Funded by the European Union

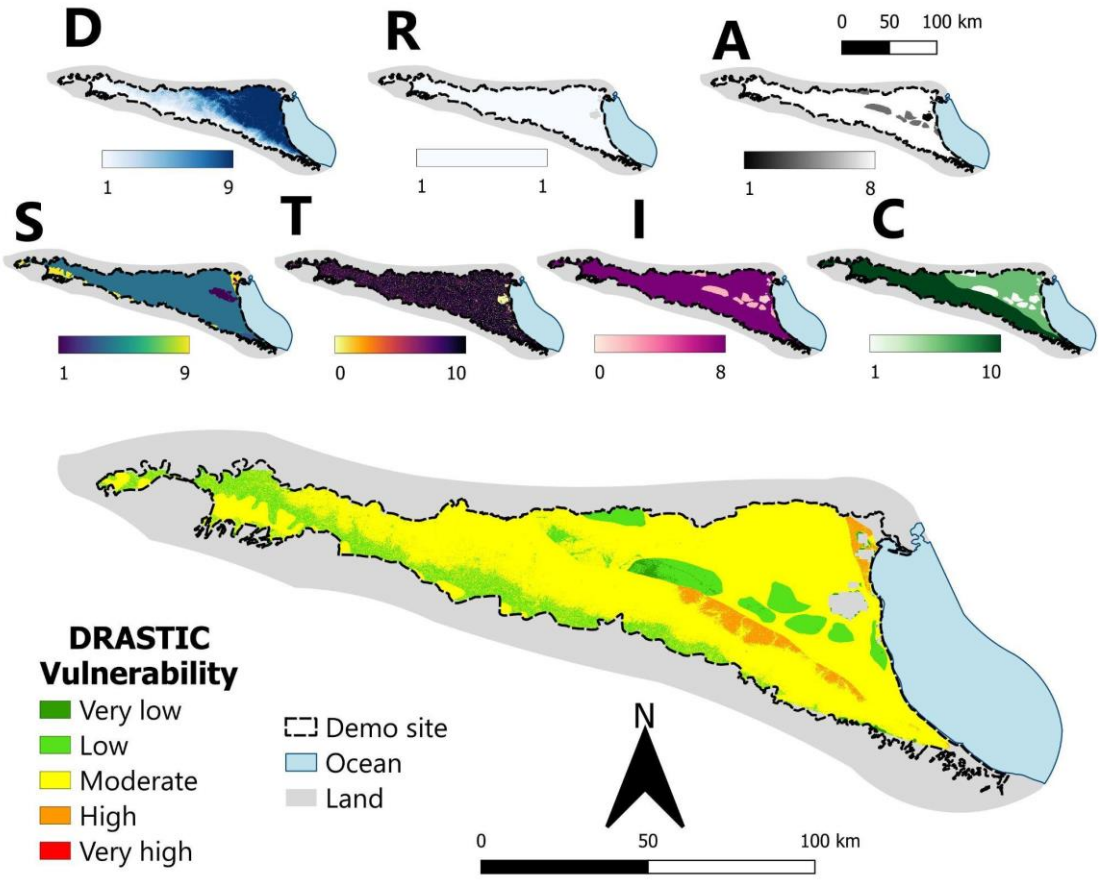

Figure H-6 Vulnerability to groundwater pollution of the Emilia-Romagna demo site, calculated using the DRASTIC method.

This project has received funding from the European Union's Horizon Europe research and innovation programme under grant agreement No GA 101082048

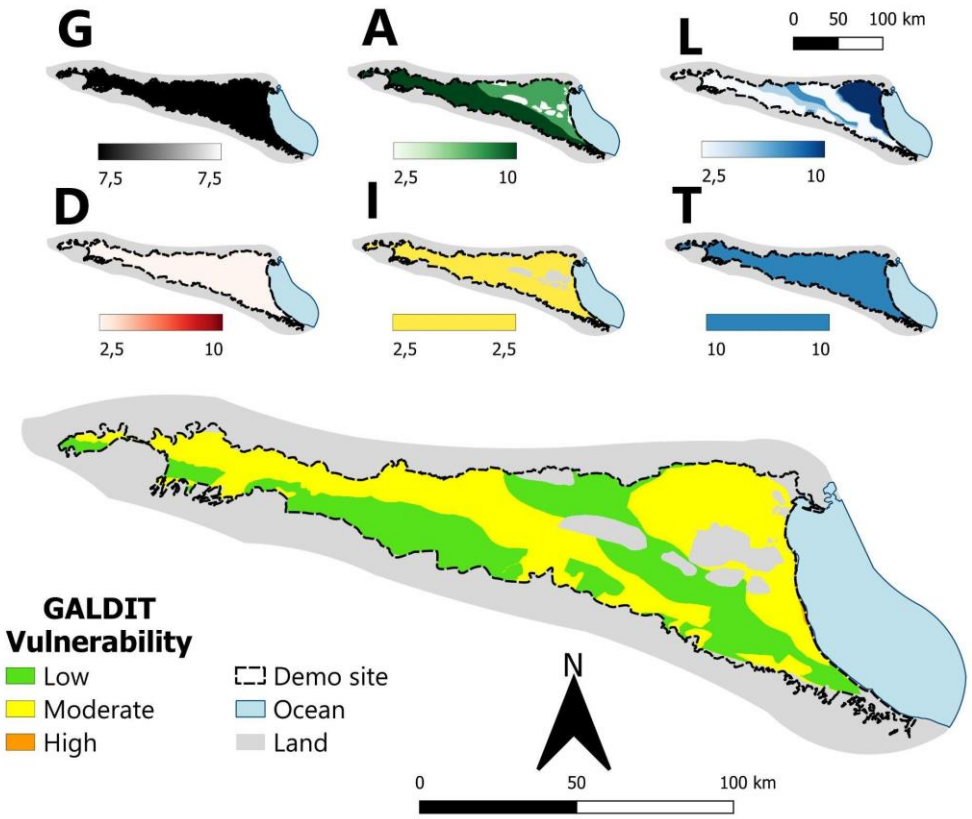

Figure H-7 Vulnerability to groundwater pollution of the Emilia-Romagna demo site, calculated using the GALDIT method.

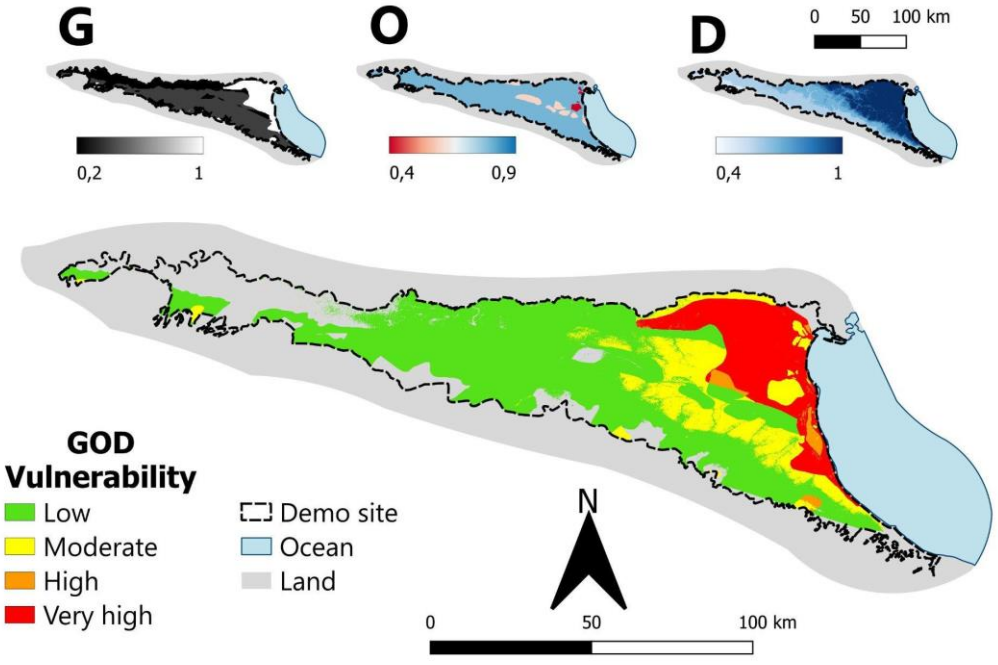

Figure H-8 Vulnerability to groundwater pollution of the Emilia-Romagna demo site, calculated using the GOD method.

This project has received funding from the European Union's Horizon Europe research and innovation programme under grant agreement No GA 101082048
Funded by the European Union

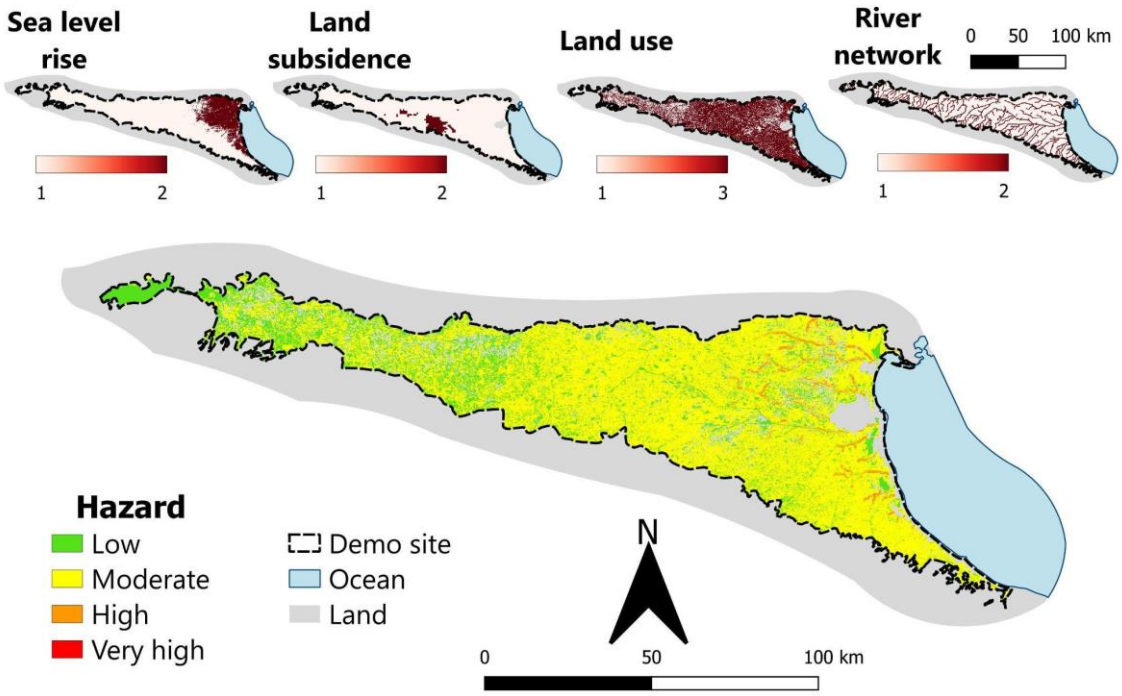

Figure H-9 Hazard to groundwater pollution of the Emilia-Romagna demo site.

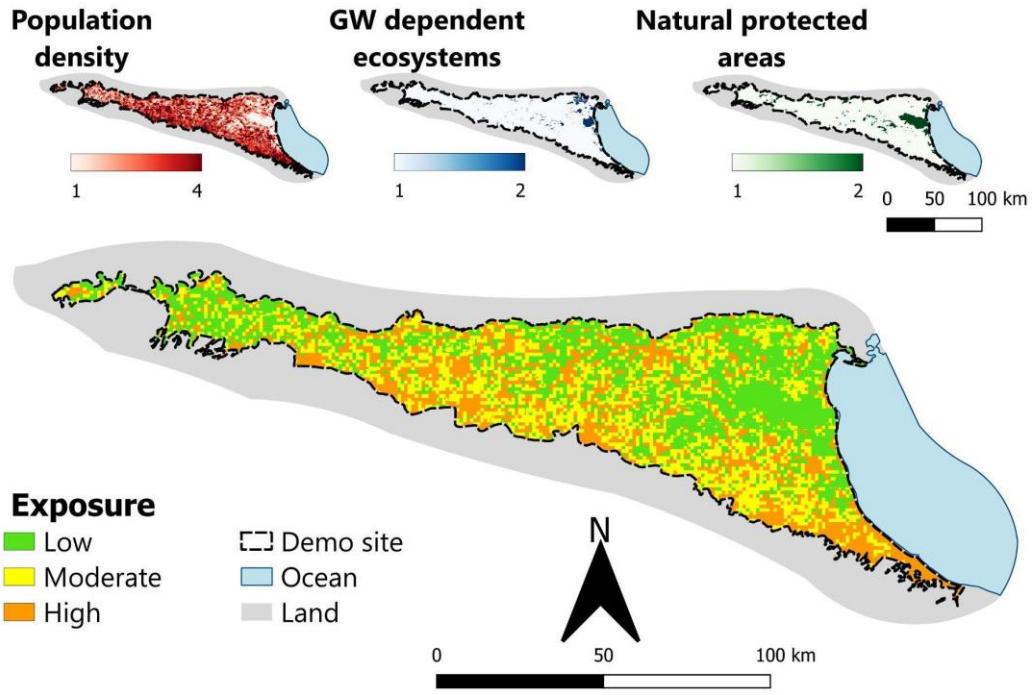

Figure H-10 Exposure to groundwater pollution of the Emilia-Romagna demo site.

This project has received funding from the European Union's Horizon Europe research and innovation programme under grant agreement No GA 101082048
Funded by the European Union

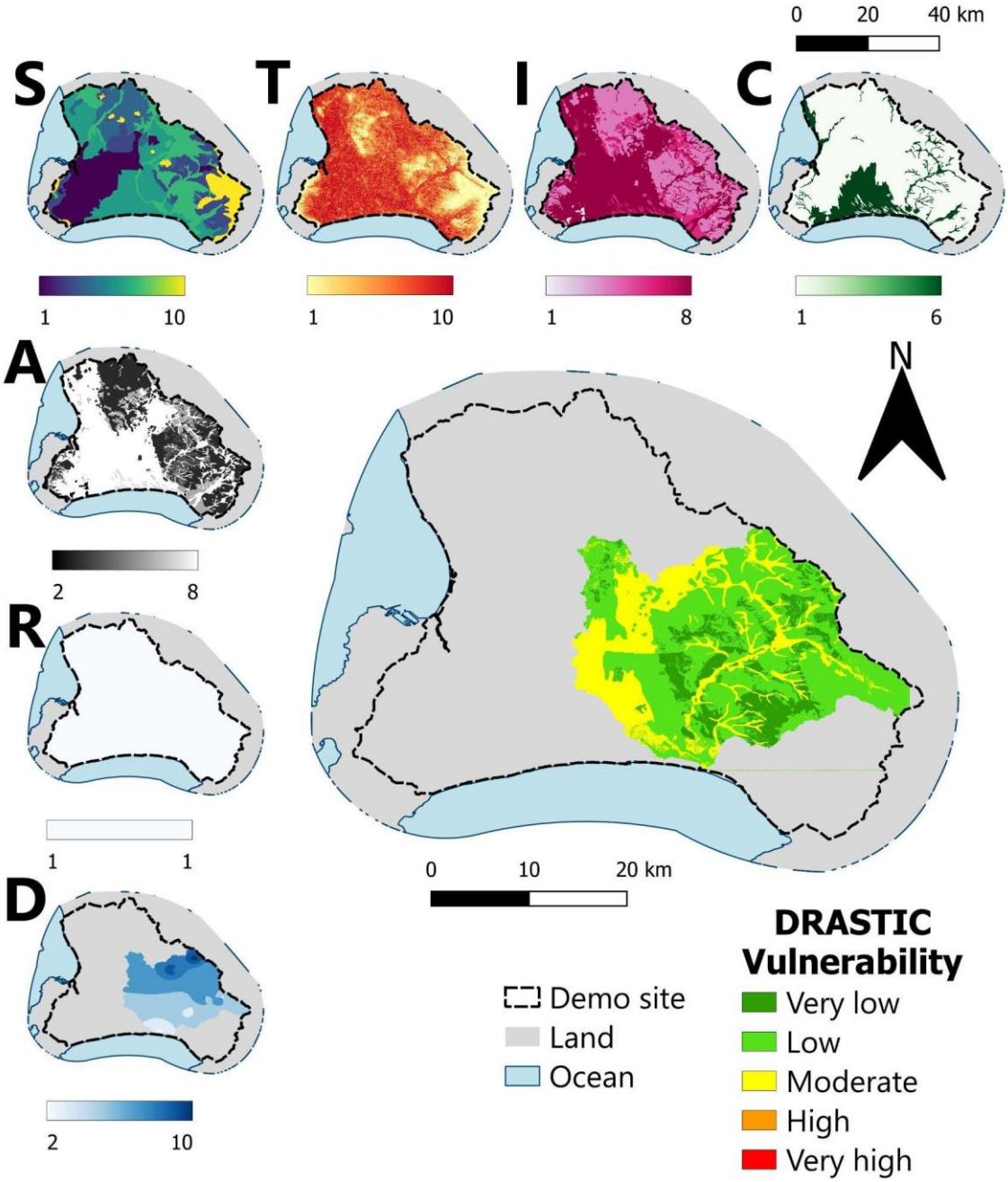

Figure H-11 Vulnerability to groundwater pollution of the Cape Flats demo site, calculated using the DRASTIC method.

This project has received funding from the European Union's Horizon Europe research and innovation programme under grant agreement No GA 101082048

Funded by the European Union

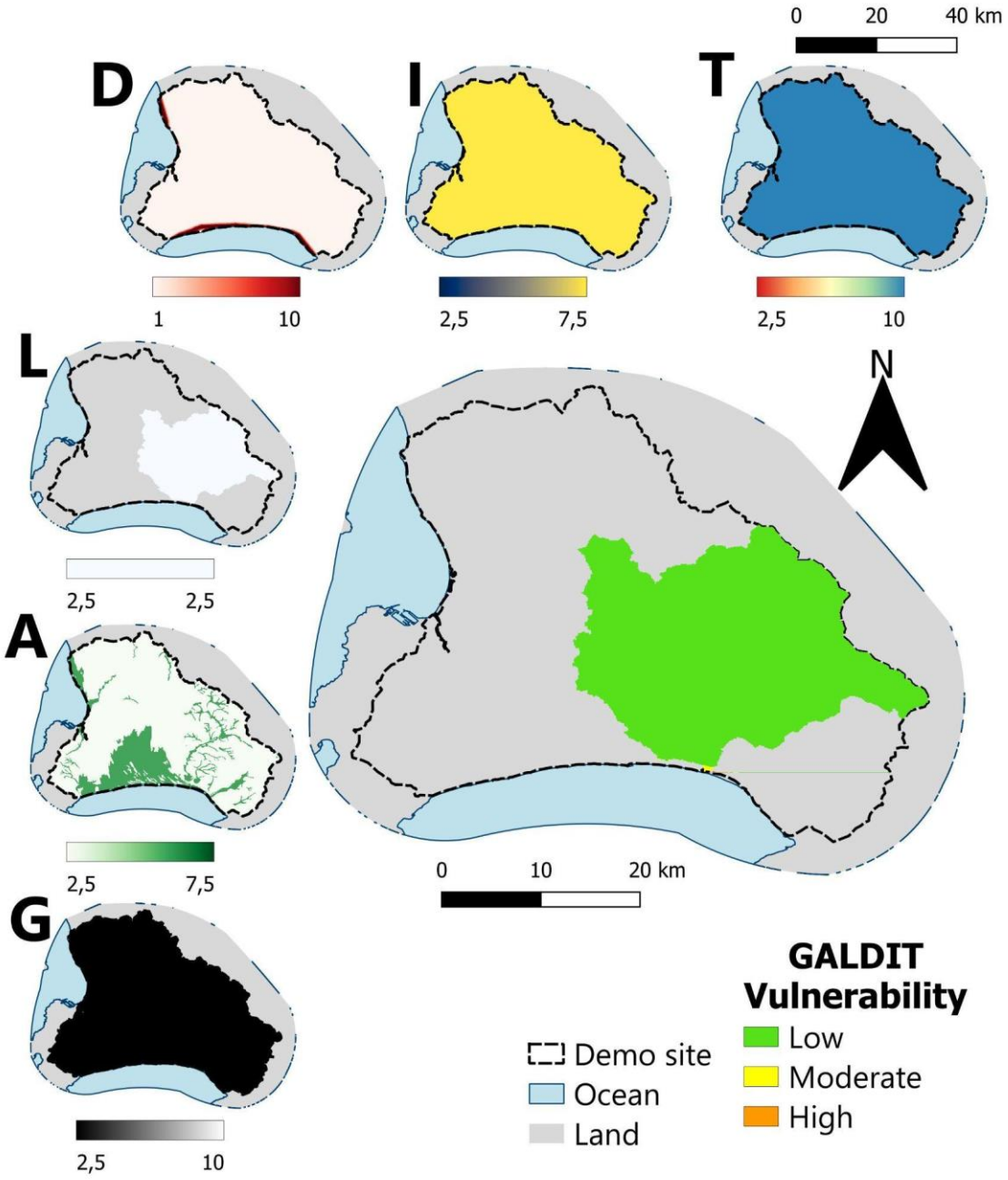

Figure H-12 Vulnerability to groundwater pollution of the Cape Flats demo site, calculated using the GALDIT method.

This project has received funding from the European Union's Horizon Europe research and innovation programme under grant agreement No GA 101082048

Funded by the European Union

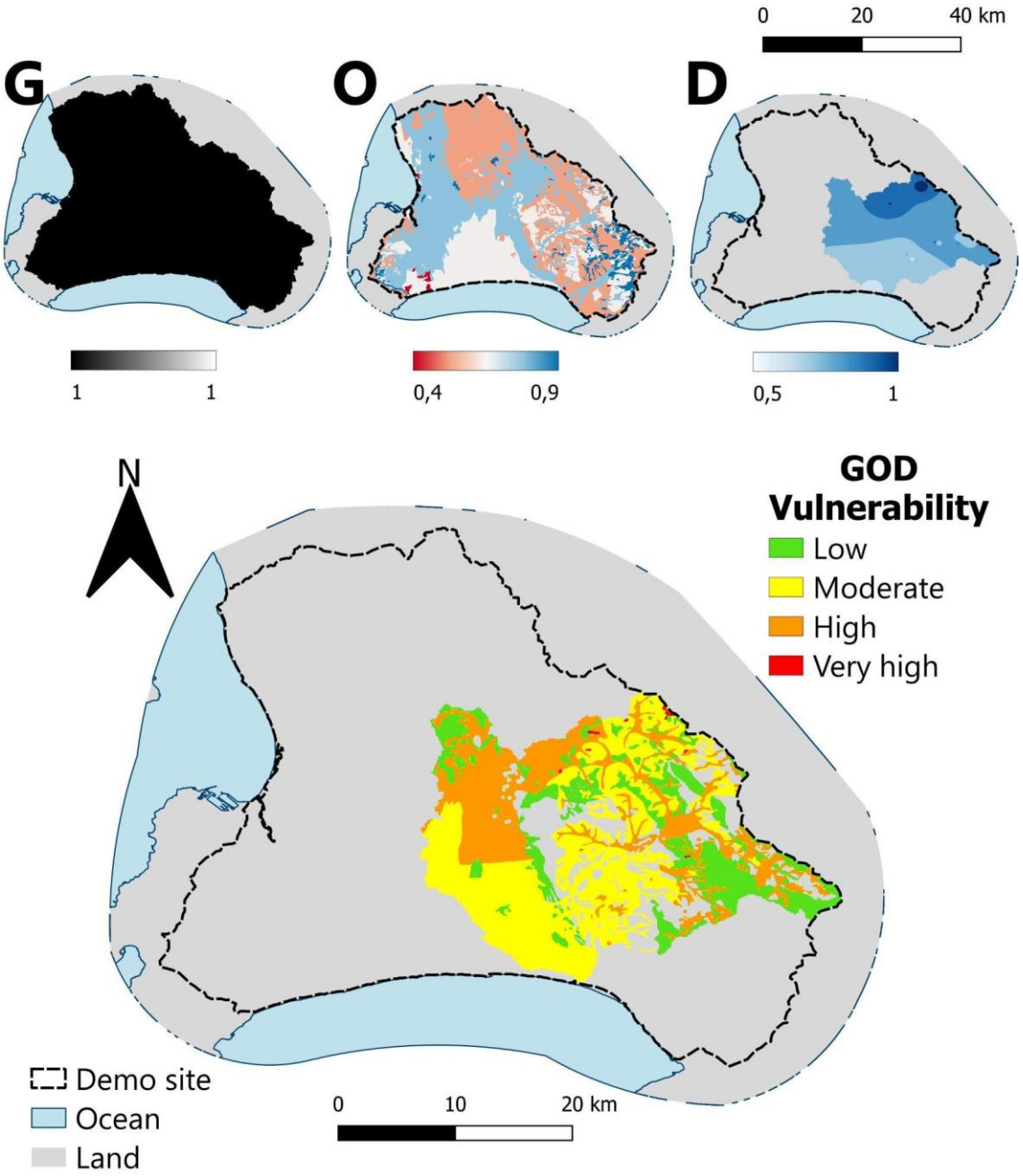

Figure H-13 Vulnerability to groundwater pollution of the Cape Flats demo site, calculated using the GOD method.

This project has received funding from the European Union's Horizon Europe research and innovation programme under grant agreement No GA 101082048

Funded by the European Union

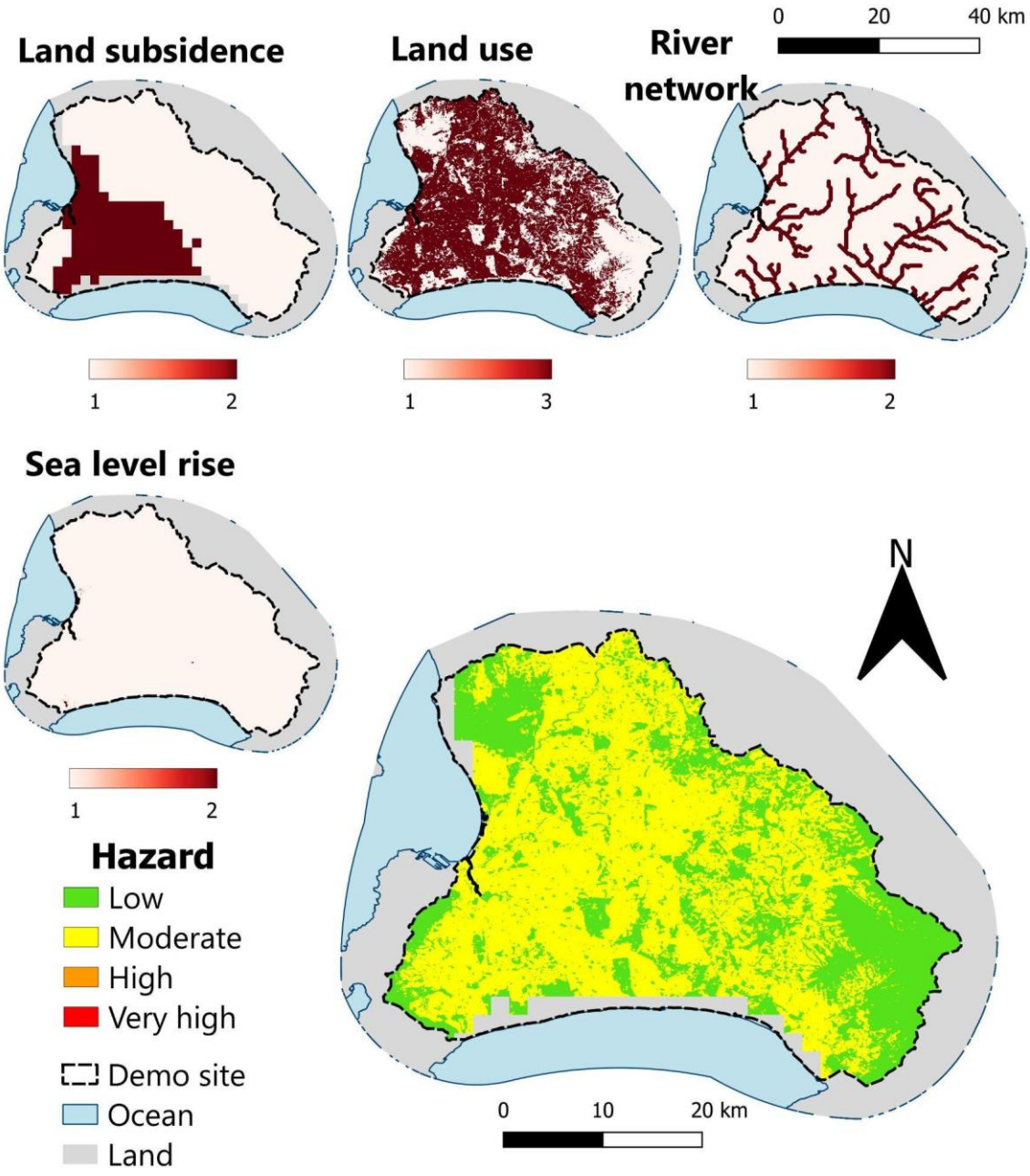

Figure H-14 Hazard to groundwater pollution of the Cape Flats demo site.

This project has received funding from the European Union's Horizon Europe research and innovation programme under grant agreement No GA 101082048

Funded by the European Union

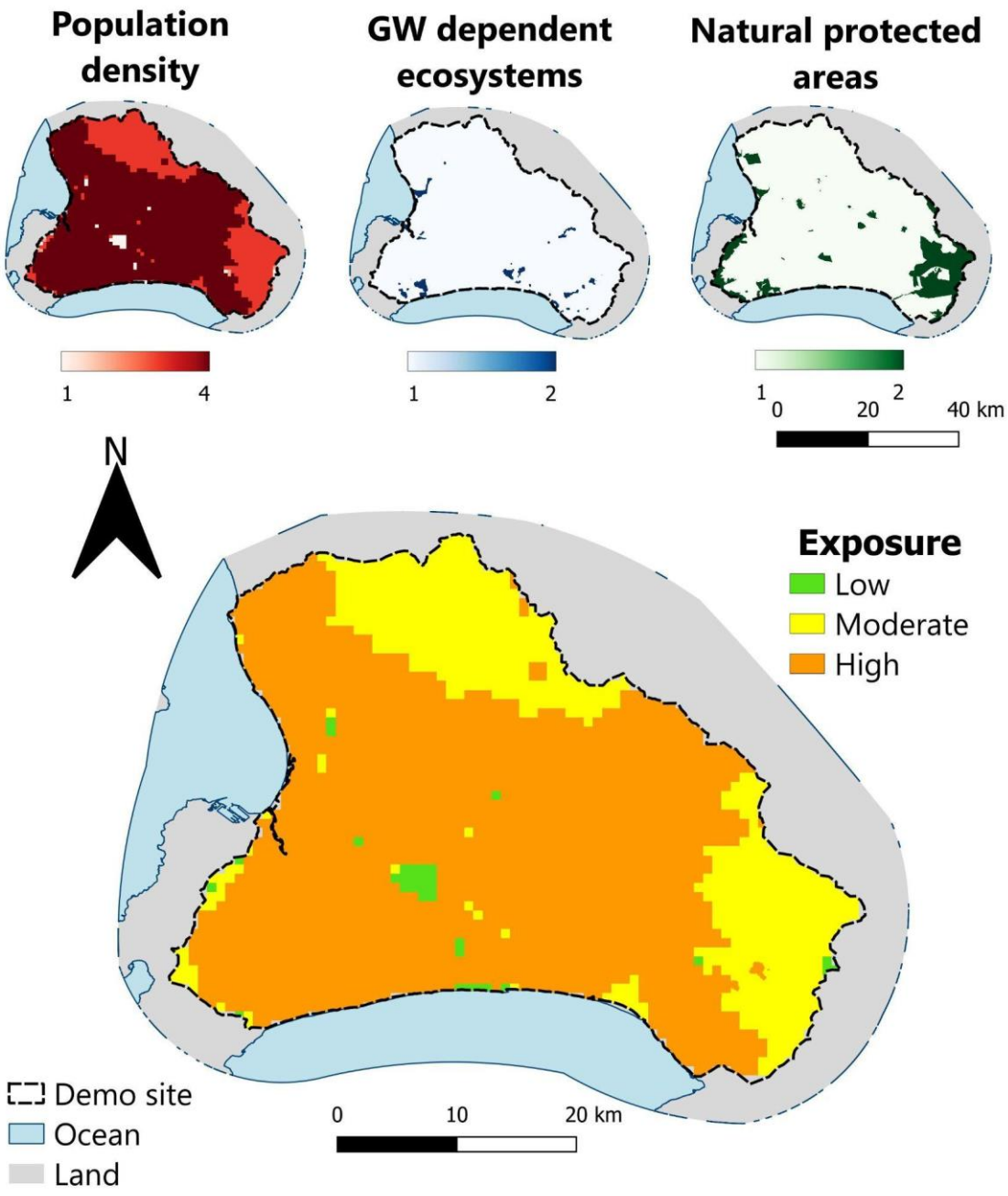

Figure H-15 Exposure to groundwater pollution of the Cape Flats demo site.

This project has received funding from the European Union's Horizon Europe research and innovation programme under grant agreement No GA 101082048

Funded by the European Union

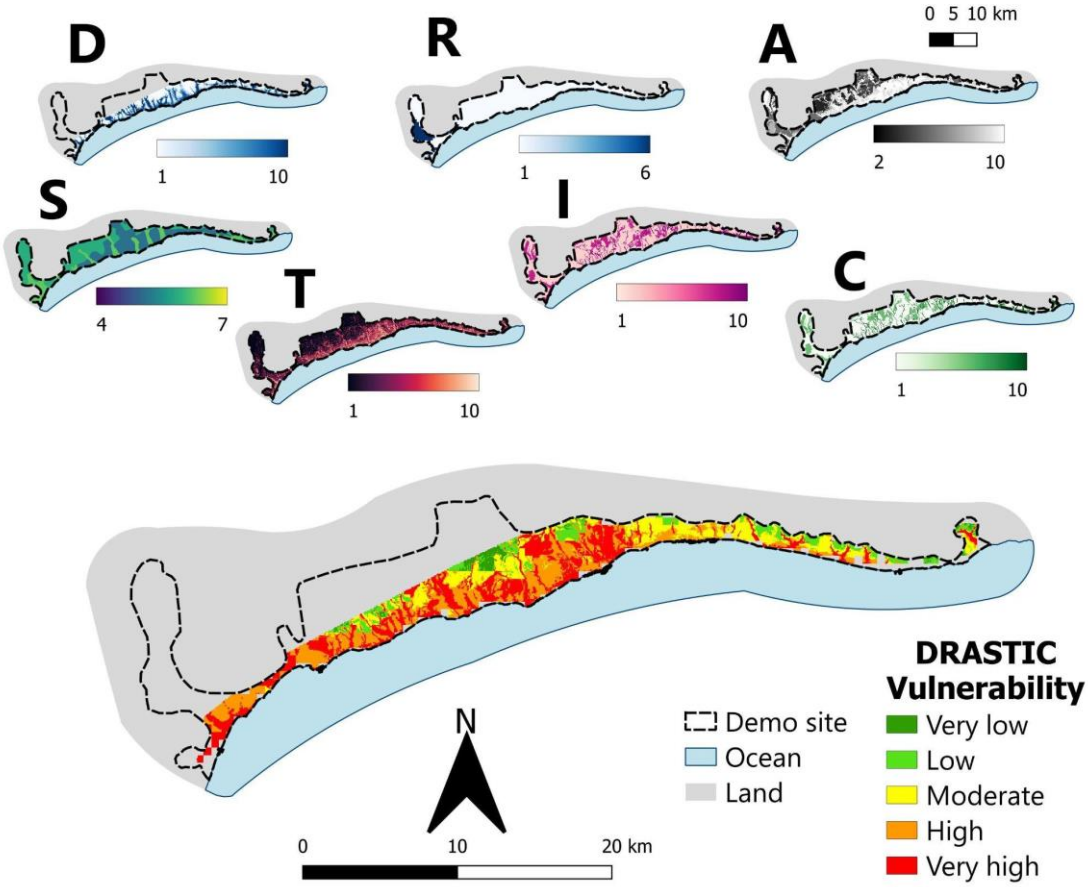

Figure H-16 Vulnerability to groundwater pollution of the Marbella demo site, calculated using the DRASTIC method.

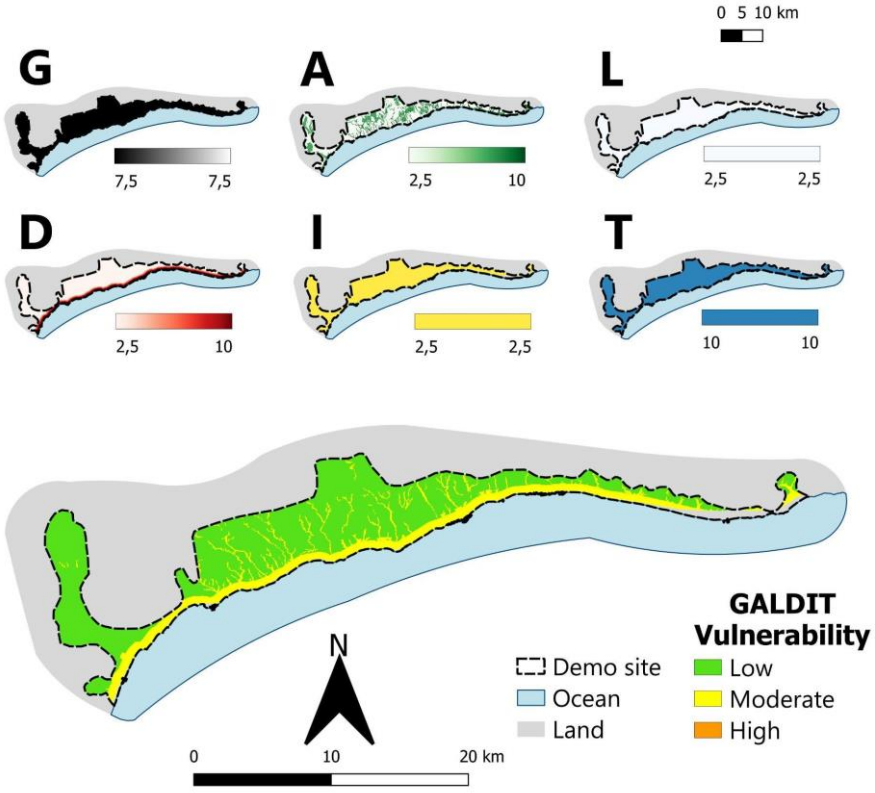

This project has received funding from the European Union's Horizon Europe research and innovation programme under grant agreement No GA 101082048

Figure H-17 Vulnerability to groundwater pollution of the Marbella demo site, calculated using the GALDIT method.

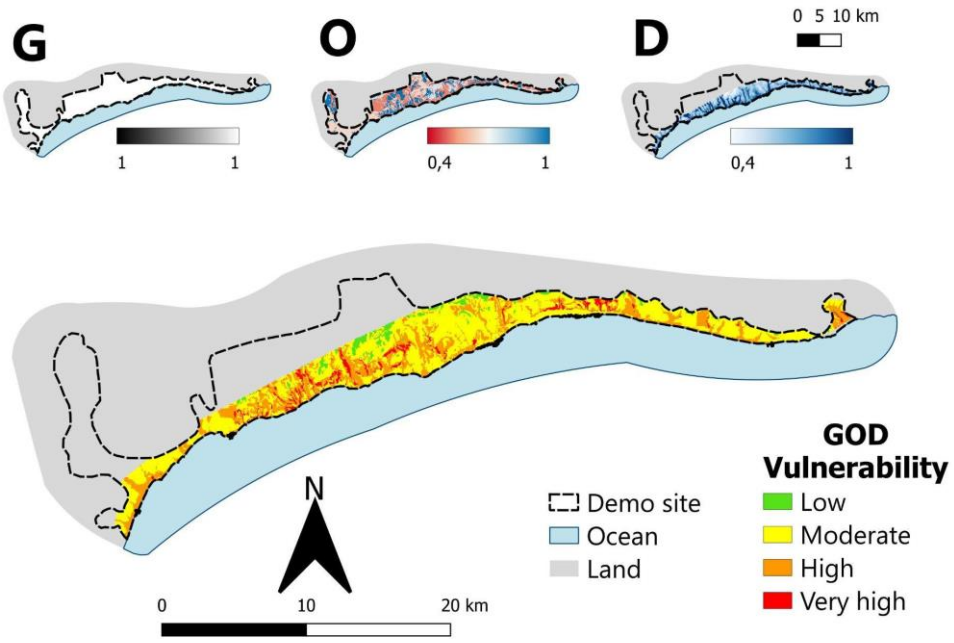

Figure H-18 Vulnerability to groundwater pollution of the Marbella demo site, calculated using the GOD method.

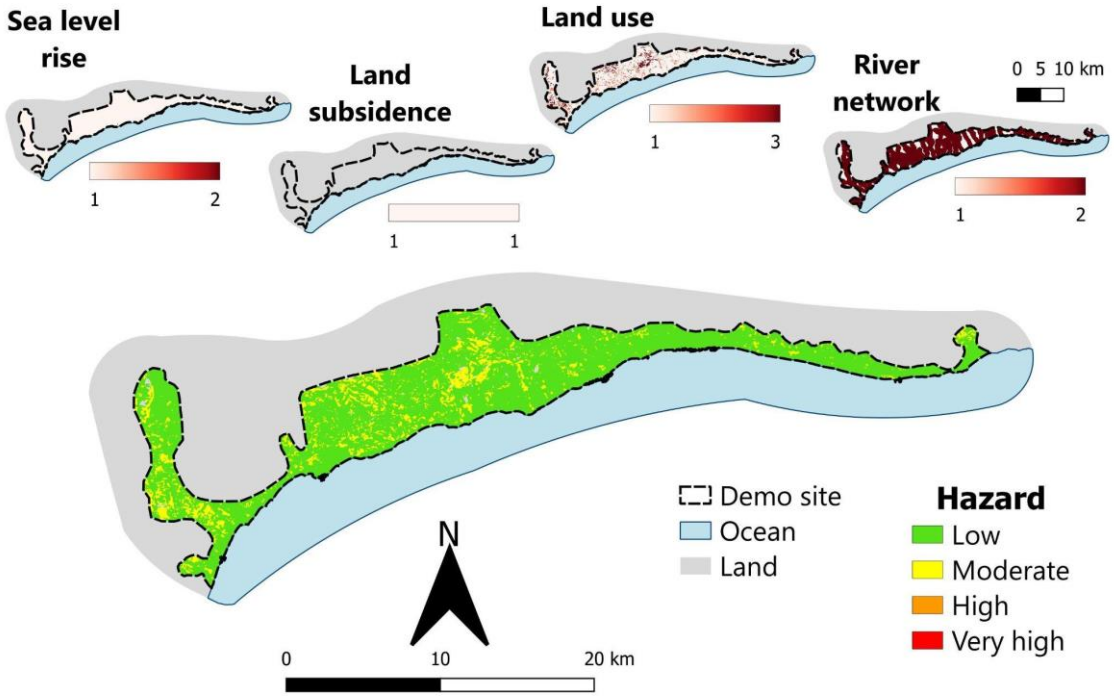

Figure H-19 Hazard to groundwater pollution of the Marbella demo site.

This project has received funding from the European Union's Horizon Europe research and innovation programme under grant agreement No GA 101082048
Funded by the European Union

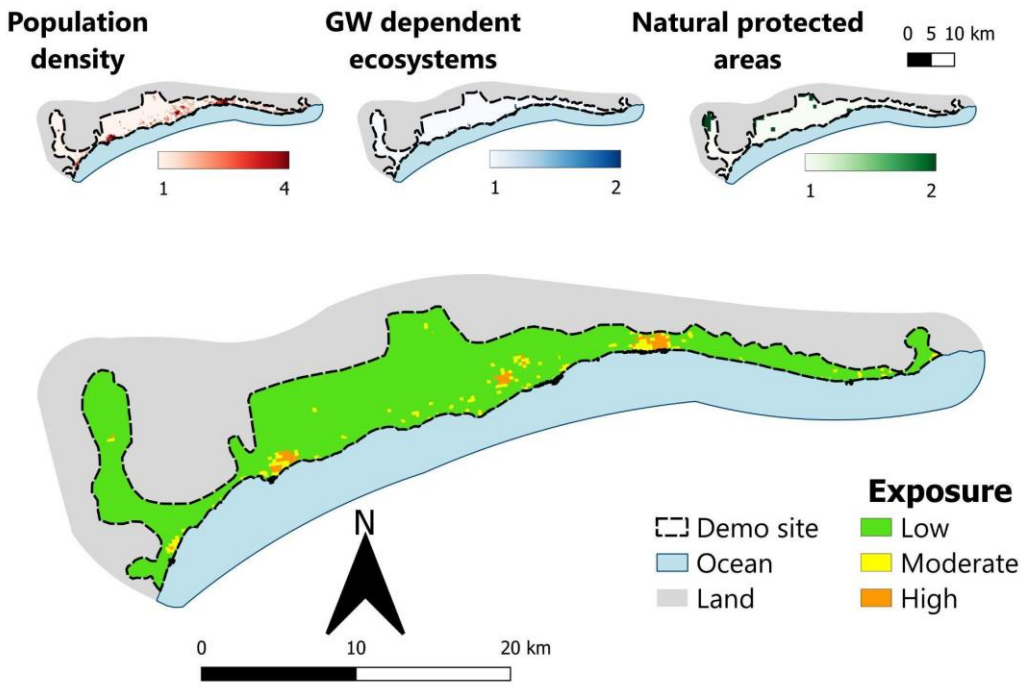

Figure H-20 Exposure to groundwater pollution of the Marbella demo site.

This project has received funding from the European Union's Horizon Europe research and innovation programme under grant agreement No GA 101082048

Funded by the European Union